

Natural Nanoparticles in Soils
and their role in
organic-mineral interactions
and colloid-facilitated transport

Thesis Committee

Thesis supervisors

Prof. Dr. R.N.J. Comans

Professor of Soil Chemistry and Chemical Soil Quality, Wageningen University

Dr. L. Weng

Associate professor, Department of Soil Quality, Wageningen University

Other members

Prof. Dr. S.A. Banwart, University of Sheffield

Prof. Dr. K. Kalbitz, University of Amsterdam

Prof. Dr. A.A. Koelmans, Wageningen University

Prof. Dr. M.F. Benedetti, Paris Diderot University

This research was conducted under the auspices of the Graduate School for Socio-Economic and Natural Sciences of the Environment (SENSE).

Natural Nanoparticles in Soils

and their role in
organic-mineral interactions
and colloid-facilitated transport

Inge C. Regelink

Thesis

submitted in fulfilment of the requirements for the degree of doctor

at Wageningen University

by the authority of the Rector Magnificus,

Prof. Dr. M.J. Kropff,

in the presence of the

Thesis Committee appointed by the Academic Board

to be defended in public

on Friday 7 November 2014

at 4 p.m. in the Aula

Inge C. Regelink

Natural nanoparticles in soils and their role in organic-mineral interactions and colloid-facilitated transport, 222 pages

PhD thesis, Wageningen University, Wageningen, NL (2014)

With references, with summaries in English and Dutch

ISBN: 978-94-6257-150-1

Table of Contents

Chapter 1.	General introduction	9
Chapter 2.	Asymmetric flow field-flow fractionation as a new approach to analyse iron-(hydr)oxide nanoparticles in soil extracts	25
Chapter 3.	Characterization of colloidal Fe from soils using field-flow fractionation and Fe K-edge X-ray absorption spectroscopy	49
Chapter 4.	Characterization of colloidal phosphorus species in drainage waters from a clay soil using asymmetric flow field-flow fractionation	71
Chapter 5.	The distribution of trace elements between organic and mineral colloidal nanoparticles in a soil extract	95
Chapter 6.	Adsorption competition between phosphate and organic matter on metal-(hydr)oxides in arable and forest soils explained by mechanistic adsorption modelling	105
Chapter 7.	Mechanistic linkages between soil aggregates, soil porosity and soil chemical properties	127
Chapter 8.	General discussion	159
Appendices		179
Summary		199
Samenvatting		205
Dankwoord		211
Curriculum Vitae & List of Publications		217
Education Certificate		220

Chapter 1

General introduction

Inge C. Regelink

1.1 Introduction

Soils provide major ecosystem services such as food production, sequestration of organic carbon (OC), and buffering of water and nutrients. Soils can provide these services because they act as biogeochemical reactors in which nutrients and contaminants are transformed, sequestered or released as a result of the numerous physical-chemical and biological processes that take place within the soil (Figure 1.1). Many of these biogeochemical processes have in common that they occur at the solid-water interface or, with other words, at the surfaces of the organic and mineral compounds within the soil (Chorover et al., 2007). Considering the mineral compounds, the total surface area of the soil minerals is more important than the mass of the soil minerals when determining the potential reactivity of the soil. As a consequence, the particle size an important parameter since the specific surface area (SSA, i.e. surface to mass ratio) of a spherical particle increases strongly with decreasing particle, in particular for particles smaller than 10 nm (Figure 1.2). Therefore, a relatively small amount of nano-sized particles can dominate the reactive surface area of the soil whereas the more abundant but larger silt- and sand-sized particles hardly contribute. As such, the characteristics of the natural nano-sized mineral fraction present in soils are of great interest because this fraction provides the interfaces which are involved in numerous geochemical processes. Therefore, natural nanoparticles and their role in soil processes form the key topic of this PhD thesis.

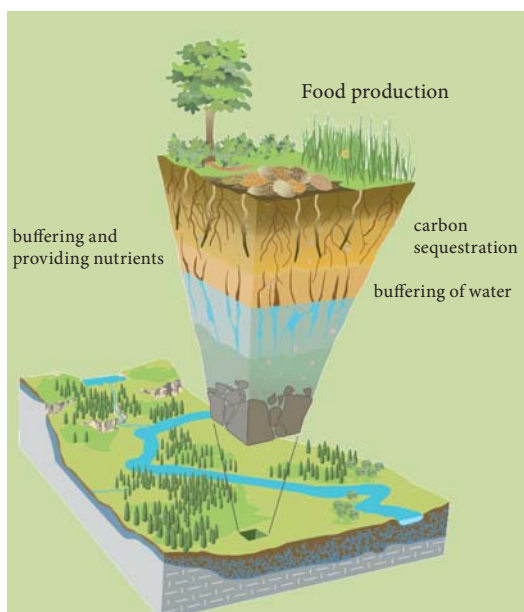


*Figure 1.1. Ecosystem services of soils.
Reprinted with permission from
www.criticalzone.org*

The research presented in this thesis can be divided into two research directions: (i) characterisation of the size and speciation of natural nanoparticles in soils and soil extracts and (ii) understanding and quantifying the role of nanoparticles in soil processes, in particular colloid-facilitated transport, sequestration of OC and phosphate, and aggregate formation. In this section, I will introduce these two research directions and the chosen experimental approaches. Finally, I will introduce the main objectives and outline of this thesis.

1.2 Natural Nanoparticles in soils

Nanoparticles are nanometre-sized hard particles. They have in general a high reactivity due to their small size and consequently large SSA. The SSA of spherical particles is proportional to the reciprocal of the particle diameter (d), according to $SSA = 6/\rho*d$. Consequently, the SSA shows a tremendous increase with decreasing size for particles smaller than 10 nm (Figure 1.2). In addition to their large specific surface area, nanoparticles may have a unique structure, making them more reactive compared to the bulk material, even after correction for the SSA (Hochella et al., 2008; Qafoku, 2010). This size-dependent surface reactivity of nanoparticles can be explained by a change in the arrangement of atoms at the surface of the nanoparticle when a large fraction of the atoms are located at the surface (Hiemstra, 2013). The official definition of nanoparticles states that nanoparticles have at least one dimension smaller than 100 nm (Figure 1.3) (Christian et al., 2008). However, Hochella et al. (2008) proposed that the upper limit of nanoparticles should be defined as the size above which the properties of the particles are indistinguishable from those of the bulk material, which is typically a few tens of nanometers. Colloidal particles are defined

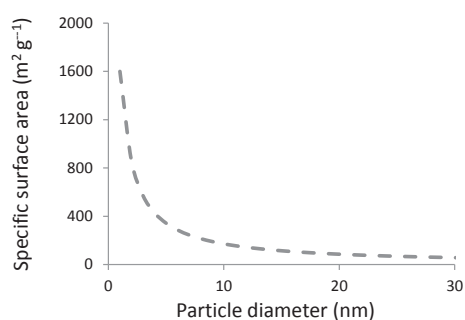


Figure 1.2. The specific surface area (SSA) of a spherical nanoparticle as a function of the particle diameter, calculated according to $SSA=6/\rho*d$ using a density (ρ) of 3.5 kg dm^{-3} . The SSA strongly increases with decreasing particle diameter for particles smaller than 10 nm.

as dispersed particles with a size between 1 nm and 1 mm (Figure 1.2) (Kretzschmar et al., 1999). Hence, nanoparticles and colloids partly overlap and nanoparticles can as such be regarded as a subfraction of colloids. Since the definitions of colloids and nanoparticles are solely based on the dimensions of the particles, the variety of colloids and nanoparticles in the environment is large and their composition is complex and heterogeneous (Kretzschmar et al., 1999; Wigginton et al., 2007).

The increasing awareness of the typical characteristics of nanomaterials compared to bulk materials has driven the tremendous increase in research on both natural and engineered nanoparticles during the last decade. As a result, the production of engineered nanoparticles has been booming and nowadays engineered nanoparticles are applied in numerous industrial applications, consumer products as well as for environmental remediation practices (Ju-Nam and Lead, 2008). For example, engineered Fe-oxide nanoparticles have several potential applications for in-situ remediation of contaminated soils (Braunschweig et al., 2013). However, whereas the engineered nanoparticles have come to the centre of spotlight only recently, natural nanoparticles have been active in various biogeochemical processes for billions of years. Examples of natural nanoparticles in soils and surface waters are metal-(hydr)oxides of iron (Fe), aluminium (Al) or manganese (Mn), aluminium-silicate clay minerals, and metal-sulphides (Braunschweig et al., 2013; Calabi-Floody et al., 2011; Hofacker et al., 2013). In soils, Fe-(hydr)oxides are the most abundant nano-sized particles in the solid phase (Plathe et al., 2013; Qafoku, 2010) and, therefore,

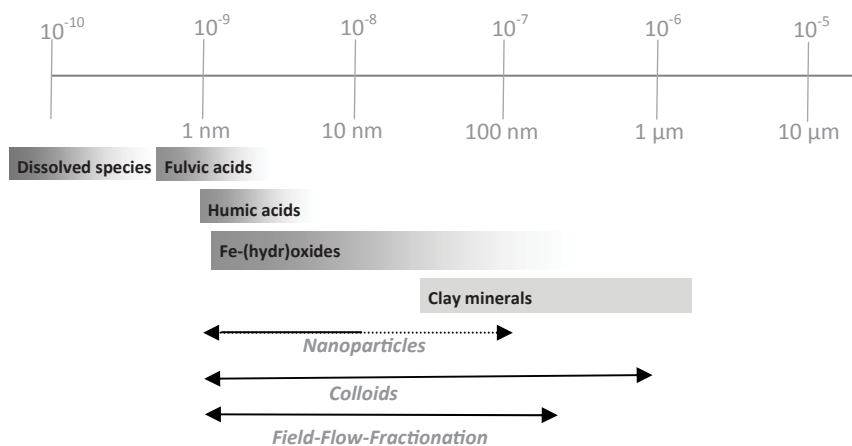


Figure 1.3. Schematic overview of the size-distribution of natural nanoparticles and colloids and the definitions used within this thesis.

these nanoparticles play a central role throughout this thesis. The dominant Fe-(hydr)oxide mineral within the nano-sized fraction of soils is ferrihydrite, which is a poorly polymerized Fe-(hydr)oxide mineral (FeOOH) characterised by its small size, large reactive surface area, and high density of reactive surface sites (Hiemstra, 2013).

In order to improve our understanding of the role of Fe-(hydr)oxide nanoparticles in colloid-facilitated transport and the sequestration of OC and phosphate, these Fe-(hydr)oxides need to be well characterized with respect to their size, surface area and speciation. However, characterization of the Fe-(hydr)oxides present in natural soils is still challenging and, therefore, in many studies, researchers have used synthetic analogues of natural Fe-(hydr)oxides to study the properties of Fe-(hydr)oxides in order to understand their adsorption characteristics. For example, adsorption models have been developed based on adsorption experiments using synthetic Fe-(hydr)oxides (Dzombak and Morel, 1990; Weng et al., 2008). However, comparison between the SSA derived for synthetic goethite ($100 \text{ m}^2\text{g}^{-1}$, Stachowicz et al., 2008) and ferrihydrite ($600 \text{ m}^2\text{g}^{-1}$, Dzombak and Morel, 1990) and the SSA determined for the Fe-(hydr)oxide fraction in natural soils revealed that natural Fe-(hydr)oxides can even be smaller than their synthetic counterparts. For example, Hiemstra et al. (2010a) derived the SSA for a range of agricultural soils and found that the SSA varied between $200\text{--}1200 \text{ m}^2\text{g}^{-1}$, which corresponds to a particle size of $10\text{--}1 \text{ nm}$, while Eusterhues et al. (2005) derived an average SSA of $800 \text{ m}^2\text{g}^{-1}$ for Fe-(hydr)oxides in a series of forest soils. Also, in heavily fertilized soils, the observed ratios between P and metal-(hydr)oxides (Koopmans et al., 2007) are higher than can be explained based on the maximum phosphate adsorption capacity as predicted from adsorption experiments with synthetic Fe-(hydr)oxides (Rahnemaie et al., 2007). Overall, these results provide indirect evidence for the presence of extremely small and highly reactive Fe-(hydr)oxides in soils. However, the presence of such small and highly reactive Fe-(hydr)oxide particles in soils is remarkable since such particles should be thermodynamically unstable relative to their larger and more crystalline counterparts (Burlinson and Penn, 2005; Christian et al., 2008; Navrotsky et al., 2008; Schwertmann and Murad, 1983). As such, synthetic Fe-(hydr)oxides rapidly increase in size over time due to aging (Burlinson and Penn, 2005). The existence of nano-sized Fe-(hydr)oxides in soils might be explained by the presence of phosphate and dissolved organic carbon in soils, since these elements inhibit further growth and polymerization of freshly precipitated Fe-(hydr)oxides (Eusterhues et al., 2008; Voegelin et al., 2010). Nevertheless, it remains questionable whether these small and highly reactive phases do actually exist in well-developed soils, which warrants further research to provide experimental evidence for

the existence and composition of nano-sized Fe-(hydr)oxide particles in soils.

Novel analytical approaches are needed in order to characterize the Fe-(hydr)oxides in the nano-sized fraction of the soil. The size of the nanoparticles can be determined by Asymmetric Flow Field-Flow Fractionation (AF4), which is an analytical technique that allows for a continuous size-fractionation of nanoparticles and colloids (1-500 nm) in water samples. AF4 can be combined with online detectors such as a UV-detector and High-Resolution Inductively Coupled Plasma Mass Spectrometry (HR-ICP-MS) for particle characterization (von der Kammer et al., 2011). Fractionation takes place in a thin water film (Figure 1.4) and particles are fractionated based on differences in their diffusion coefficient which is related to their hydrodynamic diameter. A first requirement to analyse Fe-(hydr)oxides by AF4 is that the particles should be dispersed as intact particles from the soil. However, at the beginning of this PhD thesis, no attempts had been made to extract Fe-(hydr)oxides from soils as colloidally stable particles, which was therefore my first research objective. Once dispersed, the size-distribution and elemental composition of the soil particles can be determined by AF4-HR-ICP-MS. However, one generally recognized constraint in previous AF4 studies (Plathe et al., 2013) is the inability of this technique to elucidate the speciation of the Fe-containing colloids when Fe-(hydr)oxides elute simultaneously with clay minerals during AF4 fractionation. Therefore, an additional technique such as X-ray absorption spectroscopy (XAS) is needed to analyse the speciation of the colloidal Fe. XAS probes the local coordination of Fe and has been applied before to analyze the speciation of Fe in soils, in colloids isolated from environmental water samples and in synthetic Fe-precipitates (Kleja et al., 2012; Voegelin et al., 2013). As such, in this PhD thesis, I will combine results from these novel analytical approaches since I expect that this combination leads to new insights into the size, composition and speciation of Fe in the nano-sized fraction of the soil.

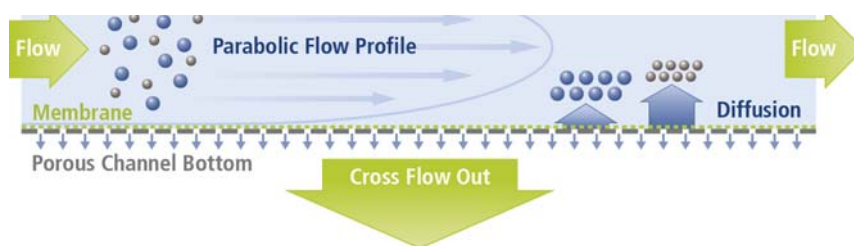


Figure 1.4. Schematic picture showing the principles of particle fractionation in Asymmetric Flow Field-Flow Fractionation (AF4). Reprinted with permission from Postnova Analytics.

1.3 Role of Fe-(hydr)oxide nanoparticles in soil processes

In this section, I will elaborate further on the role of nanoparticles in colloid facilitated transport, sequestration of OC and phosphate, and aggregate formation.

1.3.1 Colloid Facilitated Transport

Besides being present in the solid phase, mineral nanoparticles such as Fe-(hydr)oxides and clay minerals, can also be released to the pore water and consequently be transported to ground- or surface waters where they act as carriers for trace metals and phosphate (Benedetti et al., 2003; Dolfing et al., 1999; Kretzschmar et al., 1999; Lyvén et al., 2003, Plathe et al., 2013). The release of mineral nanoparticles and colloids from the soil and their mobility within the soil are strongly related to the colloidal stability of the respective particles (Kretzschmar et al., 1999). Particles are colloidally stable when the attractive Van der Waals forces are counterbalanced by electrostatic repulsive forces between the particles (Tombacz and Szekeres, 2004). The electrostatic interactions between particles are dominantly controlled by the electrostatic potential of the particles, which is a function of the inherent surface charge of the particle, the ionic strength of the solution, and the additional charge added to the surface due to adsorption of cations and anions (Rahnemaie et al., 2007). As such, the colloidal stability of Fe-(hydr)oxide and clay particles is enhanced by the adsorption of a sufficient amount of anions such as fulvic acids and phosphate, whereas multivalent cations (e.g., Ca^{2+} , Fe^{3+} , and Al^{3+}) stimulate the coagulation of these particles (Baalousha, 2009; Majzik and Tombacz, 2007). As a result, the ionic composition of the solution has a strong influence on the release of Fe-(hydr)oxides and other colloids from the soil and their stability in the water phase (Kretzschmar et al., 1999). However, the quantitative contribution of mineral nanoparticles to element transport is still poorly understood because the characterization of nanoparticles and colloids in water samples is hampered by their small size, strong tendency to aggregate and large heterogeneity. Classical fractionation techniques such as membrane filtration are therefore not suitable for in-depth characterization of nanoparticles and colloids because of artefacts due to coagulation and a low size-resolution of the obtained fractions (Bolea et al., 2006). Instead, a continuous fractionation technique is needed. Therefore, I make use of AF4 coupled to HR-ICP-MS which allows for a continuous fractionation and online analyses of the elemental composition of the colloids in a wide size-range (1-500 nm). Applications of AF4-HR-ICP-MS to unravel the speciation of colloids in surface waters or soil extracts are still scarce, but results are very promising. For example, AF4-HR-ICP-MS was used to characterize colloidal Fe species in

surface waters (Benedetti et al., 2003) and to study the contribution of organic and mineral colloids in trace element transport in surface waters (Baalousha et al., 2006; Neubauer et al., 2013; Stolpe et al., 2010). However, AF4 is a technique in development and AF4-HR-ICP-MS has not been applied before to unravel the speciation of the colloidal P fraction in surface waters and at this moment, The transport of colloidal P is of environmental concern because colloidal P contributes substantially to the overall transport of P from agricultural fields on clay soils to adjacent surface waters (van der Salm et al., 2012), thereby leading to eutrophication of surface waters (Correll, 1998). However, the speciation, and thus the mobility and bioavailability, of the colloidal P fraction is still unknown and therefore, one of my objectives is to use AF4-HR-ICP-MS to unravel the speciation of colloidal P in drain and trench waters from these fields.

1.3.2 Sequestration of organic carbon and phosphate

Humic substances and phosphate show a high affinity for adsorption to Fe-(hydr)oxides and as such, Fe-(hydr)oxides dominate the potential sequestration capacity for these anions even though they typically contribute less than 5% to the soil mass (Hiemstra et al., 2010a; Mikutta and Kaiser, 2011). Considering the sequestration of OC first, adsorption to mineral surfaces inhibits biodegradation of the organic matter (Eusterhues et al., 2014), leading to long-term sequestration of OC within organo-mineral assemblages. As such, soil can act as a sink for CO₂, thereby mitigating the greenhouse effect caused by elevated CO₂ levels (Mikutta et al., 2006). The contribution of metal-(hydr)oxides to the sequestration of OC in soil is considered more important than other factors that affect carbon sequestration such as the inherent recalcitrance of the organic substances and occlusion within aggregates (Mikutta et al., 2006). However, predictions of the amount of OC that can be sequestered by adsorption to Fe-(hydr)oxides are still uncertain due to uncertainties in (i) the SSA of the Fe-(hydr)oxides and thus the overall surface area available for sorption of the OC and in (ii) the amount of organic matter adsorbed on the surface under certain conditions. Estimated values for the organic matter layer on Fe-(hydr)oxides surfaces given in literature vary between 1.1 and 4.8 mg C per m² (Dümig et al., 2012; Eusterhues et al., 2005; Hiemstra et al., 2010b). This wide range might be explained by the wide range in properties of humic substances among different soils, such as their molecular weight, amount of carboxylic groups and hydrophobicity. Another factor that influences the adsorption of humic substances to Fe-(hydr)oxides is the competition with phosphate, which binds to the same type of surface sites on the Fe-(hydr)oxide surface (Weng et al., 2008). Adsorption experiments using synthetic

model systems have shown that high levels of phosphate strongly reduce the adsorption of humic substances to Fe-(hydr)oxides (Antelo et al., 2007; Weng et al., 2008). These findings suggest that OC sequestration is inhibited in soils with high phosphate levels, which is the case in many agricultural soils in the Western world (Reijneveld et al., 2010). However, the role of phosphate as a potential inhibitor for carbon sequestration in agricultural soils received only minor attention so far, and a quantitative understanding of this effect is still lacking. Similar problems arise in the predictions of phosphate sequestration by Fe-(hydr)oxide nanoparticles and despite the enormous amount of studies on phosphate adsorption to metal-(hydr)oxides, the maximum amount of phosphorus that can be sequestered by the metal-(hydr)oxide fraction ($P/Al_{ox}+Fe_{ox}$ ratio) in the soil is still under debate. For example, Borggaard et al. (1990) found a maximum phosphorus adsorption capacity of 0.2, which is considerably lower than the maximum $P/Al_{ox}+Fe_{ox}$ ratio (0.5) derived by Van der Zee and Van Riemsdijk (1988). In order to predict the mobility of phosphate in the soil and its availability for plant uptake, the soluble phosphate concentration is of importance. (Duffner et al., 2012; Koopmans et al., 2007). The soluble phosphate concentration can be expected to be in equilibrium with the adsorbed phase and both might be affected by the competition with humic substances (Borggaard et al., 1990; Weng et al., 2008). To obtain a better understanding of the adsorption processes occurring at the surface of Fe-(hydr)oxide nanoparticles in soils, advanced surface complexation models have been proven to be very powerful tools to describe and predict the adsorption interactions between phosphate and organic matter on synthetic Fe-(hydr)oxides (Weng et al., 2008). One of these models is the CD-MUSIC (charge-distribution multi-site complexation) model that describes the multiple interactions of ions with charged mineral surfaces and has been applied successfully to describe adsorption of phosphate and organic matter to Fe-(hydr)oxides (Hiemstra et al., 2010a; Hiemstra et al., 2013). In this thesis, I use surface complexation modelling to describe and predict the competitive adsorption interactions between organic matter and phosphate in natural soils. I expect that this modelling approach will improve our quantitative understanding of OC-sequestration in soils with varying phosphate content, and vice versa, phosphate sequestration and phosphate solubility in soils with a varying soil organic carbon content. Overall, these interactions may provide new insights into the effects of soil management practices, such as addition of organic amendments or application of high levels of phosphate, on the amount of OC and phosphate sequestered within the soil as well on the availability of these elements.

1.3.3 Soil aggregate formation

The physical structure of the soil plays a crucial role in the agricultural productivity and water retention capacity of soils. Soil structure is the result of multiple physical and chemical interactions in the soil. However, the complex interactions between physical-chemical properties and soil structure are still poorly understood which limits our ability to improve soil structural properties by adjusting soil management practices. Soil structure has been defined as ‘the size, shape and characteristics of soil particles, aggregates, and pores across the size-range from nanometers to centimeters’ (Bronick and Lal, 2005; Oades, 1993). This definition implies that soil structure is the product of various structural entities that cover a size-range of several orders of magnitude. At the smallest size-scale of aggregation, Fe-(hydr)oxide nanoparticles play an important role because they form organic-mineral assemblages due to their strong interactions with humic acids. These organic-mineral interactions have been shown to be important for the stability of nano- and micro-meter sized aggregates within the soil (Asano and Wagai, 2014; Pronk et al., 2011). It might be expected that Fe-(hydr)oxides also enhance the formation of aggregates at larger size-scales and that they thus improve the stability of soil macroaggregates and increase soil porosity. However, the role of Fe-(hydr)oxides in the formation of macro-aggregates is still poorly understood since studies are limited to typical oxide-rich soils (Barthès et al., 2008; Duiker et al., 2003; Igwe et al., 2009) meaning that the role of Fe-(hydr)oxides in soils with a low or average Fe-(hydr)oxide content is still unknown. Other major factors in aggregation include, among others, organic matter, clay minerals and divalent cations. Organic matter plays a crucial role in the aggregation of mineral particles and is by far the most intensively studied aggregation factor in literature (Angers, 1998; Bronick and Lal, 2005; Pulleman and Marinissen, 2004; Six et al., 2004). Clay minerals enhance aggregation because of their interactions with organic matter but, clay minerals that show strong swelling and shrinkage cause a decrease in aggregate stability (Angers, 1998; Fernández-Ugalde et al., 2013; Six et al., 2000). Another factor that affects aggregation is the amount of exchangeable divalent cations, in particular Ca^{2+} , since the tendency of soil particles to coagulate increases within increasing Ca^{2+} concentration (Curtin et al., 1994). However, despite the extensive knowledge on aggregation mechanisms (Bronick and Lal, 2005; Six et al., 2004), a quantitative understanding of the relationships between physical-chemical properties and the soil structure is still lacking. This is of environmental concern since intensive land use and poor agricultural management practices have led to a decline in the quality of the soil structure, leading to a decrease in the agricultural productivity and water

retention capacity of soils worldwide (Banwart, 2011; Montgomery, 2007). Therefore, there is a need for a mechanistic understanding of the physical-chemical key-factors controlling the evolution from single (nano)particles to soil aggregates, which is one of the objectives of this PhD thesis.

1.4 Objectives and Outline

The overall objective of this PhD thesis was to characterize the dominant natural nanoparticles in soils and elucidate their role in a number of major geochemical processes. More specifically, the research objectives were:

- (i) To provide experimental evidence for the extremely small size of Fe-(hydr)oxide nanoparticles naturally formed in soils using a novel analytical approach (Chapter 2, 3)
- (ii) To study the size and speciation of the mineral nanoparticles released from the soils and to identify the key-factors controlling the release of Fe-(hydr)oxide nanoparticles from soils (Chapter 2 and 3)
- (iii) To quantify the contribution of Fe-(hydr)oxide nanoparticles and other colloids to colloid-facilitated transport of trace metals and P (Chapter 4,5)
- (iv) To quantify the amount of organic matter that can be adsorptively stabilized by metal-(hydr)oxide nanoparticles in arable and forest soils (Chapter 6)
- (v) To quantify the effects of competition between organic matter and phosphate for adsorption to metal-(hydr)oxide nanoparticles on the soluble phosphate concentrations in soils (Chapter 6).
- (vi) To understand mechanistically if and how Fe-(hydr)oxide nanoparticles affect the soil physical properties for a range of soils (Chapter 7).

To reach these objectives, I made use of novel analytical techniques, mechanistic surface complexation models, and various soil and water samples collected from different field sites (Figure 1.5). First, I explore the use of AF4 coupled to HR-ICP-MS as a new approach to analyse the size of Fe-(hydr)oxide nanoparticles extracted from soils (Chapter 2). I show that the single Fe-(hydr)oxide nanoparticles (<10 nm) are strongly bound to the soil and can only be released after extraction of the organic matter associated with these particles. The speciation of these soil nanoparticles is the subject of Chapter 3, in which I show that Fe-(hydr)oxides associated with clay particles can be mobile within the soil, in contrast to the free Fe-(hydr)oxide nanoparticles. Subsequently, in Chapter 4 and 5, I show that mineral colloids can act as carriers for trace metals and P and as such facilitate the transport of

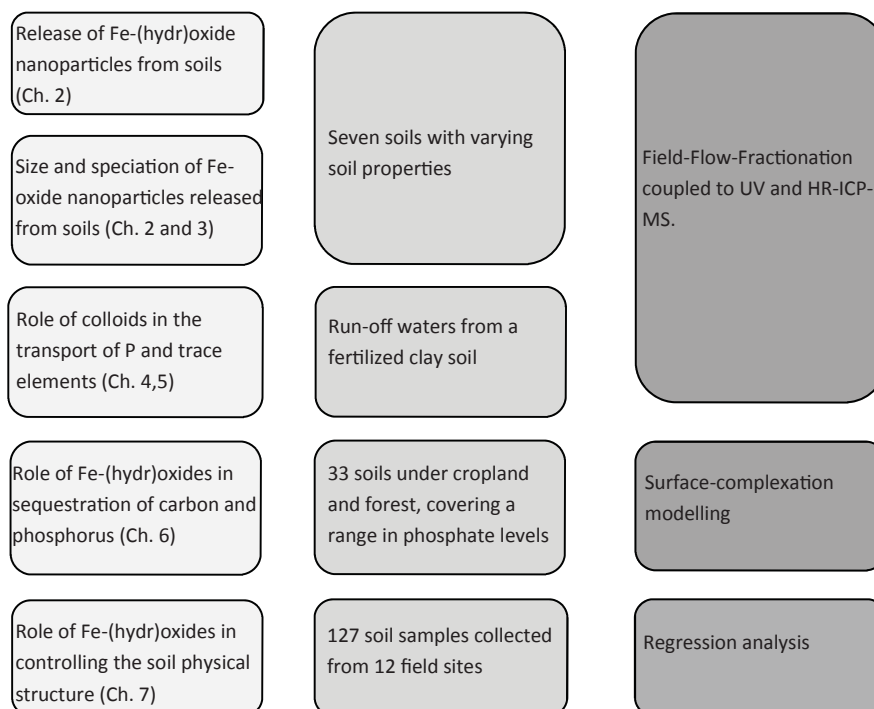


Figure 1.5. Schematic overview of the topics discussed in this thesis and the chosen experimental and modelling techniques.

phosphorus from fertilized soils to adjacent surface waters. In Chapter 6, I used a surface-complexation model to predict the surface speciation of Fe-(hydr)oxides in arable and forest soils. I show that organic matter is the dominant surface species on Fe-(hydr)oxides in forest soils whereas phosphate is the dominant surface species on Fe-oxides in arable soils, and I quantify the competition between these adsorbates. In Chapter 7, I make use of a large data-set on soil physical-chemical data to identify key-factors controlling the formation of soil aggregates. I show that Fe-(hydr)oxides play an important role in determining the soil physical properties, a mechanism that was underrated so far. In my final chapter 8, I discuss the main findings of my research.

References

- Antelo, J., Arce, F., Avena, M., Fiol, S., López, R., Macías, F., 2007. Adsorption of a soil humic acid at the surface of goethite and its competitive interaction with phosphate. *Geoderma* 138(1–2), 12-19.
- Baalousha, M., 2009. Aggregation and disaggregation of iron oxide nanoparticles; Influence of particle concentration, pH and natural organic matter. *Sci. Total. Environ.* 407(6), 2093-2101.
- Baalousha, M., Kammer, F., Motelicaheino, M., Hilal, H., Lecoustumer, P., 2006. Size fractionation and

- characterization of natural colloids by flow-field flow fractionation coupled to multi-angle laser light scattering. *J. Chromat. A* 1104(1-2), 272-281.
- Barthès, B.G., Kouakoua, E., Larré-Larrouy, M.-C., Razafimbelo, T.M., de Luca, E.F., Azontonde, A., Neves, C.S.V.J., de Freitas, P.L., Feller, C.L., 2008. Texture and sesquioxide effects on water-stable aggregates and organic matter in some tropical soils. *Geoderma* 143(1-2), 14-25.
- Benedetti, M.F., Ranville, J.F., Allard, T., Bednar, A.J., Menguy, N., 2003. The iron status in colloidal matter from the Rio Negro, Brasil. *Colloid. Surfaces A*. 217(1-3), 1-9.
- Bolea, E., Gorriz, M.P., Bouby, M., Laborda, F., Castillo, J.R., Geckeis, H., 2006. Multielement characterization of metal-humic substances complexation by size exclusion chromatography, asymmetrical flow field-flow fractionation, ultrafiltration and inductively coupled plasma-mass spectrometry detection: a comparative approach. *J. Chromat. A* 1129(2), 236-246.
- Borggaard, O.K., Jorgensen, S.S., Moberg, J.P., Raben-Lange, B., 1990. Influence of organic matter on phosphate adsorption by aluminium and iron oxides in sandy soils. *J. Soil Sci.* 41, 443-449.
- Braunschweig, J., Bosch, J., Meckenstock, R.U., 2013. Iron oxide nanoparticles in geomicrobiology: from biogeochemistry to bioremediation. *New Biotechnol.* 30(6), 793-802.
- Bronick, C.J., Lal, R., 2005. Soil structure and management: a review. *Geoderma* 124(1-2), 3-22.
- Burleson, D.J., Penn, R.L., 2005. Two-step growth of goethite from ferrihydrite. *Langmuir*. 22(1), 402-409.
- Calabi-Floody, M., Bendall, J.S., Jara, A.A., Welland, M.E., Theng, B.K.G., Rumpel, C., Mora, M.d.l.L., 2011. Nanoclays from an Andisol: Extraction, properties and carbon stabilization. *Geoderma* 161(3-4), 159-167.
- Chorover, J., Kretzschmar, R., Garcia-Pichel, F., Sparks, D.L., 2007. Soil biogeochemical processes within the critical zone. *Elements* 3(5), 321-326.
- Christian, P., Von der Kammer, F., Baalousha, M., Hofmann, T., 2008. Nanoparticles: structure, properties, preparation and behaviour in environmental media. *Ecotoxicology* 17(5), 326-343.
- Correll, D.L., 1998. The role of phosphorus in the eutrophication of receiving waters: A review. *J. Environ. Qual.* 27(2), 261-266.
- Curtin, D., Steppuhn, H., Selles, F., 1994. Effect of magnesium on cation selectivity and structural stability of sodic soils. *Soil Sci. Soc. Am. J.* 57(5), 1277-1283.
- Dolfing, J., Chardon, W., Japenga, J., 1999. Association between colloidal iron, aluminum, phosphorus, and humic acids. *Soil Sci.* 164(3), 171-179.
- Duffner, A., Hoffland, E., Temminghoff, E.J.M., 2012. Bioavailability of zinc and phosphorus in calcareous soils as affected by citrate exudation. *Plant Soil* 361, 165-175.
- Dümig, A., Häusler, W., Steffens, M., Kögel-Knabner, I., 2012. Clay fractions from a soil chronosequence after glacier retreat reveal the initial evolution of organo-mineral associations. *Geochim. Cosmochim. Ac.* 85(0), 1-18.
- Duiker, S.W., Rhoton, F.E., Torrent, J., Smeck, N.E., Lal, R., 2003. Iron (hydr)oxide crystallinity effects on soil aggregation. *Soil Sci. Soc. Am. J.* 67(2), 606-611.
- Dzombak, D.A., Morel, F.M.M., 1990. Surface complexation modeling: Hydrous ferric oxide. Wiley-Interscience.
- Eusterhues, K., Neidhardt, J., Hadrlich, A., Kusel, K., Totsche, K.U., 2014. Biodegradation of ferrihydrite-associated organic matter. *Biogeochem.* 1, 6-18.
- Eusterhues, K., Rumpel, C., Kögel-Knabner, I., 2005. Organo-mineral associations in sandy acid forest soils: Importance of specific surface area, iron oxides and micropores. *Eur. J. Soil Sci.* 56, 753-763.
- Eusterhues, K., Wagner, F.E., Häusler, W., Hanzlik, M., Knicker, H., Totsche, K.U., Kögel-Knabner, I., Schwertmann, U., 2008. Characterization of Ferrihydrite-Soil Organic Matter Coprecipitates by

- X-ray Diffraction and Mössbauer Spectroscopy. *Environ. Sci. Technol.* 42(21), 7891-7897.
- Fernández-Ugalde, O., Barré, P., Hubert, F., Virto, I., Girardin, C., Ferrage, E., Caner, L., Chenu, C., 2013. Clay mineralogy differs qualitatively in aggregate-size classes: clay-mineral-based evidence for aggregate hierarchy in temperate soils. *Eur. J. Soil Sci.* 64(4), 410-422.
- Hiemstra, T., 2013. Surface and mineral structure of ferrihydrite. *Geochim. Cosmochim. Ac.* 105, 316-325.
- Hiemstra, T., Antelo, J., Rahnemaie, R., Riemsdijk, W.H.v., 2010a. Nanoparticles in natural systems I: The effective reactive surface area of the natural oxide fraction in field samples. *Geochim. Cosmochim. Ac.* 74(1), 41-58.
- Hiemstra, T., Antelo, J., van Rotterdam, A.M.D., van Riemsdijk, W.H., 2010b. Nanoparticles in natural systems II: The natural oxide fraction at interaction with natural organic matter and phosphate. *Geochim. Cosmochim. Ac.* 74(1), 59-69.
- Hiemstra, T., Mia, S., Duhaut, P.-B., Molleman, B., 2013. Natural and Pyrogenic Humic Acids at Goethite and Natural Oxide Surfaces Interacting with Phosphate. *Environ. Sci. Technol.* 47(16), 9182-9189.
- Hochella, M.F., Lower, S.K., Maurice, P.A., Penn, R.L., Sahai, N., Sparks, D.L., Twining, B.S., 2008. Nanominerals, mineral nanoparticles, and Earth systems. *Science* 319(5870), 1631-1635.
- Hofacker, A.F., Voegelin, A., Kaegi, R., Weber, F.A., Kretzschmar, R., 2013. Temperature-dependent formation of metallic copper and metal sulfide nanoparticles during flooding of a contaminated soil. *Geochim. Cosmochim. Ac.* 103, 316-332.
- Igwe, C.A., Zarei, M., Stahr, K., 2009. Colloidal stability in some tropical soils of southeastern Nigeria as affected by iron and aluminium oxides. *Catena* 77(3), 232-237.
- Ju-Nam, Y., Lead, J.R., 2008. Manufactured nanoparticles: An overview of their chemistry, interactions and potential environmental implications. *Sci. Total. Environ.* 400(1-3), 396-414.
- Kleja, D.B., van Schaik, J.W.J., Persson, I., Gustafsson, J.P., 2012. Characterization of iron in floating surface films of some natural waters using EXAFS. *Chem. Geol.* 326-327, 19-26.
- Koopmans, G.F., Chardon, W.J., McDowell, R.W., 2007. Phosphorus Movement and Speciation in a Sandy Soil Profile after Long-Term Animal Manure Applications. *J. Environ. Qual.* 36(1), 305-315.
- Kretzschmar, R., Borkovec, M., Grolimund, D., Elimelech, M., 1999. Mobile subsurface colloids and their role in contaminant transport. *Adv. Agron.* 66, 121-193.
- Lyvén, B., Hassellöv, M., Turner, D.R., Haraldsson, C., Andersson, K., 2003. Competition between iron- and carbon-based colloidal carriers for trace metals in a freshwater assessed using flow field-flow fractionation coupled to ICPMS. *Geochim. Cosmochim. Ac.* 67(20), 3791-3802.
- Majzik, A., Tombácz, E., 2007. Interaction between humic acid and montmorillonite in the presence of calcium ions I. Interfacial and aqueous phase equilibria: Adsorption and complexation. *Org. Geochem.* 38(8), 1319-1329.
- Mikutta, R., Kaiser, K., 2011. Organic matter bound to mineral surfaces: Resistance to chemical and biological oxidation. *Soil Biol. Biochem.* 43(8), 1738-1741.
- Mikutta, R., Kleber, M., Torn, M., Jahn, R., 2006. Stabilization of soil organic matter: Association with minerals or chemical recalcitrance? *Biogeochemistry* 77(1), 25-56.
- Navrotsky, A., Mazeina, L., Majzlan, J., 2008. Size-driven structural and thermodynamic complexity in iron oxides. *Science* 318, 1635.
- Neubauer, E., von der Kammer, F., Hofmann, T., 2013a. Using FLOWFFF and HPSEC to determine trace metal-colloid associations in wetland runoff. *Water Res.* 47(8), 2757-2769.
- Neubauer, E., von der Kammer, F., Knorr, K.H., Peiffer, S., Reichert, M., Hofmann, T., 2013b. Colloid-

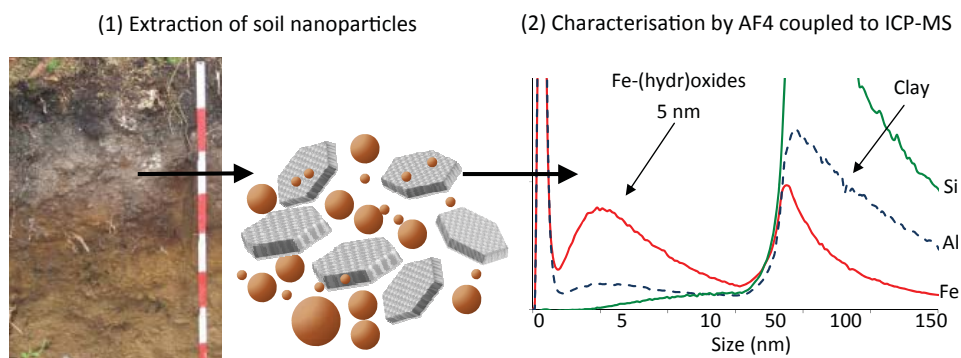
- associated export of arsenic in stream water during stormflow events. *Chem. Geol.* 352(0), 81-91.
- Oades, J.M., 1993. The role of biology in the formation, stabilization and degradation of soil structure. *Geoderma* 56, 377-400.
- Plathe, K.L., von der Kammer, F., Hassellöv, M., Moore, J.N., Murayama, M., Hofmann, T., Hochella Jr, M.F., 2013. The role of nanominerals and mineral nanoparticles in the transport of toxic trace metals: Field-flow fractionation and analytical TEM analyses after nanoparticle isolation and density separation. *Geochim. Cosmochim. Ac.* 102(0), 213-225.
- Pronk, G.J., Heister, K., Kögel-Knabner, I., 2011. Iron oxides as major available interface component in loamy arable topsoils. *Soil Sci. Soc. Am. J.* 75(6), 2158-2168.
- Pulleman, M., Marinissen, J., 2004. Physical protection of mineralizable C in aggregates from long-term pasture and arable soil. *Geoderma* 120(3), 273-282.
- Qafoku, N.P., 2010. Terrestrial nanoparticles and their controls on soil-/geo-processes and reactions. 107, 33-91.
- Rahnemaie, R., Hiemstra, T., van Riemsdijk, W.H., 2007. Geometry, charge distribution, and surface speciation of phosphate on goethite. *Langmuir* 23(7), 3680-3689.
- Reijneveld, J., Ehlert, P., Termorshuizen, A., Oenema, O., 2010. Changes in the soil phosphorus status of agricultural land in the Netherlands during the 20th century. *Soil use manag.* 26(4), 399-411.
- Salm, C.v.d., Toorn, A.v.d., Chardon, W.J., Koopmans, G.F., 2012. Water and nutrient transport on a heavy clay soil in a fluvial plain in The Netherlands. *J. Environ. Qual.* 41(1), 229-241.
- Schwertmann, U., Murad, E., 1983. Effect of pH on the formation of goethite and hematite from ferrihydrite. *Clay. Clay Min.* 31, 277-284.
- Six, J., Bossuyt, H., Degryze, S., Denef, K., 2004. A history of research on the link between (micro) aggregates, soil biota, and soil organic matter dynamics. *Soil Tillage Res.* 79(7-31).
- Stolpe, B., Guo, L., Shiller, A.M., Hassellöv, M., 2010. Size and composition of colloidal organic matter and trace elements in the Mississippi River, Pearl River and the northern Gulf of Mexico, as characterized by flow field-flow fractionation. *Mar. Chem.* 118(3-4), 119-128.
- Tombacz, E., Szekeres, M., 2004. Colloidal behavior of aqueous montmorillonite suspensions: the specific role of pH in the presence of indifferent electrolytes. *Applied Clay Sci.* 27, 75-94.
- van der Zee, S.E.A.T.M., van Riemsdijk, W.H., 1988. Model for long-term phosphate reaction kinetics in soil. *J. Environ. Qual.* 17(1), 35-41.
- Voegelin, A., Kaegi, R., Frommer, J., Vantelon, D., Hug, S.J., 2010. Effect of phosphate, silicate, and Ca on Fe(III)-precipitates formed in aerated Fe(II)- and As(III)-containing water studied by X-ray absorption spectroscopy. *Geochim. Cosmochim. Ac.* 74(1), 164-186.
- Voegelin, A., Senn, A.-C., Kaegi, R., Hug, S.J., Mangold, S., 2013. Dynamic Fe-precipitate formation induced by Fe(II) oxidation in aerated phosphate-containing water. *Geochim. Cosmochim. Ac.* 117(0), 216-231.
- von der Kammer, F., Legros, S., Hofmann, T., Larsen, E.H., Loeschner, K., 2011. Separation and characterization of nanoparticles in complex food and environmental samples by field-flow fractionation. *Trends Anal. Chem.* 30(3), 425-436.
- Weng, L., Riemsdijk, W.H.v., Hiemstra, T., 2008. Humic Nanoparticles at the Oxide-Water Interface: Interactions with Phosphate Ion Adsorption. *Environ. Sci. Tech.* 42, 8747-8752.
- Wigginton, N.S., Haus, K.L., Hochella Jr, M.F., 2007. Aquatic environmental nanoparticles. *J. Environ. Monitor.* 9(12), 1306.

Chapter 2

Asymmetric flow field-flow fractionation as a new approach to analyse iron-(hydr)oxide nanoparticles in soil extracts

Inge C. Regelink, Liping Weng, Gerwin F. Koopmans and Willem H. van Riemsdijk

Published as 'Asymmetric flow field-flow fractionation as a new approach to analyse iron-(hydr)oxide nanoparticles in soil extracts' in Geoderma, 2013, 202: 34-144



Abstract

Iron-(hydr)oxide nanoparticles are important for the sequestration of organic carbon because of their small size and consequently large specific surface area. Therefore, there is an increasing interest in analytical techniques such as asymmetric flow field-flow fractionation (AF4) that allow for a direct measurement of the size distribution of nanoparticles (1–150 nm). We used AF4 coupled to high-resolution inductively coupled plasma mass spectrometer (HR-ICP-MS) to analyse the size distribution and elemental composition of nanoparticles dispersed from three horizons of a podzol. We tested three extractants for the amount of dispersed Fe-(hydr)oxide nanoparticles. No Fe-(hydr)oxide nanoparticles were dispersed in 5 mM NaCl. In a 1 mM NaOH extraction (pH 9.0), the amount of Fe dispersed in the form of Fe-(hydr)oxide nanoparticles amounted to 0.2–0.8 g kg⁻¹, which corresponded to 2–13% of the Fe content as extracted with ammonium oxalate (Fe_{ox}). Pyrophosphate was found to be most effective extractant for Fe-(hydr)oxide nanoparticles and extracted 1.0–4.7 g kg⁻¹ Fe as Fe-(hydr)oxide nanoparticles, corresponding to 16–47% of the Fe-ox content. These Fe-(hydr)oxide nanoparticles were 2–20 nm in size and maximum concentrations were found at a particle diameter of 5 nm. The dispersion of Fe-(hydr)oxide nanoparticles in pyrophosphate coincided with the extraction of a large fraction of the soil organic carbon content (55–69%) which shows that dispersion of organo-mineral aggregates results in the release of Fe-(hydr)oxide nanoparticles from soil. The amount of Fe-(hydr)oxide nanoparticles extracted from soil did not increase after ultrasonic treatment of the pyrophosphate suspension. Since not all Fe-(hydr)oxides can be dispersed from the soil as primary particles, AF4 cannot be used as a tool to analyse the specific surface area of the Fe-(hydr)oxides in soil. Instead, AF4 should be considered as a complementary technique providing a direct measurement for the size of the Fe-(hydr)oxide nanoparticles in soil extracts.

2.1. Introduction

Iron-(hydr)oxides are important soil constituents for the retention of soil organic matter (SOM) because of their large specific surface area (SSA) and their high density of surface groups (Hiemstra, 2013; Weng et al., 2008). Retention of SOM can occur via different mechanisms including sorption, co-precipitation and occlusion (Mikutta et al., 2006). The amount of SOM that can be sorptively protected by Fe-(hydr)oxides depends on the SSA of the Fe-(hydr)oxides in the soil (Eusterhues et al., 2005; Hiemstra et al., 2010). Eusterhues et al. (2005) determined the SSA of soils by N₂ gas adsorption and they derived a SSA of

short-ranged ordered Fe-(hydr)oxides of $\approx 800 \text{ m}^2 \text{ g}^{-1}$. Hiemstra et al. (2010) developed a new approach to estimate the SSA of Fe-(hydr)oxides based on the phosphate-buffering capacity of soils. They found that the SSA ranged between 200 to $1200 \text{ m}^2 \text{ g}^{-1}$ for Fe-(hydr)oxides in large series of agricultural soils. Assuming a spherical particle geometry, the SSA of short-ranged ordered Fe-(hydr)oxides corresponds to equivalent particle diameters of 1 to 10 nm only (Hiemstra et al., 2010). This size is in agreement with other studies in which Fe-(hydr)oxide nanoparticles were detected using Mössbauer spectroscopy or transmission electron microscopy (TEM) (Penn et al. 2001; Van der Zee et al. 2005). However, spectroscopic techniques and surface area analyses give only an indirect measurement for the particle size of the Fe-(hydr)oxides. A direct measurement of the particle size-distribution in the small nano-range (<10 nm) is important because the SSA of the nanoparticles increases dramatically with a decrease in particle size for particles in this size-range. This calls for the application of an analytical approach that allows for fractionation and elemental analyses of nano-sized particles.

Asymmetric flow field-flow fractionation (AF4) is an analytical technique for size-fractionation of nanoparticles. The fractionation takes place in a thin water film and is driven by differences in diffusion coefficients, which can be related to the particle hydrodynamic diameter (Von der Kammer et al. 2011). Coupling of AF4 with high-resolution inductively coupled plasma mass spectrometer (HR-ICP-MS) allows for size-fractionation and online analyses of the elemental composition of nanoparticles. The combination of AF4 with HR-ICP-MS has been applied successfully to study colloidal nanoparticles in environmental water samples (Lyvén et al., 2003; Regelink et al., 2013; Stolpe et al., 2013). However, so far only a few attempts have been done to use AF4 for analysis of soil nanoparticles (Baalousha et al., 2006; Plathe et al., 2010). A crucial step in AF4 analyses of soils is the dispersion of the primary nanoparticles into suspension as colloidally stable particles, which means that the nanoparticles are either electrostatically or sterically stabilized. However, knowledge on suitable extraction methods to disperse Fe-(hydr)oxide nanoparticles from soil is limited, which, in turn, hampers the application of AF4 in soil analyses to characterize these nanoparticles.

A mild extractant, for example water or a dilute salt solution, can be used to mimic the soil pore-water (Koopmans and Groenenberg, 2011) and to disperse the potentially mobile soil nanoparticles (Kretzschmar and Sticher, 1997). However, Fe-(hydr)oxides in soils tend to associate with SOM (Baalousha, 2009) and these organo-mineral interactions need to be overcome to disperse the Fe-(hydr)oxide particles. Therefore, more Fe-(hydr)oxides may be

dispersed when stronger extractants are used that can reduce the interactions between Fe-(hydr)oxides and SOM. For example, large amounts of SOM can be extracted in NaOH or pyrophosphate (Tatzber et al., 2007; Van Zomeren and Comans, 2007). The latter extractant is also commonly used to disperse soils for particle size fractionation (Pronk et al., 2011) and to extract Fe associated with SOM (Dümig et al., 2012; Jeanroy and Guillet, 1981). Following these classical extraction procedures however, Fe-(hydr)oxides may dissolve in the strong alkaline extractants, which is in conflict with our aim to extract the nanoparticles as intact particles for AF4-fractionation. Therefore, these extractants should be tested at a lower pH. In addition, ultrasonic energy can be used to disperse particles from soil (An et al., 2010; Kaiser et al., 2012; Pronk et al., 2011). Ultrasonic treatment may however not release primary particles but small aggregates of particles (Calabi-Floody et al., 2011) which conflicts with our aim to measure the particle size of the primary Fe-(hydr)oxide nanoparticles. So far, our understanding of how extractant and ultrasonic treatment affects dispersion of Fe-(hydr)oxide nanoparticles is limited and no attempts have been done to analyse the released particles using AF4 coupled to HR-ICP-MS.

The objective of this study was to test three extractants for the dispersion of Fe-(hydr)oxide nanoparticles: (i) 5 mM NaCl, (ii) 1 mM NaOH and (iii) a 2 mM pyrophosphate solution. In addition to these three extractants, NaHCO₃ and pyrophosphate in combination with ultrasonic treatment were tested. The podzol was chosen because of the high Fe-(hydr)oxide content in the B horizon, where typically accumulation of Fe, Al, and OC occurs. We used AF4 coupled to an UV-analyser and HR-ICP-MS to analyse the size-distribution and elemental chemical composition of the dispersed nanoparticles. The results provide insight into (i) the size-distribution of Fe-(hydr)oxide nanoparticles and (ii) the role of organo-mineral interactions in dispersion of Fe-(hydr)oxide particles.

2.2. Material and Methods

2.2.1 Soils

The sampling area is located in the Lysina catchment, situated in the mountainous region of the Slavkov Forest Protected Landscape Area in the western part of the Czech Republic. The soil profile is characterized as a Folic Albic Podzol. Samples were taken from seven distinct soil horizons, i.e., AE, E, Bh₁, Bh₂, Bs, BC, and C. More information about the chemistry and hydrology of the Lysina catchment can be found in previous papers (Krám et al., 2009; Krám et al., 2012). The Lysina catchment has been studied by the Czech Geological Survey since

1988. The Lysina catchment is part of the Czech network of forest catchments (Global Earth Observation and Monitoring of the Atmosphere, with the acronym GEOMON) and in four international networks ([i] International Cooperative Programme [ICP] – Waters, [ii] ICP – Integrated Monitoring, [iii] International Long Term Ecological Research (ILTER), and [iv] Soil Transformations in European Catchments [SoilTrEC]).

2.2.2 Soil Characterization

Soil samples were dried at 40°C and sieved over 2 mm prior to analyses. The pH was measured in a soil-water suspension at a soil solution ratio (SSR) of 0.4 kg l⁻¹. The soil organic carbon (SOC) content was measured by dry combustion using an elemental analyser (Carlo Erba Nitrogen Analyzer). The cation exchange capacity (CEC) and exchangeable cations were determined using the unbuffered BaCl₂ method (Pansu and Gautheyrou, 2006) and cation concentrations were measured by inductively coupled plasma atomic emission spectrometer (ICP-AES; Varian Vista Pro). The clay content was determined by the pipette-method after dispersion of the soil samples in a 0.4 M pyrophosphate solution (Ashworth *et al.*, 2001). The amount of Fe and Al extractable in acid ammonium oxalate was determined according to the extraction method of Schwertmann (1973). Shortly, soil suspensions at a SSR of 0.05 kg l⁻¹ were prepared using 0.2 M ammonium oxalate solution at pH 3 and shaken for 2 h in the dark. The supernatants were analysed for Fe (Fe_{ox}) and Al (Al_{ox}) by ICP-AES. In addition to short-ranged ordered Fe- and Al-(hydr)oxides, acid ammonium oxalate can also dissolve some micro-goethite, allophane and imogolite and extracts monomeric Fe and Al (Pansu and Gautheyrou, 2006; Parfitt and Childs, 1988; Schwertmann, 1973). The total Fe-(hydr)oxide soil content, which include both short-ranged ordered Fe-(hydr)oxides and goethite, was measured using the dithionite-citrate-bicarbonate (Fe-DCB) method of Holmgren (1967). Shortly, 1 g of soil was extracted using 30 ml of 0.66 M citrate and 0.11 M sodium-bicarbonate solution and 1 g of dithionite. Soil suspensions were shaken for 16 h at room temperature, followed by centrifugation. After centrifugation, Fe concentrations in the supernatants were measured by ICP-AES.

2.2.3 Extraction of soil nanoparticles

Soil samples from three distinct horizons, the Bh₁, Bh₂ and Bs, were selected for the extraction of soil nanoparticles because of their high Fe_{ox} and Al_{ox} contents.

NaCl. Soil suspensions were prepared using a 5 mM NaCl solution at a SSR of 0.1 kg l⁻¹. The final pH values of the suspensions ranged between pH 4.0 and 4.5.

NaOH. Soil suspensions were prepared using a 1 mM NaOH solution at a SSR of 0.002 kg l⁻¹. The final pH values of the suspensions were between 9.4 and 9.7. A low SSR was chosen to increase the fraction of dispersed nanoparticles from the soil. The NaOH concentration was low compared to the concentration used in the classical method (Van Zomeren and Comans, 2007) because a higher concentration and thus a higher pH could result in dissolution of Fe- and Al-(hydr)oxides.

Pyrophosphate. Soil suspensions were prepared using a 2 mM pyrophosphate (Na₄P₂O₇) solution at a SSR of 0.002 kg l⁻¹. Prior to the addition to the soil, the pH of the pyrophosphate solution was lowered to pH 9.0 using concentrated HCl to prevent dissolution of Fe- and Al-(hydr)oxides (Kaiser and Zech, 1996). The final pH values of the suspensions after shaking were between 7.7 and 8.8. The classical pyrophosphate extraction method uses a concentration of 0.1 M pyrophosphate (Jeanroy and Guillet, 1981). We used a lower pyrophosphate concentration and a lower SSR, because a high ionic strength lowers dispersion of nanoparticles. In addition to this, P was an element of interest in our work and a higher pyrophosphate concentration would cause a higher background concentration of P, possibly leading to the formation of salt peaks in the AF4 fractograms and P contamination of the AF4 system. Despite this lower pyrophosphate concentration, the P background resulting from the use of 2 mM pyrophosphate was still too high to measure P associated to nanoparticles in the pyrophosphate extracts by AF4 coupled to HR-ICP-MS. The soil suspensions prepared with the NaCl, NaOH, and pyrophosphate solutions were shaken for 4 d at 60 rotations per minute (rpm) and centrifuged for 30 min at 3000 rpm (2000 g), which corresponds to a separation of particles smaller than 150 nm under the assumption of ideal behaviour of spherical particles.

The Bh₂ horizon was used to test the effect of ultrasonication on the dispersion of nanoparticles from soil.

NaHCO₃ + ultrasonication. The soil suspension was prepared at a SSR of 0.002 kg l⁻¹ using 5 mM NaHCO₃. The soil suspension was shaken for 24 hours at 60 rpm, treated ultrasonically (95 J cm⁻³) and centrifuged (30 min, 3000 rpm). The pH after shaking was 8.3. This extractant was chosen to test if Fe-(hydr)oxides can be mechanically dispersed from the soil without strongly altering the chemical environment of the nanoparticles. An extractant such as pyrophosphate will drastically change the chemical environment of the nanoparticles, but NaHCO₃ is expected to be chemically less invasive. The suspension was treated for 3 min with a Hielscher ultrasonicator (UP400s, 24 kHz) with a 22 mm probe-tip, operating at 80% of the maximum amplitude. The power output was determined

calorimetrically (North, 1976) and amounted to 106 W (Figure A1).

Pyrophosphate + ultrasonication. The soil suspension was prepared in 10 mM pyrophosphate (pH 8.5) at a SSR of 0.002 kg l⁻¹. The soil suspension was shaken, ultrasonically treated and centrifuged as described above.

Concentrations of Fe (HR-ICP-MS; Thermo Element 2) and dissolved organic carbon (DOC) (Sievers 900 TOC analyser) were analysed in supernatants. Supernatants were not filtered because filtration may lead to the removal of particles smaller than the theoretical cut-off size of the membrane. Because the supernatants were not filtered, the DOC may also include organic carbon that is usually referred to as particulate organic carbon. All supernatants were analysed by AF4 for the detection of nanoparticles.

2.2.4 AF4-ICPMS analyses

An AF4 system (Postnova Analytics, Germany) was used for size-fractionation of the nanoparticles in the different soil extracts. The principles of AF4 size-fractionation are described in detail elsewhere (Baalousha *et al.*, 2011; Von der Kammer *et al.*, 2011). A 3 mM NaHCO₃ solution at pH 8.3 was used as a carrier. The injected volume was 0.1 ml for the NaOH and pyrophosphate extracts and 0.5 ml for the NaCl and NaHCO₃ extracts. For comparison, we corrected for the difference in injected volume by multiplying the element concentrations of the runs using 0.1 ml by a factor 5. The injection/focussing time was 11 min using a cross flow of 3 ml min⁻¹. The cross flow rate was 3 ml min⁻¹ for the first 15 minutes (t₀-t₁₅), and thereafter, the cross flow decreased in 2 min to 0.2 ml min⁻¹ in a linear manner and was maintained at this rate from the 17th to the 30th minute (t₁₇-t₃₀). Using a stepwise change in cross flow rate allowed for fractionation of particles <14 nm in size with a high size-resolution and fractionation of particles 14–150 nm in size with a lower size-resolution. The detector flow was coupled to an UV-detector (Postnova Analytics) and to a HR-ICP-MS, which measured the Fe, Al, Si, Ca, Mg, and P concentrations every 10 s. Calibration of the HR-ICP-MS was done at the beginning and at the end of each measurement day to correct for sensitivity drifting. An overview of the AF4, UV-detector, and HR-ICP-MS analytical parameters is given in Table 2.1.

A combination of calibration, using standard particles, and AF4 theory was used to derive the relationship between particle size and retention time. Theory was used to calculate the particle diameter during t₀-t₁₅ of the elution step when the cross flow rate was constant. The theory behind AF4 fractionation, which is based on ideal behaviour of spherical particles, is well known for running conditions using a constant crossflow (Baalousha *et al.*, 2011; Von

Figure 2.1. Analytical parameters and characteristics of the AF4, UV-detector and HR-ICP-MS.

AF4	AF2000, Postnova Analytics
Membrane	1 kDa polyethersulfone (PES)
Spacer thickness	350 μm
Injection volume	0.1 or 0.5 ml
Focussing time	11 min
Cross flow during focusing	3 ml min ⁻¹
Cross flow rate t ₀ -t ₁₅	3 ml min ⁻¹
Cross flow rate t ₁₈ -t ₃₀	0.2 ml min ⁻¹
Detector flow rate	0.5 ml min ⁻¹
Slot pump flow rate	0.5 ml min ⁻¹
Carrier	3 mM NaHCO ₃
UV-Detector	Postnova Analytics
Monitored wavelength	254 nm
HR-ICP-MS	Thermo Element 2
Monitored elements	Fe, Al, Si, Ca ^a , Mg ^a , P ^a
Time per reading	12 sec

^a Results not shown

der Kammer *et al.*, 2011). The linear relation between the hydrodynamic particle diameter and the retention time can be calculated using equations (2.1) and (2.2):

$$d_h = \frac{2KT V_0 t_r}{\pi \eta Q_C w^2 t_0} \quad (2.1)$$

$$t_0 = \frac{V_0}{Q_C} \ln \left(1 + \frac{Q_C}{Q_{\text{out}}} \right) \quad (2.2)$$

where t_0 = void time (s); t_r = retention time (s); d_h = hydrodynamic diameter (m); T = absolute temperature (K); K = Boltzmann constant (1.38×10^{-23} J K⁻¹); η = viscosity (10^{-3} Pa.s); w = channel thickness (m); V_0 = void volume (m³); Q_C = cross flow rate (m³s⁻¹); Q_{out} = outlet flow rate (detector plus slot flow rate)(m³s⁻¹).

According to calculations using the above equations, particles smaller than 14 nm were eluted during t_0 - t_{15} of the elution step. In addition to this, polystyrene sulfonate standards (Postnova Analytics) with known molecular weights of 1.1, 15.8, and 75.6 kDa were used to check whether it was possible to separate particles during t_0 - t_{15} of the elution step. These

particle standards were used because polystyrene nanoparticles with a diameter smaller than 20 nm defined in terms of size were not available. The fractograms of these particle standards was well resolved, with a retention time of the particles amounting to 0.6, 2.9, and 11 min (Figure A2). Application of AF4 theory becomes more complicated when the cross flow rate is not constant, *i.e.* after 15 minutes of the elution step. Therefore, NIST-certified polystyrene nanoparticles (Postnova Analytics) with a diameter of 20, 50, and 100 nm were used for calibration for $t_{17}-t_{30}$ of the elution step. The fractogram of these standard nanoparticles was well resolved, with a retention time of the particles amounting to 17, 19, and 24 min respectively (Figure A2). Retention times from these fractograms were used to establish a linear relationship of the particle diameter versus the elution time ($R^2=0.99$). Subsequently, this relationship was used to calculate the diameter of particles eluted during $t_{17}-t_{30}$ of the elution step. Despite our effort to quantify the diameter of the nanoparticles in the different soil extracts, the actual size of the particles can deviate somewhat from the calculated hydrodynamic particle diameter due to non-ideal behaviour a non-spherical shape of the particles.

2.3. Results and discussion

2.3.1 General soil characteristics

The general soil characteristics (Table 2) are typical for soils where podsolization is the dominant soil forming process (Buurman and Jongmans, 2005). Namely, the pH was low (3.3–4.2) and Al was the dominant exchangeable cation (>60%). The AE and E horizons were depleted in Fe, Al, and SOC whereas accumulation of these elements and SOC occurred in the horizons below. The Bh₁, Bh₂, and Bs horizons were rich in Fe_{DCB} (8.5–16.8 g kg⁻¹), Fe_{ox} (6.3–12.8 g kg⁻¹), Al_{ox} (2.0–8.1 g kg⁻¹) and SOC (28.5–43.8 g kg⁻¹). The high ratio of Fe_{ox} to Fe_{DCB} (0.62–0.75) indicated a large contribution of short-ranged ordered Fe-(hydr)oxides relative to the total Fe-(hydr)oxide content. The SOC content correlated well with the Fe_{DCB} (Figure 1; $R^2=0.95$) and Fe_{ox} content ($R^2=0.96$). The correlation was less strong ($R^2=0.61$) when the Al-(hydr)oxide content, which was estimated as Al-ox minus Al-CEC, was included in the amount of metal-(hydr)oxides. Hence, SOM is strongly associated with Fe-(hydr)oxides. However, the SOC content in the AE horizon (0–5 cm) deviated from the relationship with Fe-(hydr)oxides and the high SOC content in this horizon can be explained by the presence of litter and fresh OC.

2.3.2 Fractograms of the soil extracts

The results of nanoparticles dispersed in the three extractants (NaCl, NaOH, and pyrophosphate) without ultrasonic treatment are discussed in this section whereas the results of the extracts with ultrasonic treatment are discussed later. The Fe concentration in the three extractants increased in the order of NaCl < NaOH < pyrophosphate and the DOC concentration (Table 2.2) followed the same order. The amount of DOC in the NaCl-extracts amounted to less than 3% of the SOC content. Between 16 and 31% of the SOC was extracted as DOC in NaOH, which can be explained by the higher pH (9.4–9.7) of the extractant. Pyrophosphate was the most effective extractant with respect to SOC and extracted between 55 and 69% of the SOC content, although pH (7.7–8.8) was low compared to the pH of the classical pyrophosphate extraction method (10.4) (Jeanroy and Guillet, 1981). The AF4 fractograms (Figure 2.2) show the Fe, Al and Si concentration and UV absorbance as a function of the elution time and the corresponding hydrodynamic particle diameter. In the text, the size of the dissolved organic matter (DOM) is expressed as a molecular weight (derived from calibration with particle standards) instead of the hydrodynamic diameter since this is more common for organic colloids.

NaCl. The nanoparticles dispersed in the NaCl-extracts are distributed between two different peaks (Figure 2.2). The first peak, eluting after 0.8 min (1.9 kDa), shows the presence of colloids with a high UV-absorbance and high Al and Fe concentrations. This peak can be attributed to the elution of DOM which typically absorbs UV-light at 254 nm. Elution of DOM in this size-fraction has been observed in previous AF4-studies on environmental water samples (Baalousha and Lead, 2007; Regelink *et al.*, 2013) as well. The recovered

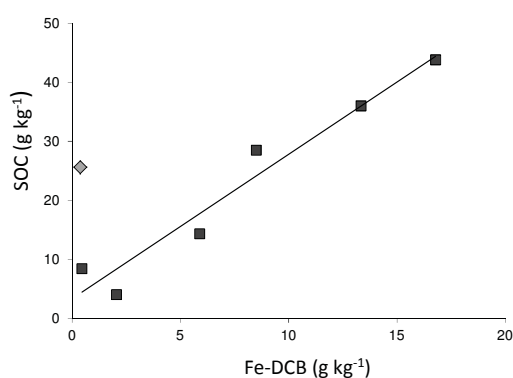


Figure 2.1. Correlation between Fe-DCB and SOC in the podzol profile ($R^2=0.95$). The diamond represents the top soil (AE-horizon) which deviates from the correlation.

Table 2.2. General soil characteristics and amounts of dissolved organic carbon (DOC) and Fe- and Al-(hydr)oxide nanoparticles (2 – 20 nm) extracted in 5 mM NaCl, 1 mM NaOH and 2 mM sodium-pyrophosphate (PP), n.d.: not detected, n.m.: not measured.

Hori- zon	pH	SOC ^a g kg ⁻¹	Clay %	Fe-DCB ^b g kg ⁻¹	Fe-ox ^c	Al-ox ^c	Al-oxides ^d g kg ⁻¹ (%)	DOC ^e			Fe-oxides < 20 nm ^f			Al-oxides < 20 nm ^f			
								NaCl	NaOH	PP	NaCl	NaOH	PP	NaCl	NaOH	PP	NaCl
AE	3.37	2.56	3.3	0.4	0.1	0.2	n.d.	n.m.	n.m.	n.m.	n.m.	n.m.	n.m.	n.m.	n.m.	n.m.	n.m.
E	3.75	0.84	3.5	0.5	0.1	0.3	n.d.	n.m.	n.m.	n.m.	n.m.	n.m.	n.m.	n.m.	n.m.	n.m.	n.m.
Bh ₁	3.29	28.5	17.4	8.5	6.3	2.0	n.d.	0.8 (2.8)	8.8 (31)	19.7 (69)	n.d.	0.8 (13)	1.0 (16)	n.d.	n.d.	n.d.	n.d.
Bh ₂	3.73	43.8	22.6	16.8	12.8	5.8	3.66	0.5 (1.1)	7.9 (18)	24.1 (55)	n.d.	0.6 (5)	4.7 (37)	n.d.	0.14 (4)	0.6 (16)	
Bs	4.08	36.0	20.0	13.3	8.2	8.1	6.09	0.4 (1.2)	5.8 (16)	20.5 (57)	n.d.	0.2 (2)	3.9 (47)	n.d.	0.15 (2)	1.1 (18)	
BC	3.92	1.43	16.4	5.9	2.2	6.3	5.21	n.m.	n.m.	n.m.	n.m.	n.m.	n.m.	n.m.	n.m.	n.m.	n.m.
C	4.17	0.4	8.5	2.0	0.5	3.2	2.36	n.m.	n.m.	n.m.	n.m.	n.m.	n.m.	n.m.	n.m.	n.m.	n.m.

^a Soil organic carbon (SOC) content

^b Fe extractable in dithionite-citrate-bicarbonate (Fe-DCB)

^c Fe and Al extractable in ammonium-oxalate (Fe-ox, Al-ox)

^d Al-(hydr)oxides, calculated as Al-ox minus exchangeable Al (Appendix D).

^e Dissolved organic carbon (DOC) in the supernatants of the NaCl, NaOH and pyrophosphate extractions. Values between brackets show DOC as percentage of SOC.

^f Iron- and Al-(hydr)oxide nanoparticles in the 2 to 20 nm size-fraction, as detected in the AF4-fractograms (Figure 2.2). Values between brackets show the amount of Fe- and Al-(hydr)oxide nanoparticles as a percentage of the Fe-ox or Al-(hydr)oxide content, respectively.

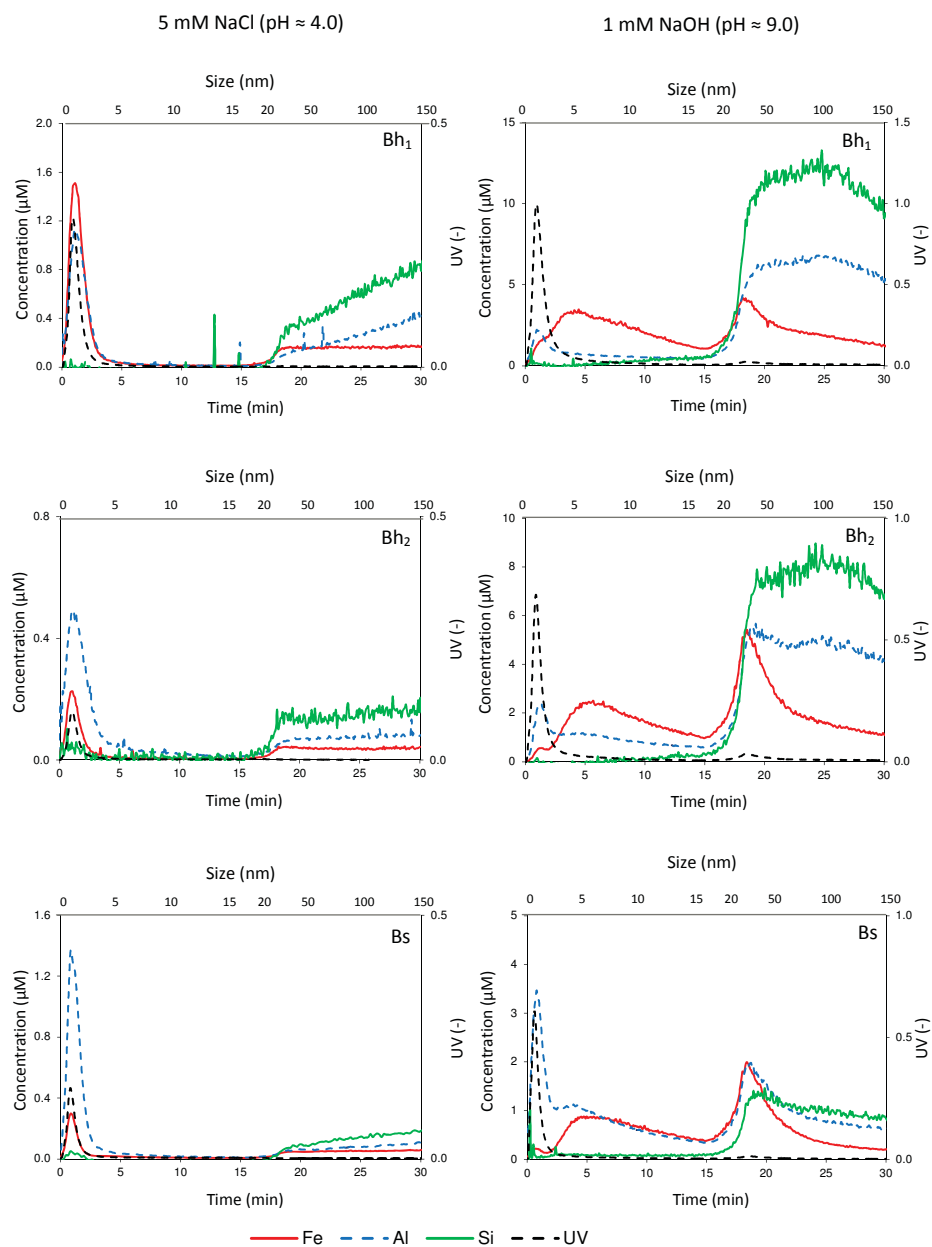


Figure 2.2. AF4-fractograms of nanoparticles dispersed in 5 mM NaCl, 1 mM NaOH and 2 mM pyrophosphate (no ultrasonication) for the three soil horizons (Bh₁, Bh₂ and Bs horizon). The fractograms show the Fe, Al and Si concentration and the UV absorbance at 254 nm as a function of elution time and the corresponding hydrodynamic particle diameter.

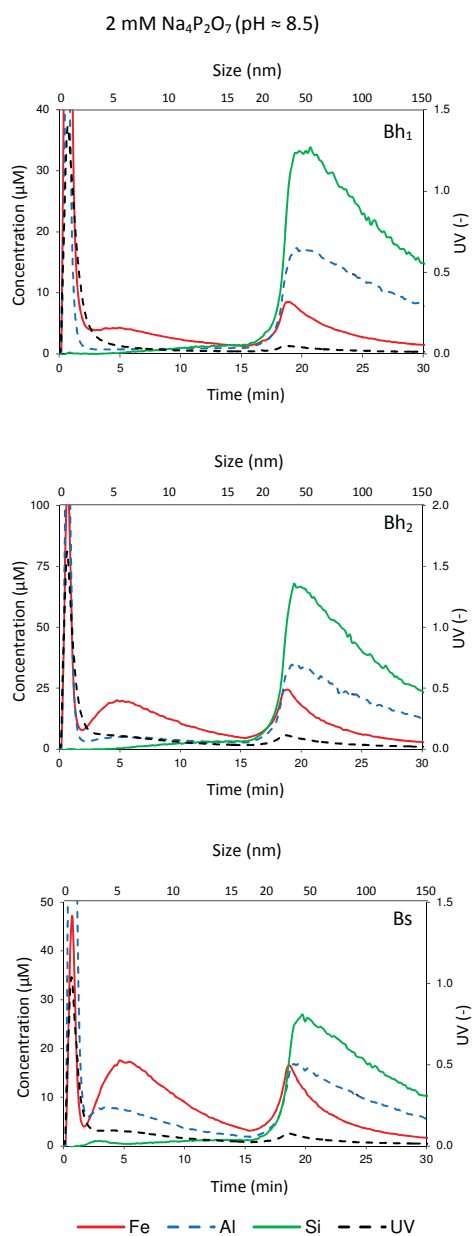


Figure 2.2. AF4-fractograms of nanoparticles dispersed in 5 mM NaCl, 1 mM NaOH and 2 mM pyrophosphate (no ultrasonication) for the three soil horizons (Bh_p, Bh₂ and Bs horizon). The fractograms show the Fe, Al and Si concentration and the UV absorbance at 254 nm as a function of elution time and the corresponding hydrodynamic particle diameter.

DOM molecules are larger than 1 kDa since molecules smaller than 1 kDa can pass the AF4 membrane and will thus be flushed out of the AF4 column. Iron and Al co-elute with DOM and these elements are probably adsorbed to the DOM. In a podzol, one can expect high amounts of Fe and Al associated with DOM due to the low soil pH (Jansen *et al.*, 2005). The nanoparticles eluting within the second peak (20–130 nm) contain Si, Al, and Fe. The average molar Si/Al ratio is about 2:1, which indicates the presence of 2:1 clay minerals or mica minerals. The elution pattern of Fe is very similar to the elution patterns of Si and Al. In this size range, Fe is probably mainly associated with the clay minerals which can be explained by Fe structurally incorporated within the clay minerals or by Fe adsorbed on the clay mineral surfaces. Generally, clay minerals such as illite and montmorillonite contain some Fe in their structure due to isomorphous substitution (Mermut and Cano, 2001). For the Bh₁ horizon, however, the molar Fe/Si ratio is elevated in the size range of 20–50 nm which may indicate that part of the Fe is present as Fe-(hydr)oxides, either as separate primary nanoparticles or associated with the clay minerals. The UV-absorbance of the 20–130 nm sized particles can be explained by UV-absorbance by the clay-particles although organic molecules associated with the clay particles may contribute to the UV-absorbance as well.

NaOH. The nanoparticles dispersed in the NaOH extracts are distributed among three different peaks (Figure 2.2). The first peak, which elutes after 0.8 min (1.9 kDa), shows the presence of DOM and associated Fe and Al. There is a second peak of Fe with maximum concentrations found at a size of 5 nm. For the Bh₂ and Bs horizons, the Al concentration shows a peak at 5 nm as well. The Fe- and Al-containing nanoparticles cannot be explained by associations of these metals with DOM since the UV absorbance is low. The metals are neither associated with clay particles because there was no co-elution of Si. Therefore, this peak likely indicates the presence of Fe- and Al-(hydr)oxide nanoparticles. For the Bh₁, Bh₂, and Bs horizons, the amount of Fe-(hydr)oxide nanoparticles in the 2–20 nm size range amount to 0.84, 0.61 and 0.19 g kg⁻¹, respectively which corresponds to 13, 5, and 2% of the Fe_{ox} content, respectively (Table 2.2). Data interpretation for Al is more complicated since there is overlap between Al associated to DOM (Al_{DOM}) and Al present as Al-(hydr)oxides. To distinguish between both Al forms, we estimated the distribution between Al_{DOM} and Al(hydr)oxides using equations 2.3 and 2.4;

$$Al_{DOM} = \alpha * UV \quad (2.3)$$

$$Al_{(hydr)oxides} = Al_{total} - Al_{DOM} \quad (2.4)$$

where Al_{total} , Al_{DOM} , and Al(hydr)oxides are expressed in M and UV in absorbance units and where the symbol α denotes the Al/UV ratio, derived from the peak maximum of the DOM peak. This set of equations is only valid in the size range below 20 nm where no clay particles elute. The amount of Al present as Al-(hydr)oxide nanoparticles (2–20 nm) amounted to 0.14 and 0.15 g kg⁻¹ in the Bh₂ and Bs horizon respectively, which corresponds to 4 and 2% of the Al-(hydr)oxide content, whereas no Al-(hydr)oxide nanoparticles were detected in the Bh₁ horizon.

The co-elution of Si and Al indicates the presence of clay particles in the size range of 20–130 nm. The elution pattern of Fe deviates from the elution pattern of Si. Therefore, Fe-(hydr)oxide nanoparticles are likely to be present in addition to Fe substituted within clay minerals. However, the amount of Fe-(hydr)oxide nanoparticles cannot be directly derived from the AF4 fractograms due to the overlap between Fe-(hydr)oxide and clay particles and equations 2.5 and 2.6 were used to estimate the distribution of Fe among Fe(hydr)oxides and Fe_{clay}.

$$Fe_{clay} = 0.09 * Si \quad (2.5)$$

$$Fe_{(hydr)oxide} = Fe_{total} - Fe_{clay} \quad (2.6)$$

In these equations, Si, Fe_{total}, Fe_{clay} and Fe(hydr)oxide are expressed in M and the factor 0.09 denotes the molar Fe/Si ratio of clay particles which is derived from the fractograms. The molar Fe/Si ratio shows a decrease with increasing particle size and levels off at about 0.09 for particles larger than 100 nm. This value is within the range of Fe substitution ratios (Fe_{clay}) of common 2:1 clay minerals (0.01–0.1) (Mermut and Cano, 2001). Appendix A (Figure A3) shows an example of the predicted distribution of Fe between Fe_{clay} and Fe(hydr)oxide for the Bh₂ horizon. The calculated amounts of Fe-(hydr)oxides in the size range of 20–150 nm amount to ≈ 0.5, 0.7 and 0.2 g kg⁻¹ (2, 6 and 9% of Fe-ox) in the Bh₁, Bh₂, and Bs horizons, respectively. Iron-(hydr)oxide nanoparticles in this size-range may be present as primary particles (*i.e.*, not associated to any other mineral particles) or as small particles attached to the surface of the clay minerals (Wagner *et al.*, 1988).

Pyrophosphate. The nanoparticles dispersed in the pyrophosphate extracts are distributed among three different peaks (Figure 2.2). The first peak elutes after 0.5 min, which is equal to the void time (*i.e.*, the elution-time of an unretarded particle). Iron, Al and P (results not shown) elute simultaneously and the peak shows all characteristics of a void peak. This void peak may be related to the use of pyrophosphate as an extractant. Preliminary testing with

a $\text{Na}_4\text{P}_2\text{O}_7$ solution did not lead to the elution of a void peak. However, a void peak did elute when the trivalent cation Al^{3+} was added to the $\text{Na}_4\text{P}_2\text{O}_7$ solution (Table A1). Pyrophosphate forms polymeric complexes in the presence of cations (Ikotun et al., 2010) and such metal-pyrophosphate complexes may be unable to pass the AF4 membrane which can explain their presence in the void peak. The metal-pyrophosphate complexes in the void peak may originate from monomeric Fe and Al that were adsorbed to SOM.

The second peak of nanoparticles with maximum concentrations found at 5 nm indicates the presence of Fe- and Al-(hydr)oxide nanoparticles. For the Bh_1 , Bh_2 and Bs horizons, the amounts of dispersed Fe-(hydr)oxide nanoparticles between 2 and 20 nm are 1.0, 4.7, and 4.8 g kg^{-1} , which corresponds to 16, 37, and 47% of Fe-ox, respectively (Table 2.2). The Al-(hydr)oxide nanoparticles amount to 0.6 and 1.1 g kg^{-1} in the 2–20 nm size-fraction of the Bh_2 and Bs horizon but they were not detected in the Bh_1 horizon (Table 2.2). The amount of Fe-(hydr)oxide nanoparticles (2–20 nm) in pyrophosphate increased with a factor of 1.2 to 23 compared to the NaOH extractions whereas the dispersion of Al-(hydr)oxide nanoparticles increased with a factor of 5 to 6. The particle sizes of the Fe-(hydr)oxides detected in NaOH and pyrophosphate are of similar size as freshly prepared synthetic ferrihydrite particles (2–6 nm) (Burlinson and Penn, 2005). The extremely small size of the Fe-(hydr)oxide particles may also indicate the presence of ferrihydrite–DOM co-precipitates (Schwertmann *et al.*, 2005). Such co-precipitates form when ferrihydrite precipitates from solutions containing both Fe and organic acids and these co-precipitates are smaller and less crystalline compared to their counterparts precipitated in the absence of DOM (Eusterhues *et al.*, 2008).

The third peak of nanoparticles, in the size range of 20–150 nm, is dominated by clay nanoparticles. Clearly, more clay particles are dispersed with pyrophosphate than with NaOH because Si and Al concentrations are 4 to 10 times higher compared to those measured in the NaOH extracts. Iron is present as well in this peak, and it shows a similar elution pattern as Si and Al. Part of the Fe in this size range may be explained by Fe substitutions in clay minerals and some Fe may be present in the form of Fe-(hydr)oxide particles. However, it is not possible to estimate the distribution between these two Fe species because of the strong similarity of the Fe, Si and Al peak.

The pH values of the 1 mM NaOH (9.4–9.7) and 2 mM pyrophosphate (7.7–8.8) extracts are relatively high compared to the initial pH-values of the soil (3.3–4.1). A possible artefact of increasing the pH of acid soils is that monomeric Fe and Al may desorb from the organic matter and may precipitate, leading to the formation of new particles. This artefact will not

occur in pyrophosphate because pyrophosphate acts as a ligand for dissolved Fe^{3+} and Al^{3+} . For the NaOH extracts, we cannot exclude the possibility of precipitation of new metal-(hydr)oxides. However, considering the strong similarities in particle size-distribution of the Fe and Al-(hydr)oxide nanoparticles in the NaOH and pyrophosphate extracts, we expect that artefacts leading to formation of new particles did not occur.

2.3.3 Factors controlling the dispersion of nanoparticles

The amount of dispersible Fe and Al-(hydr)oxide nanoparticles present in the 2–20 nm size range increases in the order of $\text{NaCl} < \text{NaOH} < \text{pyrophosphate}$ (Table 2). The differences in extraction efficiency between these three extractants can be related to the differences in their capacities to disperse nanoparticles. Electrostatic repulsion is the major factor controlling dispersion of nanoparticles from the soil solid phase to solution (Baalousha, 2009; Kretzschmar and Sticher, 1997). In the NaCl extracts, no dispersion of primary Fe-(hydr)oxide nanoparticles is observed. Apparently, the zeta-potential of the Fe-(hydr)oxide nanoparticles is not sufficiently negative to cause dispersion under these conditions. The dispersion of Fe and Al-(hydr)oxide nanoparticles in NaOH coincided with the extraction of a large fraction of the SOC (16–31%) (Table 2.2). Compared to NaOH, pyrophosphate extracted even more Fe and Al-(hydr)oxide nanoparticles and more SOC (55–69%) (Table 2.2). Therefore, the dispersion of Fe-(hydr)oxide nanoparticles seems to be related to the disaggregation of organo-mineral aggregates. This is in agreement with work of Calabi-Floody *et al.* (2011) who showed that the removal of SOM enhances the dispersion of nanoparticles from soils. The dispersing capacity of pyrophosphate can be explained by two factors (Pansu and Gautheyrou, 2006). Firstly, pyrophosphate, being a tetravalent anion, is a very effective competitor for SOM adsorbed to metal-(hydr)oxide surfaces. The replacement of SOM by pyrophosphate leads to a more negative zeta-potential of the metal-(hydr)oxides particles, which induces dispersion of these nanoparticles. Secondly, pyrophosphate acts as a ligand for di- and trivalent cations such as Ca^{2+} , Al^{3+} , and Fe^{3+} . The complexation of these metals by pyrophosphate during soil extraction will lead to less coagulation of SOM and mineral particles and increased dispersion of metal-(hydr)oxide particles.

2.3.4 Ultrasonic dispersion of Fe-(hydr)oxide nanoparticles

The results of the nanoparticles dispersed in NaHCO_3 and pyrophosphate in combination with ultrasonic treatment are discussed in this section.

NaHCO₃ + ultrasonication. The fractogram of the NaHCO_3 -extract after ultrasonic

treatment (Figure 2.3) shows the presence of DOM in the 1–5 nm size range and clay nanoparticles in the 20–100 nm size range. The concentrations of Si, Al and Fe in this latter peak were lower than those in the NaOH and pyrophosphate extracts (without ultrasonication) and no primary Fe and Al-(hydr)oxide nanoparticles were detected. Thus, in the absence of a chemical dispersant, primary Fe-(hydr)oxide nanoparticles could not be dispersed from the soil with ultrasonic treatment applied at an amount of 95 J cm^{-3} . The amount of ultrasound energy applied was low compared to other studies (Kaiser et al., 2012; Pronk et al., 2011) and we found that Fe concentrations in the supernatant increased with increasing amount of applied ultrasound energy (Appendix A, Figure A4). Nevertheless, the amount of Fe dispersed after ultrasonication at 500 J cm^{-3} (0.8 g kg^{-1}) was still less than 10% of the amount of Fe dispersed in pyrophosphate without ultrasonication (9.8 g kg^{-1}). This is in agreement with results of Pronk et al., (2011) who showed that the clay fraction was lower when determined after ultrasonic treatment compared to the clay fraction determined after chemical dispersion of the soil. Ultrasonic treatment disperses less particles from soil because ultrasonic treatment cannot detach organic matter from mineral particles (Schmidt et al., 1999) and because ultrasonic treatment cannot disperse iron-stabilized aggregates (Pronk et al., 2011). As a consequence, ultrasonic treatment releases small aggregates instead of primary particles (Calabi-Floody et al., 2011; Li et al., 2012). Ultrasonic treatment without pyrophosphate is therefore less effective in dispersion of primary Fe-(hydr)oxide particles from soil compared to extraction with pyrophosphate.

Pyrophosphate + ultrasonication. The fraction of SOC extracted in the ultrasonicated 10 mM pyrophosphate extract is somewhat higher (60%) compared to the 2 mM pyrophosphate extract without ultrasonication (55%). The fractograms of the pyrophosphate extract and ultrasonically treated pyrophosphate extract are very similar (Figure 2.2 and 2.3). Ultrasonic treatment of the pyrophosphate extract did thus not increase the amount of primary Fe and Al-(hydr)oxide nanoparticles in the 2–20 nm size-range. Therefore, we could not disperse more than 4.7 g kg^{-1} Fe as Fe-(hydr)oxide nanoparticles, which corresponds to 37% of Fe-ox. More Fe-(hydr)oxide nanoparticles may be dispersed but may elute simultaneously with the clay particles (20–150 nm) meaning that they are not recognized as Fe-(hydr)oxides in the fractograms of the pyrophosphate extracts. In addition, part of the soil Fe-(hydr)oxide particles may be larger than the analysed size range (1–150 nm). Also, dispersion of Fe-(hydr)oxide nanoparticles from soil may be incomplete because of strong associations between Fe-(hydr)oxide nanoparticles and clay minerals (Cornell and Schwertmann, 2006). Once Fe-(hydr)oxides are attached to clay minerals they do not disperse upon ultrasonic

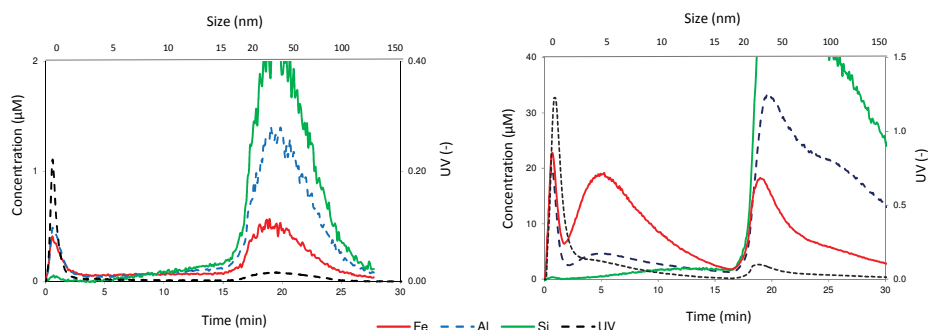


Figure 2.3. AF4-fractograms of nanoparticles dispersed from the Bh2-horizon in 5 mM NaHCO_3 (left) and 10 mM pyrophosphate (right) after ultrasonication of the soil suspensions. The fractograms show the Fe, Al and Si concentration and the UV absorbance at 254 nm as a function of elution time and the corresponding hydrodynamic particle diameter.

treatment or in alkaline extractions (Yong and Ohtsubo, 1987) meaning that they cannot be quantified with AF4.

2.4. Conclusions

Among the three chemical extractions, pyrophosphate extracted the most Fe and Al as primary (*i.e.*, not associated to other particles) metal-(hydr)oxide nanoparticles from soil and maximum concentrations of Fe-(hydr)oxide nanoparticles were found at a particle size of 5 nm. The use of NaOH caused less dispersion of Fe- and Al-(hydr)oxide particles while no metal-(hydr)oxide particles could be detected in the NaCl extracts. Dispersion of metal-(hydr)oxide nanoparticles from soil correlates positively with the amount of SOC extracted, which can be explained by disaggregation of organo-mineral soil aggregates. No Fe and Al-(hydr)oxide nanoparticles were dispersed from soil after ultrasonic treatment of a NaHCO_3 suspension. This shows that a chemical dispersant such as pyrophosphate is needed to release primary Fe- and Al-(hydr)oxide nanoparticles from the organo-mineral aggregates in soil. The amounts of Fe-(hydr)oxide nanoparticles in the 2–10 nm size range dispersed in pyrophosphate corresponded to 16–47% of the Fe-ox content in the three soil horizons. Ultrasonic treatment of the pyrophosphate suspension did not further increase the amounts of dispersed Fe-(hydr)oxide nanoparticles. The remaining part of the Fe-(hydr)oxides in soil is either larger than the analysed size range (1–150 nm), is associated with clay minerals or cannot be dispersed from soil during extraction with pyrophosphate in combination with ultrasonic treatment. Hence, dispersion of Fe-(hydr)oxides from the

podzol is not complete and as a consequence, AF4 coupled to HR-ICP-MS could not be used to derive the surface area of Fe-(hydr)oxides in the podzol. Instead, AF4 coupled to HR-ICP-MS should be considered as a complementary analytical technique, which can be used to provide a direct measurement of the particle size distribution of metal-(hydr)oxide nanoparticles in soil extracts.

Acknowledgements

This work is part of the SoilTrEC project (Soil Transformations in European Catchments) and was funded by the EU commission under the 7th Framework Program (Contract No. 244118). We thank the project partner from the Czech Geological Survey, Prague (M. Novák) for cooperation. Technical help of P. Krám, O. Myška (CGS Prague) and J. Blaha (Lesy Ceske Republiky, Lazne Kynzvalt) during the soil sampling is highly appreciated. We thank the partners from ISNNP, Sofia (S. Rousseva, M. Kercheva, E. Dimitrov, M. Nenov and T. Shishkov) and BOKU, Vienna (W. Blum and G. Lair) for their collaboration in sampling and for supplying part of the data.

References

- An, S., Mentler, A., Mayer, H., Blum, W.E.H., 2010. Soil aggregation, aggregate stability, organic carbon and nitrogen in different soil aggregate fractions under forest and shrub vegetation on the Loess Plateau China. *Catena* 81, 226-33
- Ashworth, J., Doug, K., Rhonda, K., Robert, L., 2001. Standard procedure in the hydrometer method for particle size analysis. *Commun. Soil Sci. Plan.* 32, 633-42
- Baalousha, M., 2009. Aggregation and disaggregation of iron oxide nanoparticles: Influence of particle concentration, pH and natural organic matter. *Sci. Total. Environ.* 407, 2093-101.
- Baalousha, M., Lead, J.R., 2007. Characterization of natural aquatic colloids (<5 nm) by flow-field flow fractionation and atomic force microscopy. *Environ. Sci. Technol.* 41, 1111-17.
- Baalousha, M., Stolpe, B., Lead, J.R., 2011. Flow field-flow fractionation for the analysis and characterization of natural colloids and manufactured nanoparticles in environmental systems: A critical review. *J. Chromatogr. A* 1218, 4078- 103.
- Baalousha, M., Von der Kammer, F., Motelicaheino, M., Hilal, H., Lecoustumer, P., 2006. Size fractionation and characterization of natural colloids by flow-field flow fractionation coupled to multi-angle laser light scattering. *J. Chromatogr. A* 1104, 272-81
- Burleson, D.J., Penn, R.L., 2005. Two-step growth of goethite from ferrihydrite. *Langmuir* 22, 402-9.
- Buurman, P., Jongmans, A., 2005. Podzolisation and soil organic matter dynamics. *Geoderma* 125, 71-83.
- Calabi-Floody, M., Bendall, J.S., Jara, A.A., Welland, M.E., Theng, B.K.G., Rumpel, C., De la Luz Mora, M., 2011. Nanoclays from an Andisol: Extraction, properties and carbon stabilization. *Geoderma* 161, 159-67.
- Cornell, R.M., Schwertmann, U., 2006. The iron oxides. Structure, properties, reactions, occurrences

- and use, second ed. WILEY-VCH Verlag, Weinheim
- Dümig, A., Häusler, W., Steffens, M., Kögel-Knabner, I., 2012. Clay fractions from a soil chronosequence after glacier retreat reveal the initial evolution of organo-mineral associations. *Geochim. Cosmochim. Ac.* 85, 1-18.
- Eusterhues, K., Rumpel, C., Kögel-Knabner, I., 2005. Organo-mineral associations in sandy acid forest soils: importance of specific surface area, iron oxides and micropores. *Europ. J. Soil Sci.* 56, 753-63.
- Eusterhues, K., Wagner, F.E., Häusler, W., Hanzlik, M., Knicker, H., Totsche, K.U., Kögel-Knabner, I., Schwertmann, U., 2008. Characterization of ferrihydrite-soil organic matter coprecipitates by X-ray diffraction and mössbauer spectroscopy. *Environ. Sci.Technol.* 42, 7891-97.
- Hiemstra, T., Antelo, J., Rahnemaie, R., Van Riemsdijk, W.H., 2010. Nanoparticles in natural systems I: The effective reactive surface area of the natural oxide fraction in field samples. *Geochim. Cosmochim. Ac.* 74, 41-58
- Hiemstra, T., 2013. Surface and mineral structure of ferrihydrite. *Geochim. Cosmochim. Ac.* 105, 316-25.
- Holmgren, G.G., 1967. A rapid citrate-dithionite extractable iron procedure. *Soil Sci. Soc. Am. Proc.* 31, 210-11.
- Ikotun, O.F., Marino, N., Kruger, P.E., Julve, M., Doyle, R.P., 2010. Coordination complexes incorporating pyrophosphate: Structural overview and exploration of their diverse magnetic, catalytic and biological properties. *Coordin. Chem. Rev.* 254, 890-915.
- Ilg, K., Dominik, P., Kaupenjohann, M., Siemens, J., 2008. Phosphorus-induced mobilization of colloids: model systems and soils. *Eur. J. Soil Sci.* 59, 233-46
- Jansen, B., Nierop, K. G. J., Verstraten, J. M., 2005. Mechanisms controlling the mobility of dissolved organic matter, aluminium and iron in podzol B horizons. *Eur. J. Soil Sci.* 56, 537-50.
- Jeanroy, E., Guillet, B., 1981. The occurrence of suspended ferruginous particles in pyrophosphate extracts of some soil horizons. *Geoderma* 26, 95-105.
- Kaiser, M., Berhe, A.A., Sommer, M., Kleber, M., 2012. Application of ultrasound to disperse soil aggregates of high mechanical stability. *J. Plant Nutr. Soil Sci.* 175, 521-26
- Kaiser, K., Zech, W., 1996. Defects in estimation of aluminum in humus complexes of podzolic soils by pyrophosphate extraction. *Soil Sci.* 161, 452-58.
- Koopmans, G.F., Groenenberg, J.E., 2011. Effects of soil oven-drying on concentrations and speciation of trace metals and dissolved organic matter in soil solution extracts of sandy soils. *Geoderma.* 161, 147-58
- Krám, P., Hruška, J., Driscoll, C.T., Johnson, C.E., Oulehle, F., 2009. Long-term changes in aluminum fractions of drainage waters in two forest catchments with contrasting lithology. *J. Inorg. Biochem.* 103, 1465-72.
- Krám, P., Hruška, J., Shanley, J.B., 2012. Streamwater chemistry in three contrasting monolithologic Czech catchments. *Appl. Geochem.* 27, 1854-63
- Kretzschmar, R., Sticher, H., 1997. Transport of humic-coated iron oxide colloids in a sandy soil: Influence of Ca²⁺ and trace metals. *Environ. Sci. Technol.* 31, 3497-504
- Li, W., He, Y., Wu, J., Xu, J., 2012. Extraction and characterization of natural soil nanoparticles from Chinese soils. *Eur. J. Soil Sci.* 63, 754-61
- Lyvén, B., Hassellöv, M., Turner, D.R., Haraldsson, C., Andersson, K., 2003. Competition between iron- and carbon-based colloidal carriers for trace metals in a freshwater assessed using flow field-flow fractionation coupled to ICPMS. *Geochim. Cosmochim. Ac.* 67, 3791-802.
- Mermut, A.R., Cano, A.F., 2001. Baseline studies of the clay minerals society source clays: Chemical

- analyses of major elements. *Clay. Clay Mineral.* 49, 381-6.
- Mikutta, R., Kleber, M., Torn, M.S., Jahn, R., 2006. Stabilization of soil organic matter: association with minerals or chemical recalcitrance? *Biogeochemistry* 77, 25-26
- North, P.F. 1976. Towards an absolute measurement of soil structural stability using ultrasound. *J. Soil Sci.* 27. 451-9
- Pansu, M., Gautheyrou, J., 2006. *Handbook of soil analysis: Mineralogical, organic and inorganic methods.* Springer Berlin Heidelberg, New York.
- Parfitt, R.L., Childs, C.W., 1988. Estimation of forms of Fe and Al: A review, and analysis of contrasting soils by dissolutions and moessbauer methods. *Aust. J. Soil Res.* 26, 121-44
- Penn, R.L., Zhu, C., Xu, H., Veblen, D.R., 2001. Iron oxide coatings on sand grains from the Atlantic coastal plain: High-resolution transmission electron microscopy characterization. *Geology* 29, 843-6.
- Plathe, K.L., Von der Kammer, F., Hassellöv, M., Moore, J., Murayama, M., Hofmann, T., Hochella, M.F., 2010. Using FIFFF and aTEM to determine trace metal-nanoparticle associations in riverbed sediment. *Environ. Chem.* 7, 82-93.
- Pronk, G.J., Heister, K., Kögel-Knaber, I., 2011. Iron oxides as major available interface component in loamy arable topsoils. *Soil Sci. Soc. Am. J.* 75, 2158-68
- Regelink, I.C., Koopmans, G.F., Van der Salm, C., Weng, L., Van Riemsdijk, W.H., 2013. Characterization of colloidal phosphorus species in pipe drain and trench waters from a fertilized clay soil using asymmetric flow field flow fractionation. *J. Environ. Qual.* 42, 464-73
- Schmidt, M.W.I., Rumpel, C., Kögel-Knabner, I., 1999. Evaluation of ultrasonic dispersion procedure to isolate primary organomineral complexes from soils. *Eur. J. Soil Sci.* 50, 87-94
- Schwertmann, U., 1973. Use of oxalate for Fe extraction from soils. *Can. J. Soil Sci.* 53, 244-6.
- Schwertmann, U., Wagner, F., Knicker, H., 2005. Ferrihydrite-humic associations: Magnetic hyperfine interactions. *Soil Sci. Soc. Am. J.* 69, 1009-15
- Stolpe, B., Guo, L., Shiller, A.M., Aiken, G.R., 2013. Abundance, size distributions and trace-element binding of organic and iron-rich nanocolloids in Alaskan rivers, as revealed by field-flow fractionation and ICP-MS. *Geochim. Cosmochim. Ac.* 105, 221-39
- Tatzber, M., Stemmer, M., Speigel, H., Katzlberger, C., Haberhauer, G., Mentler, A., Gerzabek, M.H., 2007. FTIR-spectroscopic characterization of humic acids and humin fractions obtained by advanced NaOH, Na₄P₂O₇ and Na₂CO₃ extraction procedures. *J. Plant Nutr. Soil Sci.* 170, 522-9.
- Van der Zee, C., Slomp, C.P., Rancourt, D.G., De Lange, G.J., Van Raaphorst, W., 2005. A Mössbauer spectroscopic study of the iron redox transition in eastern Mediterranean sediments. *Geochim. Cosmochim. Ac.* 69, 441-53.
- Van Zomeren, A., Comans, R., 2007. Measurement of humic and fulvic acid concentrations and dissolution properties by a rapid batch procedure. *Environ. Sci. Technol.* 41, 6755-61
- Von der Kammer, F., Legros, S., Hofmann, T., Larsen, E.H., Loeschner, K., 2011. Separation and characterization of nanoparticles in complex food and environmental samples by field-flow fractionation. *Trends Anal. Chem.* 30, 425-36.
- Wagner, U., Knorr, W., Forster, A., Murad, E., Salazar, R., Wagner, F., 1988. Mössbauer study of illite associated with iron oxo-hydroxides. *Hyperfine Interact.* 41, 855-8.
- Weng, L., Van Riemsdijk, W.H., Hiemstra, T., 2007. Adsorption of humic acids onto goethite: Effects of molar mass, pH and ionic strength. *J. Colloid Interf. Sci.* 314, 107-18.
- Weng, L., Van Riemsdijk, W.H., Hiemstra, T., 2008. Humic nanoparticles at the oxide-water interface: Interactions with phosphate ion adsorption. *Environ. Sci. Tech.* 42, 8747-52.

Yong, R.N., Ohtsubo, M., 1987. Interparticle action and rheology of kaolinite-amorphous iron hydroxide (ferrihydrite) complexes. *Appl. Clay Sci.* 2, 63-81.

Chapter 3

Characterization of Colloidal Fe from Soils using Field-Flow Fractionation and Fe K-edge X-ray Absorption Spectroscopy

Inge C. Regelink, Andreas Voegelin, Liping Weng, Gerwin F. Koopmans,
Rob N.J. Comans

Published as 'Characterization of Colloidal Fe from Soils using Field-Flow Fractionation and Fe K-edge X-ray Absorption Spectroscopy' in Environmental Science and Technology, (2014) 48, 4307

Abstract

Colloids may facilitate the transport of trace elements and nutrients like phosphate in soil. In this study, we characterized soil colloids (<0.45 μm), extracted from four agricultural soils by Na-bicarbonate and Na-pyrophosphate, by two complementary analytical techniques; asymmetric flow field-flow fractionation (AF4) and X-ray absorption spectroscopy (XAS). The combined results from AF4 and XAS show that colloidal Fe is present as (i) free Fe-(hydr)oxide nanoparticles, (ii) Fe-(hydr)oxides associated with clay minerals and as (iii) Fe in clay minerals. Free Fe-(hydr)oxide nanoparticles, which can be as small as 2–5 nm, are extracted with Na-pyrophosphate but not with Na-bicarbonate, except for one soil. In contrast, Fe-(hydr)oxides associated with clay minerals were dispersed by both extractants. XAS results show that the speciation of Fe in the colloidal fractions closely resembles the speciation of Fe in the bulk soil, indicating that dispersion of colloidal Fe from the studied soils was rather unselective. In one Fe-rich soil, colloidal Fe was dominantly dispersed in the form of free Fe-(hydr)oxide nanoparticles. In the other three soils, dispersed Fe-(hydr)oxides were dominantly associated with clay minerals, suggesting that their dispersion as free nanoparticles was inhibited by strong attachment. However, in these soils, Fe-(hydr)oxides can be dispersed as oxide-clay associations and may as such facilitate the transport of trace elements.

3.1 Introduction

Iron-(hydr)oxide nanoparticles are abundant in the environment (Jambor and Dutrizac, 1998) and play an important role in the sequestration of soil organic carbon (SOC), phosphate and trace metals in soils (Hiemstra et al., 2010; Kaiser et al., 2002; Mikutta and Kaiser, 2011; Regelink and Temminghoff, 2011). The high sorptive capacity of Fe-(hydr)oxide nanoparticles can be explained by the combination of a high density of reactive surface sites and a large specific surface area (SSA) (Cornell and Schwertmann, 2006; Eusterhues et al., 2005; Hiemstra, 2013). For agricultural soils, the SSA of the Fe-(hydr)oxides corresponds to average particle sizes between 1–10 nm (Hiemstra et al., 2010), which is in line with particle sizes of Fe-(hydr)oxides in the environment as measured by asymmetric flow field-flow fractionation (AF4) (Neubauer et al., 2013b; Regelink et al., 2013b; Stolpe et al., 2013) or electron microscopy (Li et al., 2012; Plathe et al., 2013). Such small nanoparticles can form when Fe is co-precipitated with humic substances, phosphate or silicate, since these elements effectively inhibit polymerization and further growth of Fe-containing nanoparticles (Eusterhues et al., 2008; Kaegi et al., 2010; Mikutta et al., 2008; Voegelin et

al., 2010; Voegelin et al., 2013). Due to their small size, Fe-(hydr)oxide nanoparticles may be released from the soil to the pore water and act as carriers for organic matter, phosphate and trace metals, thereby facilitating their transport in soils and surface waters (Braunschweig et al., 2013; Neubauer et al., 2013b; Regelink et al., 2013b; Stolpe et al., 2013). However, the mobility of Fe-(hydr)oxide nanoparticles depends, amongst others, on their aggregation behavior in the soil. As such, the release of Fe-(hydr)oxide nanoparticles from soils may be very low due to their strong tendency to form aggregates with other soil constituents such as organic carbon and clay minerals (Baalousha et al., 2008; Kretzschmar and Sticher, 1997; Pronk et al., 2011). For example, in a previous study of Regelink et al., (2013b) Fe-(hydr)oxide nanoparticles could not be dispersed from a podzol when this soil was extracted with Na-bicarbonate, whereas a large fraction of these nanoparticles could be mobilized in Na-pyrophosphate, which disperses a considerable amount of organic-mineral aggregates (Kaiser et al., 2011). However, this previous study was limited to one soil type, whereas the abundance and characteristics of dispersible Fe-(hydr)oxide nanoparticles is known to depend on soil type (Li et al., 2012). Therefore, there is a strong need to characterize colloidal Fe and Fe-(hydr)oxide nanoparticles mobilized from different soils in order to increase our understanding of their potential contribution to colloid-facilitated transport.

Iron in oxic soils can be present as various Fe species such as Fe(III)-(hydr)oxides, Fe(II)- and Fe(III)-bearing phyllosilicate minerals, and Fe(III) associated with organic matter (Kleja et al., 2012; Prietzel et al., 2007; Rennert et al., 2012). As such, in addition to the concentration of colloidal Fe extracted from soils, further characterization of the soil colloids is needed to distinguish between these Fe species. The size and elemental composition of nanoparticles can be characterized by AF4 coupled to high-resolution inductively coupled plasma mass spectrometry (HR-ICP-MS) (Van der Kammer et al., 2011). This fractionation technique has been applied successfully to characterize associations between trace elements and organic and mineral colloids in environmental water samples (Lyvén et al., 2003; Neubauer et al., 2013b; Regelink et al., 2013a; Stolpe et al., 2013). More recently, AF4-HR-ICP-MS was applied to characterize nanoparticles extracted from soils and sediments (Neubauer et al., 2013b; Plathe et al., 2013; Regelink et al., 2013b). One generally recognized constraint in previous AF4 studies (Plathe et al., 2010; Regelink et al., 2013b) is the inability of this technique to elucidate the speciation of the Fe-containing colloids when Fe-(hydr)oxides elute simultaneously with clay minerals during AF4 fractionation. Therefore, additional techniques are needed to characterize the Fe speciation of the colloids, for example Fe K-edge X-ray absorption spectroscopy (XAS), including X-ray absorption near edge structure

(XANES) and extended X-ray absorption fine structure (EXAFS) spectroscopy. XAS probes the local coordination of Fe and has been applied before to analyze the speciation of Fe in soils, in colloids isolated from environmental water samples and in synthetic Fe-precipitates (Baker et al., 2010; Gustafsson et al., 2007; Kleja et al., 2012; Mikutta et al., 2010; Sjöstedt et al., 2013; van Schaik et al., 2008; Voegelin et al., 2013; Voegelin et al., 2007).

In this study, AF4-HR-ICP-MS and EXAFS spectroscopy are combined for the first time to characterize soil colloids extracted from four Dutch agricultural soils, which vary in SOC content, Fe-(hydr)oxide content and SSA of the Fe-(hydr)oxides. The colloidal fraction, which we define as the fraction passing a 0.45- μm filter membrane, was extracted from the soils using Na-bicarbonate or Na-pyrophosphate in combination with mechanical energy in the form of ultrasonication. Na-bicarbonate is considered as a mild extractant for relatively easily dispersible colloids, whereas Na-pyrophosphate is a stronger extractant that is also able to disperse considerable amounts of organo-mineral aggregates (Jeanroy and Guillet, 1981; Kaiser et al., 2011). The size-distribution and chemical composition of dispersed nanoparticles smaller than 150 nm was characterized by AF4-HR-ICP-MS. Additionally, for two soils, Fe speciation in bulk soil and in the colloidal fractions was analyzed by Fe K-edge XAS. The combination of these two complementary techniques enables us to characterize the size-distribution and speciation of the soil colloids. The results will be discussed with respect to the release of Fe-(hydr)oxide nanoparticles and other Fe-bearing colloids from soils and their potential role in colloid-facilitated transport.

3.2 Material and Methods

3.2.1 Soils

Soil samples (0–10 cm) were collected from four agricultural soils in The Netherlands. These soils were used in a previous study of Hiemstra et al. (2010) and for reasons of comparison, we used the same soil numbers as in this previous study. The soils were dried at 40°C and sieved over 2 mm. For the determination of the total Fe content, 4 g of finely powdered soil material were mixed with 0.9 g of wax (Licowax C, Fluxana, Germany) and pressed into a 32-diameter pellet for analysis on an energy-dispersive X-ray fluorescence spectrometer (XRF) (XEPOS+, SPECTRO Analytical Instruments GmbH, Kleve, Germany) using a built-in calibration for geological materials provided by the manufacturer. The SOC content, clay content, ammonium oxalate extractable Fe, Al, and P (Fe_{ox} , Al_{ox} , and P_{ox}) (Schwertmann, 1973) and dithionite-citrate-bicarbonate extractable Fe (Fe_{d}) (Holmgren,

1967) as well as the SSA of the metal-(hydr)oxides were taken from Hiemstra et al. (2010). The SSA of the metal-(hydr)oxides was derived previously from phosphate desorption curves which were interpreted using the CD-MUSIC model and the derived reactive surface areas per mass of soil was scaled to the sum of the Fe- and Al-(hydr)oxide content (Hiemstra et al., 2010). Since Fe-(hydr)oxides are the dominant metal-(hydr)oxide phase in our four soils, we refer to these SSA values as the SSA of the Fe-(hydr)oxides.

3.2.2 Extraction of Soil Colloids

Ultrapure water was used to prepare solutions. Colloids were extracted from the soils in (i) 5 mM Na-bicarbonate (NaHCO_3 , pH 8.3) and (ii) 10 mM sodium pyrophosphate ($\text{Na}_4\text{P}_2\text{O}_7$, pH 8.5). The pH of the Na-pyrophosphate solution was adjusted to 8.5 using HCl, to prevent dissolution of Fe-(hydr)oxides which may occur at its original solution pH of 9.6 (Pansu and Gautheyrou, 2006). The pH values of the equilibrated soil-suspensions were similar to those of the initial extractants. We used a solid-solution-ratio (SSR) of 2 g l^{-1} for both extractants because preliminary tests showed that using this low SSR a larger amount of colloids could be extracted from soil than at a higher SSR. The suspensions (200 ml) were shaken end-over-end ($60 \text{ rotations min}^{-1}$) for 20 h and thereafter treated ultrasonically. The ultrasonic device (Hielscher UP400s, 24 kHz) was operated at 80% of its maximum power corresponding to a calorimetric energy output of 106 W, which was determined previously (Figure A1). The applied amount of ultrasound energy was 47.7 kJ g^{-1} soil, which is far above the threshold to disperse soil aggregates (Schmidt et al., 2008). The suspensions were centrifuged (10 min, 3500 rpm, 2100 g) and the supernatants were filtered through a $0.45\text{-}\mu\text{m}$ cellulose-nitrate filter (Aqua 30, Whatman). In these filtrates, the total dissolved concentrations of Fe, Al (inductively coupled plasma-atomic emission spectrometry, ICP-AES, Varian Vista Pro) and the concentrations of dissolved organic carbon (DOC) (Shimadzu TOC analyser) and nanoparticles (AF4-HR-ICP-MS) were measured.

For soils 3 and 17, the extraction procedure was repeated to collect a larger amount of colloidal material for analysis by Fe K-edge XAS. For each soil, five flasks each containing 200 mL of suspension were prepared, as described above. After centrifugation, the supernatants were passed through $0.45\text{-}\mu\text{m}$ cellulose-nitrate membranes using a filtration unit connected to a vacuum pump. For soil 17, the Fe concentrations in the filtrates were similar to those in filtrates prepared for AF4-HR-ICP-MS analysis, but were about 30% lower for soil 3 which can be explained by the use of a vacuum pump instead of a syringe for filtration, leading to a lower pressure drop. Next, colloids extracted in the Na-bicarbonate filtrates were coagulated

by adding $\text{Ca}(\text{NO}_3)_2$ to a final concentration of 0.5 M, whereas colloids extracted by Na-pyrophosphate were coagulated by adding NaCl to a final concentration of 2 M. Calcium was not used as a coagulant for the Na-pyrophosphate filtrates to prevent precipitation of Ca-pyrophosphate. The colloids were allowed to coagulate for 20 h and the flocculates were collected on a 0.1- μm cellulose-nitrate filter (Whatman). The total dissolved Fe, Al, and Si concentrations were measured in Na-bicarbonate and Na-pyrophosphate before and after filtration, and more than 95% of the Fe, Al and Si was recovered after filtration. The colloidal material on the filters was transferred into 15 mL of ultrapure water and these suspensions were dried at 40 C° to obtain the solid colloidal material for XAS analysis.

3.2.3 AF4-HR-ICP-MS

An AF4 system (AF 2000, Postnova Analytics, Germany) with a 1 kDa polyethersulfone (PES) membrane and 350 μm spacer was used for size fractionation of the colloids extracted in Na-bicarbonate and Na-pyrophosphate. A 3 mM NaHCO_3 solution at pH 8.3 was used as a carrier. The injection time was 11 min and the injection volume amounted to 0.5 and 0.1 ml for the Na-bicarbonate and Na-pyrophosphate extracts, respectively. During the injection time, dissolved species and colloids smaller than 1 kDa will pass the membrane and leave the column, whereas larger colloids will elute from the column during the elution step. To compare element concentrations in the presented AF4 fractograms, the element concentrations were corrected for the differences in injection volume by multiplying the concentrations eluting from the Na-pyrophosphate extracts with a factor five. The cross flow was 3 ml min^{-1} for the first 15 minutes, was then linearly decreased to 0.2 ml min^{-1} within 2 min, and maintained at this rate from 17 to 30 min. The detector flow was coupled to an ultraviolet-diode array detector (UV-DAD; Postnova Analytics) and to a HR-ICP-MS (Thermo Element 2) which measured the concentrations of Fe, Al, and Si every 10 s. The relationship between the particle diameter and elution time was derived using a combination of calibration using NIST-traceable polystyrene nanoparticles (Postnova Analytics) and AF4 theory, as described in Regelink et al. (2013b). The actual size of the particles may deviate from the calculated hydrodynamic particle diameter for non-spherical particles and for particles showing non-ideal behaviour (Baalousha and Lead, 2012).

3.2.4 Fe K-edge XAS

The speciation of Fe in bulk soil of soil 3 and 17 as well as in the respective colloidal materials extracted with Na-bicarbonate and Na-pyrophosphate was characterized by Fe

K-edge XANES and EXAFS spectroscopy. The samples were diluted in cellulose and pressed into homogeneous 13-mm pellets for analysis in transmission mode at room temperature. The measurements were performed at the Swiss Norwegian Beamline (SNBL, station BM01B) at the European Synchrotron Radiation Facility (ESRF, Grenoble, France). The beamline was operated with a Si(111) double crystal monochromator for energy selection (detuned to 65% of the maximum intensity for rejection of higher harmonic radiation). The incident and transmitted beam were recorded with ionization chambers (30 cm long; custom made) adjusted to reach 15% absorption in I_0 and 60% in I_1 and I_2 at the Fe K-edge. Beam energy was calibrated by setting the first maximum in the absorption K-edge of a metallic Fe foil to 7112 eV. The spectra were acquired in continuous scan mode from 6980 to 7900 eV (12 min each) and between 3 and 9 scans were averaged per sample depending on signal quality.

Reference and sample spectra were processed and analyzed using the software code Athena (Ravel and Newville, 2005). The E_0 was fixed at 7128.5 eV. The spectra were normalized by subtracting a first-order polynomial fitted to the data from -100 to -30 eV before the edge and subsequently dividing through a second-order polynomial fitted to the data from 60 to 450 eV above the edge. EXAFS spectra were extracted using the Autobk algorithm ($R_{\text{bkg}} = 0.9$; k -weight = 3, spline k -range 0-11.8 Å⁻¹). The k^3 -weighted EXAFS spectra were analysed by linear combination fitting (LCF) over the k -range 2-11 Å⁻¹. We initially tested a large suite of reference spectra, including different Fe(III)-(hydr)oxides (e.g., hematite, goethite, lepidocrocite, maghemite, ferrihydrite), Fe-carbonate (siderite), Fe(III)-phosphate (strengite), different Fe-bearing phyllosilicates (mica, chlorite, clay minerals), and organically complexed Fe(III) (including oligomeric Fe(III) associated with purified humic and fulvic acid from Mikutta and Kretzschmar (2011)). Starting with the best one-component fit, the number of components was increased as long as the normalized sum of the squared residuals ($\text{NSSR} = \sum(\text{data}_i - \text{fit}_i)^2 / \sum(\text{data}_i)^2$) of the best $n+1$ -component fit was at least 10% lower than the NSSR of the best n -component fit. Based on their occurrence and relevance in preliminary fits, the following 7 reference spectra were included in the final fits which allowed to reproduce all sample EXAFS spectra: Goethite (Gt), lepidocrocite (Lp), 2-line ferrihydrite (Fh), smectite (SWy-2), illite (IMt-1), nontronite (NAu-2), and biotite (Bio). The reference spectra of the Fe(III)-(hydr)oxides Gt, Lp and Fh are from Voegelin et al. (2010) and details on their synthesis as well as shell-fit results for Fh and Lp can be found there. The clays minerals SWy-2, IMt-1 and NAu-2 were obtained from the Source Clays Repository of the Clay Mineral Society (West Lafayette, USA). All phyllosilicate reference spectra are from Kiczka et al. (2011), where details can be found in the electronic annex.

Briefly, in the dioctahedral clay minerals SWy-2, IMt-1 and NAu-2, Fe(II) accounts for 7%, 12% and 0% of total Fe and Fe represents 15%, 21% and 90% of the cations in the octahedral sheets, respectively. In the trioctahedral biotite reference, Fe(II) accounts for 87% of total Fe and Fe for 71% of the octahedral cations. Shell-fits of the Fe K-edge EXAFS spectra of SWy-2, IMt-1 and NAu-2 have been published in previous studies (Gorski *et al.*, 2013; O'Day *et al.*, 2004; Vantelon *et al.*, 2003).

3.3 Results and Discussion

3.3.1 Soils and Extracted Colloidal Fractions

The soils cover a range in pH-values (5.6–7.1), SOC contents (9–37 g kg⁻¹) and total Fe contents (11–76 g kg⁻¹) (Table 3.1). The Fe_d contents vary between 4.7–47.6 g kg⁻¹, which correspond to 20–63% of the total Fe content in the soil. The Fe_{ox} contents vary between 1.8–19.1 g kg⁻¹ whereas Al_{ox} contents are much lower (0.5–0.8 g kg⁻¹) indicating that Fe dominates the metal-hydr(oxide) fraction of the soils. Sodium-bicarbonate extracted 2–13% of the total Fe content, whereas Na-pyrophosphate extracted 3–6 times more Fe, corresponding to 12–54% of the total Fe content (Table 3.1). Also, Na-pyrophosphate extracted a larger fraction of the SOC content (39–49%) than Na-bicarbonate (10–16%) (Table 3.1). This shows that Na-pyrophosphate disperses substantial amounts of organic-mineral aggregates, even although the pH of the extractant is lower (pH 8.5) than the pH used in the classical pyrophosphate extraction (pH 9.6). The large amount of Fe extracted in Na-pyrophosphate can be explained by a combination of factors: (i) pyrophosphate acts as a ligand for di- and trivalent cations desorbed from the soil and thereby lowers the free concentrations of potentially coagulation cations, (ii) pyrophosphate competes with SOC for adsorption to the surfaces of Fe-(hydr)oxides and clay minerals, leading to desorption of SOC and dispersion of organic-mineral aggregates, and (iii) adsorption of pyrophosphate to Fe-(hydr)oxides increases the negative surface charge of these colloids, leading to enhanced electrostatic repulsion of the particles (Jeanroy and Guillet, 1981; Kaiser *et al.*, 2011).

3.3.2 AF4-Fractograms

The fractograms of the Na-pyrophosphate and Na-bicarbonate extracts obtained from the four soils (Figure 3.1) show the UV absorbance and the Fe, Al, and Si concentrations as a function of the elution time and the corresponding hydrodynamic particle diameter. The fractograms were well reproducible (Appendix B, Figure B1). The peak in UV absorbance

Table 3.1. General soil characteristics and dissolved organic carbon, Fe and Fe-(hydr)oxide nanoparticles (Fe-oxide NPs) in the Na-bicarbonate and Na-pyrophosphate extracts.

Soil	pH	clay	SOC ^a	Fe _{total} ^b	Fe _d ^c	Fe _{ox} ^d	Al ^d _{ox}	Fe _{ox} /Fe _d	SSA _{oxides} ^e	Na-bicarbonate		Na-pyrophosphate				
(-)	(%)	(g/kg)	(g/kg)	(g/kg)	(g/kg)	(g/kg)	(g/kg)	(-)	(m ² /g)	DOC ^f	Fe ^f	DOC ^f	Fe ^f	NP ^g _{oxide}	NP ^g _{oxide}	
3	5.6	8	37	76	47.6 (63)	19.1 (25)	0.5	0.40	422	4.0	10	3	0.7 (4)	39	14	3.9 (21)
7	5.7	11	9	11	7.5 (68)	2.8 (25)	0.5	0.37	481	3.6	16	13	n.d. ^h	49	54	0.3 (10)
16	6.0	6	10	22	4.7 (20)	1.8 (8)	0.6	0.38	543	3.2	12	2	n.d. ^h	39	12	0.1 (8)
17	7.1	12	29	43	15.5 (36)	6.5 (15)	0.8	0.42	843	2.0	16	11	n.d. ^h	48	39	0.3 (5)

^a Soil organic carbon content.

^b Total Fe content determined by XRF.

^c Dithionite-citrate-bicarbonate extractable Fe (Holmgren, 1967). The amount of Fe_d expressed as a percentage of Fe_{total} is given in parentheses. Detection limit: 0.01 g/kg.

^d Ammonium-oxalate extractable Fe and Al (Schwertmann, 1973). The amount expressed as a percentage of Fe_{total} is given in parentheses. Detection limit: 0.01 g/kg.

^e Specific surface area of Fe-(hydr)oxide-like particles and corresponding average particle diameters, taken from ref.5.

^f Dissolved organic carbon and Fe concentration in the 0.45-µm filtered soil extracts, expressed as a percentage of the SOC and Fe_{total} content, respectively.

^g The amount of Fe present as free (i.e. not associated to other colloids) Fe-(hydr)oxide nanoparticles (2-150 nm) dispersed in Na-bicarbonate and Na-pyrophosphate, calculated from the AF4-fractograms (Figure 1). The amount of Fe-(hydr)oxide nanoparticles as a percentage of the Fe_{ox} content is given in parentheses.

^h not detected

at 1 nm indicates the elution of colloidal organic matter whereas the second UV peak, at a particle size of 20–150 nm, indicates the elution of inorganic particles. Between 40–75% of the injected colloidal Fe from the 0.45 μm -filtered extracts elutes in the 1–150 nm size range. The incomplete Fe recovery may be explained by the presence of Fe colloids with sizes larger than 150 nm which eluted from the column during the rinsing step. Additionally, some loss of Fe may have occurred because of dissolved Fe species or colloids passing the 1 kDa AF4 membrane (for example Fe bound by low-molecular-weight organic acids) or due to retention of colloids by the membrane. Three different Fe fractions can be distinguished in the AF4-fractograms: (i) Fe in the salt peak, (ii) free Fe-(hydr)oxide nanoparticles, and (iii) Fe co-eluting with clay minerals.

(i) The narrow Fe peak, which is only present in the Na-pyrophosphate extracts and elutes after 0.5 min, is a salt peak because the elution time equals the void time (*i.e.*, the time for an unretarded particle to pass the AF4 column). This Fe-salt peak can be explained by the elution of Fe-pyrophosphate complexes because previous testing showed that such complexes, prepared by adding trivalent cations to a Na-pyrophosphate solution, elute after 0.5 min meaning that pyrophosphate acts as a ligand for monomeric Fe adsorbed to humic substances in the soil (Regelink *et al.*, 2013b). To further support the origin of the Fe associated with pyrophosphate, we combined data of Na-pyrophosphate extractions for 8 different soils and show that the amount of Fe in the salt peak correlates positively with the SOC content ($R^2=0.78$, Figure B2). Furthermore, the amount of Fe in the salt peak divided by the SOC content correlates negatively with pH ($R^2=0.88$, Figure B2), which is in line with the increase in the amount of Fe adsorbed to humic substances with a decrease in pH, for soils where the Fe^{3+} concentration is in equilibrium with Fe-(hydr)oxide minerals (Hiemstra and van Riemsdijk, 2006).

(ii) Free Fe-(hydr)oxide nanoparticles, which are not associated with other particles, can be identified from the sole elution of Fe without any co-elution of Al and Si. Iron-(hydr)oxide nanoparticles are present in the 2–20 nm size-range of the Na-pyrophosphate extracts of all soils but absent in the Na-bicarbonate extracts, except for soil 3. For soil 7, 16 and 17, the concentration of free Fe-(hydr)oxide nanoparticles eluting in the 2–20 nm size range of the Na-pyrophosphate extracts, corresponds to 5.0–10.0% of the Fe_{ox} content of these soils (Table 3.1). For soil 3, the colloids extracted in Na-bicarbonate are characterized by the dominant elution of Fe in the 5–150 nm size range and the nearly complete absence of clay minerals. Hence, for soil 3, Fe is dominantly present as free Fe-(hydr)oxides and the amount of nano-sized Fe-(hydr)oxides corresponds to 4% of the Fe_{ox} content (Table

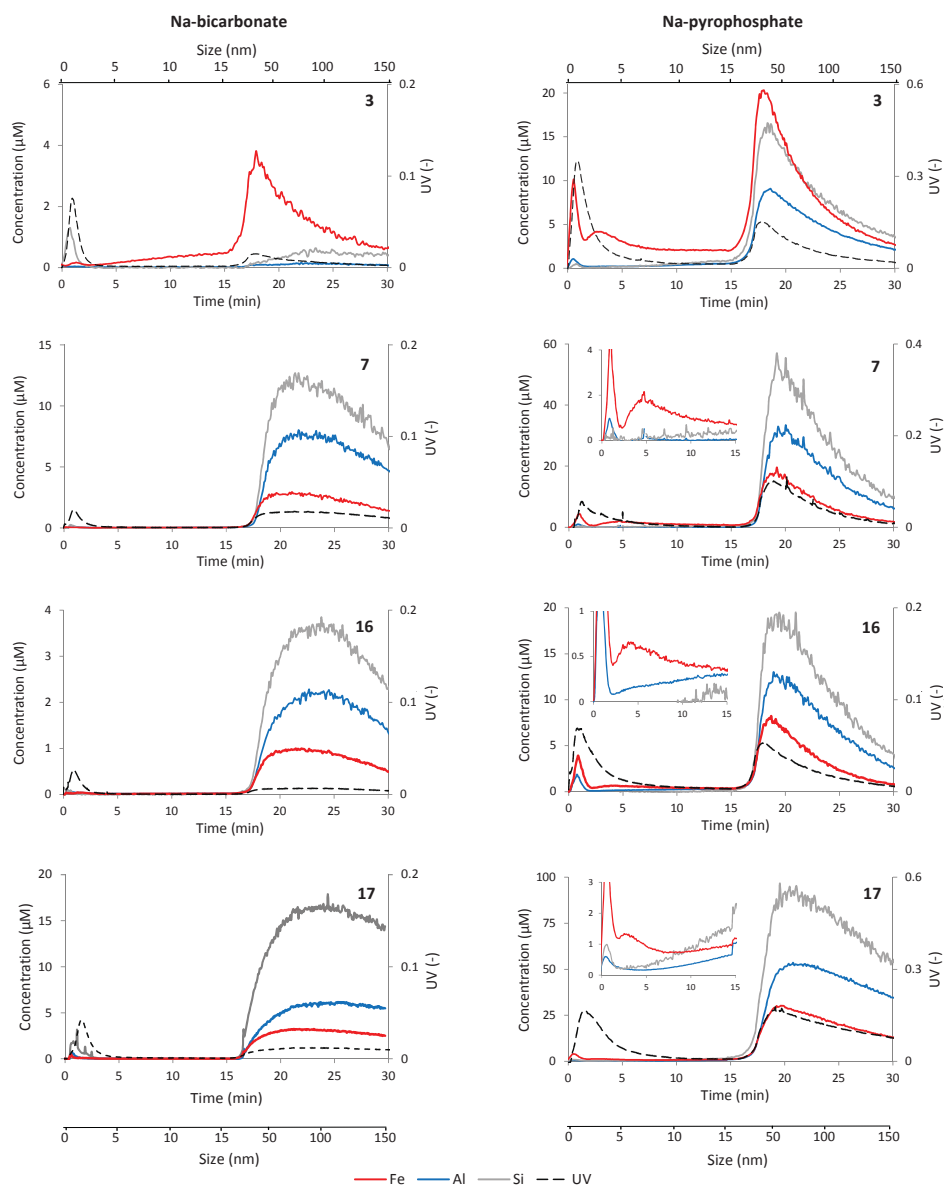


Figure 3.1. Fractograms showing the UV-absorbance (254 nm) and the Fe, Al and Si concentration as a function of the elution time and the corresponding hydrodynamic particle diameter for colloidal fractions ($<0.45 \mu\text{m}$) extracted in Na-bicarbonate and Na-pyrophosphate. The insets show the fractograms at a smaller scale. The amount of Fe present as free Fe-(hydr) oxide nanoparticles is given in Table 3.1.

3.1). The colloidal Fe extracted from soil 3 in Na-pyrophosphate is present as free Fe-(hydr)oxides (2–20 nm) and co-elutes with the Si/Al peak (20–150 nm). The Fe co-eluting with the Si/Al peak is likely present as free Fe-(hydr)oxides because Fe is the dominant element and the shape of the Fe peak deviates from the Si/Al peak. Assuming that all Fe is indeed be present in the form of free Fe-(hydr)oxides, this form corresponds to 21% of the Fe_{ox} content of soil 3 (Table 3.1). However, a small but unknown part of this Fe may be associated with phyllosilicate minerals.

(iii) Iron co-elutes with phyllosilicate minerals (Si/Al peak) in the 20–150 nm size-fraction of the Na-bicarbonate and Na-pyrophosphate extracts of soil 7, 16, and 17. The co-elution of Fe with clay minerals may be explained in various ways: (a) Fe is structurally incorporated within the phyllosilicate minerals via isomorphic substitution, (b) Fe is present as small Fe-(hydr)oxide particles attached to the surface of these clay minerals, or (c) Fe is present as Fe-(hydr)oxide particles exhibiting a similar size as the phyllosilicate minerals and therefore both particles elute simultaneously. The molar Fe/Si ratio of the colloids in this size-fraction (0.2–0.3) is not very illustrative in this perspective since the degree of Fe substitution strongly differs among clay minerals (Mermut and Cano, 2001). Thus, the speciation of the Fe co-eluting with the clay minerals cannot be elucidated from AF4-HR-ICP-MS analysis only, emphasizing the need for further characterization of these Fe colloids with alternative analytical techniques.

Table 3.2. Analysis of Fe K-edge EXAFS spectra of bulk soils 3 and 17 and colloids, dispersed in Na-bicarbonate (Na-bic) and Na-pyrophosphate (Na-PP), by linear combination fitting (LCF)^a.

	Gt	Lp	Fh	SWy-2	IMt-1	NAu-2	Bio	Sum	NSSR	Fe-oxides ^b	Fe(II) ^c
soil 3	0.33		0.54		0.12			1.15	9.3e-3	0.88	0.01
Na-bic.	0.38	0.09	0.42	0.10				1.13	8.3e-3	0.90	0.01
Na-PP	0.22	0.08	0.39	0.16		0.15		1.17	4.5e-3	0.70	0.01
soil 17		0.06	0.32	0.28		0.20	0.13	1.11	3.6e-3	0.39	0.13
Na-bic.		0.14	0.22	0.30		0.30	0.04	1.11	6.5e-3	0.36	0.05
Na-PP.		0.11	0.23	0.28		0.33	0.05	1.13	6.0e-3	0.34	0.06

^a Fits were conducted over k-range 2–11 Å⁻¹ based on spectra of goethite (Gt), lepidocrocite (Lp), 2-line ferrihydrite (Fh), smectite (SWy-2), illite (IMt-1), nontronite (NAu-2) and biotite (Bio). Individual fractions normalized to a sum of 100% are reported together with the effective sum of the fitted fractions. NSSR=normalized sum of squared residuals ($=\sum(\text{data}_i - \text{fit}_i)^2/\sum(\text{data}_i)^2$). The statistical uncertainties of fitted fractions ranged between 0.004 and 0.023, the corresponding relative uncertainties between 2% and 24%. Reference and sample spectra and LCF fits are shown in Fig. 3.2.

^b Fe-oxides fraction corresponds to sum of Gt, Lp and Fh.

^c Fe(II) fraction derived from Fe(II) contents of 7% in SWy-2, 12% in IMt-1, 0% in NAu-2 and 87% in Bio (Kiczka et al., 2011).

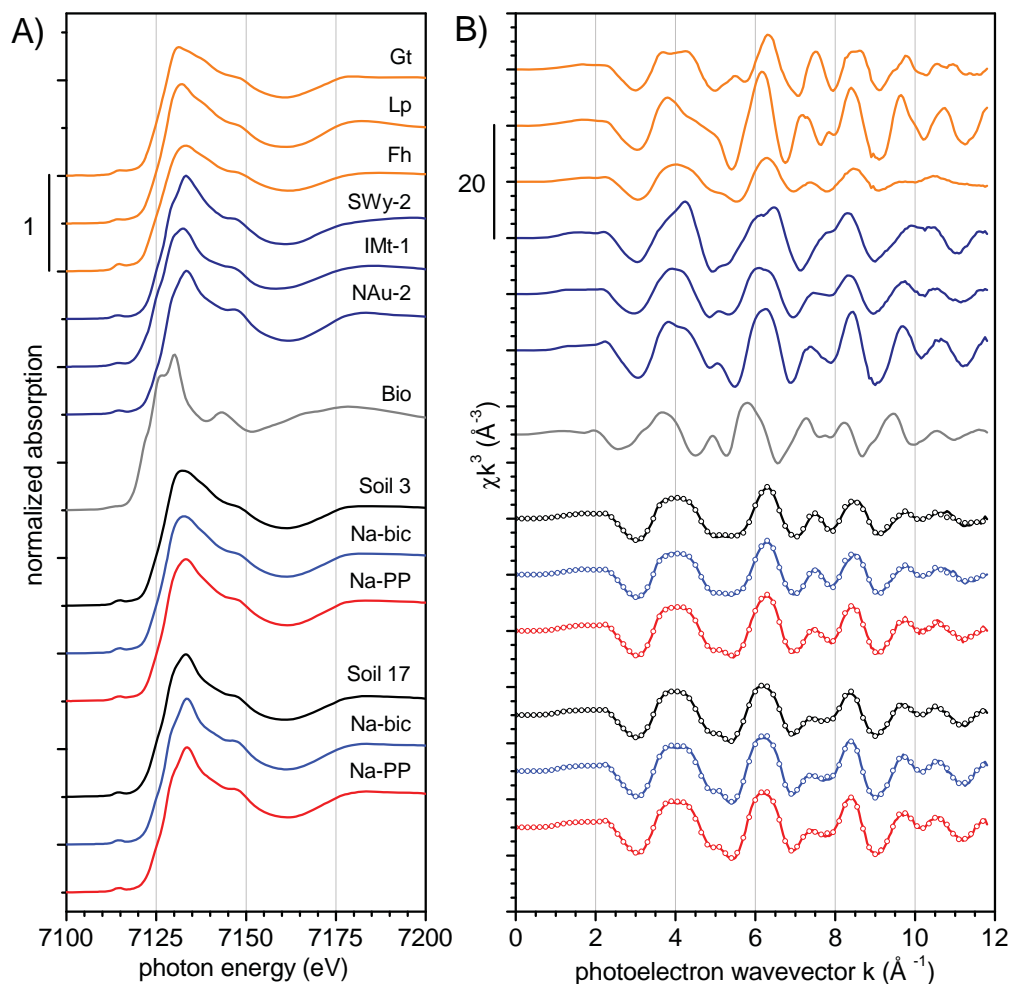


Figure 3.2. Fe K-edge XANES (A) and EXAFS (B) spectra of references used for EXAFS LCF analysis (Gt: goethite; Lp: lepidocrocite; Fh: ferrihydrite; SWy-2: smectite; IMt-1: illite; NAu-2: nontronite; Bio: biotite) and spectra of soil 3 and 17 and their respective colloids (<0.45 μm) extracted in Na-bicarbonate (Na-bic) and Na-pyrophosphate (Na-PP). The solid lines represent the measured spectra whereas the open symbols represent the results of the EXAFS LCF fits (Table 3.2)

3.3.3 X-ray Absorption Spectroscopy

Among the studied soils, the colloids extracted from soil 3 and 17 exhibit distinct features in the AF4 fractograms, suggesting that colloidal Fe extracted from soil 3 is mainly contained in Fe-(hydr)oxides whereas colloidal Fe extracted from soil 17 is dominantly associated with clay minerals. The speciation of Fe in these two soils and their respective

extracts was therefore characterized by Fe K-edge XAS. Reference and sample spectra are shown in Figure 3.2 and the results from EXAFS linear combination fitting (LCF) analysis are listed in Table 3.2. In the EXAFS, the different references exhibit distinct structural features, whereas the XANES spectra of the references reveal a limited sensitivity for the type of Fe-(hydr)oxide present. Therefore, only the EXAFS spectra were evaluated by LCF. According to the LCF results (Table 3.2), Fe in soil 3 is dominantly present in Fe(III)-(hydr)oxides (80%) and both goethite (33%) and ferrihydrite (54%) contribute significantly to the total Fe content of the soil. Qualitatively, this result is also reflected in the respective XANES spectrum, which more closely resembled the Fe-(hydr)oxide than the Fe-phyllsilicate reference spectra. The extracted colloids exhibit an Fe speciation similar to the bulk soil, although phyllosilicate-Fe seems to be mobilized to a larger extent by Na-pyrophosphate, which extracted about 5 times more colloidal Fe than Na-bicarbonate (Table 3.1). In soil 17, Fe in phyllosilicates dominates (61%) the Fe speciation in the bulk soil, as is also reflected in the shape of the respective XANES spectrum. The Fe-(hydr)oxide fraction of soil 17 (39%) is dominated by ferrihydrite whereas goethite did not contribute to the LCF fits. The colloids extracted from soil 17 exhibit a similar Fe speciation as the bulk soil. With respect to phyllosilicate-Fe, the references used for LCF indicate the average oxidation state and coordination of phyllosilicate-Fe rather than the presence of distinct phyllosilicate minerals. The LCF results thus suggest that phyllosilicate-Fe in both soils was dominantly Fe(III) contained in dioctahedral clay minerals, with a small contribution from Fe(II) in soil 17 and its colloid extracts that was probably due to the presence of minor fractions of Fe(II)-phyllosilicates such as biotite or chlorite. For both soils and the extracted colloids, the analysis of the XAS spectra by LCF suggested that organically complexed Fe(III) is not a dominant species, although this does not rule out the presence of a minor fraction of organically complexed Fe(III). Minor fractions of organically complexed Fe can be explained by the slightly acidic to neutral pH of the examined soils, at which Fe complexation to HA is low (Hiemstra and Van Riemsdijk, 2006) and by the high total Fe contents relative to SOC contents, which limits the potential contribution of organically-complexed Fe(III) to total soil Fe.

3.3.4 *Iron Speciation and Extractability by Oxalate and Dithionite*

Comparison of the Fe speciation determined by EXAFS spectroscopy (Table 3.2) and the Fe_d and Fe_{ox} fractions (Table 3.1) enables us to test to which extent Fe speciation can be inferred from Fe extractions. For soil 17, the LCF results suggest that 39% of the soil

Fe is contained in Fe-(hydr)oxides, which is in close agreement with the percentage of Fe extractable as Fe_d (36%). In soil 3, on the other hand, the fraction of Fe-(hydr)oxides determined by LCF (88%) is larger than the Fe_d fraction (63%). This discrepancy may reflect a limited sensitivity of XAS to differentiate between Fe in clay minerals and Fe(III)-(hydr)oxides in complex multi-component systems, but could also arise from a limited ability of DCB to extract Fe-(hydr)oxides from soil 3. With respect to the type of Fe(III)-(hydr)oxides as derived from the LCF results, ferrihydrite dominates the Fe-(hydr)oxide fraction in soil 17, whereas both ferrihydrite and goethite are present in soil 3. Despite these differences in Fe-(hydr)oxide speciation, the Fe_{ox}/Fe_d ratio, which is often taken as an indicator of the crystallinity of the Fe-(hydr)oxide fraction (Schwertmann, 1991), is similar for soil 3 and 17 (0.40 and 0.42, respectively, Table 3.1). Such a discrepancy between EXAFS-derived Fe speciation and Fe extractability has been reported previously (Baker et al., 2010) and may be related to factors such as the crystallinity, crystallite size, and degree of Al substitution in Fe-(hydr)oxides (Navrotsky et al., 2008; Schwertmann, 1991).

3.3.5 *Non-Selective Dispersion of Colloidal Fe from Soils*

The EXAFS spectra of soil 3 and 17 show that the speciation of Fe in the colloidal fractions, extracted with Na-pyrophosphate and Na-bicarbonate, is very similar to the speciation in the corresponding bulk soils (Table 3.2). For soil 3, goethite and ferrihydrite are present in both extracts. The rather non-selective dispersion of Fe-(hydr)oxides in Na-pyrophosphate is in contrast with the common thinking that pyrophosphate selectively extracts monomeric Fe and poorly polymerized Fe-(hydr)oxide particles (Jeanroy and Guillet, 1981; Pansu and Gautheyrou, 2006) However, these results are supported by previous EXAFS work of Karlsson *et al.* (2008) who showed for an organic soil that Fe-speciation in the bulk soil did not significantly change after removal of the pyrophosphate-extractable Fe. For soil 17, the non-selective dispersion of Fe, and thus the rather constant oxide/clay ratio in the soil and the extracted colloids, suggests that colloidal Fe is released in the form of oxide-clay assemblages rather than as two physically separated phases, as will be discussed later. Furthermore, the similar Fe speciation in the Na-bicarbonate and Na-pyrophosphate extracts shows that the strong quantitative differences in colloidal Fe concentrations between these extracts cannot be explained by preferential dispersion of certain Fe species. Instead, for these two soils, the dispersion of colloidal Fe seems rather non-selective.

3.3.6 Fractionation and Speciation of Colloidal Fe

For soil 3 and 17, the speciation of the nanoparticles can be assessed by comparing the fractograms (Figure 3.1) and the Fe speciation (Table 3.2) for the colloids extracted in Na-bicarbonate and Na-pyrophosphate from soil 3 and 17. Considering soil 3 first, Fe-(hydr)oxides dominate Fe speciation of the colloids extracted in Na-bicarbonate (90%) and Na-pyrophosphate (70%) according to the LCF results. This is in line with the amount of colloidal Fe-(hydr)oxides (0.8 and 5.9 g kg⁻¹) extracted with Na-bicarbonate and Na-pyrophosphate, which were calculated from the LCF results and the total dissolved Fe concentrations in the 0.45 µm-filtrates of these extracts. These amounts are somewhat higher than the amounts of Fe-(hydr)oxides derived from AF4 results (0.7 and 3.9 g kg⁻¹, respectively) which can be explained by the difference in the analysed size-range. Thus, the colloidal Fe dispersed from soil 3 is dominantly present as free Fe-(hydr)oxide nanoparticles.

For soil 17, the LCF results show that colloidal Fe extracted in Na-bicarbonate and Na-pyrophosphate is mainly contained in phyllosilicates (64–66%) and to a lesser extent Fe-(hydr)oxides (36–34%) (Table 3.2). The amount of Fe-(hydr)oxides extracted with Na-bicarbonate and Na-pyrophosphate amounts to 1.9 and 6.4 g kg⁻¹, which corresponds to 30 and 99% of the Fe_{ox} content or 12 and 42% of the Fe_d content, respectively. Thus, based on the LCF results, a large fraction of the Fe-(hydr)oxides in the soil can be dispersed from soil 17. However, in the corresponding fractograms, Fe-(hydr)oxides were not, or only in very small amounts, detected as free particles. This apparent discrepancy most likely indicates that Fe-(hydr)oxides co-elute with the clay particles as oxide-clay assemblages, which is in line with the strong similarity between the Fe- and Si/Al peak. Iron-(hydr)oxides exhibit a high affinity to clay minerals due to electrostatic interactions between the generally positively charged Fe-(hydr)oxides and negatively charged clay minerals (Wei et al., 2011; Yong and Ohtsubo, 1987). Similar to our study, Plathe et al., (2010) who characterized nanoparticles extracted from a sediment, were unable to separate Fe-(hydr)oxides from clay minerals by a combination of density fractionation and AF4 size-fractionation, indicating that the Fe-(hydr)oxides were physically associated with clay minerals. Accordingly, the combined interpretation of the EXAFS and AF4 results for soil 17 suggests that Fe-(hydr)oxides are mostly dispersed from this soil in association with clay minerals.

To disperse Fe-(hydr)oxide nanoparticles from the soil, we used extractants with a slightly alkaline pH (8.3–8.5) since a higher pH promotes the solubility of SOC and the dispersion of mineral colloids from soils (Liang et al., 2010; Weng et al., 2011). However, it is questionable whether the difference between the pH of the soil (5.6–7.1) and the pH of

the extractants (pH 8.3–8.5), which may lead to desorption of monomeric Fe from humic substances and subsequent precipitation of Fe-(hydr)oxides, is responsible for the fact that we observe Fe-(hydr)oxide nanoparticles in the pyrophosphate extracts. Recently, Neubauer et al. (2013a) tested the effect of pH on the release of Fe-(hydr)oxide nanoparticles from an acid podzol soil in pure water, but their results are ambiguous and they conclude that the Fe-(hydr)oxide nanoparticles extracted at pH 7 and 9 may have either formed during extraction or were mobilized from the soil. For our soils, with a pH between 5.6 and 7.1, Fe-(hydr)oxide nanoparticles are released in Na-pyrophosphate but absent in Na-bicarbonate, which had a similar pH as the Na-pyrophosphate extractant. Therefore, we argue that the release of Fe-(hydr)oxide nanoparticles in Na-pyrophosphate is not solely related to the pH of the extractant, but rather to the ability of pyrophosphate to disperse organic-mineral aggregates (Kaiser et al. 2011; Jeanroy, 1981). Additionally, pyrophosphate acts as a ligand for monomeric Fe desorbed from humic substances (Regelink et al., 2013b), thereby preventing polymerization and precipitation of monomeric Fe as Fe-(hydr)oxide nanoparticles. Also, the similar speciation of Fe in the colloid extracts and corresponding bulk soils as revealed by XAS supports our reasoning that the speciation of the extracted Fe-(hydr)oxides is not significantly affected by the extraction procedure.

3.3.7 Dispersion of Fe-(hydr)oxide Nanoparticles From Soils

The large SSA of the Fe-(hydr)oxides, as estimated previously by Hiemstra *et al.*, (2010) suggests that the majority of the Fe-(hydr)oxides in the soils should be as small as 2–4 nm (Table 3.1). These predicted average particle diameters are in line with the particle sizes at which the maximum concentrations of free Fe-(hydr)oxide nanoparticles elute in the AF4 (2–5 nm). However, only a small fraction of the soil Fe-(hydr)oxides (5–21% of Fe_{ox}) can be dispersed as free nanoparticles by the combination of Na-pyrophosphate and ultrasonic treatment (5–21% of Fe_{ox} , Table 3.1), and no free nanoparticles are dispersed by the combination of Na-bicarbonate and ultrasonic treatment, except for soil 3 (4% of Fe_{ox} , Table 3.1). The remaining Fe-(hydr)oxide nanoparticles either form strong aggregates in the soil, or are dispersed as oxide-clay assemblages, as was found for soil 17. Iron-(hydr)oxides in soils can be associated with humic substances, clay particles and silt/sand particles and these associations differ with respect to their resistance to chemical and mechanical dispersion. The binding of Fe-(hydr)oxides to silt/sand particles is relatively weak and previous work showed that Fe-(hydr)oxides can be detached from sand particles by ultrasonic treatment (Farmer et al., 2000). Iron-(hydr)oxides associated with humic substances can be dispersed in

substantial amounts as free particles in Na-pyrophosphate (Regelink et al., 2013b). However, these organic-oxide associations cannot be dispersed using ultrasonic treatment, because of their high mechanical strength (Calabi-Floody et al., 2011; Regelink et al., 2013b). The strongest interactions are found between Fe-(hydr)oxides and clay minerals and Fe-(hydr)oxides cannot be dispersed as free particles from clay minerals by ultrasonic treatment or alkaline extractants Pronk et al., 2011; Yong and Ohtsubo, 1987). As such, we suggest that these different sequestration mechanisms for Fe-(hydr)oxides in soils can explain the differences in the amount and setting of the Fe-(hydr)oxides released from the four soils and the different extractants. The dominant presence of free Fe-(hydr)oxide nanoparticles in the colloidal fractions of soil 3 may thus be explained by detachment of Fe-(hydr)oxides from silt/sand particles. Additionally, in the Na-pyrophosphate extract, Fe-(hydr)oxides nanoparticles may be released from organic-oxide associations. For the other soils, the majority of the dispersible Fe-(hydr)oxides seem associated with clay minerals, and only a small amount of free Fe-(hydr)oxide nanoparticles is released from organic-oxide associated in the Na-pyrophosphate extracts. These strong differences between the soils may be due to differences in soil characteristics. As such, we argue that the dispersion free Fe-(hydr)oxides from soil 3 may be related to the combination of a high Fe_d content and low a clay content, as compared to the other soils. The results of this study are in contrast with previous results for a podzol soil, for which a large fraction of the soil Fe-(hydr)oxides (16–47% of Fe_{ox}) was dispersed as free 5-nm sized Fe-(hydr)oxide nanoparticles in Na-pyrophosphate, which was explained by their association with humic substances (Regelink et al. 2013b). As such, the differences in the amount, speciation and setting (i.e., attached to oxides or freely dispersed) of the dispersed colloidal Fe seem related to differences in soil characteristics.

These findings are of environmental importance since the dispersion of colloids from soils due to changes in solution chemistry is the most common source of colloids in soils and groundwater (Kretzschmar et al., 1997). Our findings show that, although Fe-(hydr)oxides have a strong tendency to aggregate, they can be dispersed from soil as free Fe-(hydr)oxide nanoparticles and as oxide-clay associations. The contribution of free Fe-(hydr)oxides and oxide-clay associations depends on the soil type. Once dispersed, Fe-(hydr)oxides may facilitate the transport of trace elements in the soil and water. This warrants further research to understand the differences between free Fe-(hydr)oxides and oxide-clay associations with respect to their colloidal stability and mobility in soils and surface waters.

Acknowledgments

The EU commission is acknowledged for financing the SoilTrEC (Soil Transformations in European Catchments) project in its 7th Framework Program. The Swiss Norwegian Beamline (SNBL) at the European Synchrotron Radiation Facility (ESRF, Grenoble, France) is acknowledged for providing XAS beamtime. We thank Herman Emerich (SNBL) and Wouter van Beek (SNBL) for providing technical support at the beamline, Anna-Caterina Senn (Eawag, Switzerland) for her help with XAS sample preparation and data collection, and Christian Mikutta (ETH Zurich, Switzerland) for providing XAS reference spectra.

References

- Baalousha, M., Lead, J.R., 2012. Rationalizing nanomaterial sizes measured by Atomic Force Microscopy, Flow Field-Flow Fractionation, and Dynamic Light Scattering: Sample preparation, polydispersity, and particle structure. *Environ. Sci. Technol.* 46(11), 6134-6142.
- Baalousha, M., Manciuola, A., Cumberland, S., Kendall, K., Lead, J.R., 2008. Aggregation and surface properties of iron oxide nanoparticles: Influence of pH and natural organic matter. *Environ. Tox. Chem.* 27(9), 1875-1882.
- Baker, L.L., Strawn, D.G., Vaughan, K.L., McDaniel, P.A., 2010. XAS study of Fe mineralogy in a chronosequence of soil clays formed in basaltic cinders. *Clay. Clay Min.* 58(6), 772-782.
- Braunschweig, J., Bosch, J., Meckenstock, R.U., 2013. Iron oxide nanoparticles in geomicrobiology: From biogeochemistry to bioremediation. *New Biotechnol.* 30(6), 793-802.
- Calabi-Floody, M., Bendall, J.S., Jara, A.A., Welland, M.E., Theng, B.K.G., Rumpel, C., de la Luz Mora, M., 2011. Nanoclays from an Andisol: Extraction, properties and carbon stabilization. *Geoderma* 161(3-4), 159-167.
- Cornell, R.M., Schwertmann, U., 2006. The iron oxides. Structure, properties, reactions, occurrences and uses. 2nd edition. Wiley-VCH Verlag.
- Eusterhues, K., Rumpel, C., Kögel-Knabner, I., 2005. Organo-mineral associations in sandy acid forest soils: Importance of specific surface area, iron oxides and micropores. *Eur. J. Soil Sci.* 56, 753-763.
- Eusterhues, K., Wagner, F.E., Häusler, W., Hanzlik, M., Knicker, H., Totsche, K.U., Kögel-Knabner, I., Schwertmann, U., 2008. Characterization of ferrihydrite-soil organic matter coprecipitates by X-ray diffraction and Mössbauer spectroscopy. *Environ. Sci. Technol.* 42(21), 7891-7897.
- Farmer, A.D., Collings, A.F., Jameson, G.J., 2000. Effect of ultrasound on surface cleaning of silica particles. *Int. J. Miner. Process.* 60, 101-113.
- Gorski, C.A., Klüpfel, L.E., Voegelin, A., Sander, M., Hofstetter, T.B., 2013. Redox properties of structural Fe in clay minerals: 3. Relationships between smectite redox and structural properties. *Environ. Sci. Technol.* 47, 13477-13485.
- Gustafsson, J.P., Persson, I., Kleja, D.B., van Schaik, J.W.J., 2007. Binding of iron(III) to organic soils: EXAFS spectroscopy and chemical equilibrium modeling. *Environ. Sci. Technol.* 41(4), 1232-1237.
- Hiemstra, T., 2013. Surface and mineral structure of ferrihydrite. *Geochim. Cosmochim. Ac.* 105, 316-325.
- Hiemstra, T., Antelo, J., Rahnemaie, R., Van Riemsdijk, W.H., 2010. Nanoparticles in natural systems I: The effective reactive surface area of the natural oxide fraction in field samples. *Geochim. Cosmochim. Ac.* 74(1), 41-58.
- Hiemstra, T., Van Riemsdijk, W.H., 2006. Biogeochemical speciation of Fe in ocean water. *Mar. Chem.* 102(3-4), 181-197.
- Holmgren, G.G.S., 1967. A rapid citrate-ditionite extractable iron procedure. *Soil Sci. Soc. Am. J.* 31(2), 210-211.
- Jambor, J.L., Dutrizac, J.E., 1998. Occurrence and constitution of natural and synthetic ferrihydrite, a widespread iron oxyhydroxide. *Chem. Rev.* 98(7), 2549-2586.
- Jeanroy, E., Guillet, B., 1981. The occurrence of suspended ferruginous particles in pyrophosphate extracts of some soil horizons. *Geoderma* 26, 95-105.

- Kaegi, R., Voegelin, A., Folini, D., Hug, S.J., 2010. Effect of phosphate, silicate, and Ca on the morphology, structure and elemental composition of Fe(III)-precipitates formed in aerated Fe(II) and As(III) containing water. *Geochim. Cosmochim. Ac.* 74(20), 5798-5816.
- Kaiser, K., Eusterhues, K., Rumpel, C., Guggenberger, G., Kögel-Knabner, I., 2002. Stabilization of organic matter by soil minerals—investigations of density and particle-size fractions from two acid forest soils. *J. Plant Nutr. Soil Sci.* 165(4), 451-459.
- Kaiser, K., Walter, K., Ellerbrock, R.H., Sommer, M., 2011. Effects of land use and mineral characteristics on the organic carbon content, and the amount and composition of Na-pyrophosphate-soluble organic matter, in subsurface soils. *Eur. J. Soil. Sci.* 62, 226-236.
- Karlsson, T.R., Persson, P., Skyllberg, U., Mörth, C.M., Giesler, R., 2008. Characterization of iron(III) in organic soils using Extended X-ray Absorption Fine Structure Spectroscopy. *Env. Sci. Technol.* 42(15), 5449-5454.
- Kiczka, M., Wiederhold, J.G., Frommer, J., Voegelin, A., Kraemer, S.M., Bourdon, B., Kretzschmar, R., 2011. Iron speciation and isotope fractionation during silicate weathering and soil formation in an alpine glacier forefield chronosequence. *Geochim. Cosmochim. Ac.* 75(19), 5559-5573.
- Kleja, D.B., van Schaik, J.W.J., Persson, I., Gustafsson, J.P., 2012. Characterization of iron in floating surface films of some natural waters using EXAFS. *Chem. Geol.* 326-327, 19-26.
- Kretzschmar, R., Borkovec, M., Grolimund, D., Elimelech, M., Mobile subsurface colloids and their role in contaminant transport. *Adv. Agron.* 66, 121-193.
- Kretzschmar, R., Sticher, H., 1997. Transport of humic-coated iron oxide colloids in a sandy soil: Influence of Ca²⁺ and trace metals. *Environ. Sci. Technol.* 31(12), 3497-3504.
- Li, W., He, Y., Wu, J., Xu, J., 2012. Extraction and characterization of natural soil nanoparticles from Chinese soils. *Eur. J. Soil Sci.* 63, 751
- Liang, X., Liu, J., Chen, Y., Li, H., Ye, Y., Nie, Z., Su, M., Xu, Z., 2010. Effect of pH on the release of soil colloidal phosphorus. *J. Soil. Sed.* 10(8), 1548-1556.
- Lyvén, B., Hassellöv, M., Turner, D.R., Haraldsson, C., Andersson, K., 2003. Competition between iron- and carbon-based colloidal carriers for trace metals in a freshwater assessed using flow field-flow fractionation coupled to ICPMS. *Geochim. Cosmochim. Ac.* 67(20), 3791-3802.
- Mermut, A.R., Cano, A.F., 2001. Baseline studies of the clay minerals society source clays: Chemical analyses of major elements *Clay. Clay Mineral.* 49(5), 381-386.
- Mikutta, C., Frommer, J., Voegelin, A., Kaegi, R., Kretzschmar, R., 2010. Effect of citrate on the local Fe coordination in ferrihydrite, arsenate binding, and ternary arsenate complex formation. *Geochim. Cosmoch. Ac.* 74, 5574
- Mikutta, C., Kretzschmar, R., 2011. Spectroscopic evidence for ternary complex formation between arsenate and ferric iron complexes of humic substances. *Environ. Sci. Technol.* 45(22), 9550-9557.
- Mikutta, C., Mikutta, R., Bonneville, S., Wagner, F., Voegelin, A., Christl, I., Kretzschmar, R., 2008. Synthetic coprecipitates of exopolysaccharides and ferrihydrite. Part I: Characterization. *Geochim. Cosmochim. Ac.* 72(4), 1111-1127.
- Mikutta, R., Kaiser, K., 2011. Organic matter bound to mineral surfaces: Resistance to chemical and biological oxidation. *Soil Biol. Biochem.* 43(8), 1738-1741.
- Navrotsky, A., Mazeina, L., Majzlan, J., 2008. Size-driven structural and thermodynamic complexity in iron oxides. *Science* 319(5870), 1635-1638.
- Neubauer, E., Schenkeveld, W.D.C., Plathe, K.L., Rentenberger, C., Von der Kammer, F., Kraemer, S.M., Hofmann, T., 2013a. The influence of pH on iron speciation in podzol extracts: Iron complexes with natural organic matter, and iron mineral nanoparticles. *Sci. Total Environ.* 461-462(0), 108-116.
- Neubauer, E., Von der Kammer, F., Hofmann, T., 2013b. Using FLOWFFF and HPSEC to determine trace metal-colloid associations in wetland runoff. *Water Research* 47(8), 2757-2769.
- O'Day, P.A., Rivera, N., Root, R., Carroll, S.A., 2004. X-ray absorption spectroscopic study of Fe reference compounds for the analysis of natural sediments. *Am. Min.* 89, 572-585.
- Pansu, M., Gautheyrou, J., 2006. *Handbook of Soil Analysis: Mineralogical, Organic and Inorganic Methods.* Springer Berlin Heidelberg New York.
- Plathe, K.L., Von der Kammer, F., Hassellöv, M., Moore, J., Murayama, M., Hofmann, T., Hochella, M.F., 2010. Using FIFFF and aTEM to determine trace metal-nanoparticle associations in riverbed sediment. *Environ. Chem.* 7(1), 82-93.

- Plathe, K.L., Von der Kammer, F., Hassellöv, M., Moore, J.N., Murayama, M., Hofmann, T., Hochella Jr, M.F., 2013. The role of nanominerals and mineral nanoparticles in the transport of toxic trace metals: Field-flow fractionation and analytical TEM analyses after nanoparticle isolation and density separation. *Geochim. Cosmochim. Ac.* 102(0), 213-225.
- Prietzl, J., Thieme, J., Eusterhues, K., Eichert, D., 2007. Iron speciation in soils and soil aggregates by synchrotron-based X-ray microspectroscopy (XANES, μ -XANES). *Eur. J. Soil Sci.* 58(5), 1027-1041.
- Pronk, G.J., Heister, K., Kögel-Knabner, I., 2011. Iron oxides as major available interface component in loamy arable topsoils. *Soil Sci. Soc. Am. J.* 75(6), 2158-2168.
- Ravel, B., Newville, M., 2005. ATHENA, ARTEMIS, HEPHAESTUS: Data analysis for X-ray absorption spectroscopy using IFEFFIT. *J. Synchrotron Rad.* 12(4), 537-541.
- Regelink, I.C., Koopmans, G.F., van der Salm, C., Weng, L., Van Riemsdijk, W.H., 2013a. Characterization of colloidal phosphorus species in drainage waters from a clay soil using Asymmetric flow field-flow fractionation. *J. Environ. Qual.* 42(0), 464-473.
- Regelink, I.C., Temminghoff, E.J.M., 2011. Ni adsorption and Ni-Al LDH precipitation in a sandy aquifer: An experimental and mechanistic modeling study. *Environ. Pollut* 159(3), 716-721.
- Regelink, I.C., Weng, L., Koopmans, G.F., Van Riemsdijk, W.H., 2013b. Asymmetric flow field-flow fractionation as a new approach to analyse iron-(hydr) oxide nanoparticles in soil extracts. *Geoderma* 202, 134-141.
- Rennert, T., Eusterhues, K., De Andrade, V., Totsche, K.U., 2012. Iron species in soils on a mofette site studied by Fe K-edge X-ray absorption near-edge spectroscopy. *Chem. Geol.* 332-333, 116-123.
- Schmidt, M., Rumpel, C., Kögel-Knabner, I., 2008. Evaluation of an ultrasonic dispersion procedure to isolate primary organomineral complexes from soils. *Europ. J. Soil Sci.* 50(1), 87-94.
- Schwertmann, U., 1973. Use of oxalate for Fe extraction from soils. *Can. J. Soil. Sci.* 53(2), 244-246.
- Schwertmann, U., 1991. Solubility and dissolution of iron oxides. *Plant Soil* 130, 1-25.
- Sjöstedt, C., Persson, I., Hesterberg, D., Kleja, D.B., Borg, H., Gustafsson, J.P., 2013. Iron speciation in soft-water lakes and soils as determined by EXAFS spectroscopy and geochemical modelling. *Geochim. Cosmochim. Ac.* 105, 172-186.
- Stolpe, B., Guo, L., Shiller, A.M., Aiken, G.R., 2013. Abundance, size distributions and trace-element binding of organic and iron-rich nanocolloids in Alaskan rivers, as revealed by field-flow fractionation and ICP-MS. *Geochim. Cosmochim. Ac.* 105(0), 221-239.
- Von der Kammer, F., Legros, S., Larsen, E.H., Loeschner, K., Hofmann, T., 2011. Separation and characterization of nanoparticles in complex food and environmental samples by field-flow fractionation. *Trend. Anal. Chem.* 30(3), 425-436.
- Van Schaik, J.W.J., Persson, I., Kleja, D.B., Gustafsson, J.P., 2008. EXAFS Study on the reactions between iron and fulvic acid in acid aqueous solutions. *Environ. Sci. Technol.* 42(7), 2367-2373.
- Vantelon, D., Montarges-Pelletier, E., Moichot, L.J., Briois, V., Pelletier, M., Thomas, F., 2003. Iron distribution in the octahedral smectites. An Fe K-edge X-ray absorption spectroscopy study. *Phys. Chem. Miner.* 30, 44-53.
- Voegelin, A., Kaegi, R., Frommer, J., Vantelon, D., Hug, S.J., 2010. Effect of phosphate, silicate, and Ca on Fe(III)-precipitates formed in aerated Fe(II)- and As(III)-containing water studied by X-ray absorption spectroscopy. *Geochim. Cosmochim. Ac.* 74(1), 164-186.
- Voegelin, A., Senn, A.C., Kaegi, R., Hug, S.J., Mangold, S., 2013. Dynamic Fe-precipitate formation induced by Fe(II) oxidation in aerated phosphate-containing water. *Geochim. Cosmochim. Ac.* 117(0), 216-231.
- Voegelin, A., Weber, F.-A., Kretzschmar, R., 2007. Distribution and speciation of arsenic around roots in a contaminated riparian floodplain soil: Micro-XRF element mapping and EXAFS spectroscopy. *Geochim. Cosmochim. Ac.* 71(23), 5804-5820.
- Wahlund, K.G., Giddings, J.C., 1987. Properties of an Asymmetrical flow field-flow fractionation channel having one permeable wall. *Anal. Chem.* 59(9), 1332-1339.
- Wei, S.Y., Liu, F., Feng, X.H., Tan, W.F., Koopal, L.K., 2011. Formation and transformation of iron oxide-kaolinite associations in the presence of iron(II). *Soil Sci. Soc. Am. J.* 75(1), 45.
- Weng, L., Vega, F.A., Van Riemsdijk, W.H., 2011. Competitive and synergistic effects in pH dependent phosphate adsorption in soils: LCD modeling. *Environ. Sci. Technol.* 45(19), 8420-8428.
- Yong, R.N., Ohtsubo, M., 1987. Interparticle action and rheology of kaolinite-amorphous iron hydroxide complexes. *Appl. Clay Sci.* 2(1), 63-81.

Chapter 4

Characterization of colloidal phosphorus species in drainage waters from a clay soil using asymmetric flow field-flow fractionation

Inge C. Regelink, Gerwin F. Koopmans, Liping Weng, Caroline van der Salm, and Willem H. van Riemsdijk

Published as 'Characterization of colloidal phosphorus species in drainage waters from a clay soil using asymmetric flow field-flow fractionation' in Journal of Environmental Quality, 2013, 42: 464-473



Abstract

Phosphorus (P) transport from agricultural land contributes to eutrophication of surface waters. Pipe drain and trench waters from a grassland field on a heavy clay soil in The Netherlands were sampled before and after manure application. Phosphorus speciation was analyzed by physico-chemical P fractionation and the colloidal P fraction in the dissolved fraction ($<0.45\mu\text{m}$) was analyzed by Asymmetric Flow Field-Flow Fractionation (AF4) coupled to High-Resolution Inductively Coupled Plasma Mass-Spectrometry and Ultraviolet-Diode Array Detector. When no manure was applied for almost seven months, Total P (TP) concentrations were low ($<21\ \mu\text{M}$), and TP was almost evenly distributed among Dissolved Reactive Phosphorus (DRP), Dissolved Unreactive P (DUP), and Particulate P (PP). Total P concentrations increased by a factor of 60 and 4 when rainfall followed shortly after application of cattle slurry or its solid fraction, respectively. Under these conditions, DRP contributed 50% or more to TP. The P speciation within the DUP and PP fractions varied among the different sampling times. Phosphorus associated to dissolved organic matter, likely via cation bridging, comprised a small fraction of DUP at all sampling times. Colloidal P co-eluted with clay particles when P application was withheld for almost seven months and after application of the solid cattle slurry fraction. At these sampling times, PP correlated well with particulate Fe, Al, and Si indicating that P is associated with colloidal clay particles. After cattle slurry application, part of DUP was likely present as phospholipids. Physico-chemical fractionation combined with AF4 analysis is a promising tool to unravel the speciation of colloidal P in environmental water samples.

4.1 Introduction

Transport of Phosphorus (P) from agricultural land contributes to P enrichment and eutrophication of surface waters (Correll, 1998). Clay soils represent 42% of the agricultural land in The Netherlands (Wolf et al., 2003) and are an important source of P losses to Dutch surface waters (Van der Salm et al., 2012). Phosphorus transport via trenches is an important and rapid pathway for P losses from Dutch clay soils to surface waters, owing to the low water conductivity of these soils (Van der Salm et al., 2012). Similar artificial drainage networks such as grassed waterways, surface or field drains, and furrows are common on heavier textured soils worldwide (Lentz and Lehrsch, 2010; Udawatta et al., 2004). In addition, significant P losses from clay soils via pipe drain water have been found as well, despite the high P sorption capacity of the subsoil (Addiscot et al., 2000; Van der Salm et al.,

2012; Turtola and Paajanen, 1995). This has been attributed to the rapid transport of water and P via preferential pathways such as clay shrinkage cracks and macropores (Addiscot et al., 2000; Van der Salm et al., 2012; Turtola and Paajanen, 1995).

A wide variety of organic and inorganic P species can be present in environmental water samples (Van Moorlegghem et al., 2011). For example, organic P species such as inositol hexakisphosphate (phytic acid), deoxyribonucleic acids (DNA), and phospholipids were found in leachate waters (Espinosa et al., 1999; Toor et al., 2003) and water extracts from agricultural soils (Turner et al., 2002). Orthophosphate is the major inorganic P form in environmental water samples. Besides the dissolved orthophosphate species, P can be present as orthophosphate-metal-humic matter complexes (Gerke, 2010; Hens and Merckx, 2001), colloidal Ca-phosphate precipitates, or it can be associated with colloidal clay and metal oxide particles (Dominik et al., 2008; Uusitalo et al., 2001). Transport of organic and inorganic P associated to colloidal particles is especially important in clay soils, and has been demonstrated to contribute significantly to P losses from clay soils to surface waters (Uusitalo et al., 1999; Uusitalo et al., 2001; Van der Salm et al., 2012). Understanding the speciation of P in agricultural discharge waters is important, because the various P species differ in their bioavailability in aquatic ecosystems (Ekholm, 1994). For example, P in the form of dissolved orthophosphate is directly available for uptake by algae (Ekholm, 1994) whereas orthophosphate associated to mineral colloids first has to be released by desorption before it becomes available for uptake by biota (Uusitalo et al., 1999). In addition to this, knowledge on the P speciation in agricultural discharge waters is essential to the development of strategies to minimize P losses to surface water (Buda et al., 2012). Physico-chemical fractionation of P is a popular method to distinguish between different P forms in environmental water samples (Chardon et al., 2007; Heathwaite et al., 2005; Van der Salm et al., 2012; Toor et al., 2003; Uusitalo et al., 2001). In this approach, the fraction of P larger than 0.45 μm is defined as Particulate P (PP), while the P fraction able to pass the filter is defined as dissolved P. The P fraction smaller than 0.45 μm is often further fractionated into Dissolved Reactive P (DRP), as measured by a colorimetric method (Murphy and Riley, 1962). The DRP fraction is generally considered to represent orthophosphate, although inorganic colloidal P forms can contribute to this fraction (Sinaj et al., 1998; Van Moorlegghem et al., 2011). The difference between Total Dissolved Phosphorus (TDP) and DRP is called Dissolved Unreactive P (DUP), which can consist of both dissolved organic P species and orthophosphate associated with inorganic colloids (Turner et al., 2002). Hence, with physico-chemical fractionation, the speciation of P within the DUP fraction but also

within the PP fraction remains unclear.

In a previous study, P losses from a heavy clay soil under agricultural grassland in a Dutch fluvial plain to surface water were monitored during a five-year period (Van der Salm et al., 2012). Phosphorus transport by rapid discharge through trenches was found to be the most important transport pathway for P losses (60–90%) and annual P losses were dominated by PP (69–71%). The contributions of DUP and DRP were lower but still significant (18–19% and 10–13%). The extent of the P losses largely depended on the amount of P added in the form of inorganic P fertilizer and cattle slurry and on the timing of P application in relation to local weather conditions (Van der Salm et al., 2012). In this follow-up study, we analyzed the P speciation in water discharge samples from the trenches and pipe drains from the same grassland field as in the previous monitoring study (Van der Salm et al., 2012). Since the application of cattle slurry was expected to influence the P speciation in the water discharge samples, we took samples at different occasions, i.e., when P application was withheld for almost seven months and shortly after cattle slurry application. Also, samples were taken at a third occasion when the solid fraction of cattle slurry was applied. In The Netherlands, solid-liquid separation of cattle slurry is increasingly used in practice because it reduces the volume of the manure and thus costs are lower when the manure has to be transported off-farm (Verloop et al., 2009). In addition to physico-chemical fractionation, we analyzed the DUP fraction in the pipe drain and trench water samples using Asymmetric Flow Field-Flow Fractionation (AF4) coupled to a High Resolution-Inductively Coupled Plasma-Mass Spectrometer (HR-ICP-MS) and Ultraviolet-Diode Array Detection (UV-DAD). AF4 is a chromatographic-like technique for size-fractionation of colloids and allows for online multi-element detection in combination with HR-ICP-MS. This technique was successfully applied to analyze (trace)elements associated to colloids in environmental water samples (Lyvén et al., 2003; Plathe et al., 2010; Regelink et al., 2011; Stolpe et al., 2010), but, to the best of our knowledge, it has not been used yet to characterize colloidal P in natural waters (pipe drain and trench waters). Our specific objectives were (1) to measure the speciation of P in the water discharge samples from trenches and pipe drains from a grassland field by physico-chemical P fractionation, (2) to unravel the P speciation contained within the DUP fraction by AF4 coupled to HR-ICP-MS and UV-DAD, and (3) to understand the link between P speciation and the agricultural P management conditions at the time of sampling.

4.2 Material and Methods

4.2.1 *Experimental Field and Agricultural Management*

The pipe drain and trench water samples were collected from a grassland field on a dairy farm near Waardenburg, which is located in a fluvial plain in the central part of The Netherlands. The grassland field and the soil sampling protocol and the physical and chemical soil characteristics were previously described in detail by Koopmans et al. (2005) and Van der Salm et al. (2012). In short, the soil is a heavy clay and can be classified as a Eutric Fluvisol. The soil profile was characterized by the presence of an Apg horizon (0-0.4 m) and a Cg horizon (0.4-1.0 m). The clay content in the Apg and Cg horizons was 56.8 and 58.5%, respectively. The Apg horizon had a pH-CaCl₂ (0.01 M CaCl₂) of 6.7 and Soil Organic Matter (SOM) and CaCO₃ amounted to 5.4 and 0.4%, respectively. The Cg horizon had a pH-CaCl₂ of 7.6, a SOM content of 2.3%, and a CaCO₃ content of 0.7%. The total P content, as measured after combustion of SOM in a muffle furnace and subsequent extraction of the soil by 0.5 M H₂SO₄, in the Apg and Cg horizons was 747 and 494 mg kg⁻¹, respectively, of which 60 and 32% was organic. The field is about 175 m long and 90 m wide and drained by two trenches and twelve pipe drains. The short side of the field adjoined a ditch which received all water from the field. The trenches and pipe drains were installed perpendicular to the ditch. The trenches have a width and depth of 0.5 m and an intermediate distance of 45 m. The land between the trenches is slightly elevated (0.4 m) to facilitate rapid water drainage. The pipe drains have an intermediate distance of about 7 m and were installed at about 0.8 m below the soil surface. The grassland field is dominated by *Lolium perenne* and the grass is cut for silage and grazed between cuts, which is a common practice on dairy farms in The Netherlands. Cattle slurry is applied two to three times a year in spring and summer using a trailing foot and inorganic P fertilizer is applied once a year in early spring. In addition, the solid fraction of cattle slurry obtained after solid-liquid separation (based on filtration) was applied in early spring of 2011. The 30-yr average precipitation and evapotranspiration amount to respectively 785 and 543 mm yr⁻¹, which leads to an average precipitation surplus of 242 mm yr⁻¹. The 30-yr average temperature is 9.8 °C, with a minimum monthly average of 2.8 °C in January and a maximum of 17.4 °C in July (Royal Meteorological Dutch Institute, 2011).

4.2.2 *Sampling Program*

We used the same experimental set-up and equipment for the sampling of pipe drain and trench waters as used in the previous monitoring study (Van der Salm et al., 2012), which was performed in the period 2002-2008. In short, the twelve pipe drains were grouped into two sets of six adjacent drains. The water discharge of the two trenches and the two sets of drains was led to small collectors with a V-notch opening and water discharge rates were monitored by measuring the water level in the collectors (ISCO 3220 flow meter). Water samples were taken by an autosampler (ISCO 3700 sampler) in a flow proportional manner at fixed water discharge intervals (0.12 mm) and stored in the dark at 5 °C in the field. In this follow-up study, pipe drain and trench waters were collected at three occasions in 2010 and 2011 representing three different agricultural P management conditions. Water discharge samples were collected when:

- 1) no cattle slurry or inorganic P fertilizer had been applied for almost seven months. During the sampling period, a rainfall event with 28 mm of precipitation occurred and the pipe drain and trench water samples were collected on February 7, 2011 (t1).
- 2) P was applied on February 21, 2011 in the form of the solid fraction of cattle slurry, which was obtained after solid-liquid separation (Verloop et al., 2009), at a rate of 6.6 kg P ha⁻¹. This P application was followed by 19 mm of precipitation until the time of sampling of pipe drain and trench waters on March 1, 2011 (t2).
- 3) P was applied on March 29, 2010 in the form of cattle slurry at a rate of 19 kg P ha⁻¹, followed by 20 mm of precipitation until the time of sampling of drain and trench waters on April 1, 2010 (t3).

The sampling period lasted seven days for t1 and t2 and eight days for t3. The two trenches and the two sets of pipe drains were treated in this follow-up study as replicates. The water discharge samples were stored in the dark at 5 °C after addition of sodium azide (NaN₃) with a final concentration of 1 mM to prevent microbial activity. Addition of NaN₃ at this concentration does not cause lysis of microbial cells (Koshlukova et al., 1999). The AF4 and UV-DAD equipment was implemented in our laboratory in March 2011. Hence, all AF4-related work was carried out in this period.

4.2.3 *Chemical Analyses and Physico-Chemical Fractionation of the Water Discharge Samples*

Total P (TP) was measured spectrophotometrically using the molybdenum-blue method (Murphy and Riley, 1962) in the unfiltered water discharge samples after acid digestion of the

sample with $K_2S_2O_8$ (Ebina et al., 1983). Furthermore, total P, Fe, Si, and Al were determined after digestion of the unfiltered water samples with Aqua Regia (ISO 15587-1). Phosphorus and metal concentrations in the digests were measured by an Inductively Coupled Plasma-Atomic Emission Spectrometer (ICP-AES; Varian Vista Pro). Total P measured in the water discharge samples after digestion with Aqua Regia (results not shown) was similar to total P measured after digestion with $K_2S_2O_8$. The pH and EC were measured in the unfiltered water samples. Before analysis of the dissolved P fractions, the water samples were passed through a $0.45\ \mu\text{m}$ filter (Aqua 30, Whatman). Total dissolved P, Fe, Si, Al, and Ca were measured by ICP-AES and orthophosphate was measured spectrophotometrically as DRP using the molybdenum-blue method (Murphy and Riley, 1962). Dissolved Unreactive P was calculated as TDP minus DRP. Particulate P, Fe, Si, and Al were calculated as the total concentration in the unfiltered water samples minus their total dissolved concentration in the filtered water samples. Dissolved Organic Carbon (DOC) in the filtered samples was measured using a fully automated segmented flow analyzer (Skalar SK12) by persulfate and tetraborate oxidation under UV light and infrared detection.

4.2.4 Analyzes of the Colloidal Fraction in the Water Discharge Samples

An AF4 system (Postnova Analytics, Germany) was used for size-fractionation of the colloidal particles. The principles of AF4 size-fractionation are described in detail elsewhere (Von der Kammer et al., 2011). A 3 mM NaHCO_3 solution at pH 8.3 was used as carrier. Overnight, the system was flushed with 15% (v/v) ethanol to prevent microbial activity. The injection volume was 1 ml and the injection/focusing time was 15 min, using a cross flow of $3\ \text{ml}\ \text{min}^{-1}$. A sufficiently large focusing time is needed to focus the particles in the right position, and to remove the truly dissolved species from the column. In a preliminary test, an injection/focusing time of 15 min was found to be sufficiently long to remove more than 95% of the truly dissolved orthophosphate when using a 100 mM Na_2HPO_4 solution. The remaining orthophosphate eluted as a narrow salt peak at t_0 .

The cross flow rate was $3\ \text{ml}\ \text{min}^{-1}$ for the first 14 minutes (t_0 - t_{14}) and thereafter, the cross flow decreased in 2 min to $0.2\ \text{ml}\ \text{min}^{-1}$ in a linear manner and was maintained at this rate from the 16th to the 30th minute (t_{16} - t_{30}). The use of a stepwise change in cross flow rate allows for fractionation of particles $<13\ \text{nm}$ in size with a high size-resolution and fractionation of particles 13-100 nm in size with a lower size-resolution. These running parameters were chosen since we expected a broad size-distribution of colloids in the water discharge samples. The detector flow was coupled to an UV-DAD detector (Postnova Analytics), which

measured the UV/VIS spectrum (210-800 nm) every 0.6 s. Consecutively, the detector flow was coupled to a HR-ICP-MS (Thermo Element 2), which measured the Fe, Al, Si, Ca, Mg, and P concentrations every 10 s. Calibration of the HR-ICP-MS was done at the beginning and at the end of each measurement day to correct for a decrease in sensitivity over time. An overview of the AF4, UV-DAD, and HR-ICP-MS parameters is given in Table 4.1.

Table 4.1. Analytical instrumentation parameters used for particle separation by AF4 coupled to UV-DAD and HR-ICP-MS.

AF4	AF2000, Postnova Analytics
Membrane	1 kDa polyethersulfone (PES)
Spacer thickness	350 μm
Injection volume	1 ml
Focussing time	15 min
Cross flow during focusing	3 ml min ⁻¹
Cross flow rate t ₀ -t ₁₅	3 ml min ⁻¹
Cross flow rate t ₁₈ -t ₃₀	0.2 ml min ⁻¹
Detector flow rate	0.5 ml min ⁻¹
Slot pump flow rate	0.5 ml min ⁻¹
Carrier	3 mM NaHCO ₃
UV-Detector	Postnova Analytics
Monitored wavelength	254 nm
HR-ICP-MS	Thermo Element 2
Monitored elements ^a	Fe(56), Al(27), Si(28), Ca(44), Mg(24), P(31)
Time per reading	10 sec

a Monitored mass of the elements is given between brackets.

A combination of calibration, using standard particles, and AF4 theory was used to derive the relationship between particle size and retention time. AF4 theory was used to calculate the particle diameter during t_0 - t_{14} of the elution step when the cross flow rate was constant. The theory behind AF4 fractionation, based on ideal behavior of spherical particles, is well known for running conditions using a constant cross flow (Litzén, 1993; Wahlund and Giddings, 1987). The linear relation between the hydrodynamic particle diameter and the retention time can be calculated using Eq. 4.1 and Eq. 4.2.

$$d_h = \frac{2KT V_0 t_r}{\pi \eta Q_c w^2 t_0} \quad (4.1)$$

$$t_0 = \frac{V_0}{Q_c} \ln \left(1 + \frac{Q_c}{Q_{out}} \right) \quad (4.2)$$

where t_0 = void time (s); t_r = retention time (s); d_h = hydrodynamic diameter (m); T = absolute temperature (K); K = Boltzmann constant (1.38×10^{-23} J K⁻¹); η = viscosity (1.00×10^{-3} Pa.s); w = channel thickness (m); V_0 = void volume (m³); Q_c = cross-flow rate (m³s⁻¹); Q_{out} = outlet flow rate (detector plus slot flow rate)(m³s⁻¹). According to AF4 theory, particles smaller than 13 nm were eluted during t_0 - t_{14} of the elution step. In addition to this, polystyrene sulfonate standards (Postnova Analytics) with known molecular weights of 1.1, 15.8, and 75.6 kDa were used to check whether it was possible to separate particles during t_0 - t_{14} of the elution step. These particle standards were used because polystyrene nanoparticles with a diameter smaller than 13 nm defined in terms of size were not available. The fractogram of these particle standards was well resolved, with a retention time of the particles amounting to 0.6, 2.9, and 11 min (Figure A2). Application of AF4 theory becomes more complicated when the cross flow rate is not constant, i.e., after 14 minutes of the elution step. Therefore, NIST-certified polystyrene nanoparticles (Postnova Analytics) with a diameter of 20, 50, and 100 nm were used for calibration for t_{16} - t_{30} of the elution step. The fractogram of these standard nanoparticles was well resolved, with a retention time of the particles amounting to 16, 18, and 23 min, respectively (Figure A2). Retention time from this fractogram was used to establish a linear relationship of the particle diameter versus the elution time ($R^2=0.99$). Subsequently, this relationship was used to calculate the diameter of particles eluted during t_{16} - t_{30} . Despite our effort to quantify the particle diameter of the colloids in the agricultural discharge waters, the actual size of the colloids can deviate somewhat from the calculated particle diameters, due to non-ideal behavior of the colloids or the particle standards or due to a non-spherical shape of the particles.

The filtered (0.45 μ m) pipe drain and trench water samples taken at t_1 , t_2 , and t_3 were analyzed using AF4 coupled to UV-DAD and HR-ICP-MS. For t_1 and t_2 , one replicate of the pipe drain and trench water samples was analyzed. For t_3 , both replicate samples of the pipe drain and trench waters were analyzed.

Concentrations of DOC eluted during the first 5 min of the AF4 runs were estimated based on calibration of the UV-signal with standard Suwannee River Fulvic Acid (FA)

(International Humic Substances Society). Fulvic Acid was dissolved in ultrapure water at a concentration of 2, 4, 8 and 16 mg l⁻¹, and the UV-absorbance was recorded with UV-DAD. Based on the UV-DAD results and the FA concentrations, a linear relationship was established ($R^2=0.99$) (results not shown), which was used to estimate the DOC concentrations eluted during the first 5 min.

In an accompanying experiment, the UV spectrum of phytic acid was obtained by measuring the UV spectrum of a 3 mM NaHCO₃ solution containing dodeca-sodium-phytic acid solution at a P concentration of 10 µM by the UV-DAD detector.

4.2.5 *Statistical Analysis*

Data of TP, DRP, DUP, and PP concentrations were log-transformed to meet analysis of variance (ANOVA) requirements and subjected to ANOVA. The means of parameters for which significant treatment effects were found were separated using the Least Significant Difference (LSD) test ($P<0.05$).

4.3 **Results and Discussion**

4.3.1 *General Characteristics of the Pipe Drain and Trench Waters*

Total water volumes discharged by the pipe drains and trenches of the grassland field varied substantially between sampling times, with 5 mm of water discharged over seven days at t2 to 27 mm over eight days at t3 (Table 4.2). The trenches contributed 54 to 95% of the total water discharge at the three sampling times, despite the level terrain of the field (slope <1%). The pipe drain and trench waters had neutral to slightly alkaline pH values varying between 7.0 and 7.5. Both dissolved and particulate concentrations of Fe, Si, and Al were higher in the trench waters than those in the pipe drain waters at all sampling times. In contrast, the dissolved Ca concentrations in the pipe drain waters was higher than those in the trench waters, which may be due to a longer contact time of the water transported through the solid phase before it entered the pipe drains (Van der Salm et al., 2012). The dissolved and particulate metal concentrations strongly differ among the three sampling times, which may be caused by factors such as temporal differences in water discharge and ionic strength. The DOC concentrations in the pipe drain and trench waters at t3 were much higher than those at the other sampling times, probably resulting from the application of cattle slurry shortly before sampling at t3.

Characterization of colloidal phosphorus in drainage waters

Table 4.2. General and chemical characteristics of the pipe drain and trench water samples.^a

Fertilizer	t1		t2		t3	
	No ^b		Solid fraction of cattle slurry		Cattle slurry	
	Trenches	Drains	Trenches	Drains	Trenches	Drains
Discharge(mm)	3.8 ± 0.6	5 ± 0.7	4.8 ± 0.3	0.3 ± 0.3	19.1 ± 0.1	7.8 ± 0.1
pH (-) ^d	7.07 ± 0.0	7.12 ± 0.0	7.49 ± 0.0	6.98 ± 0.0	7.23 ± 0.0	7.30 ± 0.2
EC (µS cm ⁻¹) ^d	108 ± 15	753 ± 45	185 ± 4.2	589 ± 57	995 ± 7.0	733 ± 164.1
DOC (mg l ⁻¹) ^e	17.3 ± 2.5	8.8 ± 0.1	26.5 ± 0.1	12.5 ± 1.8	100.5 ± 2.1	41.9 ± 6.2
Ca (mM) ^e	0.3 ± 0.0	3.4 ± 0.3	0.5 ± 0.0	2.5 ± 0.3	1.7 ± 0.1	2.1 ± 0.5
Fe (µM) ^e	25.7 ± 13.4	0.4 ± 0.3	25.9 ± 6.7	5.6 ± 2.5	8.8 ± 1.6	7.3 ± 1.3
Al (µM) ^e	65.6 ± 38.2	0.19 ± 0.0	76.7 ± 21.4	15 ± 8.1	11.1 ± 1.4	1.35 ± 0.9
Si (µM) ^e	308 ± 235	165 ± 6.8	204 ± 45	156 ± 3.5	220 ± 0.2.2	160 ± 22.1
P-Fe (µM) ^f	126.9 ± 10.6	11.0 ± 21.1	114.1 ± 59.8	31.8 ± 19.2	21.23 ± 3.6	26.07 ± 8.9
P-Al (µM) ^f	221.0 ± 41.1	3.6 ± 3.0	151.6 ± 95.4	51.4 ± 30.6	50.9 ± 6.3	47.9 ± 14.0
P-Si (µM) ^f	374.2 ± 184.4	< d.l. ^g	371.9 ± 281	118.6 ± 71.4	114.9 ± 16.0	107.6 ± 22.3

a Values are mean and standard deviation of the two replicates.

b No cattle slurry or inorganic P fertilizer was applied for almost seven months.

c Total discharge measured over seven days (t1 and t2) or eight days (t3).

d Measured in unfiltered samples.

e Measured in filtered samples (0.45 µm).

f Particulate Fe, Al, and Si; no Ca was not detectable in the particulate form.

g Detection limit.

Table 4.3. Physico-chemical fractionation of total P (TP) in Dissolved Reactive P (DRP), Dissolved Unreactive P (DUP) and Particulate P (PP).^a

Fertilizer	t1		t2		t3	
	No		Solid fraction of cattle slurry		Cattle slurry	
	Trenches	Drains	Trenches	Drains	Trenches	Drains
DRP (µM)	7.7 ± 6.9 ^a (34 ± 21)	0.3 ± 0.1 ^d (15 ± 15)	64.7 ± 42.2 ^{ab} (78 ± 14)	6.9 ± 4.2 ^e (54 ± 7)	164 ± 12.6 ^b (65 ± 1)	57.8 ± 5.5 ^f (50 ± 2)
DUP (µM)	6.2 ± 1.9 ^a (30 ± 1)	0.8 ± 0.1 ^d (38 ± 29)	7.1 ± 2.3 ^a (9 ± 2)	1.5 ± 0.8 ^d (12 ± 1)	37.5 ± 5.0 ^b (15 ± 1)	11.1 ± 5.3 ^e (10 ± 4)
PP (µM)	6.8 ± 4.1 ^a (36 ± 20)	2.0 ± 1.1 ^d (48 ± 44)	8.1 ± 4.1 ^a (13 ± 12)	4.0 ± 1.1 ^d (34 ± 8)	49.2 ± 1.6 ^b (20 ± 2)	46.2 ± 0.5 ^e (40 ± 4)
TP (µM)	20.7 ± 7.3 ^a (100)	3.1 ± 2.5 ^d (100)	79.9 ± 40.4 ^b (100)	12.4 ± 6.2 ^d (100)	251 ± 16.0 ^c (100)	115 ± 10.3 ^c (100)

a Values are average ± standard deviation of the two replicates. Percentage of each fraction to TP is presented between brackets. Different letters denote a significant difference (P<0.05) between the different sampling times for either trenches (a,b, and c) or pipe drains (d,e, and f).

4.3.2 *Total Phosphorus in the Pipe Drain and Trench Waters*

The TP concentrations in the pipe drain and trench waters varied among sampling times, and followed the order $t_1 < t_2 < t_3$ (Table 4.3). When no P was applied for almost seven months (t_1), the TP concentrations in the pipe drain and trench waters were 3.1 and 20.7 μM , respectively. After the application of P at a rate of 6.6 kg P ha^{-1} with the solid fraction of the cattle slurry at t_2 , the TP concentrations in the pipe drain and trench waters increased to 12 and 80 μM , respectively. The TP concentrations in drain and trench waters were significantly higher at t_3 (115 and 251 μM), when precipitation followed shortly after P application of 19 kg P ha^{-1} with cattle slurry. With the exception of the TP concentration in the pipe drain water at t_1 , all TP concentrations clearly exceeded the Dutch threshold for TP in surface waters (5 μM). The TP concentrations in the pipe drain waters were on average a factor of 5 lower than those in the trench waters, which can be explained by retention of P in the subsoil. Nevertheless, TP concentrations in pipe drain waters quickly increased when precipitation interacted with the manure applied in the solid form at t_2 and in the slurry form at t_3 . Since the soil matrix of the field has a very low saturated conductivity of about 1.3 mm d^{-1} (Van der Salm et al., 2012), this fast response of TP in the pipe drain waters indicates the existence of rapid preferential transport pathways. The TP losses at t_1 and t_2 amounted to 0.03 and 0.12 kg ha^{-1} , respectively, which correspond to 1 and 4% of the five-year average annual TP loss from the same grassland field (3.0 kg $\text{ha}^{-1} \text{y}^{-1}$) (Van der Salm et al., 2012). In contrast, the TP loss at t_3 amounted to 1.7 kg ha^{-1} , which equals 58% of this five-year average annual TP loss. Hence, the TP loss from the grassland field at t_3 was largely controlled by an Incidental Loss (IL). Fresh P applications may cause an IL of P to surface waters when precipitation interacts directly with the animal manure or inorganic P fertilizer spread onto the soil surface and although these events occur only once or twice per year, they can typically make the dominant contribution of >50% of the annual TP loss (Van der Salm et al., 2012; Withers et al., 2003).

4.3.3 *Physico-chemical Fractionation of Phosphorus in the Pipe Drain and Trench Waters*

Results of the physico-chemical fractionation of TP into DRP, DUP, and PP are presented in Table 4.3. The lowest DRP concentrations were found in the trench and pipe drain waters of t_1 (7.7 and 0.3 μM) when no P was applied for almost seven months. However, the DRP concentrations in the trench and pipe drain waters increased at t_2 to 64.7 and 6.9 μM , respectively. At t_3 , significantly higher DRP concentrations of 164.2 and 57.8 μM were found

in the trench and pipe drain waters, respectively. Thus, rainfall following application of solid cattle manure (t2) or cattle slurry (t3) results in an increase of the DRP concentration in the water discharge samples. This is not surprising since P in cattle manure is known to consist for a large part of orthophosphate (Toor et al., 2005; Turner and Leytem, 2004). The DUP concentrations in the trench and pipe drain waters were low at t1 (6.2 and 0.8 μM) and t2 (7.1 and 1.5 μM). In contrast, significantly higher DUP concentrations were found at t3 in both the trench (37.5 μM) and pipe drain waters (11.1 μM). Hence, the DUP concentrations strongly increased when rainfall interacted with cattle slurry. So the source of DUP and, therefore, the P species present in the DUP fraction, is likely to be different between sampling times. With traditional physico-chemical P fractionation, DUP cannot be further speciated. For this purpose, other techniques like AF4 coupled to HR-ICP-MS and UV-DAD may be helpful, as will be demonstrated in a later stage of this paper.

For all sampling times, the PP fraction contributed 13 to 48% to TP. For the pipe drain and trench water samples collected at t1 and t2, the PP concentrations show a strong

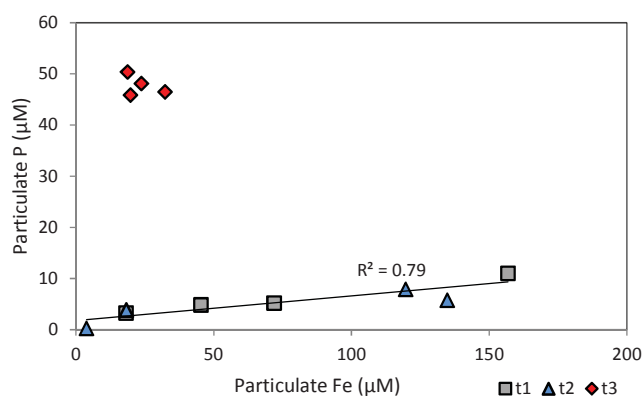


Figure 4.1. Particulate P plotted against particulate Fe in drain and trench waters sampled at t1, t2 and t3.

correlation with the particulate Fe concentrations (Figure 4.1). This can be explained by the association of P in the PP fraction to particulate clay particles. However, the data points of t3, when the PP concentrations were strongly elevated (Table 4.3), clearly deviate from this relationship (Appendix C, Figure C1). At t3, the ratios of PP to particulate Fe, Al, and Si are much higher than those at t1 and t2. Based on the particulate Si and Al concentrations, we calculated the P/clay ratio in these samples, assuming all Al and Si to be present in the form of the clay mineral illite ($\text{Si}_{6.77}\text{Al}_{3.92}\text{Fe}_{0.82}\text{O}_{20}(\text{OH})_4$) (Mermut and Cano, 2001). Illite

is the dominant clay mineral in Dutch fluvial clay soils (Van der Salm et al., 1998). The P/clay ratio ($4.2 \text{ mmol g}^{-1} \text{ clay}$) but also the P/Fe ratio (2.1 mol mol^{-1}) are much higher than the P sorption capacities of clay minerals ($0.08 \text{ mmol g}^{-1} \text{ clay}$) (Edzwald et al., 1976) and Fe-(hydr)oxides (P/Fe: 0.5 mol mol^{-1}) (Dominik et al., 2008). Thus, the high PP concentrations in the water samples of t3 cannot be explained by P associated to mineral particles and the nature of PP at this sampling time remains unknown. This will be further elaborated when discussing the results of AF4 analyses.

4.3.4 AF4 of the Pipe Drain and Trench Waters

The colloids contained within the ≈ 1 to 100 nm size fraction of the filtered ($0.45 \text{ }\mu\text{m}$) water discharge samples were analyzed by AF4 coupled online to HR-ICP-MS and UV-DAD. The colloids were fractionated based on size and online analyzed for their elemental composition and UV spectrum. Truly dissolved P species are removed from the column and are thus not recovered. Recoveries of colloid-sized P concentrations in terms of DUP were between 42 and 65%. Incomplete recoveries of the DUP fraction can be explained by the difference between the studied size-range of the colloids during the AF4 analyses (hydrodynamic diameter of ≈ 1 nm to 100 nm) and the pore size of the filter (450 nm) used to separate DUP from PP. Also, some loss of colloidal particles can occur due to binding of particles to the polyethersulfone (PES) membrane.

Since the fractionation results of the colloidal P in the trench and pipe drain waters is similar for the samples taken at t1 and t2, the results of these sampling times are discussed simultaneously here, whereas the results for t3 will be discussed separately below. Fractograms of the trench waters sampled at t1 and t2 are presented in Figure 4.2, whereas the results for the pipe drain waters at these sampling times are available in Appendix C, Figures C1. The fractograms of the pipe drain and trench waters show the presence of colloidal Dissolved Organic Matter (DOM) molecules in the 1-5 nm size range. This peak is characterized by a high UV absorbance at 254 nm, which is typical for FA and humic acids. Humic-rich colloidal particles with a similar size were found with flow field-flow fractionation coupled to UV in surface waters (Baalousha and Lead, 2007). In the pipe drain and trench waters, Fe and Ca elute simultaneously with the DOM in the 1-5 nm size range (Figure 4.2). Hence, these cations are likely to be associated to the DOM. Also, P co-elutes with the DOM, although only in very low concentrations. Some of this P may be incorporated with humic substances, because standard purified FA contain on average 0.4% P (w/w), *i.e.*, the molar P/DOC ratio is 0.0003 (International Humic Substances Society,

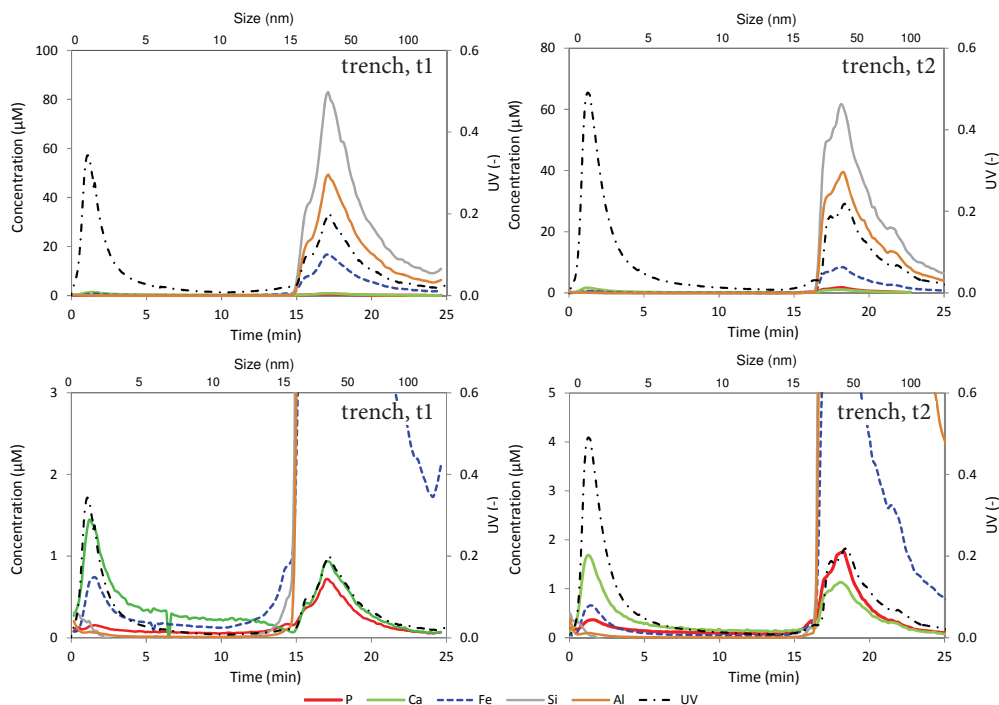


Figure 4.2. AF4 fractograms showing the elemental composition and UV absorbance (254 nm) of the colloids in the trench waters collected at t1 (when no manure was applied for almost 7 months) and at t2 (when rainfall followed after application of the solid fraction of cattle slurry). Figures in the upper panel are at a large scale whereas figures in the lower panel are at a smaller scale.

2011). We used the UV-absorbance in the DOM peak to estimate the FA concentration using a calibration curve of UV-absorbance for a standard FA. Estimated FA concentrations were below 1 mg C l^{-1} in the pipe drain and trench waters for t1 and t2. The FA concentrations in the water discharge waters were low compared to total DOC concentrations (Table 4.2), which can be explained by a large fraction of smaller organic compounds able to pass the 1 kDa membrane of the AF4. Using this FA concentration, the amount of P incorporated within FA can at most explain 10% of the amount of P associated with the DOM fraction. Therefore, the majority of P is likely to be present as a complex with the DOM molecules. Orthophosphate does not bind directly to humic substances, but metal ions can form a bridge between orthophosphate and DOM leading to the formation of Orthophosphate-Metal-DOM ($\text{PO}_4\text{-M-DOM}$) complexes. Trivalent cations like Fe^{3+} are thought to be the most important metals for the formation of such ternary complexes (Gerke, 2010). Measured

molar ratios between Fe and P in the DOM peak of the fractograms are above 1, which supports the presence of $\text{PO}_4\text{-M-DOM}$ complexes. The amount of P associated to the DOM in the 1-5 nm size range, which is likely to be in the form of $\text{PO}_4\text{-M-DOM}$ complexes, is $\approx 6\%$ of the DUP concentration in the trench water at t1 and $\approx 7\%$ and $\approx 12\%$ in the trench and pipe drain waters at t2, respectively. Concentrations of colloidal P in the pipe drain water collected at t1 were below the detection limit of the HR-ICP-MS. There is some uncertainty in these values because the concentrations of P associated to DOM are near the detection limit of the HR-ICP-MS, and, although hardly detectable, there may be a small contribution of orthophosphate eluting as a void peak at t0. Also, in other studies, P containing ternary complexes have been found in soil solutions of sandy and loamy soils (Gerke, 1992; Hens and Merckx, 2001). In a study of Hens and Merckx (2001) using Gel Permeation Chromatography (GPC), $\text{PO}_4\text{-M-DOM}$ complexes were present in the high molecular weight organic matter (>600 kDa) fraction of DOM. In contrast, the $\text{PO}_4\text{-M-DOM}$ complexes found in this study were in the 1-5 nm size-range, which corresponds to a molecular weight of 1 to ≈ 10 kDa. This difference may be related to the much higher ionic strength used in the GPC analyses (0.15 M NaCl) of Hens and Merckx (2001) as compared to the ionic strength of the carrier used in our AF4 analyses (3 mM NaHCO_3). A higher ionic strength can lead to coagulation of humic substances, leading to a larger particle size (Weng et al., 2002).

The fractograms of the trench waters (Figure 4.2) and pipe drain waters (Appendix C, Figure C1) collected at t1 and t2 show the presence of a second peak at 15-100 nm containing Si, Al, and Fe. The average molar Si/Al ratio of these particles is about 1.7 indicating the presence of 2:1 clay minerals, which is likely to be illite (Van der Salm et al., 1998). The average molar Fe/Si ratio in this size range is 0.3, which is higher than the molar Fe/Si ratio of illite, i.e., 0.13, as reported by Mermut and Cano (2001). Apparently, besides Fe being structurally incorporated within clay minerals, some additional Fe may be present on the clay surface as a Fe-(hydr)oxide coating. The concentrations of colloidal clay particles were higher in the trench waters (Figure 4.2) than those in the pipe drain waters (Appendix C, C1). This is in line with the higher total dissolved concentrations of Fe, Si, and Al in the trench waters as compared with those in the pipe drain waters (Table 4.2). In the fractograms of the trench waters of t1 and t2 (Figure 4.2) and the pipe drain water of t2 (Appendix C, Figure C1), P co-elutes with the colloidal clay particles. For the pipe drain water sampled at t1, the P concentrations were too low to be measured accurately by the HR-ICP-MS. Phosphorus associated with colloidal clay minerals in the 15-100 nm size fraction contributes 41, 35, and 52% to the DUP concentrations in the trench waters of t1 and t2 and the pipe drain water

of t2, respectively. This P can be either inorganic or organic in nature. For example, both orthophosphate and phytic acid are known to bind strongly to clay particles and Fe-(hydr) oxides (Dominik et al., 2008; Edzwald et al., 1976; Toor et al., 2003; Weng et al., 2011). Also, Ca co-elutes with the clay particles, which may be explained by Ca bound electrostatically to the negatively-charged clay particles. In addition, part of the Ca and P could be presents as small Ca-P precipitates on the surface of the clay minerals (Ulén and Snäll, 2007). With the combination of techniques as employed in this study, P associated to colloidal clay particles was shown to contribute largely to the colloidal P fraction at t1 and t2 in pipe drain and trench waters. However, we are unable to discriminate between the possible forms of P associated to colloidal clay minerals.

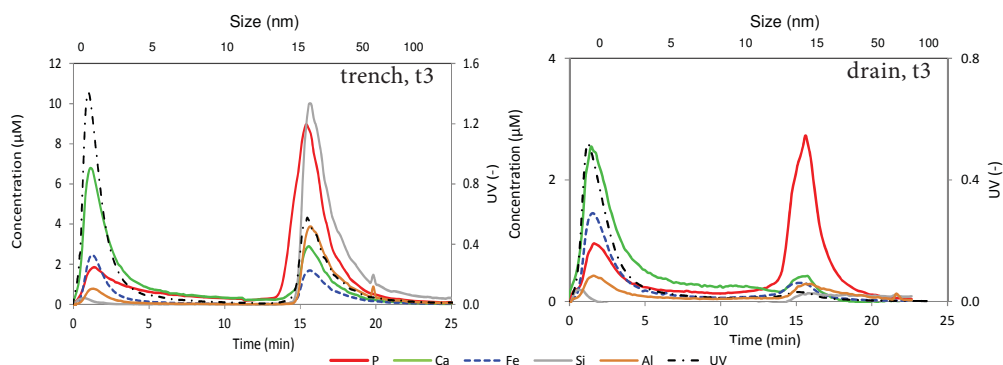


Figure 4.3. AF4 fractograms showing the elemental composition and UV absorbance (254 nm) of the colloids in the trench water and pipe drain water collected at t3 (when rainfall followed after application of cattle slurry).

The fractograms of the pipe drain and trench waters collected at t3 are given in Figure 4.3 whereas the fractograms of the replicate water samples are given in Appendix C, Figure C2. Similar to the results of t1 and t2, colloidal DOM particles are present in the 1-5 nm size range. The UV absorbance of this DOM peak is higher in the water discharge samples of t3 than at t1 and 2, which is in agreement with the higher total DOC concentrations at t3 (Table 4.2). Calcium, Fe, Al, and P co-elute with the DOM and, as discussed above, this P may be associated to DOM in the form of $\text{PO}_4\text{-M-DOM}$ complexes. However, in the trench waters, the shape of the P peak differs from the shape of the UV and Fe peaks, which may indicate the presence of other P species overlapping in size with the colloidal DOM particles. Possibly, this P is of the same nature as the organic P species detected in these water discharge samples, as will be discussed below. Based on the Si, Al, and Fe peaks in the

15-100 nm size range, colloidal clay particles are clearly present in the trench waters whereas almost no clay particles were detected in the pipe drain waters.

In contrast to t1 and t2, a clear P peak is visible in the 10-50 nm size range of the pipe drain and trench waters collected at t3. Remarkably, the P in this size range is not associated to clay particles, which is evident from the absence of Si and Al in the pipe drain waters and from the difference in peak position of P and Si and Al in the trench waters. This unknown P species in the 10-50 nm size range cannot be explained by the presence of colloidal Ca-phosphate or Ca-phytate precipitates, since the measured molar Ca/P ratios of 0.1 to 0.3 are too low to support the presence of these P colloids (Grynspan and Cheryan, 1983; Lindsay et al., 1979). Furthermore, Ca-P particles in manure form micrometer-sized aggregates and are, therefore, too large to fall within the colloidal size range (Cooperband and Good, 2002). Thus, another P species must be present in the 10-50 nm size range in our water discharge samples. Since the pipe drain and trench water samples were collected shortly after cattle slurry application and because of the presence of rapid transport pathways for water and P at this grassland field (Van der Salm et al., 2012), the unknown P species in the water discharge samples is likely to originate directly from the cattle slurry. Based on a study of Toor et al. (2005), orthophosphate (73%) is the dominant P species in cattle manure, while organic P species such as phytic acid (9%), DNA (1.9%), and phospholipids (3.7%) comprise a smaller fraction of total P. The presence of free (*i.e.*, not associated to colloidal particles) phytic acid in our water discharge samples is unlikely because of its very low water solubility in animal manure (Turner and Leytem, 2004). Furthermore, the unknown P species cannot be explained by phytic acid associated with colloidal clay particles, since the peak positions of P and clay colloids are clearly different. In contrast to phytic acid, DNA and phospholipids are readily soluble in water (Turner and Leytem, 2004). In a previous study of Gerritse (1981), the high molecular weight organic P, which was thought to consist of DNA and phospholipids, was responsible for the fast transport of P through soil columns after addition of pig slurry. Such organic P molecules have typical UV spectra. Therefore, we compared the UV spectra of the unknown P species in the 10-50 nm size range with the spectra of phytic acid, DNA, and phospholipids for further identification of the unknown P species. The UV spectra of pure material of DNA and phospholipids were obtained from literature (Ogram et al., 1987; Xu et al., 2009) while the spectrum of phytic acid was measured in this study. Figure 4A shows the UV spectrum of DNA, phytic acid, and phospholipids over the 200-400 nm wavelength. The UV spectrum of DNA is characterized by a maximum absorbance at 260 nm (Ogram et al., 1987). Phospholipids show only absorbance at wavelengths below

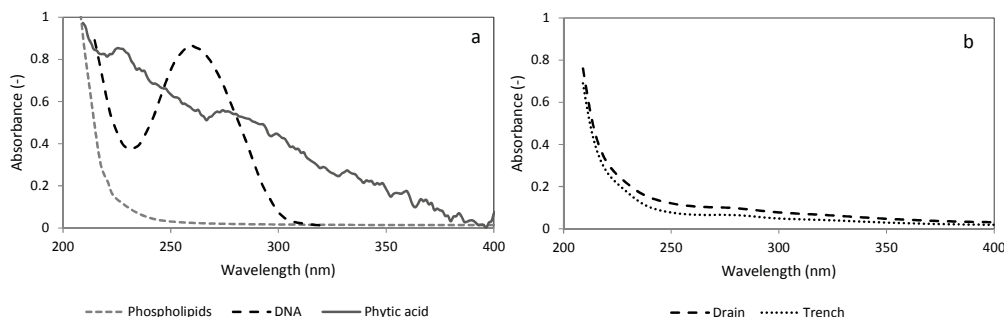


Figure 4.4. (a) UV spectrum of phytic acid, DNA (Ogram et al., 1987) and phospholipids (Xu et al., 2009) and (b) UV spectrum of the unknown P species detected in the 10-50 nm size range in the pipe drain and trench waters sampled at t3, when rainfall followed after application of dairy slurry. The UV spectrums of this unknown P species were collected using AF4 coupled online with UV-DAD, and the presented spectrums were taken at the peak maximum of the P peak.

250 nm (Xu et al., 2009), while phytic acid shows a featureless spectrum decreasing almost linearly from 200 to 400 nm. Hence, these strong differences in the UV spectra of DNA, phospholipids, and phytic acid allow for discrimination between these three organic P species. There is a strong similarity between the UV spectrum of phospholipids (Figure 4a) and the unknown P species in the pipe drain and trench water samples (Figure 4b). Hence, phospholipids can explain the presence of the P peak in the 10-50 nm size range in the water discharge samples of t3. Furthermore, the UV spectrum of the P peak in the 1-5 nm size range is similar to the UV spectrum of phospholipids (data not shown). Apparently, phospholipids may be present in the pipe drain and trench waters in the form of smaller colloids as well. The average P concentrations as phospholipids in 10-50 nm size range of the two replicates amounted to 12.5 ± 0.9 and 4.7 ± 1.7 μM P in the trench and pipe drain waters, respectively. These concentrations correspond to $33 \pm 2.5\%$ and $43 \pm 14.0\%$ of their DUP concentrations. Phospholipids are the building blocks of microbial cell walls and their presence in cattle manure is thought to be from microbial origin (Toor et al., 2005). Phospholipids can form vesicles of varying size, which can even be much larger than 0.45 μm (Yohannes et al., 2006). Therefore, phospholipids may have contributed to the elevated PP concentrations in the water discharge samples collected at t3 explaining the deviation of these samples from the relationship between PP and particulate Fe, Si, and Al for t1 and t2 (Figure 4.1). Alternatively, the formation of particulate associations between phytic acid and particulate clay and/or metal-(hydr)oxides (Hens and Merckx, 2001; Toor et al., 2003) may have contributed to the elevated PP concentrations at t3. Not all orthophosphate anion

groups of phytic acid are necessarily involved in the formation of the bonding between this organic P species and clay and/or metal-(hydr)oxides. For example, sorption of phytic acid on goethite was suggested to occur through four of the six P anion groups with the remaining two groups being free (Ognalaga et al., 1994; Celi et al., 1999). The formation of particulate associations between phytic acid and clay and metal-(hydr)oxides may, therefore, exceed the P sorption capacities of these particulates. However, this still would not explain the high ratios of P/clay ($4.2 \text{ mmol g}^{-1} \text{ clay}$) and P/Fe (2.1 mol mol^{-1}) observed in the particulate fraction in the pipe and drain waters of t3.

4.4 Conclusions

In conclusion, three types of colloidal P species could be distinguished within the DUP fraction in pipe drain and trench waters using AF4 coupled to HR-ICP-MS and UV-DAD. When P application was withheld for almost seven months, TP concentrations were low and P was almost evenly distributed among DRP, DUP, and PP. At this sampling time, P associated to colloidal clay particles comprised a large fraction of DUP and PP. Phosphorus associated to DOM, likely as $\text{PO}_4\text{-M-DOM}$ complexes, comprised a small fraction of DUP, as was the case in all water discharge samples of all sampling times. Total P concentrations in pipe drain and trench waters increased by a factor of 4 to 60 when rainfall followed after the application of the solid fraction of cattle slurry and cattle slurry. The contribution of DRP was 50% or more under these agricultural P management conditions. The DUP fractionation results were, however, different among these two sampling times. Phospholipids contributed largely to the DUP concentration in the water discharge samples when rainfall followed shortly after application of cattle slurry, with the concentration of this organic P species equaling or exceeding the Dutch threshold for TP in surface waters. Hence, phospholipids can be of environmental concern because of their high mobility in soil, even though this organic P species comprises only a small P fraction of cattle slurry (Toor et al., 2005). However, when rainfall followed after application of the solid fraction of cattle slurry, the DUP fraction was mainly comprised of P associated to clay colloids and no phospholipids were detected. Phospholipids, being highly water-soluble, were probably removed from the cattle slurry when the solid fraction was obtained by solid-liquid separation. Hence, P speciation of the DUP fraction in water discharge samples can vary strongly following different agricultural P management conditions. The combination of physico-chemical fractionation and analysis of the colloidal P fraction using AF4 coupled to HR-ICPMS and UV-DAD is a powerful and promising tool to unravel the speciation of P in environmental water samples.

References

- Addiscot, T.M., Brockie, D., Catt, J.A., Christian, D.G., Harris, G.L., Howse, K.R., Mirza, N.A., Pepper, T.J., 2000. Phosphate losses through field drains in a heavy cultivated soil. *J. Environ. Qual.* 29, 522-32.
- Chardon, W.J., Aalderink, G.H., Van der Salm, C., 2007. Phosphorus leaching from cow manure patches on soil columns. *J. Environ. Qual.* 36, 17-22.
- Cooperband, L.R., Good, L.W., 2002. Biogenic Phosphate Minerals in Manure: Implications for Phosphorus Loss to Surface Waters. *Environ. Sci. Tech.* 36, 5075-82.
- Correll, D.L., 1998. The role of phosphorus in the eutrophication of receiving waters: A review *J. Environ. Qual.* 27, 261-6.
- Dominik, K.I.P., Kaupenjohann, M., Siemens, J., 2008. Phosphorus-induced mobilization of colloids: model systems and soils. *Eur. J. Soil Sci.* 59, 233-46.
- Ebina, J., Tsutsui, T., Shirai, T., 1983. Simultaneous determination of total nitrogen and total phosphorus in water using peroxodisulfate oxidation. *Wat. Res.* 17, 1721-16.
- Edzwald, J.K., Toensing, D.C., Leung, M.C., 1976. Phosphate Adsorption Reactions with Clay Minerals. *Environ. Sci. Tech.* 10, 485-90.
- Ekhholm, P., 1994. Bioavailability of phosphorus in agriculturally loaded rivers in southern Finland. *Hydrobiologia* 287, 179-94.
- Gerke, J., 1992. Orthophosphate and organic phosphate in the soil solution of four sandy soils in relation to pH-evidence for humic-Fe-(Al)-phosphate complexes. *Commun. Soil Sci. Plant Anal.* 23, 601-12.
- Gerke, J., 2010. Humic (organic matter)-Al(Fe)-phosphate complexes. *Soil Sci.* 175, 417-25.
- Gerritse, R.G., 1981. Mobility of phosphorus from pig slurry in soils. In: T.W.G. Hucker, G. Catroux (Eds.), *Phosphorus in Sewage Sludge and Animal Waste Slurries*. Reidel, Dordrecht.
- Heathwaite, L., Haygarth, P.M., Matthews, R., Preedy, N., Butler, P., 2005. Evaluating colloidal phosphorus delivery to surface waters from diffuse agricultural sources. *J. Environ. Qual.* 34, 287-98.
- Hens, M., Merckx, R., 2001. Functional characterization of colloidal phosphorus species in the soil solution of sandy soils. *Environ. Sci. Technol.* 35, 493-500
- International Humic Substances Society. 2011. Data available at <http://www.humicsubstances.org> (verified 5 Dec. 2011)
- Lentz, R.D., Lehrsch, G.A., 2010. Nutrients in runoff from a furrow-irrigated field after incorporating inorganic fertilizer or manure. *J. Environ. Qual.* 39, 1402-15.
- Litzén, A., 1993. Separation Speed, Retention, and Dispersion in Asymmetrical Flow Field-Flow Fractionation as Functions of Channel Dimensions and Flow Rates. *Anal. Chem.* 65, 461-70.
- Lyvén, B., Hassellöv, M., Turner, D.R., Haraldsson, C., Andersson, K., 2003. Competition between iron- and carbon-based colloidal carriers for trace metals in a freshwater assessed using flow field-flow fractionation coupled to ICPMS. *Geochim. Cosmochim. Ac.* 67, 3791-802.
- Mermut, A.R., Cano, A.F., 2001. Baseline studies of the clay minerals society source clays: Chemical analyses of major elements *Clay. Clay Mineral.* 49, 381-6.
- Moorlegghem, C.V., Six, L., Degryse, F., Smolders, E., Merckx, R., 2011. Effect of organic p forms and p present in inorganic colloids on the determination of dissolved p in environmental samples by the diffusive gradient in thin films technique, ion chromatography, and colorimetry. *Anal Chem* 83, 5317-23.
- Murphy, J., Riley, J.P., 1962. A modified single solution method for the determination of phosphate in natural waters. *Anal. Chim. Acta.* 27, 31-36.

- Ogram, A., Sayler, G.S., Barkay, T., 1987. The extraction and purification of microbial DNA from sediments. *J. Micr. Meth.* 7, 57-66.
- Plathe, K.L., Von der Kammer, F., Hassellöv, M., Moore, J., Murayama, M., Hofmann, T., Hochella, M.F., 2010. Using FIFFF and aTEM to determine trace metal-nanoparticle associations in riverbed sediment. *Environ. Chem.* 7, 82-93.
- Regelink, I.C., Weng, L., Van Riemsdijk, W.H., 2011. The contribution of organic and mineral colloidal nanoparticles to element transport in a podzol soil. *Appl. Geochem.* 26, Supplement, S241-S244.
- Stolpe, B., Guo, L., Shiller, A.M., Hassellöv, M., 2010. Size and composition of colloidal organic matter and trace elements in the Mississippi River, Pearl River and the northern Gulf of Mexico, as characterized by flow field-flow fractionation. *Mar. Chem.* 118, 119-28.
- Toor, G., 2003. Characterization of organic phosphorus in leachate from a grassland soil. *Soil Biol. Biochem.* 35, 1317-1323.
- Toor, G.S., Cade-Menun, B.J., Sims, J.T., 2005. Establishing a linkage between phosphorus forms in dairy diets, feces, and manures. *J. Environ. Qual.* 34, 1380-1391.
- Turner, B.L., Leytem, A.B., 2004. Phosphorus compounds in sequential extracts of animal manures: Chemical speciation and a novel fractionation procedure. *Environ. Sci. Technol.* 38, 6101.
- Turner, B.L., McKelvie, I.D., Haygarth, P.M., 2002. Characterisation of water-extractable soil organic phosphorus by phosphatase hydrolysis. *Soil Biol. Biochem.* 34, 27-35.
- Turtola, E., Paajanen, A., 1995. Influence of improved subsurface drainage on phosphorus losses and nitrogen leaching from a heavy clay soil. *Agric. Water Manage.* 28, 295-310.
- Udawatta, R.P., Motavalli, P.P., Garrett, H.E., 2004. Phosphorus loss and runoff characteristics in three adjacent agricultural watersheds with claypan soils. *J. Environ. Qual.* 33, 1709-1719.
- Ulén, B., Snäll, S., 2007. Forms and retention of phosphorus in an illite-clay soil profile with a history of fertilisation with pig manure and mineral fertilisers. *Geoderma* 137, 455-465.
- Uusitalo, R., Turtola, E., Kauppila, T., Lilja, T., 2001. Particulate phosphorus and sediment in surface runoff and drainflow from clayey soils. *J. Environ. Qual.* 30, 589-595.
- Uusitalo, R., Yli-Halla, M., Turtola, E., 1999. Suspended soil as a source of potentially bioavailable phosphorus in surface runoff waters from clay soils. *Wat. Res.* 34(9), 2477-2482.
- van der Salm, C., Köhlerberg, L., de Vries, W., 1998. Assessment of weathering rates in Dutch loess and river-clay soils at pH 3.5, using laboratory experiments. *Geoderma* 85, 41-62.
- Verloop, K., Hilhorst, G., Meerkerk, B., de Buissonje, F., Schroder, J., De Haan, M., 2009. Mestscheiding op melkveebedrijven; resultaten van MOBIEDIK, Mobiele Mestscheiding in Dik en Dun, Plant Research International B.V., Wageningen, The Netherlands.
- Van der Salm, C., Van der Toorn, A., Chardon, W.J., Koopmans, G.F., 2012. Water and nutrient transport on a heavy clay soil in a fluvial plain in The Netherlands. *J. Environ. Qual.* 41, 229-41.
- Von der Kammer, F., Legros, S., Hofmann, T., Larsen, E.H., Loeschner, K., 2011. Separation and characterization of nanoparticles in complex food and environmental samples by field-flow fractionation. *Trends Anal. Chem.* 30, 425-436.
- Wahlund, K.G., Giddings, J.C., 1987. Properties of an asymmetrical flow field-flow fractionation channel having one permeable wall. *Anal Chem* 59, 1332-1339.
- Weng, L., Vega, F.A., Van Riemsdijk, W.H., 2011. Competitive and synergistic effects in pH dependent phosphate adsorption in soils: LCD modeling. *Environ. Sci. Technol.* 45, 8420-8428.
- Withers, P.J.A., Ulén, B., Stamm, C., Bechmann, M., 2003. Incidental phosphorus losses - are they significant and can they be predicted. *J. Plant. Nutr. Soil. Sci.* 166, 459-468.
- Wolf, J., Beusen, A.H.W., Groenendijk, P., Kroon, T., Rötter, R., Zeijts, H., 2003. The integrated modeling

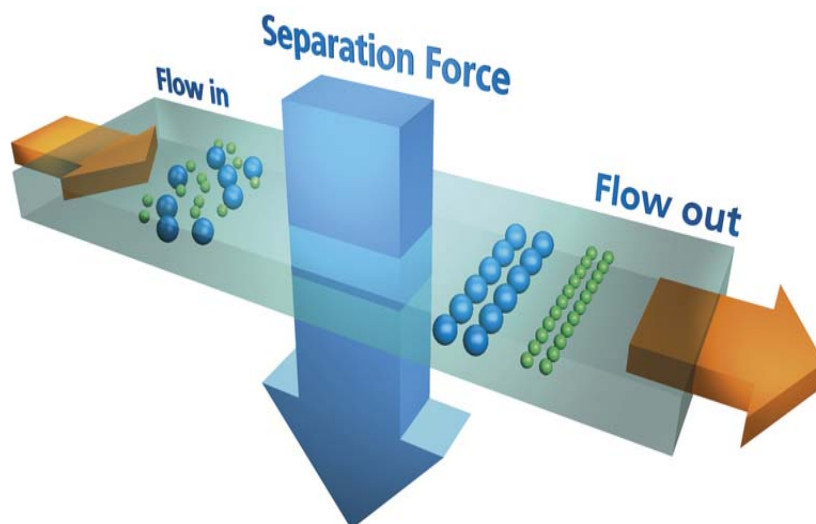
- system STONE for calculating nutrient emissions from agriculture in the Netherlands. *Environ. Modell. Softw.* 18, 597-617.
- Xu, K., Liu, B., Ma, Y., Du, J., Li, G., Gao, H., Zhang, Y., Ning, Z., 2009. Physicochemical properties and antioxidant activities of luteolin-phospholipid complex. *Molecules* 14, 3486-3493.
- Yohannes, G., Pystynen, K., Riekkola, M., Wiedmer, S., 2006. Stability of phospholipid vesicles studied by asymmetrical flow field-flow fractionation and capillary electrophoresis. *Anal. Chim. Acta* 560, 50-56.

Chapter 5

The distribution of trace elements between organic and mineral colloidal nanoparticles in a soil extract

Inge C. Regelink, Liping Weng, Willem H. van Riemsdijk

Based on Regelink, I.C., Weng, L., van Riemsdijk, W.H. (2011) The contribution of organic and mineral colloidal nanoparticles to element transport in a podzol soil. Applied Geochemistry, 26 Supplement, S241-S244



Abstract

Colloidal particles such as fulvic and humic acids, clay minerals and Fe-(hydr)oxides can facilitate the transport of trace metals and phosphorus (P) in soils and surface waters. However, the speciation of the colloidal fraction and the contribution of organic and mineral particles to colloid-facilitated transport are still poorly understood. Our objective was to unravel the associations between trace elements and organic and inorganic colloidal particles in a soil extract using a novel analytical technique: Asymmetric Flow Field-Flow Fractionation (AF4) in combination with Inductively Coupled Plasma Mass Spectrometry (ICP-MS). The colloids were extracted in water from a B-horizon of a podzol, which was characterized by a high Fe-(hydr)oxide content (6.3 g Fe kg^{-1}), high soil organic carbon content (28 g kg^{-1}) and a low pH (3.3). The results show that the majority of the trace elements are associated with inorganic colloidal particles (1–150 nm), whereas a smaller fraction is associated with organic colloids. The inorganic colloidal fraction dominantly consists of clay minerals and might additionally contain Fe-(hydr)oxides and organic substances that are associated with the clay minerals. The contribution of inorganic colloids to the total colloidal concentration decreased in the order: Pb, P, Zn, Ni and Cu. As such, AF4-ICP-MS provided evidence for the relative adsorption affinity of these trace metals for adsorption to organic versus inorganic colloids.

5.1 Introduction

Nanoparticles are ubiquitous in the environment. Commonly present soil constituents such as iron-oxides, organic matter and clay particles can be present in the nanometer size-range and, once dispersed, these particles can act as carriers for trace metals and phosphorus. Nanoparticles are of interest because of their high reactivity compared to their bigger counterparts and because they can become mobilized (Plathe et al., 2010a). Nanoparticles play an important role in the transport of various elements in soils and surface-waters. Various studies have reported a large contribution of organic colloids to the mobility of metals or phosphate (Krám et al., 2009; Patel-Sorrentino et al., 2007; Plathe et al., 2010b; Weng et al., 2002b). Additionally, inorganic colloids, such as clay minerals or Fe-(hydr)oxides, have been detected in surface waters and might contribute to the mobility of trace elements in soils and surface waters (Lyvén et al., 2003).

Podzol soils are characterized by the transport of Al, Fe and organic carbon from the eluviated E horizon to the spodic B-horizon. It is generally accepted that dissolved organic matter (DOM) plays an important role in the transport of Al and Fe in the podzol profile

(Buurman, 2005; Patel-Sorrentino et al., 2007). Besides, experimental studies showed that a significant part of mobile Al in podzol soils is present in the particulate phase (Krám et al., 2009; Patel-Sorrentino et al., 2007). Analysis of the composition of colloidal nanoparticles can increase our understanding of element and colloid transport in soils. In this study we used Asymmetric Flow Field-Flow Fractionation (AF4) in combination with Inductively Coupled Plasma Mass Spectrometry (ICP-MS) to measure the size-distribution and composition of colloids in a water-extract a podzol B-horizon.

5.2 Material and Methods

5.1.1 *Extraction and characterization of colloids*

Soil samples were taken from an acid forest soil profile, located in the Lysina catchment, Czech Republic. Soils were dried at 40C° and sieved over 2 mm. The soil sample from the BE horizon (18–25 cm depth) was used in this study. The general physical-chemical properties of the soil were taken from Regelink et al. (2011) (Chapter 2). The colloidal particles were extracted in a water-extract using a soil-solution ratio (SSR) of 1 kg l⁻¹. A high SSR was chosen so that the colloidal particles are extracted at a pH and salt concentration which is similar to the pH and salt concentration of the pore-water. The suspension was shaken end-over-end for 24 hours and thereafter centrifuged for 30 minutes at 3000 rpm and filtered over a 0.45 µm membrane filter.

An AF4 system (Postnova Analytics, Germany) was used for size-fractionation of the colloids in the soil extract. AF4 is a fractionation technique in which particles are fractionated in a water column (spacer thickness is 350 µm) based on differences in their diffusion coefficient. Dissolved species are removed from the column by the crossflow passing a polyethersulfone (PES) membrane with a cut-off of 1 kDa. A 4 mM NaHCO₃ solution at pH 8.3 was used as a carrier. Carriers with a low ionic strength, a neutral to high pH, and which do not interfere with ICP-MS analysis are in general suitable carriers for fractionation of environmental samples (Dubascoux et al., 2008). The injected sample volume was 0.5 ml and the injection/focusing time took 11 min using a cross flow of 3 ml min⁻¹. The cross flow rate was 3 ml min⁻¹ for the first 20 minutes, and thereafter, the cross flow decreased in 2 min to 0.5 ml min⁻¹ in a linear manner and was maintained at this rate from the 23th to the 41th minute. Using a stepwise change in cross flow rate allowed for fractionation of particles <20 nm in size with a high size-resolution and fractionation of particles 20–150 nm in size with a lower size-resolution. The detector flow was coupled to

an UV-detector (Postnova Analytics) and to a HR-ICP-MS, which measured the Mg, Al, Si, P, Ca, Fe, Cu, Ni, Zn and Pb concentrations every 12 s. Calibration of the HR-ICP-MS was done at the beginning and at the end of each measurement day to correct for sensitivity drifting. A combination of calibration, using standard particles, and AF4 theory was used to derive the relationship between particle size and retention time (Figure A1).

5.2 Results and Discussion

The soil is characterized by a low pH (3.3), high amount of oxalate-extractable Fe and Al (6.3 and 2.0 g kg⁻¹) and high SOC content (23.5 g kg⁻¹), which is typical for spodic horizons in which Fe, Al and SOC accumulate. The DOC concentration in the water-extract amounted to 148 mg l⁻¹.

The AF4 fractograms (Figure 5.1) show the size-distribution of the 10 monitored elements within the size-range between 1 and 150 nm. Two groups of particles can be distinguished: the first peak (1-6 nm) is characterized by a high UV-absorbance and the second peak (20-150 nm) is characterized by a low UV-absorbance and high concentrations of Si, Al and Fe. The concentrations of Si, Al and Fe continuously increase with increasing particle size and the high concentrations at the end of the AF4 run suggest the presence of substantial amounts of particles larger than the maximum particle size (150 nm) recovered during the AF4 run.

The first peak, which elution time corresponds to a particle size of 1–6 nm, can be attributed to the presence of ‘dissolved’ organic matter (DOM) such as humic acids and fulvic acids. Humic and fulvic acids fall within this size-range and have a high UV-absorbance at 254 nm (Amery et al. 2009). Smaller organic molecules, such as citric acid and other hydrophilic acids, will pass the 1 kDa membrane and are therefore not recovered during the AF4 run. The co-elution of Al and Fe with the UV peak in the 1–6 nm size range shows that Fe and Al are associated with the DOM. This association is likely due to complexation of Fe and Al with HA and FA, although previous studies have shown that Fe and Al can also elute in this size range as metal-(hydr)oxides (Lyvén et al.). If we can assume that the UV-peak corresponds to the total DOC concentration of the sample (148 mg l⁻¹), then the Al/OM and Fe/OM ratios amount to 0.03 and 0.04 mol kg⁻¹, respectively. These values are in the same order of magnitude as loadings of Al and Fe that can adsorb to DOM under acid conditions (Hiemstra and van Riemsdijk, 2006; Weng et al., 2002b). As such, the Al and Fe in this peak are likely adsorbed to the DOM rather than being present as metal-(hydr)oxide particles. In podzol soils, one can expect relatively high Fe and Al loadings associated with DOC because

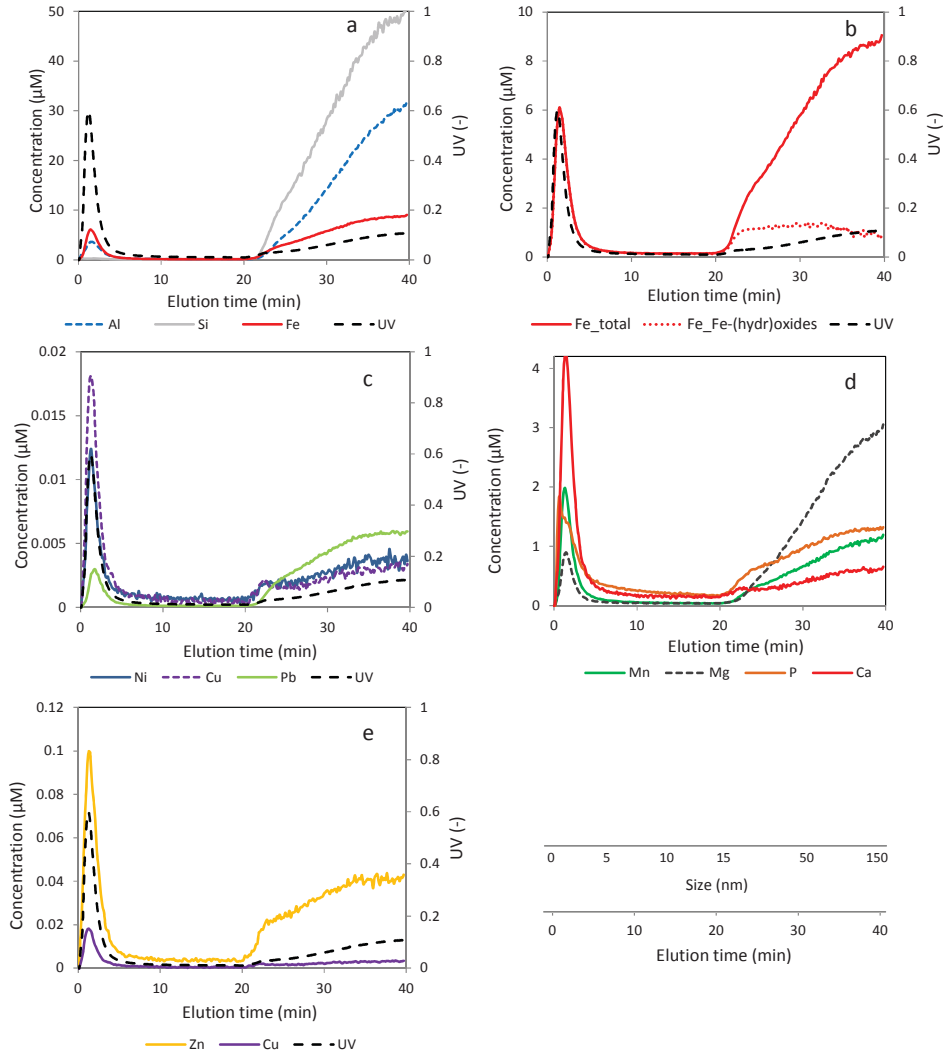


Figure 5.1. AF4-ICP-MS fractograms showing the elution of Si, Al, Fe, Ca, Mg, Mn, P, Ni, Cu, Pb and Zn as a function of the elution time and corresponding hydrodynamic particle diameter

of the low pH and consequently high total dissolved Al and Fe concentrations.

The second peak (>20 nm) is characterized by a lower UV absorbance compared to the first peak and the particles eluting in this peak dominantly consists of Si, Al and Fe. The Si:Al ratio amounts to two, which suggests the elution of 2:1 Si-Al clay minerals. For Fe, the slope of the Fe peak is steeper than the slope of the Al and Si peak, showing that the composition of the mineral particles changes with particle size. The Fe/Si ratio strongly decreases within

increasing particle size. Between 20 and 25 minutes, the Fe/Si ratio decreases from 1.2 to 0.24 and thereafter levels off to 0.16. The Fe/Si ratio is higher than the structural Fe/Si ratio of common 2:1-clay minerals (0.01–0.05) (Mermut and Cano, 2001). As such, the high Fe/Si ratio's in the fractogram indicates the presence of Fe-(hydr)oxide minerals that are attached to the clay mineral surfaces. Additionally, Fe-(hydr)oxides might also be present as a physically separated phase with a similar size as the clay minerals. The distribution of the total Fe concentration between Fe-(hydr)oxides and Fe substituted within clay minerals can be estimated if we can assume that the Fe/Si ratio of the clay minerals is constant with size. For this calculation, I assumed that the Fe/Si ratio of the clay minerals amounts to 0.16, which was the lowest ratio measured in the studies size range, and used this value to calculate the distribution of Fe between clay minerals and Fe-(hydr)oxides. The calculated amount of Fe present as Fe-(hydr)oxides is shown in Figure 5.1b, and this simple approach predicts a small peak of Fe-(hydr)oxides in the size-range between 15 to 50 nm. The presence of iron-oxides between 20-25 minutes coincides with an increase in the concentration of trace metals (Figure 5.1).

The UV absorbance of the particles in the 20 - 150 nm range is much lower than in the range of 1 - 6 nm and can probably be explained by absorbance by the mineral particles. Another possible explanation for the UV absorbance of the mineral colloids is the presence of a OM coating on the mineral particles. OM has a high affinity for adsorption to mineral surfaces and an OM coating on mineral particles strongly increases the colloidal stability of the mineral particles (Majzik and Tombacz, 2007). Furthermore, the OM loading can facilitate the transport of trace metals because of the high affinity of trace metals for

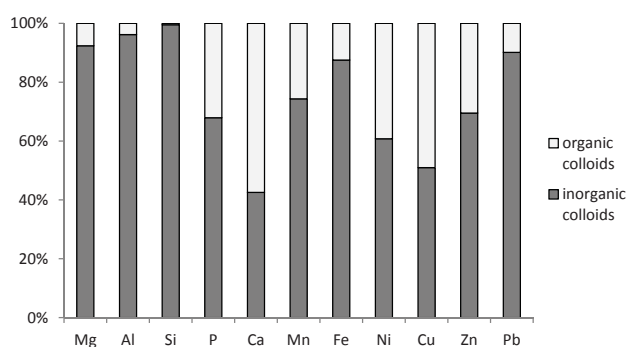


Figure 5.2. Distribution of elements between the organic and inorganic colloids in the soil extract, as determined by AF4-ICP-MS (Figure 5.1).

adsorption to OM.

The dominant colloidal nanoparticles in the soil extract are: DOM, clay particles and, to a minor extent, Fe-(hydr)oxides. These colloidal nanoparticles can facilitate the transport of associated elements. The distribution of the measured elements between the DOM peak (1–6 nm) and inorganic colloids (20–150 nm) is given in Figure 5.2. The colloidal Ca concentration is equally distributed between the DOM and mineral nanoparticles. The co-elution of Ca with DOM and clay minerals can be explained by adsorption of Ca to humic and fulvic acids and clay mineral surfaces. The presence of Ca precipitates with carbonate or phosphate is not expected because of the low soil pH. In contrast to Ca, Mg is for 94% associated with the inorganic colloids (Figure 5.2). Mg is a common substitute in octahedral sheets of clay-minerals and the measured Mg/Si ratio (0.04–0.06) is similar to Mg/Si ratio's found for 2:1 clay minerals (0.03–0.09) (Mermut and Cano, 2001). So the majority of Mg co-eluting with the inorganic colloids is present as Mg substituted within the clay mineral structure rather than as exchangeable cations.

The analyzed trace-metals show some differences in their distribution between OM and inorganic particles. Pb has a relatively high affinity for adsorption to the inorganic colloids compared to the organic colloids. The high affinity of Pb for adsorption to inorganic particles compared to organic is in agreement with previous AF4-ICP-MS studies (Lyvén et al., 2003) and modeling studies (Weng et al., 2001). Zn also shows a preference for adsorption to inorganic colloids over colloids whereas Cu and Ni is almost equally distributed between the two colloidal fractions. Overall, the contribution of inorganic colloids to the total colloidal concentration decreased in the order: Pb, Zn, Ni and Cu. The relatively high affinity of Zn and Ni for adsorption to the inorganic particles compared to Cu is in line with previous multi-surface modelling studies (Fest et al., 2005; Weng et al., 2001). However, the large contribution of inorganic colloids to the colloidal concentrations of trace metals was not expected since it is commonly thought that transport of trace metals is controlled by the concentration of DOC in the soil solution (Fest et al., 2008; Weng et al., 2002a). This discrepancy might be explained by the difference in the extraction solution used to prepare the soil extracts. In this study, water was used as extractant whereas the previous modelling studies used 0.01 M CaCl₂ as extractant. Possibly, dispersion of clay particles is inhibited in the CaCl₂ solutions due to the higher ionic strength, leading to coagulation of clay particles (Tombacz and Szekeres, 2004). Nevertheless, our results suggest that the role of inorganic colloids, such a clay minerals and Fe-(hydr)oxides, to the transport of trace metals, is underestimated so far.

The majority of colloidal P in the soil extract (72%) is associated with the inorganic fraction, likely as innersphere complexes of orthophosphate with reactive surface groups on iron-oxides and on edges of clay minerals (Manning and Goldberg, 1996; Rahnemaie et al., 2007). The remaining fraction of P is present in the smaller size-range (1–5 nm) (Figure 5.1). These particles elute somewhat earlier than the UV-peak meaning that this P is not associated with the DOM fraction in the form of metal-PO₄-DOM bindings (Gerke, 2010). Instead, P in this size-fraction might be present as small organic phosphate compounds. Phosphate-monoesters (e.g. inositol-phosphates) and diesters (e.g. DNA) can contribute to the leaching of P in soils (Toor et al., 2005). The presence of organic-phosphorus as a smaller peak within the UV-peak shows that a size-fractionation of various types of organic compounds occurred within the UV-peak. DOM is a complex mixture of organic compounds and the various groups of organic compounds cannot be completely separated by AF4 because of these compounds likely overlap in size.

Overall, this study shows that AF4 coupled to online ICP-MS is a powerful tool to analyze colloids in soil-extracts because of the high size-resolution, the low detection limits and the capability to measure multiple elements. Both organic and inorganic colloids were found to contribute substantially to the colloidal concentrations of trace elements and P and may as such contribute to the transport of these elements in soils. The contribution of inorganic colloids, which consists of clay minerals and Fe-(hydr)oxides, to the total colloidal concentration decreased in the order: Pb, Zn, Ni and Cu. The relative of these trace metals for adsorption to the inorganic particles compared to the organic particles is in line with previous multi-surface modelling studies. As such, AF4-ICP-MS provides valuable information to very modelling predictions. Overall, our results suggest that the role of inorganic colloids, such a clay minerals and Fe-(hydr)oxides, to the transport of trace metals, is underestimated so far.

References

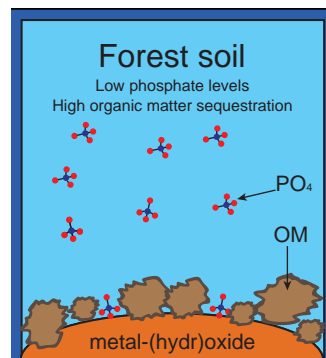
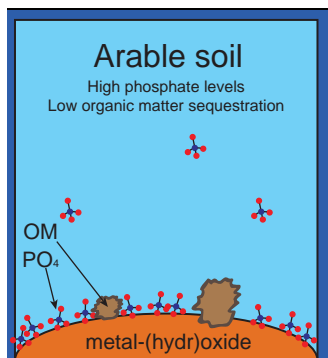
- Amery, F; Van Moorlegghem, C; Smolders, E., 2009. Adapted DAX-8 fractionation method for dissolved organic matter from soils: development, calibration with test components and application to contrasting soil solutions. *Eur. J. Soil Sci.* 60, 956-965
- Buurman, P., 2005. Podzolisation and soil organic matter dynamics. *Geoderma* 125, 71-83.
- Dubascoux, S., Von Der Kammer, F., Le Hécho, I., Gautier, M.P., Lespes, G., 2008. Optimisation of asymmetrical flow field flow fractionation for environmental nanoparticles separation. *J. Chromatog. A* 1206(2), 160-165.
- Fest, E.P.M.J., Temminghoff, E.J., Griffioen, J., Van Riemsdijk, W.H., 2005. Proton buffering and metal leaching in sandy soils. *Environ. Sci. Tech.* 39, 7901-7908.

- Fest, E.P.M.J., Temminghoff, E.J.M., Comans, R.N.J., van Riemsdijk, W.H., 2008. Partitioning of organic matter and heavy metals in a sandy soil: Effects of extracting solution, solid to liquid ratio and pH. *Geoderma* 146(1-2), 66-74.
- Gerke, J., 2010. Humic (organic matter)-Al(Fe)-phosphate complexes. *Soil Sci.* 175(9), 417-425.
- Hiemstra, T., van Riemsdijk, W.H., 2006. Biogeochemical speciation of Fe in ocean water. *Mar. Chem.* 102(3-4), 181-197.
- Krám, P., Hruska, J., Driscoll, C.T., Johnson, C.E., Oulehle, F., 2009. Long-term changes in aluminum fractions of drainage waters in two forest catchments with contrasting lithology. *J. Inorg. Biochem.* 103(11), 1465-1472.
- Lyvén, B., Hassellöv, M., Turner, D.R., Haraldsson, C., Andersson, K., 2003. Competition between iron- and carbon-based colloidal carriers for trace metals in a freshwater assessed using flow field-flow fractionation coupled to ICPMS. *Geochim. Cosmochim. Ac.* 67(20), 3791-3802.
- Majzik, A., Tombacz, E., 2007. Interaction between humic acid and montmorillonite in the presence of calcium ions II. Colloidal interactions: Charge state, dispersing and/or aggregation of particles in suspension. *Org. Geochem.* 38(8), 1330-1340.
- Manning, B.A., Goldberg, S., 1996. Modeling Arsenate Competitive Adsorption on Kaolinite, Montmorillonite and Illite. *Clay. Clay Min.* 44(5), 609-623.
- Mermut, A.R., Cano, A.F., 2001. Baseline studies of the clay minerals society source clays: Chemical analyses of major elements. *Clay. Clay Min.* 49, 381-386.
- Patel-Sorrentino, N., Lucas, Y., Eyrolle, F., Melfi, A.J., 2007. Fe, Al and Si species and organic matter leached off a ferrallitic and podzolic soil system from Central Amazonia. *Geoderma* 137(3-4), 444-454.
- Plathe, K.L., von der Kammer, F., Hassellöv, M., Moore, J., Murayama, M., Hofmann, T., Hochella, M.F., 2010a. Using FIFFF and aTEM to determine trace metal-nanoparticle associations in riverbed sediment. *Environ. Chem.* 7(1), 82-93.
- Plathe, K.L., von der Kammer, F., Hassellöv, M., Moore, J., Murayama, M., Hofmann, T., Hochella, M.F., 2010b. Using FIFFF and aTEM to determine trace metal-nanoparticle associations in riverbed sediment. *Environ. Chem.* 7(1), 82-93.
- Rahnemaie, R., Hiemstra, T., van Riemsdijk, W.H., 2007. Carbonate adsorption on goethite in competition with phosphate. *J. Colloid Interf. Sci.* 315(2), 415-425.
- Tombacz, E., Szekeres, M., 2004. Colloidal behavior of aqueous montmorillonite suspensions: the specific role of pH in the presence of indifferent electrolytes. *Appl. Clay Sci.* 27, 75-94.
- Toor, G.S., Condrón, L.M., Cade-Menun, B.J., Di, H.J., Cameron, K.C., 2005. Preferential phosphorus leaching from an irrigated grassland soil. *Eur. J. Soil. Sci.* 56(2), 155-168.
- Weng, L., Fest, E.P.M.J., Filius, J.D., Temminghoff, E.J., Van Riemsdijk, W.H., 2002a. Transport of humic and fulvic acids in relation to metal mobility in a copper-contaminated acid sandy soil. *Environ. Sci. Tech.* 38, 1699-1704.
- Weng, L., Temminghoff, E.J.M., Van Riemsdijk, W.H., 2001. Contribution of Individual Sorbents to the Control of Heavy Metal Activity in Sandy Soil. *Environ. Sci. Technol.* 35(22), 4436-4443.
- Weng, L., Temminghoff, E.J.M., Van Riemsdijk, W.H., 2002b. Aluminum speciation in natural waters: measurement using Donnan membrane technique and modeling using NICA-Donnan. *Water Res.* 36(17), 4215-4226.

Chapter 6

Phosphate solubility and carbon sequestration in cropland and forest soils explained by mechanistic adsorption modelling

Inge C. Regelink, Liping Weng, Georg J. Lair, and Rob N.J. Comans



Abstract

Phosphate (PO_4) and organic matter (OM) compete for adsorption to metal-(hydr)oxides, and these interactions affect the soluble PO_4 concentrations and the amounts of OM adsorbed to metal-(hydr)oxides. Using a mechanistic surface complexation model, we explained the adsorption interactions in 33 calcareous soils which vary in land use (arable vs. forest), sampling depth (0–80 cm), and soil age (≈ 50 –2500 y) and cover a range in soil organic carbon (SOC) contents (5.6–43.5 g kg^{-1}) and total PO_4 contents (0.2–5.9 mmol kg^{-1}). Water-soluble PO_4 concentrations are poorly related to the PO_4 loading on the metal-(hydr)oxides. Instead, at a similar PO_4 loading, PO_4 solubility increases with increasing SOC content, which can be explained by a higher OM loading on the metal-(hydr)oxides and thus a stronger competition for adsorption. Thus, due to the higher SOC content in forest soils, a similar PO_4 loading corresponds to a higher soluble PO_4 concentration in the forest soils than in the arable soils. Neglecting the competition with OM leads to an underestimating of the soluble PO_4 concentrations with several orders of magnitude. The OM loading on the metal-(hydr)oxides slightly increases with increasing soil age for the forest fields, but land use has a much stronger effect on the OM loading. The OM loading is 2–28 times lower in topsoils of the arable fields than in the forest fields, which can be explained by replacement of OM for PO_4 in the arable soils. As such, high levels of P fertilization may decline the C-sequestration potential of arable soils due to a loss of OM adsorbed to metal-(hydr)oxides.

6.1 Introduction

Iron and aluminum-(hydr)oxides generally dominate the soil's surface area available for anion adsorption and consequently play an important role in the sequestration of phosphate (PO_4) and organic matter (OM) in soils (Hiemstra et al., 2010a; Kaiser et al., 2012; Schneider et al. 2010). Both PO_4 and organic substances, such as humic acids (HA), fulvic acids (FA), and small organic acids, show a high affinity for adsorption to metal-(hydr)oxides, leading to a strong competition for adsorption between PO_4 and OM (Antelo et al., 2007; Weng et al., 2008; Hiemstra et al., 2013). The competitive adsorption interactions affect the PO_4 solubility as well as the amount of OM adsorbed to the metal-(hydr)oxides. In batch experiments, soluble PO_4 concentrations increased by a factor 2–100 whereas the amounts of adsorbed FA decreased by a factor 2–4 when PO_4 and FA were added simultaneously to synthetic goethite compared to the corresponding mono-adsorbate adsorption experiments (Antelo et al., 2007; Weng et al., 2008). Similar, in soils, addition of large quantities of PO_4

led to an increase in dissolved organic carbon (DOC) concentrations (Chardon et al., 2012; Zhang & Zhang, 2010) whereas the addition of organic substances to soils led to an increase in PO_4 solubility due to competition for adsorption (Cui et al., 2011; Duffner et al., 2012), although there are also studies reporting no significant effect in soils (Guppy et al., 2005). However, the adsorption interactions are mostly studied at PO_4 or DOC concentrations that are much higher than normally occur in soils. As a consequence, the adsorption interactions between PO_4 and OM under relevant soil conditions are still poorly understood.

Surface complexation (SC) modelling is a powerful tool to describe and predict the adsorption interactions between PO_4 and OM in soils under natural conditions. SC models, such as the charge distribution multi-site complexation (CD-MUSIC) model, describe the multiple interactions of ions with charged mineral surfaces. When using the CD-MUSIC model, the adsorbed organic molecules have been represented by one or more hypothetical surface species (Hiemstra et al., 2013) or treated as variable charged molecules simulated with the Non-Ideal consistent Competitive Adsorption (NICA) model (Weng et al., 2008). In the latter case, combination of the CD-MUSIC and NICA model forms the structure of the Ligand and Charge Distribution (LCD) model (Weng et al., 2008). These SC models have been applied successfully to describe adsorption interactions in well-defined batch experiments using synthetic Fe-(hydr)oxides and purified humic substances (Weng et al., 2005; Weng et al., 2008; Hiemstra et al., 2013). However, application of SC-models to describe PO_4 adsorption in soils by considering the competitive and synergistic effects of OM, pH and Ca are still scarce (Duputel et al., 2013; Hiemstra et al., 2010b; Weng et al., 2011; Hiemstra et al., 2013). The study of Hiemstra et al. (2010b) predicted that the OM loading, naturally present in the arable soils, leads to a 10–1000 times higher PO_4 concentration in the soil solution compared to a situation without adsorbed OM. In contrast, Devau et al. (2011) showed that PO_4 solubility in soils can be predicted by SC modelling without considering competition with organic matter and Duputel et al. (2013) predicted that citrate can either increase or decrease P solubility, depending on the citrate concentration and composition of the soil. Furthermore, PO_4 solubility and risks for PO_4 leaching from soils are normally predicted from the degree of P saturation of the metal-(hydr)oxides, without considering competition with OM (Koopmans et al., 2007). Thus, the quantitative effect of the OM loading on the soluble PO_4 concentration is still poorly understood which hampers an accurate prediction of PO_4 bioavailability and mobility in soils.

Arable and forest soils show strong differences with respect to their SOC and PO_4 content (Lair et al., 2009b; Zehetner et al., 2009) and as such, can be expected to show strong

differences in their OM and PO_4 loading on the metal-(hydr)oxide surfaces. However, estimating the OM loading is still challenging since OM is a mixture of various poorly defined compounds which differ in their affinities for adsorption to oxides and no selective extraction procedures for the oxide-associated OM exists. Alternatively, the OM loading on the metal-(hydr)oxides can be derived by SC modelling using the PO_4 concentration and PO_4 loading and taking the competitive and synergistic effects of Ca and pH into account (Hiemstra et al., 2010b). Further development and application of this approach to derive the OM loading will improve our understanding of PO_4 solubility in soils with varying SOC content, and will reveal quantitative insight into the amount of OM that can be stabilized via adsorption to metal-(hydr)oxides in soils with varying PO_4 content.

In this study, we use SC-modelling to obtain a mechanistic and more quantitative understanding of the competition between PO_4 and OM for adsorption to metal-(hydr)oxides in a set of 33 calcareous soils developed on alluvial sediments in the Marchfeld (Austria), collected from arable and forest fields. The soil samples were collected from topsoils and subsoils along an age gradient (Lair et al., 2009a; Lair et al., 2009b; Zehetner et al., 2009; Zehetner et al., 2008). The soils covers a wide range in PO_4 and SOC contents but a low range in pH and soluble Ca concentration due to the similar parent material. As such, this set is deal for studying the effect of the OM loading on PO_4 solubility since the synergistic effects of pH and Ca concentration are similar among all soils. Furthermore, this dataset allows to study the effect of landuse, PO_4 content, soil age and sampling depth on the OM loading on the metal-(hydr)oxide surfaces. Overall, the objective of this study is to obtain a quantitative understanding of the processes controlling PO_4 solubility and carbon sequestration by metal-(hydr)oxides in arable and forest soils with varying sampling depth (0–80 cm) and soil age (50–2500 y) using SC modelling.

6.2 Material and Methods

6.2.1 Soils

The three forest sites and two croplands sites are located near the Danube river in the Marchfeld area, east of Vienna, Austria. The soils are calcareous and classified as Fluvisols (site 1, 2) and Chernozems (site 3, 4 and 5, Table 6.1). The sites are part of a well-studied chronosequence (Lair et al., 2009b; Zehetner et al., 2009; Zehetner et al., 2008) and soil ages were determined previously by Lair et al., (2009a) using a combination of dating procedures including Cs-137, optically stimulated luminescence (OSL), historical maps and

the Fe_{ox}/Fe_d ratio of the soils. For the subsoil, samples were taken from each distinct soil horizon (down to 70 cm soil depth) in one pit per site, whereas the topsoils were sampled in triplicate, leading to a set of 33 soil samples (Table 6.2). For the forest sites, the upper 10 cm was considered as topsoil, whereas for the arable soils, the ploughing layer (25 cm) was taken as the border between the topsoil and subsoil. The Marchfeld area is one of the critical zone observatories (CZO's) studied in the EU-project SoilTrEC (Soil Transformations in European Catchments) and soil numbers and field-codes correspond to the coding used within this project (Table 6.2).

6.2.2 Soil Characterisation.

Soils were oven dried at 40°C and sieved over 2 mm prior to analysis. The SOC content was determined by an elemental analyzer (Carlo Erba Nitrogen analyzer 1500) after removal of the carbonates by concentrated HCl. The total amount of Fe-(hydr)oxides (including amorphous and crystalline oxides) was extracted in dithionite-citrate-bicarbonate (Fe_d) at 80°C, following the procedure of Mehra and Jackson (Mehra and Jackson, 1960). Iron concentrations in the 0.45- μ m filtrates (cellulose-nitrate filter, Whatman) were measured by inductively coupled plasma-atomic emission spectrometry (ICP-AES; Varian Vista Pro). Aluminum-(hydr)oxides and amorphous Fe-(hydr)oxides were extracted in 0.2 M ammonium-oxalate at pH 3.0 during 2 h of shaking (horizontal shaker, 85 rpm) in the dark (Schwertmann, 1973) and the 0.45- μ m filtrates were analyzed for Fe (Fe_{ox}), Al (Al_{ox}) and P (P_{ox}) by ICP-AES. The P_{ox} content is commonly used as a measurement for the amount of oxide-associated PO_4 . However, in calcareous soils, P_{ox} may also dissolve calcium-phosphate

Table 6.1. Description of the sampling sites and estimated age of the soils (taken from Lair et al. 2009)

Site	Landuse	Soil classification	soil age (year)	Description
1	Forest	Fluvisol	<50	Island in Danube river-bed, soft wood forest
2	Forest	Fluvisol	50-400	Inside a flood control dike (inundated once within 10 years), soft-wood forest
3	Forest	Chernozem	400-800	Outside the flood control dike, hard wood forest
4	Arable	Chernozem	>2500	Old cropland site (since 12th century)
5	Arable	Chernozem	>2500	Old cropland site (since 12th century)

minerals. Therefore, an alkaline extractant should be used to extract the oxide-associated PO_4 from calcareous soils. Following the procedure of Bowman & Moir (1993), P was extracted in a 0.125 M NaOH + 0.05 M EDTA solution during 24 h of shaking at a soil/solution ratio (SSR) of 0.05 kg l^{-1} and the total P (TP) and PO_4 concentrations were analyzed in the 0.45- μm filtrates of the soil extracts. Total P was measured by ICP-AES. Phosphate was measured colorimetrically using the molybdenum-blue method (Murphy and Riley, 1962) in filtrates acidified to 0.1% HCl on a Segmented Flow Analyser (Skalar SK). Organic P (Porg) was calculated as the difference between TP and PO_4 . The extraction of oxide-associated PO_4 by this extraction solution can be explained by the combination of a high pH and low Ca activity (due to complexation with EDTA), which leads to an almost complete desorption of PO_4 from oxides (Rahnemaie et al., 2007) whereas apatite is not expected to dissolve at this pH (Zehetner et al., 2008). The HA-like substances were extracted from the soil in 0.1 M Na-pyrophosphate at pH 9.6 during 24 h of shaking (SSR=0.1 kg l^{-1}) and the total organic carbon (TOC) concentration in the extracts was determined by a Shimadzu TOC analyzer (TC5000). Pyrophosphate was chosen since Tatzber et al. (2007) showed for soils from the Marchfeld area that pyrophosphate extracted 5-times more organic carbon (OC) than NaOH, which may be explained by the ability of pyrophosphate to extract OC associated with Fe- and Al-(hydr)oxides and stabilized by divalent cations (Kaiser et al., 2012).

6.2.3 Desorption Experiment.

Soil suspensions (soil solution ratio SSR=0.1 kg l^{-1}), prepared with ultrapure water (UPW), were shaken for 5 days at a horizontal shaker (85 rpm) in a climate-controlled room at 20°C. The pH was measured in the suspensions and the 0.45- μm filtrates were analyzed for total soluble Ca, Mg, Na, and P (ICP-AES), inorganic carbon (IC, TOC analyzer), TOC (TOC analyzer) and PO_4 (molybdenum-blue method (Murphy and Riley, 1962)).

6.2.4 Modelling.

The model calculation was carried out in two steps. The solution speciation was calculated and the free ion activities derived from this first step were used as input for the surface complexation modelling.

(i) Solution Speciation. Speciation of the ions in the water-extracts was calculated using the measured pH and Ca, Mg, Na, CO_3 , PO_4 and dissolved organic carbon (DOC) concentrations as model input. A monovalent anion (NO_3^-) was added to the solution

to balance the charge of ions. The ionic strength was calculated by the model from the solution speciation using the Davies equation. The aqueous speciation reactions and their equilibrium constants are given in Hiemstra *et al.* (2010a). Adsorption of Ca, Mg and Na to DOC was calculated using the NICA-Donnan model (Milne *et al.*, 2003) using fulvic acid (FA) as a proxy for the DOC, assuming that 50% of the DOC behaved as FA and that 50% was non-reactive. The model calculations showed that the effect of DOC on the solution speciation was negligible since less than 3% of the Ca and Mg in solution was associated with DOC. The predicted free ion activities were used to calculate the degree of saturation of the solutions with respect to calcium-phosphate (CaHPO_4 , log K: -19.25), tricalcium-phosphate ($\text{Ca}_3(\text{PO}_4)_2$, log K: -25.5), octa-calcium-phosphate ($\text{Ca}_4\text{H}(\text{PO}_4)_3$, log K: -46.9) and apatite ($\text{Ca}_5(\text{PO}_4)_3\text{OH}$, log K: -58.2) (Lindsay, 1979). Furthermore, the free ion activities were used as model input in step ii of the modeling.

(ii) Surface Complexation Modelling. Goethite was used as a proxy for the metal-(hydr)oxide fraction in the soil, although also Al-(hydr)oxides may contribute or dominate the oxide fraction. This simplification can be justified since the competitive adsorption behavior of PO_4 and HA is comparable for Fe-(hydr)oxides and Al-(hydr)oxides (Hunt *et al.*, 2007; Sibanda and Young, 1986). The CD-MUSIC model (Hiemstra and Riemsdijk, 1996) was used to describe the adsorption of H, Ca, Mg, Na, PO_4 , CO_3 and OM to the goethite surface using the extended Stern model to represent the electrostatic structure of the surface. Model parameters, including surface species, adsorption affinities (log K) and charge distributions, are available in the supporting information (Table D2). The amount of amorphous oxides was calculated from the Fe_{ox} and Al_{ox} content using the molar mass of ferrihydrite (89 g mol^{-1} , FeOOH) and gibbsite (78 g mol^{-1} , $\text{Al}(\text{OH})_3$), respectively. The amount of crystalline Fe-(hydr)oxides was defined as Fe_{d} minus Fe_{ox} . The SSA (specific surface area) of the amorphous oxides was set equal to the SSA of ferrihydrite ($600 \text{ m}^2\text{g}^{-1}$) (Hiemstra and Van Riemsdijk, 2009) and the SSA of the crystalline Fe-(hydr)oxides was set equal to the SSA of goethite ($100 \text{ m}^2\text{g}^{-1}$) (Stachowicz *et al.*, 2008). Adsorption to clay minerals was not considered because the binding capacity of clay minerals for ortho-P is low compared to that of metal-(hydr)oxides (Borgnino *et al.*, 2009; Manning and Goldberg, 1996).

Adsorption of OM was described in the CD-MUSIC model by defining an OM surface species using FA as a proxy for OM (Hiemstra *et al.*, 2010b; Hiemstra *et al.*, 2013). The speciation and charge distribution of the adsorbed FA was taken from the LCD-modelling work of Filius *et al.*, (2002) and Weng *et al.*, (2005). A typical FA molecule contains 4 carboxyl groups (COO^-). Upon adsorption, one of the carboxylate groups will form an

innersphere complex ($=\text{FeOH}^{0.5} + \text{H}^+ + \text{RCOO}^{-1} \longleftrightarrow \text{FeOOCR}^{0.5} + \text{H}_2\text{O}$) and two of the carboxylate groups will form an outersphere complex ($=\text{FeOH}^{0.5} + \text{H}^+ + \text{RCOO}^{-1} \longleftrightarrow \text{FeOH}_2\cdots\text{OOCR}^{0.5}$) in the pH-range relevant for this study (7.0–8.5). There is no additional charge added to the surface upon adsorption of a carboxylate group because the sum of H^+ and RCOO^{-1} is zero, but there is a redistribution of charge over the 0- and 1-plane. The amount of redistributed charge ($\Delta z_0 = -\Delta z_1$) amounts to 0.5 and 0.8 v.u. (valence unit) for the innersphere and outersphere complexes, respectively. The fourth carboxylate group of the FA molecule remains unprotonated (COO^{-1}) and adds a charge of -1 v.u. to the Stern layer and this charge is equally distributed over the 1- ($\Delta z_1 = -0.5$) and 2-plane ($\Delta z_2 = -0.5$). The phenolic groups of adsorbed FA can be assumed to remain protonated and thus have no charge and no influence on phosphate adsorption (Hiemstra *et al.*, 2013; Weng *et al.*, 2005). In the CD-MUSIC model, the adsorption of one FA molecule can be simplified by introducing a $\text{H}_3\text{SOM}^{-1}$ species which contains four carboxylate groups. Including the adsorbed protons in the defined species ($\text{H}_3\text{SOM}^{-1}$) improves the mathematical stability of the model. The $\text{H}_3\text{SOM}^{-1}$ species adsorbs to three $=\text{FeOH}^{0.5}$ surface groups via the formation reaction: $3 =\text{FeOH}^{0.5} + \text{H}_3\text{SOM}^{-1} \longleftrightarrow =(\text{FeO})(\text{FeOH}_2)_2.\text{SOM}^{-1} + \text{H}_2\text{O}$. The overall distribution of charge over the three electrostatic planes (0-, 1-, 2-plane), as defined by the charge distribution coefficients Δz_0 , Δz_1 , Δz_2 , amounts to 2.1 (0.5 + 0.8 + 0.8), -2.6 (-0.5 - 0.8 - 0.8 - 0.5) and -0.5 respectively (Table D3). The amount of adsorbed $\text{H}_3\text{SOM}^{-1}$, or the effective OM-loading, was fitted until the predicted ortho-P concentration equals the ortho-P concentration in the water extracts, using the pH, the free ion activities of Ca, Mg, Na, and CO_3 , the oxide surface area and the NaOH-EDTA extractable ortho-P content as model input. All calculations were performed with the ECOSAT software.

6.3 Results and Discussion

6.3.1 Soil Properties.

The SOC contents vary between 6 and 44 g kg⁻¹ and decrease with an increase in soil depth (Table 6.2). For the topsoils, SOC contents are lower in the cropland (16–21 g kg⁻¹) than in the forest (22–44 g kg⁻¹). The fraction of SOC extractable in Na-pyrophosphate varies between 6 and 40% and does not show a trend with land use or soil depth. The clay (6–24%) and silt content (20–71%) varied considerably among the 33 soil samples, indicating differences in sedimentation conditions across the studied floodplain. The Fe_d content correlates positively with the silt content ($R^2=0.73$) which explains the variation in Fe_d

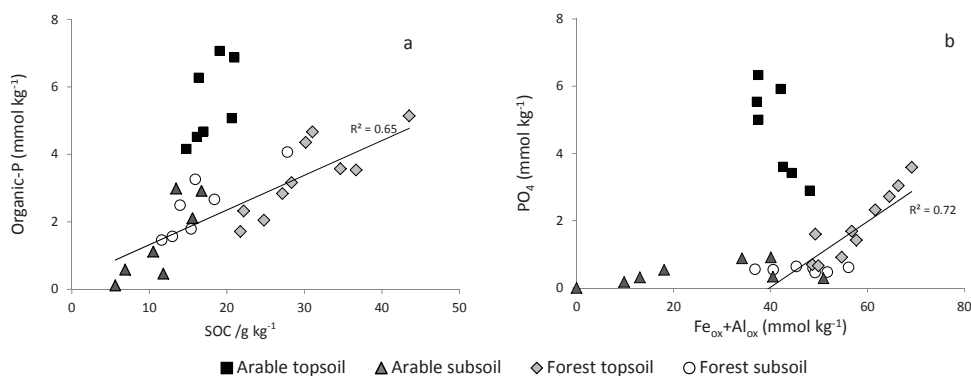


Figure 6.1. (a) The organic-P content plotted against the soil organic carbon (SOC) content for 33 samples from arable and forest soils. The line represents the correlation for all soils except the topsoils of the arable fields. (b) The phosphate content, extracted in NaOH-EDTA, plotted against the amount of amorphous Fe- plus Al-(hydr)oxides ($Fe_{ox} + Al_{ox}$). The line represents the correlation for the forest soils.

content between the sites (45–130 $mmol\ kg^{-1}$, Table 6.2). In contrast, the variation in Fe_{ox} is mainly related to soil age and the Fe_{ox} content is lower in the older arable soils (2.2–18.7 $mmol\ kg^{-1}$) than in the younger forest soils (26–52 $mmol\ kg^{-1}$) as is discussed in detail by Lair *et al.* (2009a). The Al_{ox} content varies between 7–34 $mmol\ kg^{-1}$ and, for soils with a low Fe_{ox} content, Al-(hydr)oxides dominate the amorphous metal-(hydr)oxide fraction.

6.3.2 Phosphorus speciation in the solid phase.

In the top soils, the TP content extracted in NaOH-EDTA is higher in the arable soils (9.7–11 $g\ kg^{-1}$, Table 6.2) than in the forest soils (2.4–5.9 $g\ kg^{-1}$), which can be explained by the long-term P-fertilization of the arable soils. For the arable soils, TP strongly decreases with increasing sampling depth (Table 6.2), indicating that transport of TP to deeper layers is limited. The strong accumulation of TP in the topsoils of arable sites can be explained by the high affinity of phosphate for adsorption to metal-(hydr)oxides (Rahnemaie *et al.*, 2007) and by the low solubility of calcium-phosphate and calcium-inositol-hexaphosphate precipitates (Graf, 1983; Grynspan and Cheryan, 1983; Koopmans *et al.*, 2007; Zee and Riemsdijk, 1986). The distribution of TP between organic-P (38–88%) and PO_4 (12–62%) does not show a trend with land use or sampling depth (results not shown).

Phosphate and organic-P strongly differ with respect to their interactions with the metal-(hydr)oxides in the soil. Organic-P does not correlate with the $Fe_{ox} + Al_{ox}$ content ($R^2=0.08$, results not shown), which can be explained by the nature of the organic P fraction. Organic-P

Table 6.2. General soil characteristics of the forest soil (site F1-F3) and arable soils (site F4, F5)

Nr.	Site	Depth (cm)	SOC ^a (g kg ⁻¹)	OC ^b _{pyr} (%)	Clay (%)	pH (-)	Fe _d ^c (mmol kg ⁻¹)	Fe _{ox} ^d (mmol kg ⁻¹)	Al _{ox} ^d (mmol kg ⁻¹)	P _{ox} ^d (mmol kg ⁻¹)	TP ^e (mmol kg ⁻¹)	PO ₄ ^e (mmol kg ⁻¹)	SSA ^f (m ² g ⁻¹)	PO ₄ loading ^g (μmol m ⁻²)	PO ₄ water ^h (μM)	OM loading ⁱ (μmol m ⁻²)
1	F1/1	0-5	25	3.1	8	7.8	102	8	16	7.5	5.1	3.0	4.1	0.75	3.66	1.33
5	F1/2	0-5	22	2.9	10	8.2	104	52	17	8.1	5.9	3.6	4.2	0.85	2.04	1.11
7	F1/3	0-5	22	2.9	7	8.1	99	49	15	7.2	4.4	2.7	4.0	0.69	2.01	1.25
9	F2/1	0-5	37	6.0	8	7.9	105	44	17	9.3	5.9	2.3	3.9	0.60	6.78	1.48
10	F2/1	5-10	28	5.6	9	7.9	102	40	16	7.8	4.8	1.7	3.6	0.47	4.53	1.55
11	F2/1	35-40	15	2.7	9	8.1	87	32	13	5.0	2.4	0.6	2.9	0.22	0.59	1.52
12	F2/1	41-46	13	1.8	8	8.2	80	28	13	4.6	2.1	0.5	2.6	0.21	0.82	1.54
13	F2/1	47-52	12	1.7	6	8.2	76	25	12	4.0	2.0	0.6	2.4	0.23	0.66	1.48
15	F2/2	5-10	27	4.5	8	8.3	112	34	15	7.0	4.4	1.6	3.3	0.48	4.08	1.46
18	F2/3	5-10	35	7.4	8	8.1	110	39	19	8.2	5.0	1.4	3.7	0.38	2.37	1.50
21	F3/1	0-5	44	6.7	10	8.0	124	31	24	8.3	6.1	0.9	3.7	0.25	2.85	1.65
22	F3/1	5-10	30	5.2	13	7.8	127	27	22	7.3	5.0	0.7	3.4	0.20	2.24	1.71
23	F3/1	12-17	28	5.7	14	8.0	129	31	25	8.0	4.7	0.6	3.8	0.16	0.88	1.63
24	F3/1	35-40	18	1.8	15	8.2	130	29	22	7.4	3.1	0.5	3.6	0.13	0.37	1.47
26	F3/1	45-50	16	4.1	18	8.2	126	28	20	6.3	3.8	0.6	3.4	0.17	0.40	1.52
27	F3/1	50-55	14	2.1	18	8.4	124	29	20	6.3	3.0	0.5	3.4	0.14	0.24	1.47
29	F3/2	5-10	31	6.6	14	8.2	122	29	21	6.6	5.3	0.7	3.4	0.19	1.69	1.64
32	F3/3	5-10	28	4.2	14	8.1	116	26	21	3.6	2.4	0.6	3.3	0.19	1.03	1.60
35	F4/1	5-10	16	3.1	19	8.3	75	7	30	12.3	10.1	5.5	2.4	2.32	9.69	0.20
36	F4/1	30-35	21	3.1	19	8.2	78	9	33	13.3	11.0	5.9	2.6	2.24	13.20	0.16
37	F4/1	46-51	13	2.2	18	8.3	73	6	34	6.1	3.9	0.9	2.5	0.36	0.30	1.24
38	F4/1	55-60	17	1.7	17	8.5	68	6	29	4.9	3.8	0.9	2.2	0.40	0.37	1.19

Table 6.2. continued

Nr.	Site	Depth (cm)	SOC ^a (g kg ⁻¹)	OC _{pyr} ^b -----	Clay (%)	pH	Fe _d ^c (mmol kg ⁻¹)	Fe _{ox} ^d -----	Al _{ox} ^d -----	P _{ox} ^d -----	TP ^e	PO ₄ ^e	SSA ^f m ² g ⁻¹	PO ₄ loading ^g μmol m ⁻²	PO ₄ water ^h μM	OM loading ^j μmol m ⁻²
39	F4/1	70-75	11	0.7	7	8.6	63	6	12	2.5	1.7	0.5	1.4	0.39	0.24	1.10
40	F4/2	5-10	15	3.3	21	8.4	82	9	29	13.0	10.5	6.3	2.5	2.57	13.43	0.06
42	F4/3	5-10	17	3.2	20	8.3	84	8	29	11.8	9.7	5.0	2.5	2.01	7.88	0.37
44	F5/1	2-7	19	4.9	16	8.3	58	9	39	10.8	10.0	2.9	2.8	1.05	1.59	0.91
45	F5/1	25-30	15	4.2	18	8.3	55	9	39	5.2	4.7	3.2	2.7	1.18	3.78	0.98
46	F5/1	35-40	16	5.4	25	8.4	51	4	36	6.2	2.4	0.3	2.3	0.14	0.03	1.20
47	F5/1	40-45	12	3.0	24	8.4	45	19	32	5.0	0.7	0.3	2.8	0.10	0.03	1.25
48	F5/1	45-50	7	2.8	24	8.5	45	2	11	1.9	0.9	0.3	1.0	0.31	0.03	0.91
50	F5/1	70-75	6	1.2	11	7.7	46	3	7	1.9	0.3	0.2	0.9	0.21	0.03	1.20
51	F5/2	2-7	16	5.2	16	8.3	62	8	34	11.1	9.9	3.6	2.5	1.42	4.27	0.73
55	F5/3	2-7	21	5.2	14	8.3	59	9	35	10.8	10.3	3.4	2.6	1.32	3.14	0.78

in soils is normally present as inositol-hexaphosphate (Koopmans et al., 2007; Murphy et al., 2009), which can be sequestered in the soil as poorly soluble Ca-precipitates (Graf, 1983; Grynspan and Cheryan, 1983) or due to adsorption to metal-(hydr)oxides (Celi et al., 2001; Graf, 1983; Grynspan and Cheryan, 1983). Precipitation of inositol-hexaphosphate with Ca is thermodynamically favored over adsorption to metal-(hydr)oxides at a neutral to alkaline pH (Celi et al., 2001; Graf, 1983; Grynspan and Cheryan, 1983). Therefore, in these calcareous soils, inositol-hexaphosphate is likely sequestered as Ca-precipitates rather than being associated with metal-(hydr)oxides in the soil. The amount of organic P is correlated with the SOC content ($R^2=0.65$, Figure 6.1a) except the topsoils of the arable fields which deviate from the correlation with SOC by having a much higher organic-P content due to probably the application of organic-P via manure fertilizer.

In contrast to organic-P, PO_4 is strongly associated with metal-(hydr)oxides in the soils. For the forest soils, the PO_4 contents shows a strong correlation with the Fe_{ox} content ($R^2=0.93$, results not shown) as well as with the $\text{Fe}_{\text{ox}}+\text{Al}_{\text{ox}}$ content ($R^2=0.73$, Figure 6.1b), which is in line with results from a previous PO_4 adsorption study for these sites (Lair et al., 2009c). The topsoils of the arable fields deviate from this correlation (Figure 6.1b) by having a much higher PO_4 content, relative to the $\text{Fe}_{\text{ox}}+\text{Al}_{\text{ox}}$ content, compared to the forest soils. This indicates a higher PO_4 saturation of the metal-(hydr)oxides in the arable soils. There was no correlation between the PO_4 content and the clay content (results not shown), which can be explained by the low PO_4 adsorption capacity of clay minerals compared to metal-(hydr)oxides (Borgnino et al., 2009). Furthermore, the PO_4 content in the forest soils does not correlate with the Fe_d content, indicating that the crystalline Fe-(hydr)oxides ($\text{Fe}_d-\text{Fe}_{\text{ox}}$) hardly contribute to the surface area available for anion adsorption, although crystalline Fe-(hydr)oxides make up 50–90% of the total Fe-(hydr)oxide content. The low contribution of the crystalline Fe-(hydr)oxides to the anion-adsorption capacity of the soil is in line with the low SSA of crystalline Fe-(hydr)oxides ($100 \text{ m}^2\text{g}^{-1}$) compared to the SSA of amorphous Fe-(hydr)oxides ($600 \text{ m}^2\text{g}^{-1}$) (Cornell and Schwertmann, 2006). These regressions show that the surface area available for PO_4 adsorption is dominated by the amount of amorphous metal-(hydr)oxides (i.e. $\text{Fe}_{\text{ox}}+\text{Al}_{\text{ox}}$).

Comparing the P_{ox} content with the TP and PO_4 content extracted in NaOH-EDTA enables us to evaluate whether the commonly used P_{ox} can be used as a measurement for the amount of oxide-associated PO_4 in calcareous soils. The P_{ox} content correlates strongly with the TP and PO_4 content ($R^2=0.91$ and 0.74 , respectively, Figure D1). However, the P_{ox} content is on average 1.8 times higher than the TP content and 6 times higher than

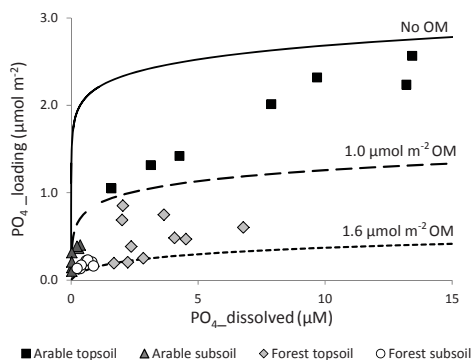


Figure 6.2. The PO_4 loading on the metal-(hydr)oxide surfaces as a function of the water-soluble PO_4 concentrations for 33 soil samples from arable and forest soils. The lines show the PO_4 adsorption isotherms which were calculated by surface-complexation modelling for an organic matter (OM) loading on the metal-(hydr)oxides of 0, 1.0, and 1.6 $\mu\text{mol m}^{-2}$ and using the average pH (8.2) and soluble Ca concentration (1 mM) in the water extracts.

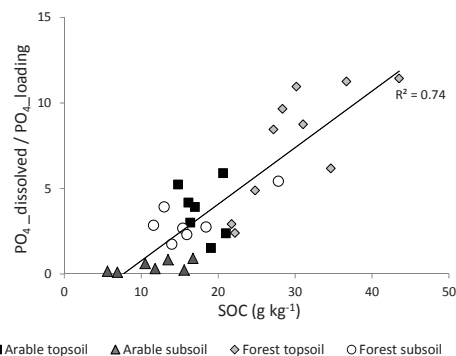


Figure 6.3. The ratio between the water-soluble PO_4 concentration and the PO_4 loading on the metal-(hydr)oxides ($PO_4\text{-water}:PO_4\text{-loading}$) as a function of the soil organic carbon (SOC) content for 33 soil samples from arable and forest soils.

the PO_4 content (Figure D1). These results indicate that P_{ox} seriously overestimates the amount of oxide-associated PO_4 in these calcareous soils, which is likely due to dissolution of calcium-phosphate minerals in the acid-oxalate extractant (pH 3.0) and extraction of organic-P. Recently, Cui and Weng (2013) showed that organic-P explains up to 25% of the P_{ox} content in non-calcareous arable soils. Thus, our results show that P_{ox} cannot be used as a measurement for the oxide-associated PO_4 in calcareous soils.

6.3.3 Phosphate solubility is controlled by competition with OM.

Water-soluble PO_4 concentrations vary between 0.03 and 13.4 μM (0.001–0.42 mg l^{-1}) and decrease with increasing sampling depth (Table 6.1). Remarkably, PO_4 concentrations are rather similar in the arable and forest soils, which is in contrast with the higher $PO_4:(Fe_{ox}+Al_{ox})$ ratio in the arable soils (Figure 6.1b). DOC concentrations in water extract range between 4 and 44 mg l^{-1} and Ca is the dominant cation in the water-extracts (0.3–1.7 mM) (Table D1). First, we tested whether precipitation of PO_4 with Ca^{2+} could have occurred after desorption of PO_4 from the soil. Therefore, the degree of saturation of the solutions with respect to common calcium-phosphate minerals was calculated using the pH and free Ca^{2+} and PO_4^{3-} activities obtained from the solution speciation modelling. The results

show that PO_4 concentrations in the water extracts are far below saturation with respect to calcium-phosphate and tricalcium-phosphate, meaning that precipitation of these minerals did not occur. In contrast, most extracts were oversaturated with respect to poorly soluble octa-calcium-phosphate and hydroxy-apatite (Table D2), however, direct precipitation of these minerals from solutions is kinetically inhibited since these minerals cannot form without the presence of the more soluble tricalcium-phosphate mineral as a pre-cursor (van Kemenade and de Bruyn, 1987; Weng et al., 2011). These model calculations are supported by the previous study of Weng et al. (2011) who found for similar pH range that precipitation of PO_4 did not occur in soil extracts with a Ca^{2+} concentration below 5 mM. Furthermore, it can be expected that PO_4 concentrations were not significantly influenced by dissolution of hydroxy-apatite since this mineral has extremely low solubility in water (Lindsay, 1979). Therefore, we conclude that the water-soluble PO_4 concentrations are controlled by desorption rather than by precipitation or dissolution.

The water-soluble PO_4 concentrations are poorly correlated to the PO_4 loading on the oxide surfaces (Figure 6.2). The PO_4 loading (Table 6.2) was calculated from the PO_4 content, extracted in the NaOH-EDTA, divided by the estimated surface area of the amorphous ($\text{Fe}_{\text{ox}} + \text{Al}_{\text{ox}}$) and crystalline metal-(hydr)oxides ($\text{Fe}_d - \text{Fe}_{\text{ox}}$), using a SSA of 600 and 100 m^2g^{-1} for amorphous and crystalline metal-(hydr)oxides, respectively (Stachowicz et al., 2008). For the topsoils, PO_4 loadings (0.2–2.3 $\mu\text{mol m}^{-2}$) are higher in the arable soils than in the forest soils. For the subsoils, PO_4 loadings are all below 0.5 $\mu\text{mol m}^{-2}$, irrespective of land use. Remarkably, the same soluble PO_4 concentration corresponds to a much higher PO_4 loading in the arable soils than in the forest soils. For example, for the top soils, the PO_4 loading is 3.5–6.5 times higher in the arable soils than in the forest soils for a similar water-soluble PO_4 concentration. For the subsoils, PO_4 concentrations are 2–10 times higher in the forest soils compared to the arable soils at the same PO_4 loading. Thus, the PO_4 loading alone is a poor predictor for the water-soluble PO_4 , meaning that other factors control the distribution of PO_4 between the adsorbed and dissolved phase.

The strong differences in PO_4 solubility at the same PO_4 loading can be explained by competition with organic matter. First, the ratio between $\text{PO}_{4,\text{water}}/\text{PO}_{4,\text{loading}}$ shows a strong and positive correlation with the SOC content ($R^2=0.74$, Figure 6.3). Thus, for soils with a similar pH and soluble Ca concentration, a higher SOC content corresponds to a higher PO_4 solubility at the same PO_4 loading, indicating competition for adsorption. To our best knowledge, this is the first time a correlation between the SOC content and the distribution of PO_4 between the dissolved and adsorbed phase is presented in literature. Secondly, the

SC-model predictions show that the differences in PO_4 concentration can be explained by competition between OM on PO_4 for adsorption to the metal-(hydr)oxides (Figure 6.2). Without considering simultaneous adsorption of OM, the model strongly overestimates the PO_4 loading needed to explain the observed soluble PO_4 concentrations, as is shown from the predicted adsorption isotherm (solid line) in Figure 6.2. This adsorption isotherm was calculated for the average pH (8.2) and Ca concentration (1 mM) in the water extracts. The variation in pH and Ca concentration among the individual samples is low and has therefore only a minor effect on the position of the predicted adsorption isotherm. When simultaneous adsorption of OM is considered, the model predicts a decrease in the apparent adsorption affinity of PO_4 with increasing OM loading, as is shown in Figure 6.2 for an OM loading of 1.0 and 1.6 $\mu\text{mol m}^{-2}$ (Figure 6.2). Based on these isotherms, the OM loading in the topsoils of the arable fields should be below 1.0 $\mu\text{mol m}^{-2}$, whereas the OM loading in the forest soils and subsoils of the arable fields should vary between 1.0 and 1.6 $\mu\text{mol m}^{-2}$ in order to explain the observed distribution of PO_4 between the adsorbed and dissolved phase. In contrast to previous modelling studies (Hiemstra et al., 2010a; Hiemstra et al., 2013; Weng et al., 2011), which were limited to topsoils of arable fields with high PO_4 and SOC contents, we show that the competition between PO_4 and OM also affects PO_4 solubility in subsoils and forest soils despite their lower PO_4 content. Neglecting the competition with OM results in an underestimation of the soluble PO_4 concentrations with several orders of magnitude. For example, for the forest soils, which have a PO_4 loading below 0.5 $\mu\text{mol m}^{-2}$, the PO_4 concentrations predicted for a soil without OM are below 0.001 μM whereas the measured PO_4 concentrations vary between 0.24 and 6.78 μM . Thus, the model predictions (Figure 6.2) and the observed correlation (Figure 6.3) show that the higher PO_4 solubility in the forest soils, relative to the PO_4 loading, can be explained by a stronger competition with organic matter in the forest soils compared to the arable soils. These results imply that the solubility of PO_4 , and its availability for plant uptake, is higher in soils with a higher SOC content, suggesting that organic amendments will enhance availability of PO_4 .

6.3.4 *The effective OM loading is higher in forest soils than in arable soils*

The OM loadings on the metal-(hydr)oxides (Table 6.2), which were fitted by the SC-model until the predicted and measured soluble PO_4 concentrations were similar, are shown in Figure 6.4 for the different land use types, sampling depths and soil ages. For the topsoils, predicted OM loadings are 2–28 times higher for the forest soils (1.1–1.7 $\mu\text{mol m}^{-2}$) than for the arable soils (0.06–0.91 $\mu\text{mol m}^{-2}$). For the arable soils, the OM loading is lower in

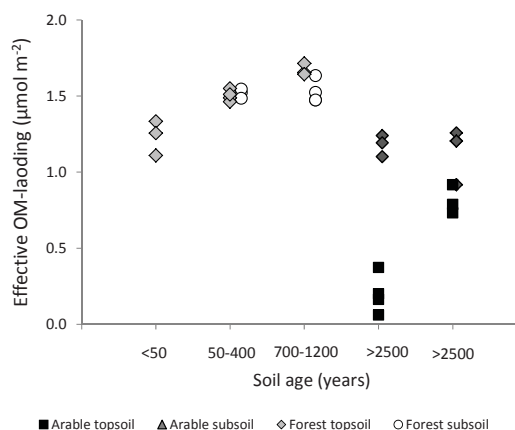


Figure 6.4. The effective OM loading for 33 soil samples from forest and arable soils ranked to the soil age, which was previously derived by Lair *et al.*, 2009a. The effective OM loading was estimated by surface complexation modelling as described in the main text.

the topsoils than in the subsoils, which can be explained by the high PO_4 loading in the topsoils. For the forest soils, the OM loading is similar in the topsoils and subsoils, which seems in contrast with the decrease of the SOC content with increasing sampling depth. However, the predicted OM loading should be interpreted as an effective OM loading since it reflects the level of competition experienced by a phosphate molecule adsorbed on the oxide surface rather than the actual amount of OM adsorbed on the surface. Since adsorbed humic substances can extend far beyond the Stern layer (Hiemstra *et al.*, 2013; Weng *et al.*, 2008), a similar effective OM loading in the top and subsoils can correspond to a lower actual OM loading in the subsoils when the average molecular weight (MW) of the humic substances in the subsoils is lower than in the topsoils.

The amount of oxide-associated OC in the soil ($\text{OC}_{\text{oxides}}$) can be estimated from the calculated OM loading using some assumptions with respect to the MW and carbon content of the adsorbed OM. We assume that the adsorbed OM has a MW of 1.9 kD and a carbon content of 50%, which is reasonable for FA (Weng *et al.*, 2008). Multiplying the effective OM loading by the MW and carbon content gives the estimated OC loading (0.05–1.7 mg C m^{-2}). The OC loading multiplied by the total oxide's surface area (Table 6.2) gives the amount of OC adsorbed to metal-(hydr)oxides ($\text{OC}_{\text{oxides}}$) in the soils, which varies between 0.1–5.9 g C kg^{-1} soil. The correlation between $\text{OC}_{\text{oxides}}$ and SOC ($R^2=0.46$, results not shown) is rather poor, and even worse for the pyrophosphate-extractable OC ($R^2=0.18$, results not shown). In contrast, Gustafson (2006) found a rather good correlation between the pyrophosphate-

extractable OC and the oxide-associated OC predicted by SC-modelling, however, for a set of four soils only. The poor correlation between OCoxides and the pyrophosphate-extractable OC may indicate that pyrophosphate does not selectively extract OC associated with metal-(hydr)oxides, but also extracts OC associated to calcium as coagulated OC (Kaiser et al., 2011). Another plausible explanation for the poor correlations is that soils show considerable variation with respect to the average MW of the oxide-associated OC (Perminova et al., 2003). Thus, the currently poorly understood relationship between the predicted and actual OC contents warrants further research on the molecular properties of oxide-associated OC in soils.

The effective OM loading correlates negatively with the PO_4 loading ($R^2=0.85$, Figure D2), which is in agreement with previous findings of Hiemstra et al. (2010b). This correlation suggests that there is a causal relationship between excessive PO_4 application and the decline in the OM loading in arable soils. Adsorption experiments with goethite showed a strong decrease in FA and HA adsorption in the presence of PO_4 (Antelo et al., 2007; Weng et al., 2008). Also for soils, experiments showed an increase in DOC when PO_4 was added in large quantities to the soil, which points to desorption of OM from mineral surfaces due to competition with PO_4 (Chardon et al., 2012; Cui et al., 2011; Duffner et al., 2012; Hunt et al., 2007; Kang et al., 2011; Zhang and Zhang, 2010). Desorption of humic substances from metal-(hydr)oxide surfaces in soils is extremely slow (Zhou et al., 2001), which may explain why some authors did not find a significant effect (Guppy et al., 2005a; Guppy et al., 2005b). The soils in this study have been equilibrated for years to decades in the field, suggesting that soils should be near equilibrium with respect to the PO_4 and OM loading. Organic matter adsorbed to Fe-(hydr)oxides is protected against biodegradation (Eusterhues et al., 2014, however, once desorbed, the OM may be lost from the soil due to leaching or biodegradation, or may remain in the soil as coagulated OM. Besides P-fertilization, other differences in soil management between forest and cropland soils, such as low C-inputs and mechanical disturbances, may also affect OM contents (Guo and Gifford, 2002; Six et al., 2002; Zehetner et al., 2009). However, low C-inputs and mechanical disturbances of soil aggregates normally lead to a decrease in the easily biodegradable particulate organic matter (POM) fraction whereas the mineral-associated OM remains unaffected (Helfrich et al., 2006; John et al., 2005). Thus, mechanical disturbances and low C inputs cannot fully explain the lower OM loading predicted in the arable soils. Therefore, our interpretation of the results and model predictions shows that the low OM loadings in the arable fields are caused by the strong competition with PO_4 due to excessive P-fertilization.

In addition to land use, also the soil age affects the effective OM loading. For the forest soils, the OM loading in the topsoils shows an increasing trend with increasing soil age (Figure 6.4). The predicted OM loading in the youngest forest site (≈ 50 year) is already rather high and corresponds to 70% of the OM loading in the oldest forest site, which is 700–1200 year old. Thus, the effective OM-loading seems to develop rapidly during the initial stages of soil formation. This finding is in agreement with the conclusion of Zehetner et al., (2009) who analyzed SOC contents along the Marchfeld chronosequence and found that SOC rapidly accumulates during the first 100 year of soil formation. From our results, it cannot be concluded whether the OM loadings are near equilibrium at 1200 year or will continue to increase over time since the oldest sites (>2500 year) are used as cropland. The use of these soils for arable farming has resulted in a loss of oxide-associated OM, likely due to excessive P-fertilization. As such, land use has a much stronger effect on the OM loading than soil age.

6.4 Conclusions

Our experimental and modelling results show that the competition between PO_4 and OM for adsorption to metal (hydr)oxides affects the solubility of PO_4 as well as the amount of OM adsorbed to the metal-(hydr)oxides. This competition is of importance in the topsoils as well as in the subsoils, despite the much lower SOC and PO_4 contents in the subsoils. The soluble PO_4 concentrations were underestimated with several orders of magnitude if competition with OM was not considered in SC-modelling. As a consequence of the higher SOC content in forest soils, a similar PO_4 loading corresponds to a higher soluble PO_4 concentration in the forest soils than in the arable soils. These results have important implications for predictions of P bioavailability and mobility. We suggest that predictions of bioavailability and mobility can be significantly improved when soluble PO_4 concentrations are predicted by SC modelling taking the competition with OM into account, rather than by the using solely the $\text{P}_{\text{ox}}/\text{Fe}_{\text{ox}}+\text{Al}_{\text{ox}}$ ratio. Furthermore, our results suggest that the availability of PO_4 in soils can be enhanced by the application of organic amendments that compete with PO_4 for adsorption to the oxide surfaces. The predicted OM loading on metal-(hydr)oxides is 2–28 times lower in topsoils of the arable fields than in the forest fields, which can be explained by replacement of OM for PO_4 in the arable soils. As such, high levels of P fertilization may in time lead to a loss of the oxide-associated OM in arable soils due to saturation of the metal-(hydr)oxide surfaces with PO_4 . Therefore, we suggest that the potential to sequester carbon by adsorption to metal-(hydr)oxides is lower in PO_4 -rich arable soils than in PO_4 -poor forest soils. Furthermore, OM loadings increase with increasing soil age, although

land use has a much stronger effect on the OM loading. Overall, this study demonstrates that competitive adsorption interactions can be successfully described by SC-modelling and that these interactions should receive more attention in further research on PO_4 solubility and carbon stabilization by metal-(hydr)oxides.

Acknowledgement

We gratefully acknowledge funding from the European Commission FP 7 Project “Soil Transformations in European Catchments” (SoilTrEC) and we thank the project partners for their help in soil sampling and data collection.

References

- Antelo, J., Arce, F., Avena, M., Fiol, S., López, R., Macías, F., 2007. Adsorption of a soil humic acid at the surface of goethite and its competitive interaction with phosphate. *Geoderma* 138(1-2), 12-19.
- Banwart, S., Menon, M., Bernasconi, S.M., Bloem, J., Blum, W.E., de Souza, D.M., Davidsdotir, B., Duffy, C., Lair, G.J., Kram, P., 2012. Soil processes and functions across an international network of Critical Zone Observatories: Introduction to experimental methods and initial results. *Comptes Rendus Geoscience*.
- Borgnino, L., Avena, M.J., De Pauli, C.P., 2009. Synthesis and characterization of Fe(III)-montmorillonites for phosphate adsorption. *Colloids and Surfaces A: Phys. Eng. As.* 341(1-3), 46-52.
- Celi, L., Presta, M., Ajmore-Marsan, F., Barberis, E., 2001. Effects of pH and electrolytes on inositol hexaphosphate interaction with goethite. *Soil Sci. Soc. Am. J.* 65, 753-760.
- Chardon, W.J., Groenenberg, J.E., Temminghoff, E.J.M., Koopmans, G.F., 2012. Use of reactive materials to bind phosphorus. *J. Environ. Qual.* 41(3), 636-646.
- Cornell, R.M., Schwertmann, U., 2006. *The iron oxides. Structure, properties, reactions, occurrences and uses.* 2nd edition ed. Wiley-VCH Verlag.
- Cui, H., Wang, M.K., Fu, M., Ci, E., 2011. Enhancing phosphorus availability in phosphorus-fertilized zones by reducing phosphate adsorbed on ferrihydrite using rice straw-derived biochar. *J. Soil. Sed.* 11, 1135-1141.
- Duffner, A., Hoffland, E., Temminghoff, E.J.M., 2012. Bioavailability of zinc and phosphorus in calcareous soils as affected by citrate exudation. *Plant Soil* 361, 165-175.
- Eusterhues, K., Neidhardt, J., Hadrich, A., Kusel, K., Totsche, K.U., 2014. Biodegradation of ferrihydrite-associated organic matter. *Biogeochem.* 1, 6.
- Graf, E., 1983. Calcium binding to phytic acid. *J. Agric. Food Chem.* 31(4), 851-853.
- Grynsan, F., Cheryan, M., 1983. Calcium phytate: Effect of pH and molar ratio on in vitro solubility. *J. Am. Oil Chem. Soc.* 60(10), 1763-1765.
- Guo, L.B., Gifford, R.M., 2002. Soil carbon stocks and land use change: a meta analysis. *Glob. change. biol.* 8(4), 345.
- Guppy, C.N., Menzies, N.W., Blamey, F.P.C., Moody, P.W., 2005a. Do decomposing organic matter residues reduce phosphorus sorption in highly weathered soils? *Soil Sci. Soc. Am. J.* 69, 1405-1411.
- Guppy, C.N., Menzies, N.W., Moody, P.W., Blamey, F.P.C., 2005b. Competitive sorption reactions between phosphorus and organic matter in soil: a review. *Soil Research* 43(2), 189-202.

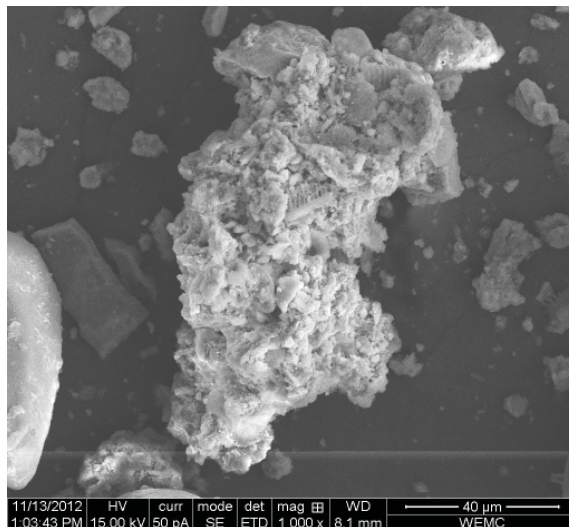
- Helfrich, M., Ludwig, B., Buurman, P., Flessa, H., 2006. Effect of land use on the composition of soil organic matter in density and aggregate fractions as revealed by solid-state ^{13}C NMR spectroscopy. *Geoderma* 136, 331-341.
- Hiemstra, T., Antelo, J., Rahnemaie, R., Van Riemsdijk, W.H., 2010a. Nanoparticles in natural systems I: The effective reactive surface area of the natural oxide fraction in field samples. *Geochim. Cosmochim. Ac.* 74(1), 41-58.
- Hiemstra, T., Antelo, J., Van Rotterdam, A.M.D., Van Riemsdijk, W.H., 2010b. Nanoparticles in natural systems II: The natural oxide fraction at interaction with natural organic matter and phosphate. *Geochim. Cosmochim. Ac.* 74(1), 59-69.
- Hiemstra, T., Mia, S., Duhaut, P.B., Molleman, B., 2013. Natural and pyrogenic humic acids at goethite and natural oxide surfaces interacting with phosphate. *Environ. Sci. Technol.* 47(16), 9182-9189.
- Hiemstra, T., Van Riemsdijk, W.H., 1996. A surface structural approach to ion adsorption: the charge distribution (CD) model. *J. Colloid Interf. Sci.* 179, 488-508.
- Hiemstra, T., Van Riemsdijk, W.H., 2009. A surface structural model for ferrihydrite I: Sites related to primary charge, molar mass, and mass density. *Geochim. Cosmochim. Ac.* 73(15), 4423-4436.
- Hunt, J.F., Ohno, T., He, Z., Honeycutt, C.W., Dail, D.B., 2007. Inhibition of phosphorus sorption to goethite, gibbsite and kaolin by fresh and decomposed organic matter. *Biol. Fertil. Soils* 44, 277-288.
- John, B., Yamashita, T., Ludwig, B., Flessa, H., 2005. Storage of organic carbon in aggregate and density fractions of silty soils under different types of land use. *Geoderma* 128, 63-79.
- Kaiser, K., Walter, K., Ellerbrock, R.H., Sommer, M., 2011. Effects of land use and mineral characteristics on the organic carbon content, and the amount and composition of Na-pyrophosphate-soluble organic matter, in subsurface soils. *Eur. J. Soil. Sci.* 62, 226-236.
- Kaiser, M., Ellerbrock, R.H., Wulf, M., Dultz, S., Hierath, C., Sommer, M., 2012. The influence of mineral characteristics on organic matter content, composition, and stability of topsoils under long-term arable and forest land use. *J. Geophys. Res.* 117(G2).
- Kang, J., Amoozegar, A., Hesterberg, D., Osmond, D.L., 2011. Phosphorus leaching in a sandy soil as affected by organic and inorganic fertilizer sources. *Geoderma* 161, 194-201.
- Koopmans, G.F., Chardon, W.J., McDowell, R.W., 2007. Phosphorus movement and speciation in a sandy soil profile after long-term animal manure applications. *J. Environ. Qual.* 36(1), 305-315.
- Lair, G.J., Zehetner, F., Fiebig, M., Gerzabek, M.H., van Gestel, C.A., Hein, T., Hohensinner, S., Hsu, P., Jones, K.C., Jordan, G., Koelmans, A.A., Poot, A., Slijkerman, D.M., Totsche, K.U., Bondar-Kunze, E., Barth, J.A., 2009a. How do long-term development and periodical changes of river-floodplain systems affect the fate of contaminants? Results from European rivers. *Environ. Poll.* 157(12), 3336-3346.
- Lair, G.J., Zehetner, F., Hrachowitz, M., Franz, N., Maringer, F.J., Gerzabek, M.H., 2009b. Dating of soil layers in a young floodplain using iron oxide crystallinity. *Quat. Geochron.* 4(3), 260-266.
- Lair, G.J., Zehetner, F., Khan, Z.H., Gerzabek, M.H., 2009c. Phosphorus sorption-desorption in alluvial soils of a young weathering sequence at the Danube River. *Geoderma* 149(2), 39-44.
- Lindsay, W.L., 1979. *Chemical Equilibria in Soils*. Wiley-Interscience.
- Manning, B.A., Goldberg, S., 1996. Modeling arsenate competitive adsorption on kaolinite, montmorillonite and illite. *Clays Clay Miner.* 44(5), 609-623.
- Mehra, O.P., Jackson, M.L., 1960. Iron oxide removal from the soils and clays by dithionite-citrate system buffered with sodium bicarbonate. *Clays Clay Miner.* 7, 317-327.
- Mikutta, R., Kaiser, K., 2011. Organic matter bound to mineral surfaces: Resistance to chemical and biological oxidation. *Soil Biol. Biochem.* 43(8), 1738-1741.

- Milne, C.J., Kinniburgh, D.G., van Riemsdijk, W.H., Tipping, E., 2003. Generic NICA-Donnan model parameters for metal-ion binding by humic substances. *Environ. Sci. Tech.* 37, 958-971.
- Murphy, J., Riley, J.P., 1962. A modified single solution method for the determination of phosphate in natural waters. *Anal. Chim. Acta.* 27(1), 31-36.
- Murphy, P., Bell, A., Turner, B., 2009. Phosphorus speciation in temperate basaltic grassland soils by solution ³¹P NMR spectroscopy. *Eur. J. Soil Sci.* 60(4), 638-651.
- Perminova, I.V., Frimmel, F.H., Kudryavtsev, A.V., Kulikova, N.A., Abbt-Braun, G., Hesse, S., Petrosyan, V.S., 2003. Molecular weight characteristics of humic substances from different environments as determined by size exclusion chromatography and their statistical evaluation. *Environ. Sci. Technol.* 37(11), 2477-2485.
- Rahnemaie, R., Hiemstra, T., van Riemsdijk, W.H., 2007. Geometry, charge distribution, and surface speciation of phosphate on goethite. *Langmuir* 23(7), 3680-3689.
- Schneider, M.P.W., Scheel, T., Mikutta, R., van Hees, P., Kaiser, K., Kalbitz, K., 2010. Sorptive stabilization of organic matter by amorphous Al hydroxide. *Geochim. Cosmochim. A.* 74, 1606-1619.
- Schwertmann, U., 1973. Use of oxalate for Fe extraction from soils. *Can. J. Soil. Sci.* 53(2), 244-246.
- Sibanda, H.M., Young, S.D., 1986. Competitive adsorption of humus acids and phosphate on goethite, gibbsite and two tropical soils. *J. Soil Sci.* 37(2), 197-204.
- Six, J., Callewaert, P., Lenders, S., De Gryze, S., Morris, S.J., Gregorich, E.G., Paul, E.A., Paustian, K., 2002. Measuring and understanding carbon storage in afforested soils by physical fractionation. *Soil Sci. Soc. Am. J.* 66(6), 1981-1987.
- Stachowicz, M., Hiemstra, T., van Riemsdijk, W.H., 2008. Multi-competitive interaction of As(III) and As(V) oxyanions with Ca, Mg, PO₄, and CO₃ ions on goethite. *J. colloid interf. sci.* 320(2), 400-414.
- van Kemenade, M.J.J.M., de Bruyn, P.L., 1987. A kinetic study of precipitation from supersaturated calcium phosphate solutions. *J. colloid interf. sci.* 118(2), 564-585.
- van der Zee, S.E.A.T.M., van Riemsdijk, W.H., 1986. Transport of phosphate in a heterogeneous field. *Transport Porous. Med.* 1, 339-359.
- Weng, L., van Riemsdijk, W.H., Hiemstra, T., 2008. Humic nanoparticles at the oxide-water interface: Interactions with phosphate ion adsorption. *Environ. Sci. Tech.* 42, 8747-8752.
- Weng, L., Vega, F.A., van Riemsdijk, W.H., 2011. Competitive and synergistic effects in pH dependent phosphate adsorption in soils: LCD Modeling. *Environ. Sci. Technol.* 45(19), 8420-8428.
- Weng, L.P., Koopal, L.K., Hiemstra, T., Meeussen, J.C.L., van Riemsdijk, W.H., 2005. Interactions of calcium and fulvic acid at the goethite-water interface. *Geochim. Cosmochim. Ac.* 69(2), 325-339.
- Zehetner, F., Lair, G.J., Gerzabek, M.H., 2009. Rapid carbon accretion and organic matter pool stabilization in riverine floodplain soils. *Global Biogeochem. Cycles* 23(4).
- Zehetner, F., Lair, G.J., Maringer, F.J., Gerzabek, M.H., Hein, T., 2008. From sediment to soil: floodplain phosphorus transformations at the Danube River. *Biogeochem.* 88(2), 117-126.
- Zhang, M., Zhang, H., 2010. Co-transport of dissolved organic matter and heavy metals in soils induced by excessive phosphorus applications. *J. Environ. Sci.* 22(4), 598-606.
- Zhou, Q., Maurice, P.A., Cabaniss, S.E., 2001. Size fractionation upon adsorption of fulvic acid on goethite: equilibrium and kinetic studies. *Geochim. Cosmochim. Ac.* 65(5), 803-812.

Chapter 7

Mechanistic linkages between soil aggregates, soil porosity and soil physical-chemical properties

Inge C. Regelink, Cathelijne R. Stoof, Svetla Rousseva, Liping Weng,
Georg J. Lair, Pavel Kram, Nikolaos P Nikolaidis, Milena Kercheva, Steve
Banwart, Rob N.J. Comans



Abstract

The mechanistic linkages between soil structure and physical-chemical soil properties are still poorly understood due to the wide size-range at which aggregation occurs and the variety of aggregation factors and processes involved. To understand these processes, we collected data on aggregate fractions, soil porosity and physical-chemical properties of 127 soils, which covered a wide range in characteristics and were collected from three European Critical Zone Observatories. First, we established the mechanistic linkages between porosity and aggregates. Soil micro and micro+meso porosity increased with increasing fraction of water-stable aggregates (>0.25 mm, WSA), whereas this correlation was not significant for the fraction of dry-sieved aggregates (> 1mm, DSA). The fraction of DSA showed a strong, positive correlation with the ratio between microporosity and micro+mesoporosity ratio ($\theta_{30 \text{ kPa}}/\theta_{0.25 \text{ kPa}}$), suggesting that micropores are dominantly located within DSA whereas mesopores are located in-between DSA and loose particles. The fractions of DSA and WSA were not correlated showing that the presence of WSA is not a prerequisite to form DSA. Secondly, we studied the relations between the physical-chemical properties and soil structure. Soil texture had only a minor effect on the fractions of WSA and DSA whereas Fe-(hydr)oxides correlated positively with the fraction of WSA and with the micro-porosity. We suggest that Fe-(hydr)oxides provide adsorption sites for organic substances on larger minerals and thereby enable poorly reactive mineral particles to be taken up in the network of organic substances. Furthermore, the fraction of WSA increased with an increase in the soil organic carbon (SOC) content and with a decrease in pH. This pH-effect was explained by the enhanced coagulation of organically-coated particles at a lower pH. Overall, this study provides, for the first time, evidence for the mechanistic linkages between aggregate fractions and porosity, and shows that the role of Fe-(hydr)oxides in the formation of aggregates and pores is of higher importance than previously thought.

7.1 Introduction

Soils provide major ecosystem services such as food production, water retention and sequestration of soil organic carbon (SOC). The physical structure of the soil plays a crucial role in the processes that facilitate these soil functions. Yet, intensive land use and poor agricultural management practices have led to a decline in the quality of the soil structure, leading to a decrease in the agricultural productivity and SOC stabilization capacity of soils worldwide (Banwart, 2011; Montgomery, 2007). Soil structure is the result of multiple

physical, chemical and biological interactions in the soil. However, the complex interactions between physical-chemical properties and soil structure are still poorly understood which limits our ability to improve soil structural properties by adjusting soil management practices. Therefore, there is a need for a mechanistic understanding of the physical and chemical key-factors controlling the formation of soil aggregates from loose mineral particles.

Soil structure has been defined as 'the size, shape and characteristics of soil particles, aggregates, and pores across the size-range from nanometers to centimeters' (Bronick and Lal, 2005; Oades, 1993). This definition implies that soil structure is the product of various structural entities that cover a size-range of several orders of magnitude. According to the widely used aggregate hierarchy theory (Oades and Waters, 1991), soil aggregates and soil pores are formed in a hierarchical manner meaning that micro-aggregates (<0.25 mm) are the building blocks for macro-aggregates (>0.25 mm) and that aggregation is controlled by different aggregation factors at each size scale. In order to verify the aggregate hierarchy theory, we propose to quantify the soil structure at the various hierarchical levels by a combination of (i) the size distribution and stability of the aggregates and (ii) the volume and size distribution of the pores. Soil aggregates and soil porosity reflect different aspects of the structure, with micropores reflecting much smaller structural entities than mesopores, and water-stable aggregates (WSA) reflecting much stronger aggregates than dry-sieved aggregates (DSA). Because pores are the voids within and in between aggregates, it can be expected that the number of aggregates and the pore volume are related to each other (Boix Fayos, 1997; Nyamangara et al., 2001). This relationship was described by Dexter (1988) who stated that, if aggregate hierarchy exists, smaller aggregates should have a lower porosity than larger aggregates because the latter contain also the pores between the smaller aggregates that comprise them. However, experimental evidence for the relation between aggregate fractions and porosity for various soil types are still very scarce. Insight into these relationships may help to understand how the various hierarchal levels are related. As such, we expect that a combination of aggregate and porosity measurements can be used to quantify soil structure at different size scales and different levels of aggregate strength, which is a prerequisite for understanding at which level the various physical-chemical interactions affect aggregation.

The interplay between the various physical-chemical processes involved in aggregate formation is highly complex and affected by various soil properties. Various factors have been reported in literature to affect or control aggregation (Bronick and Lal, 2005). The

most commonly mentioned parameters are (i) soil texture, (ii) the amount of metal-(hydr)oxides, (iii) the amount and characteristics of organic binding agents and (iv) the pH and the concentration of multivalent cations. Clay minerals affect aggregation because of their interactions with organic matter (OM), leading to the formation of organo-mineral assemblages (Angers, 1998; Fernández-Ugalde et al., 2013; Six et al., 2000a). Similar, Fe-(hydr)oxides play an important role in the formation of organic-mineral assemblages due to their strong interactions with humic acids (HA) (Asano and Wagai, 2014; Pronk et al., 2011). However, the role of Fe-(hydr)oxides in the aggregate formation in soils with low Fe-(hydr)oxide content is still poorly understood since studies are mostly limited to typical oxide-rich soils (Barthès et al., 2008; Duiker et al., 2003; Igwe et al., 2009). OM plays a crucial role in the aggregation of mineral particles and is by far the most intensively studied aggregation factor in literature (Angers, 1998; Bronick and Lal, 2005; Dilkova et al., 1998; Pulleman and Marinissen, 2004; Six et al., 2004). OM is a complex mixture of multiple organic substances such as humic-like substances, polysaccharides, proteins, lignin's and poorly soluble aliphatic compounds (Calabi-Floody et al., 2011; Wattel-Koekkoek et al., 2001) and this range of properties enables OM to affect aggregation via different mechanisms and at different scales (Tisdall and Oades, 1982). Another factor that affects aggregation is the amount of exchangeable multi-valent cations, such as Ca^{2+} and Al^{3+} , since the tendency of soil particles to coagulate depends on the presence of these cations (Curtin et al., 1994).

Despite the extensive knowledge on aggregation mechanisms (Bronick and Lal, 2005; Six et al., 2004), a quantitative understanding of the relationships between physical-chemical properties and the soil structure is still lacking. Therefore, we collected data on aggregate fractions, porosity and physical-chemical properties for 126 soil samples collected from 12 different soil profiles in three diverse European Critical Zone Observatories (CZO). Our objective was (i) to assess the interactions between physical-chemical processes and soil structure at different size scales of aggregation, and (ii) to develop a conceptual model describing the physical-chemical interactions at the different size scales and their relation with aggregate stability and porosity.

7.2 Material and Methods

7.2.1 Sites

The soils for this study were collected at 12 sampling sites at three European critical zone observatories (CZO's), which are described in detail by Banwart et al. (2012). The CZO's are

characterized by different parent material, land use, and climate and are located in Austria (Marchfeld CZO), in the Czech Republic (Slavkov Forest CZO), and on the island of Crete, Greece (Koiliaris CZO):

The Marchfeld CZO is located on the former floodplains of the River Danube downstream of Vienna in Austria. This CZO includes six sites that are part of a chronosequence (20–20,000 year old) (Lair et al., 2009a). Climate is temperate with dry and hot summers, and soils are covered by deciduous foresty and annual crop. The soils, classified as Fluvisols and Chernozems, are calcareous and the clay mineralogy is dominated by illite and chlorite (Banwart et al. 2012). This site has been extensively studied, in particular in terms of soil dating (Lair et al., 2009a), phosphorus speciation and adsorption (Lair et al., 2009b; Zehetner et al., 2008) and carbon sequestration (Regelink et al., 2014b; Zehetner et al., 2009).

The Koiliaris CZO is located on Crete, east of the city of Chania. Climate is mediterranean and soils are covered by natural vegetation (shrubs and herbaceous species). The three sites have been formed at different sedimentary deposits: fluvial, unconsolidated and consolidated bedrock. Soils are classified as Fluvisols (site K1,2) and Cambisols (site K3), respectively, and are degraded due to deforestation for cropping and grazing. Organic matter contents and aggregate stability are therefore low (Stamati et al., 2013) and soils are susceptible to erosion and desertification. Further information about this site can be found in Stamati et al. (2013) and Moraetis et al. (2014).

The Slavkov Forest CZO, in western Czech Republic, is located in a national protected area. Climate is temperate and the soils are used for forestry (mainly Norway spruce). This CZO includes three sites, which are located on the slopes of three first-order catchments (Lysina, Pluhuv Bor, Na Zelenem). The catchments are characterized by different parent material (granite, serpentinite and amphibolite) and therefore by three distinct soil types (Podzol, Stagnosol and Cambisol, respectively). They therefore show strong differences with respect to their mineralogy and chemical composition (Table 7.1). Detailed information about the chemistry and hydrology of the three catchments can be found in Kram et al. (2012) and Banwart et al. (2012).

7.2.2 Soil sampling

Soils samples were taken from all 12 sampling sites in spring 2010. Three soil profile pits were dug at each site, yielding a total of 36 pits. Bulk soil samples and undisturbed soil cores were taken from each distinct soil horizon (Table 7.1) down to the C-horizon, which was always within 1.2 m below the surface. Bulk soil samples were sampled for the

analysis of soil texture, aggregates, and chemical properties. The field-moist samples were gently broken up by hand so that the larger clods broke along natural fissures, and roots and any rock fragments were removed by hand. Undisturbed soil cores (5 cm high, 5 cm diameter, 100 cm³) were taken for the analysis of soil water retention and bulk density. Organic horizons (O, AO, Ah), which were only present at sampling sites of the Slavkov Forest CZO, were excluded. Soil samples taken from the upper 10 cm were considered as topsoils whereas samples from deeper horizons were considered as subsoils. This yielded a total of 126 samples, of which 39 topsoils and 87 subsoils.

7.2.3 *Chemical soil characterization*

Homogenized soils samples were oven dried at 40°C and sieved over 2 mm. The pH was measured potentiometrically in a soil-water suspension at a soil/solution ratio (SSR) of 0.4 kg l⁻¹. The total C (TC) and N (TN) content were determined by a CN-analyzer (Carlo Erba Nitrogen analyzer 1500). For calcareous soils, the carbonate content was measured gas-volumetrically (Pansu and Gautheyrou, 2006) and the SOC content was calculated as the difference between TC and carbonate-C. The C:N ratio of the OM was defined as the ratio between SOC and TN. The amount of amorphous Fe- and Al-(hydr)oxides were determined by an ammonium-oxalate extraction at pH 3.0 (Pansu and Gautheyrou, 2006; Schwertmann, 1991) for which suspensions (0.05 kg l⁻¹) were shaken for 2 h (horizontal shaker, 85 rpm) in the dark and the oxalate-extractable Fe (Fe_{ox}) and Al (Al_{ox}) concentrations were analysed in the 0.45-µm filtered extracts by inductively coupled plasma-atomic emission spectrometry (ICP-AES; Varian Vista Pro). For the Marchfeld site, Al_{ox} was not determined since the oxalate extraction was performed by the local CZO partner where Al_{ox} is not part of the routine analysis. The total amount of Fe-(hydr)oxides (i.e. the amorphous and crystalline oxides) was determined by a dithionite-citrate-bicarbonate extraction (Fe_d). For the Marchfeld CZO, Fe_d was determined for all soil samples following the procedure of (Mehra and Jackson, 1960). For the Koiliaris and Slavkov Forest CZO, Fe_d was determined following the procedure of (Holmgren, 1967), however, for a selection of soils only, since these data were solely used for site description and not for statistical analysis.

7.2.4 *Physical soil characterization*

Soil texture. Ten g of air-dried soil was chemically dispersed in 25 ml 0.4 M Na-pyrophosphate (Na₄P₂O₇). The gravel (>2mm) and sand fraction (0.05–2.0 mm) were determined by wet sieving and the silt (0.002–0.05 mm) and clay fraction (<0.002 mm) were

Table. 7.1. General description of three European Critical Zone Observatories (CZO's) and their 12 subsites.

Critical Zone Observatory	Subsite	Coordinates	Elevation ^b	Soil type	Horizons	Land use/ cover	Description ^c
Marchfeld CZO, Austria (n=64) Six subsites with varying stage of soil development	M1 (n=8)	48°07.688 16°43.611	157	Fluvisol	AC, C	Soft wood forest	Island in Danube river-bed, soil age: <50 y. Calcareous, high Fe _{ox} content (>3 g kg ⁻¹), low clay content (<10%), SOC content: 15–25 g/kg. CEC dominated by Ca for all Marchfeld soils.
	M2 (n=12)	48°08.028 16°39.693	156	Fluvisol	A1, A2, AC, C	Soft wood forest	Forest site inside a flood control dam, soil age: ≈50–400. Calcareous, SOC content: 10–36 g kg ⁻¹ .
	M3 (n=14)	48°08.692 16°41.634	157	Chernozem	A1, A2, AC, C	Hard-wood forest	Outside flood control dike, soil age: ≈400–800. Calcareous, SOC content: 10–45 g kg ⁻¹ .
	M4 (n=9)	48°09.483 16°41.135	155	Chernozem	A, AC1, AC2, C	Cropland	Old cropland site, soil age: >2500 y. Calcareous, low Fe _{ox} content (<1 g kg ⁻¹), low SOC content (<20 g kg ⁻¹)
	M5 (n=13)	48°11.709 16°44.712	148	Chernozem	A1, A2, AC, C	Cropland	Old cropland site, soil age: >2500 y. Calcareous, low Fe _{ox} content (<1 g kg ⁻¹), low SOC content (<20 g kg ⁻¹)
	M6 (n=8)	48°17.005 16°39.834	165	Chernozem	A, AE, Ab, BC, C	Hard-wood forest	Old forest site, soil age: >15,000 y. pH: 6.0–7.7, clay content: ≈15%, Fe _{ox} content: ≈1 g kg ⁻¹ , SOC content < 24 g kg ⁻¹ .
Koiliaris CZO, Crete (n=29) Three subsites, varying in parent material and elevation	K1 (n=11)	35°26.900 24°08.253	10	Fluvisol	A, AC, C1, C2, C3	Shrubland	Degraded soil, Elevation: 10 m, parent material: fluvial sediments. Calcareous, clay content: 15–23%, Fe _{ox} content: 0.2–1.5 g kg ⁻¹
	K2 (n=9)	35°26.666 24°08.209	9	Fluvisol	AC, C1, C2, C3	Shrubland	Degraded soil, parent material: unconsolidated sedimentary rock, calcareous, low clay content (<6%), low Fe _{ox} content (<0.6 g kg ⁻¹),
	K3 (n=9)	35°21.653 24°04.308	1062	Cambisol	Ab, AC1 AC2 AC3	Shrubland	Degraded soil, abandoned terrace, parent material: consolidated sedimentary rock, pH 5.5–6.2, clay content: 15–30%, Fe _{ox} content: 2.2–4.2 g kg ⁻¹
Slavkov Forest CZO, Czech Republic (n=33) Three subsites, varying in parent material	S1 (n=16)	50°2.085 12°39.316	890	Podzol	AE, E, Bh, Bs, C	Norway spruce	Lysina catchment, Parent material: granite, pH: 3.3–4.0, CEC dominated by Al. Translocation of Fe and Al. High gravel content (20–35%)
	S2 (n=11)	50°3.840 12°46.908	773	Stagnosol	AE, BE, Bt, Cr	Norway spruce	Pluhuv Bor catchment, Parent material: Mg-rich serpentinite, pH 4.0–6.6, CEC dominated by Al and Mg. High Fe _{ox} content (2–6 g kg ⁻¹)
	S3 (n=6)	49°59.785 12°42.530	771	Cambisol	A, B	Norway spruce	Na Zelenem catchment, Parent material: amphibolite, pH 3.5–5.0, CEC dominated by Al and Ca. High Feox content (2–8 g kg ⁻¹)

^aThe amount of soil samples taken per CZO and subsite are given between brackets. For each subsite, soil samples were taken from each distinct soil horizon from three different soil pits.

^bElevation in meter above mean sea level.

^cSOC: Soil organic carbon; Fe_{ox}: Oxalate-extractable Fe; CEC: Cation-exchange-capacity.

determined by the pipette method (Pansu and Gautheyrou, 2006).

Dry-sieved aggregates. The size-distribution of the dry aggregates was determined by manual dry-sieving of air-dried bulk soil (500 g) for aggregate fractions >10, 10-5, 5-3, 3-1 and < 1 mm, respectively. The results of the dry-sieving were expressed as the mass of the aggregates larger than 1 mm (DSA) calculated according to Equation 1;

$$DSA = \frac{w_{>1mm}}{w_{total}} \quad (\text{Eq. 1})$$

where DSA is the fraction of dry sieved aggregates (w/w), $w_{>1mm}$ is the mass of soil larger than 1 mm, and w_{total} is the total mass of the soil.

Additionally, the dry sieving results were expressed as the mean weight diameter (MWD_{dry}), calculated according to Equation 2;

$$MWD_{dry} = \sum_{i=1}^n \frac{w_i}{100} \bar{d}_i \quad (\text{Eq. 2})$$

where MWD is the mean weight diameter (mm), n is the number of aggregate fractions (five), d_i is the mean diameter of the i^{th} fraction and w_i is the weight of soil in the fraction i expressed as a percentage of the dry soil mass.

Water-stable aggregates. The fraction of water-stable aggregates (WSA) was determined following the wet-sieving method similar to the method of Haynes and Swift (1990) using 20 g of 1–3 mm sized dry-sieved aggregates. Kercheva et al. (2011) found a very good relationship between the water stability determined on a single aggregate fraction (3-1 mm) and a sample composed of different aggregate fractions. The aggregates were immersed in water and sieved manually over two sieves with mesh-sizes of 1 and 0.25 mm by moving the sieves ten times up and down for 10 cm while the aggregates remained under water. The mass of soil in each fraction (1–3 mm, 0.25–1 mm, and <0.25 mm) was determined after oven-drying (105 C°). Subsequently, for the 1–3 mm fraction, the fraction of sand particles larger than 1 mm was determined by dispersion of the aggregates in 0.4 M Na-pyrophosphate and subsequent sieving over 1 mm. The fraction of water-stable macro-aggregates, corrected for the sand particles larger than 1 mm, was calculated using Equation 3;

$$WSA = \frac{w_{0.25} - w_{sand>1}}{w_{dry} - w_{sand>1}} \quad (\text{Eq. 3})$$

where $w_{0.25}$ is the mass of soil in the fraction larger than 0.25 mm after wet-sieving, $w_{sand>1}$ is the mass of soil particles larger than 1 mm and w_{dry} is the mass of the initial dry-sieved aggregates (1–3 mm). For most soils, the coarse fraction amounted to less than 3% of the

recovered soil mass, except for the gravel-rich site S1 of the Slavkov Forest where 10–50% of the soil mass was larger than 1 mm. The wet sieving procedure was performed in triplicate and the average of three replicates was taken. Standard deviations of the mass fractions calculated from the triplicates were <20%.

Water retention and bulk density. Water retention and bulk density were measured in triplicate on undisturbed soil cores (100 cm³). Bulk density was determined on oven-dried soils. For water retention, samples were brought to near-saturation (0.25 kPa) over the course of 20 days, after which the drying branch of the water retention characteristic was determined at six tensions (0.25, 1, 5, 10, 30, 1500 kPa) using a suction plate apparatus (0.25–30 kPa,) and a membrane pressure plate device (1500 kPa) (Dane and Topp, 2002). For each water potential, equilibrium was established within 5–7 days. Standard deviations of the water contents, calculated from the three replicates, were below 10% for samples and average values were used in data analysis. Soil porosity was calculated from the water retention curves. Following the definitions of Luxmoore (1981), we defined microporosity as the volume of water stored at 30 kPa, which is equivalent to a pore size smaller than 10 µm, and mesoporosity as the volume of water stored between 0.25 and 30 kPa, which is equivalent to a pore size between 10 and 1000 µm (Table 7.2).

Table 7.2. Overview of the soil physical parameters.

Parameter	Pore size/Aggregate size	Method	Comment
Dry-sieved aggregates	Aggregate size: 1–10 mm	Dry sieving of air-dried soil	Macro-aggregates
Water-stable aggregates	Aggregate size: 0.25–3 mm	Wet-sieving of 1–3 mm sized dry-sieved aggregates.	Macro-aggregates with a high mechanical stability
Micro-mesoporosity	Pore size: <1000 µm	Volumetric water content at 0.25 kPa	Sum of micro- and mesoporosity
Mesoporosity	Pore size: 9–1000 µm	Volumetric water content stored between 0.25–30 kPa	Storage of gravitational water
Microporosity	Pore size: <9 µm.	Volumetric water content at 30 kPa.	Storage of plant-available and unavailable water. Indicator for micro-aggregates.

7.2.5 Statistical analysis

Relationships between soil properties were assessed using single and multiple regression analysis. All statistical calculations were performed in SPSS.

7.2.6 NICA Donnan model prediction.

The surface charge of humic acid (HA) as a function of the pH was predicted by the NICA (non-ideal competitive adsorption) - Donnan model (Milne et al., 2003) for HA in a 0.01 M CaCl₂ solution using the ECOSAT geochemical model. Concentrations of Fe³⁺, Al³⁺ and Ca²⁺ were in equilibrium with amorphous Fe-(hydr)oxides (FeOOH), gibbsite (Al(OH)₃) and calcium-carbonate (CaCO₃) using the solubility constants of Lindsay (1979).

7.3 Results

For each CZO, mean, minimum and maximum values of the soil chemical and physical parameters are given in Table A1 and the coefficient of determination (R²) from the linear regression analysis is given in Table A2-4. First, the results of the soil chemical characterization of the three CZO's will be given followed by the relations between the physical and physical-chemical properties.

7.3.1 Soil Chemical Properties

Marchfeld CZO. The six sites of the Marchfeld CZO were calcareous (2–386 g CaCO₃ kg⁻¹) and characterized by a neutral to alkaline pH (5.9–8.4) (Table E1). The textural composition strongly differed among the sites and the clay content varied between 5 and 34%. The Fe_{ox} content varied between 0.3 and 1.5 g kg⁻¹ whereas the Fed content was higher (2.5 and 8.1 g kg⁻¹). The Fe_{ox}/Fe_d ratio varied between 0.1 and 0.6 and decreased with increasing soil age as described in Lair et al. (2009). As expected, the SOC content was generally higher in the topsoils (15–45 g kg⁻¹) than in the subsoils (5–25 g kg⁻¹). For the topsoils, the SOC content was lower in the arable fields than in the forest fields, which may be explained by lower carbon inputs and enhanced biodegradation due to mechanical disturbance of soil aggregates (Six et al., 2002; Zehetner et al., 2009) and by the loss of the oxide-associated SOC due to competition with phosphate (Regelink et al., 2014b). The SOC content correlated poorly with the Fe_{ox} content (R²=0.31, Figure E1) but did not correlate with the clay content (Figure E1) and neither with the Fed content (Table E2).

Koiliaris CZO. The three sites of the Koiliaris CZO distinctly differed with respect to their textural and chemical composition (Table E1). Site K1 (Fluvisol) was characterized by a high pH (7.4–8.1), high CaCO₃ content (38–160 g kg⁻¹), low Fe_{ox} content (<0.5 g kg⁻¹) and high clay content (15–23%). Site K2 (Fluvisol) was also calcareous but characterized by a very low clay fraction (<6%) and low Fe_{ox} content (<0.5 g kg⁻¹). In contrast, site K5 (Cambisol) was characterized by a rather high Fe_{ox} content (2.0–4.2 g kg⁻¹), high clay content (13–30%) and

a slightly acid pH (5.5–6.0). Despite the rather low Fe_{ox} content, the Fe_d content was high for all sites (10–25 $g\ kg^{-1}$, Table E1) and Fe_{ox}/Fe_d ratios were consequently very low (0.05–0.15) indicating that the majority of the Fe-(hydr)oxides in these soils is crystalline. The Fe_{ox} content was strongly correlated with the Al_{ox} content ($R^2=0.89$, Table E3). The SOC content (2.9–50 $g\ kg^{-1}$) was higher in the topsoils than in the subsoils (Figure 7.1) and correlated positively with the Fe_{ox} content ($R^2=0.47$, Figure E1) but not with the clay fraction (Figure E1).

Slavkov Forest CZO. The three sites of the Slavkov Forest CZO covered a wide range in soil textural and chemical properties (Table E1). The gravel content varied between 20 and 30% in site S1 (Podzol), whereas the gravel content was below 20% for the other sites (Stagnosol and Cambisol). The clay content varied between 3 and 25% and the pH values varied between 3.3 and 6.6 in the three sites. Most soil samples were characterized by a high Fe_{ox} (1.5–13 $g\ kg^{-1}$) and Al_{ox} (0.5–9 $g\ kg^{-1}$) content, except for the E-horizons in which the Fe_{ox} and Al_{ox} content were typically below 0.15 $g\ kg^{-1}$ and 0.5 $g\ kg^{-1}$, respectively. The SOC content (2–17 $g\ kg^{-1}$) was higher in the topsoils and B-horizons than in the E- and C-horizons. The SOC content showed a positive correlation with the Fe_{ox} content ($R^2=0.62$), however, only

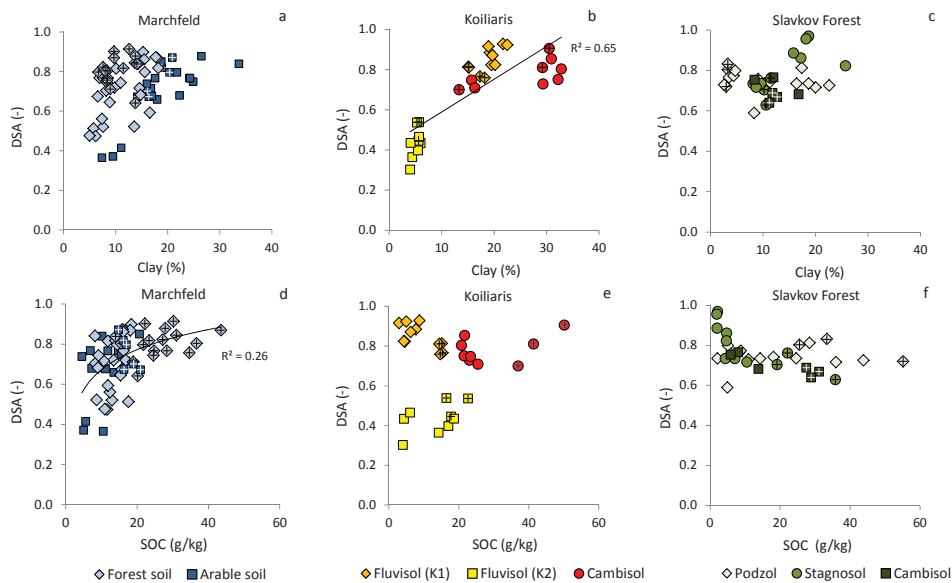


Figure 7.1. The fraction of dry-sieved aggregates ($> 1mm$, DSA, w/w), a function of the clay content (a-c) and the soil organic carbon (SOC) content (d-f) in the Marchfeld, Koiliaris and Slavkov Forest CZO. Different colors represent the various sites and symbols with crosses represent the topsoils (0–10 cm).

when the three topsoils of the Podzol site were excluded from the correlation (Figure E1). In contrast, the SOC content did not correlate with the clay content (Figure E1).

7.3.2 Soil aggregates

Dry-sieved aggregates. Results from the dry-sieving were expressed as the MWD_{dry} and as the fraction of DSA (>1 mm). Both parameters were strongly correlated ($R^2=0.65$, Figure E2) and therefore, the results presented here are restricted to the fraction of DSA. The fraction of DSA varied between 0.3 and 0.9 and showed a poor correlation with the SOC content for the Marchfeld ($R^2=0.26$), Figure 1d, whereas this correlation was not significant for the other two CZO's (Figure 7.1e,f). For the Koiliaris CZO, the fraction of DSA correlated positively with the clay content ($R^2=0.65$, Figure 7.1b), however, this correlation was dominantly caused by the low fraction of DSA in the clay-poor soils of site K2 (Fluvisol). For the other CZO's, the clay content did not correlate with the fraction of DSA (Figure 7.1a,c). Neither was there a correlation with the Fe_{ox} content or any other physical-chemical parameter (Table E2-4).

Water-stable aggregates. The fraction of WSA was generally higher in the topsoils than in the subsoils (Figure 7.2) and correlated positively with the SOC content at all sites (Marchfeld, $R^2=0.42$, Koiliaris, $R^2=0.85$ and Slavkov Forest, $R^2=0.76$, Figure 7.2a-c). However, the correlation between WSA and SOC was poor when the data of the three CZO's were combined (Figure 7.2d) because a similar SOC content corresponded to a higher fraction of WSA in acid soils compared to neutral or alkaline soils (Figure 7.3). The role of

Table 7.3. Multiple-regression relations between soil properties and the fraction of water-stable aggregates^a

Marchfeld CZO (n=64)	R ²
WSA = 2.2 + 0.16 Fe _{ox} - 0.25 pH	0.67
WSA = 1.80 + 0.13 Fe _{ox} + 0.086 SOC - 0.22 pH	0.72
Koiliaris CZO (n=36)	
WSA = -0.11 + 0.28 ln(SOC)	0.85
Slavkov Forest CZO (n=33)	
WSA = 0.89 + 0.12 ln(SOC) - 0.09 pH	0.83
All (n= 127)	
WSA = 1.2 + 0.18 ln(SOC) - 0.11 pH	0.66

^aBest fits obtained by stepwise multiple-regression using the soil physical-chemical properties as possible parameters. WSA=fraction of water-stable aggregates (w/w); SOC=Soil organic carbon (%); Fe_{ox}=oxalate-extractable Fe (g kg⁻¹). Multiple regression models are significant at p < 0.001 and the coefficients of the included variables are significant at p < 0.05.

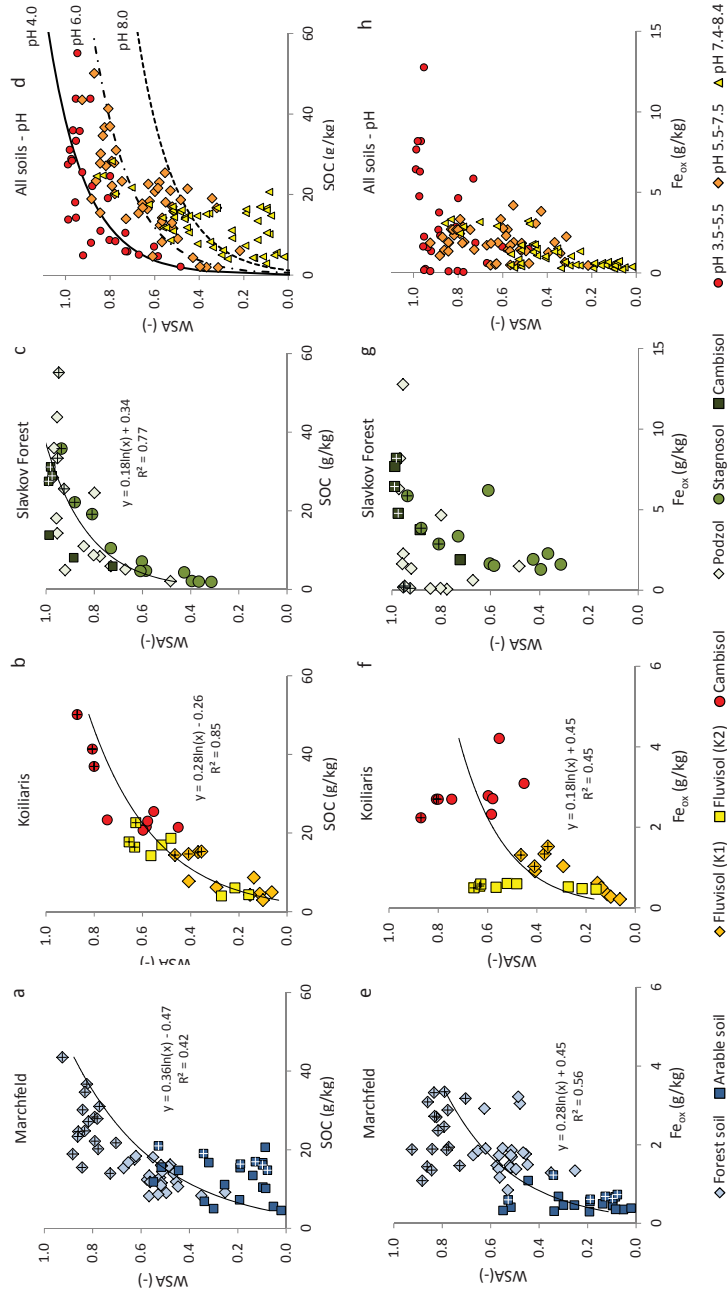


Figure 7.2. The fraction of water-stable aggregates (>0.25 mm, WSA, w/w) as a function of the soil organic carbon (SOC) content (a-d) and the amorphous Fe-(hydr)oxide (Fe_{ox}) content (e-h) in the Marchfeld, Koiliaris, Slavkov Forest CZO. Figure 7.2d and 7.2h show the data grouped as a function of the pH and the different colours represent the acid (pH 3.5-5.5), neutral (5.5-7.5) and slightly alkaline (pH 7.5-8.5) soils. The lines in Figure 7.2d shows the model predictions from the multiple regression model given in Table 7.3 (WSA = $1.2 + 0.18 \ln(SOC) - 0.11$ pH).

pH was further confirmed by multiple regression analysis, which showed that the fraction of WSA in the three CZO's was best predicted from the combination of SOC and pH. This combination explained 63% of the observed variance in WSA whereas SOC alone explained only 31% of the observed variance (Table 7.3). The coefficient for the pH is negative meaning that the fraction of WSA decreased with increasing pH.

The Fe_{ox} content was the best single predictor for WSA in the Marchfeld ($R^2=0.56$, Figure 7.2e) and the combination of Fe_{ox} , SOC and pH explained 72% of the variance in WSA in soils from this CZO (Table 7.3). Fe_{ox} was also correlated with the fraction of WSA in the Koiliaris CZO ($R^2=0.45$, Figure 7.3f). In contrast, the fraction of WSA did not correlate with Fe_{ox} for the Slavkov Forest due to the high fraction of WSA in the iron-poor soils of the Podzol site, meaning that Fe-(hydr)oxides were not a prerequisite to form stable aggregates in this acid forest soil (Figure 7.2g). Similar results were found when the $\text{Fe}_{\text{ox}}+\text{Al}_{\text{ox}}$ content was used instead of the Fe_{ox} content (Table E3-4). Correlations between the fraction of WSA and soil texture were not significant ($p=0.0001$) for any of the CZO's (Table E2-4).

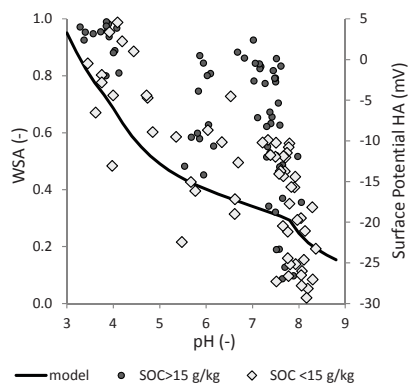


Figure 7.3. The fraction of water-stable aggregates (>0.25 mm, WSA, w/w) as a function of the pH for the soil samples taken from the Marchfeld, Koiliaris, Slavkov Forest CZO. The blue data points represent soils with a soil organic carbon (SOC) content above 15 g kg^{-1} , whereas the yellow datapoints represent the soils with a SOC content below 15 g kg^{-1} . The line shows the predicted surface potential of humic acid (HA) as a function of the pH, calculated using the NICA-Donnan model, as described in section 7.4.2. The surface potential is an indicator for the strength of the electrostatic repulsive force between organically coated particles.

7.3.3 Soil Porosity

Microporosity. Microporosity varied between 0.05 and $0.6 \text{ (m}^3/\text{m}^3)$ in the three CZO's. For the Marchfeld CZO, microporosity correlated well with the silt content ($R^2=0.57$,

Linkages between soil physical-chemical properties, aggregates and porosity

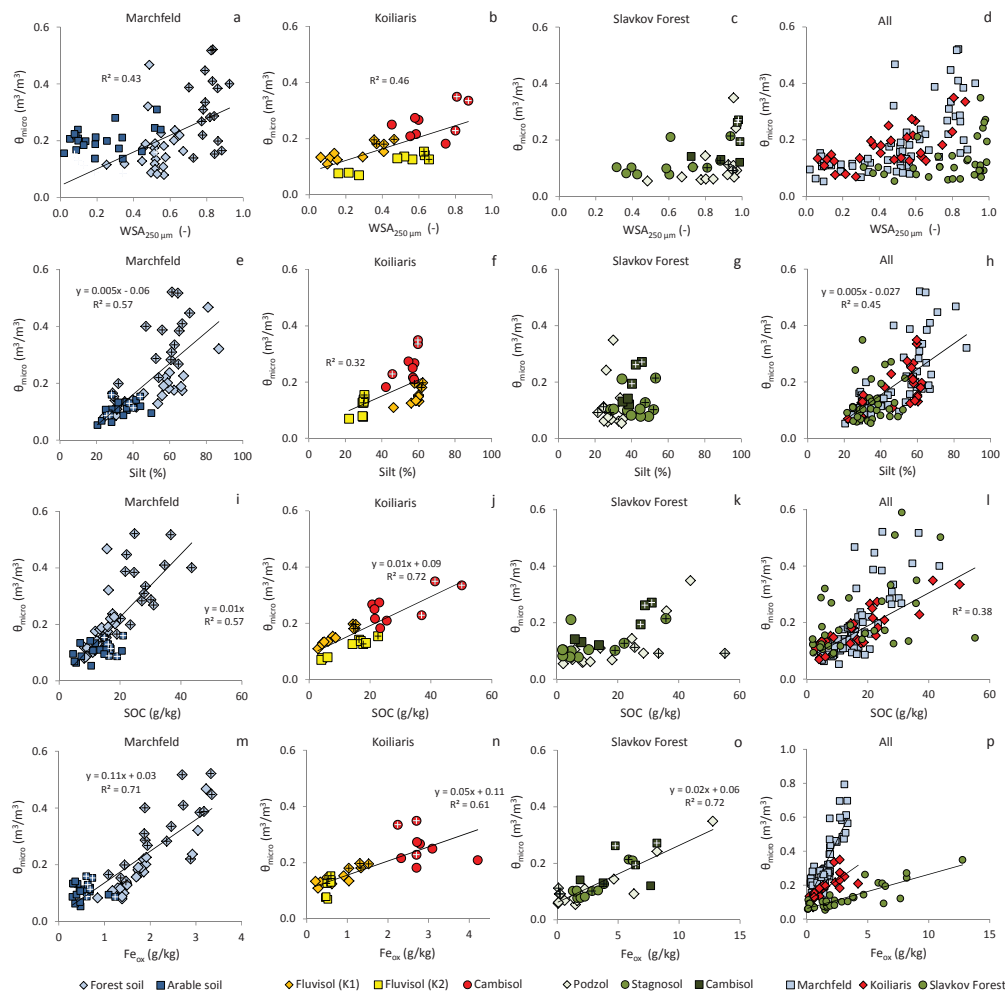


Figure 7.4. Microporosity (θ_{micro}) as a function of the fraction of water-stable aggregates (WSA, a-d) the silt content (e-h), the soil organic carbon (SOC) content (i-l) and the Fe_{ox} content (m-p) in the Marchfeld, Koiliaris, Slavkov Forest, and in the three CZO's together. Microporosity was defined as the volumetric water-content stored at 30 kPa, which is equivalent to the volume of pores smaller than 9 μ m.

Figure 7.4e) whereas this correlation was poor in the Koiliaris CZO ($R^2=0.32$) and not significant in the Slavkov Forest (Figure 7.4f and g). The silt content was the best single predictor for microporosity when the data of the three CZO's were put together ($R^2=0.45$, Figure 7.3h). The silt content was a better predictor for microporosity than the clay content, since correlations between microporosity and the clay content were only significant for

the Koiliaris CZO and not for other two sites (Table E2-5). The Fe_{ox} content was a good predictor for microporosity and the correlation coefficients amounted to 0.74, 0.61 and 0.72 for the Marchfeld, Koiliaris and Slavkov Forest CZO, respectively. However, Fe_{ox} was not a good predictor for microporosity when the data of the three CZO's was lumped (Figure 7.4d) because the slope of the regression line was different for the Slavkov Forest compared to the other two CZO's. Multiple regression analysis showed that the microporosity in the Marchfeld and Koiliaris CZO was best predicted by the combination of the Fe_{ox} , silt and clay content (Table 7.4). In contrast, when the soils of the Slavkov Forest were included as well, microporosity was best predicted from the silt and SOC content (Table 7.4).

Table 7.4. Multiple-regression relations between soil properties and microporosity^a

Marchfeld + Koiliaris CZO (n=100)	R²
$\theta_{micro} = -0.1 + 0.004 \text{ Silt} + 0.21 \text{ WSA}$	0.72
$\theta_{micro} = 0.03 + 0.07 * Fe_{ox}$	0.58
$\theta_{micro} = -0.02 + 0.05 Fe_{ox} + 0.002 \text{ Silt}$	0.64
$\theta_{micro} = 0.006 + 0.04 Fe_{ox} + 0.002 \text{ Silt} - 0.003 \text{ Clay}$	0.70
Slavkov Forest CZO (n=33)	
$\theta_{micro} = 0.06 + 0.02 Fe_{ox}$	0.72
All (n= 127)	
$\theta_{micro} = -0.07 + 0.003 \text{ Silt} + 0.03 \text{ SOC}$	0.62

^aBest fits obtained by stepwise multiple-regression. θ_{micro} =microporosity ($m^3 m^{-3}$); WSA= water-stable aggregates (w/w) SOC=Soil organic carbon (%); Fe_{ox} =oxalate-extractable Fe ($g kg^{-1}$). Multiple regression models are significant at $p < 0.001$ and the coefficients of the included variables are significant at $p < 0.05$.

Mesoporosity. The mesoporosity varied between 0.01–0.36 $m^3 m^{-3}$ and was generally lower than the microporosity. The mesoporosity did not show a clear difference between topsoils and subsoils (Figure E3). For the Marchfeld siteKoiliaris CZO, mesoporosity showed a poor correlation with the clay silt content, whereas correlations between soil texturethe silt content (Figure E3e) and mesoporosity were not significant for the Koiliaris and Slavkov Forest CZO (Figure E3d, E3f, respectively). The Fe_{ox} content correlated poorly with mesoporosity in the Marchfeld and Slavkov Forest (Figure E3g, E3i, respectively). For the Koiliaris CZO, Fe_{ox} correlated strongly with mesoporosity when the data are split up for the sandy Fluvisol (site K2, >64% sand) and the silty Fluvisol and Cambisol (site K1,3 >45% silt) indicating that an increase in the Fe_{ox} content corresponds to an increase in mesoporosity in soils with a similar texture (Figure E3h). In contrast, correlations between the SOC content and mesoporosity were not significant for any of the sites CZO's (Figure E3j-l).

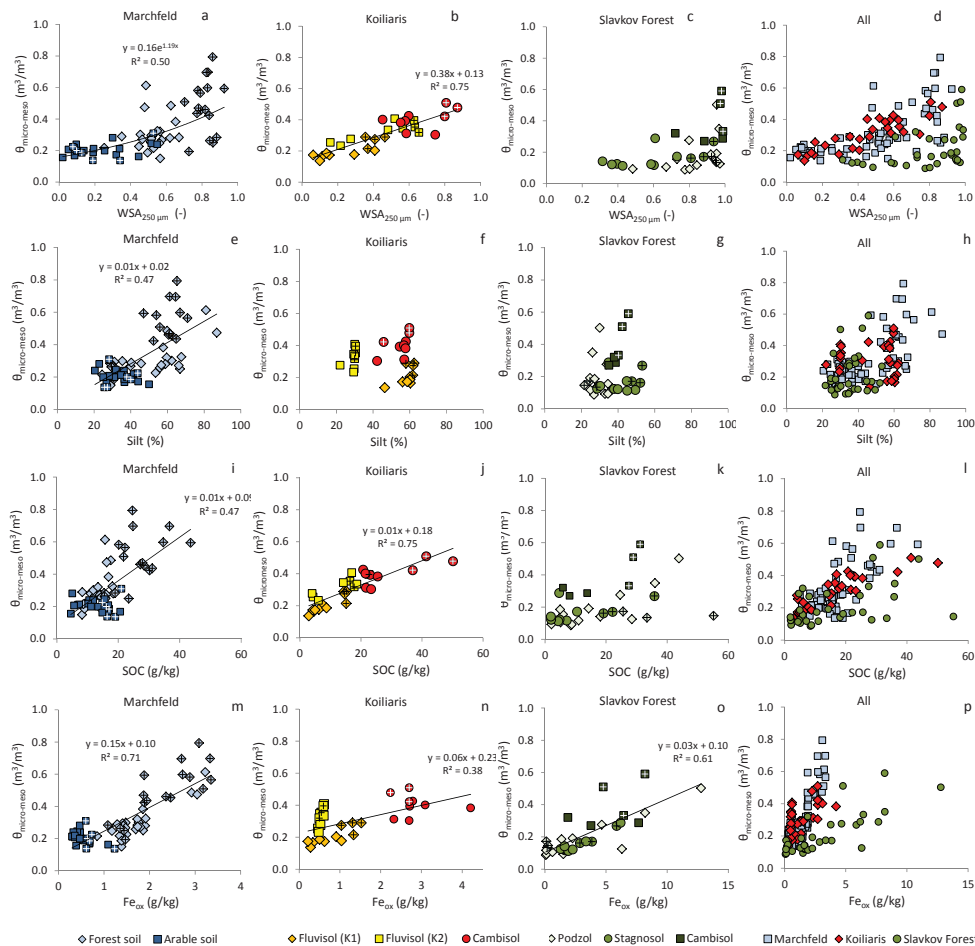


Figure 7.5. Micro+mesoporosity ($\theta_{micro+meso}$) as a function of the fraction of water-stable aggregates (WSA, a-d), the silt content (e-h), the SOC content (i-l) and the Fe_{ox} content (m-p) in the Marchfeld, Koiliaris and Slavkov Forest site, and the three CZO's together. Micro+mesoporosity was defined as the volumetric water-content stored at 0.25 kPa, which is equivalent to the volume of pores smaller than 1 mm.

Micro+mesoporosity. The micro+mesoporosity varied between 0.1 and 0.8 m³m⁻³ and showed a good, positive correlation with the fraction of WSA for the Marchfeld (R²=0.50) and Koiliaris CZO (R²=0.75) (Figure 7.5a and 7.5b, respectively), whereas this correlation was not significant for the Slavkov Forest CZO (Figure 7.5c). Correlations with the fraction of WSA were stronger for the micro+mesoporosity than for the microporosity (Figure 7.4, 7.5). Similar as for the microporosity, the micro+mesoporosity correlated strongly with

the Fe_{ox} content for the three CZO's (Marchfeld, $R^2=0.71$, Koiliaris, $R^2=0.38$ and Slavkov Forest, $R^2=0.61$, Figure 7.5m, 7.5n, 7.5o, respectively) and with the SOC content for the Marchfeld and Koiliaris CZO ($R^2=0.47$ and 0.75 , respectively, Figure 7.5i, 7.5j, respectively). Furthermore, micro+mesoporosity correlated strongly with the bulk density for all soils together (Figure E4).

The ratio between the microporosity and micro+mesoporosity ($\theta_{30}/\theta_{0.25}$) showed a strong, positive correlation with the fraction of DSA for the Marchfeld ($R^2=0.69$), Koiliaris ($R^2=0.92$) and Slavkov Forest CZO ($R^2=0.33$) (Figure 7.6a,b,c). For the three CZO's together, DSA explained 70% of the observed variance in the $\theta_{30}/\theta_{0.25}$ ratio (Figure 7.6d). In contrast, correlations between the DSA and the microporosity itself were poor or not significant (Table E2-4) meaning that an increase in DSA led to an increase in the contribution of the micropores, and consequently a similar decrease in the contribution of mesopores.

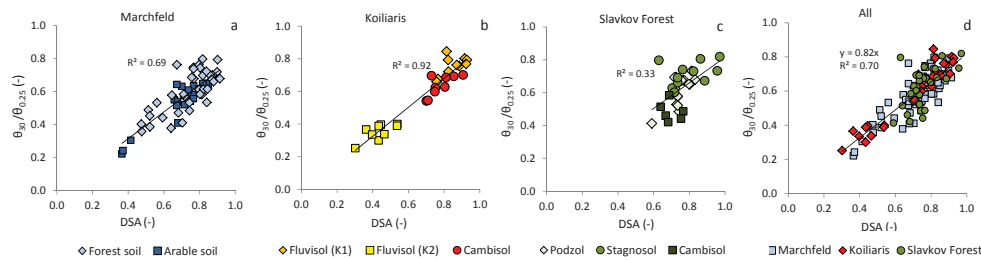


Figure 7.6. The ratio between the microporosity and the micro+mesoporosity ($\theta_{30}/\theta_{0.25}$) plotted against the fraction of dry-sieved aggregates (DSA, w/w) for the Marchfeld (a), Koiliaris (b), Slavkov Forest site (c), and three CZO's together (d). Microporosity was defined as the volumetric water-content stored at 30 kPa and the micro+mesoporosity was defined as the volumetric water-content at 0.25 kPa.

7.4 Discussion

7.4.1 Mechanistic linkages between aggregates and porosity

Soil porosity correlated only poorly to moderately with the silt content (Figure 7.4, 7.5) and other texture fractions (Table E2-4) which suggests that soil porosity is not solely determined by particle size fractions but that aggregates may also affect porosity. Indeed, the fraction of WSA showed a good correlation with the micro+mesoporosity (Figure 7.5) and a moderate correlation with microporosity for the Koiliaris and Marchfeld site (Figure

7.4). For these latter two CZO's, microporosity was well predicted from the combination of WSA and the silt content (Table 7.4). The Slavkov Forest CZO deviated from these trends (Figure 7.4, 7.5) and the poor correlations between the WSA and porosity in this CZO can be explained by the large amount of gravel (>2 mm) in the soils from this site, which results in discrepancies between water-retention data and aggregate fractions. The correlations between the fraction of WSA and soil porosity do not necessarily mean that the soil pores are either located within or in-between the water-stable aggregates since the soils pores cover a wide size range. For example, micropores (<9 μm) are expected to be located within water-stable aggregates whereas mesopores (9–1000 μm) can be located both within and in between aggregates. Instead, we suggest that an increase in the fraction of WSA corresponds to a decrease in the number of small dispersible particles that may otherwise cause clogging of pores within the soil. Overall, our results show that soil porosity is the sum of the inherent porosity, determined by its texture, and the additional porosity due to the presence of soil aggregates. This conclusion is in line with previous conceptual models (Currie, 1966; Dexter, 1988) and suggestions (Wösten et al., 2001) however, to our best knowledge, experimental evidence for the correlation between WSA and porosity has not been shown before on a large data set including various soil types as covered by the three CZO's in this study.

In contrast to the WSA, the DSA did not correlate with the microporosity or micro+mesoporosity (Table E2-4). However, the fraction of DSA showed a strong, positive correlation with the ratio between microporosity and micro+mesoporosity ($\theta_{30}/\theta_{0.25}$) for the three CZO's together (Figure 7.6). Thus, the fraction of DSA controls the distribution of soil pores between micro- and mesopores. An increase in the fraction of DSA corresponds to an increase in the contribution of micropores, suggesting that micropores are dominantly located within DSA whereas mesopores are dominantly located in between 'loose' particles, which may also include aggregates smaller than 1 mm. The slope of the regression line between DSA and the ($\theta_{30}/\theta_{0.25}$) ratio was very similar for the three CZO's (Figure 7.6), which shows that this relation is valid for a wide range of soil types and textural compositions. Studies in which both DSA and soil water retention curves have been measured are scarce. Our study shows that the distribution of micro- and mesopores is strongly linked to the presence of DSA larger than 1 mm.

DSA and WSA are controlled by different aggregation mechanisms as is shown by the lack of a correlation between the two aggregate fractions (Figure E2). Another difference between these two aggregate measurements is that the fraction of WSA is sensitive to differences in sampling depth and land use type (Figure 7.2) whereas these differences are not reflected in

the fraction of DSA (Figure 7.1). Previous studies also found that WSA is a more sensitive indicator for the soil structure (Pulleman et al., 2003; Six et al., 2000b) and therefore, wet-sieving has become a popular approach to characterize aggregates in soils under different land use (Amézqueta, 1999; Kercheva et al., 2011). Wet-sieving was performed on the 1-3 mm sized dry aggregates and the results of the wet-sieving therefore reflect the breakdown of dry aggregates (1-3 mm) into WSA (0.25–3 mm) and dispersible particles (<0.25 mm). Therefore, these results can be used to elucidate the role of aggregate hierarchy in the formation of DSA. The fraction of WSA covered a wide range (1-95%), meaning that DSA can be build-up from WSA and dispersible particles in any ratio. The presence of WSA is apparently not a prerequisite to form larger DSA, meaning that aggregate hierarchy does not necessarily plays a role in the formation of DSA.

7.4.2 Mechanistic linkages between physical-chemical properties, aggregates, and porosity

The relations between the physical-chemical properties, aggregates, and porosity are discussed for four aggregation factors: (i) soil texture, (ii) Fe-(hydr)oxides, (iii) organic binding agents and (iv) coagulation conditions.

Soil texture. Soil texture is a measure for the size-distribution of the primary mineral particles which are the building blocks for all aggregates at any larger size. The limited correlation between texture and the fraction of DSA and WSA (Figure E2) was therefore not expected. Only for the Koiliaris site an effect of texture was observed since the formation of DSA was inhibited in the sandy Fluvisol (K2, Figure 7.1), which has a very low clay (<6%) and Fe_{ox} content (<0.5 g kg⁻¹) compared to other sites. For the other CZO's, the size and stability of the aggregates were independent of the clay, silt and sand fractions (Table E2-4), despite the wide range in texture among the studied soils (Table E1). The absence of a correlation between the clay content and the fraction of WSA is in contrast with previous observations that argued that clay minerals are important for aggregation because of their interactions with OM (Angers, 1998). However, for the three CZO's used in this study, the clay fraction is not the dominant surface for sorption of OM, since there was no correlation between the clay fraction and the SOC content (Figure E1). Instead, in our soils, Fe-(hydr)oxides seem to dominate the sorption capacity for OM, since the Fe_{ox} content correlated moderately with the SOC content (Figure E1). The role of the clay fraction in aggregate formation also depends on the mineralogy of the clay fraction (Six et al., 2000a), for example, swelling clay minerals, such as montmorillonite, can have a negative impact on the soil structural

properties in soils (Brubaker et al., 1993). However, soil texture has only a minor effect on aggregation in the soils used in this study, which cover a wide variety in soil types and textural composition.

Iron-(hydr)oxides. Iron-(hydr)oxides play a crucial role in the binding of particles to aggregates as is shown by the strong correlations between the Fe_{ox} content and the micro- and micro+mesoporosity in the three CZO's (Figure 7.4, 7.5) as well as by the positive correlation between the Fe_{ox} content and the fraction of WSA in the Marchfeld and Koiliaris site (Figure 7.2). To our knowledge, a strong, positive correlation between the Fe_{ox} content and soil porosity has not been shown before in literature. Thus, Fe-(hydr)oxides play an important role in aggregation, despite the small contribution of the Fe_{ox} content to the soil mass (<1 %). This can be explained by the small size (<10 nm) and consequently large surface-to-mass ratio (100–1000 m^2g^{-1}) of Fe-(hydr)oxides in soils (Eusterhues et al., 2005; Hiemstra et al., 2010; Mikutta et al., 2006; Regelink et al., 2014a). As a result, Fe-(hydr)oxides generally dominate the surface area available for sorption of SOC and consequently play an important role in the stabilization of SOC and in the formation of organo-mineral assemblages within soils (Kögel-Knabner et al., 2008; Regelink et al., 2013). However, the correlation between the Fe_{ox} content and porosity cannot be solely explained by the co-correlation with the SOC content since the Fe_{ox} content is a better predictor for porosity than the SOC content (Figure 7.4). As such, we suggest that Fe-(hydr)oxides have a more fundamental role in aggregation. Fe-(hydr)oxides have the ability to form strong bindings with clay, silt and sand particles, meaning that Fe-(hydr)oxides can provide sorption sites for organic substances on the surfaces of these otherwise low to moderately reactive particles (Arias et al., 1996; Sei et al., 2002). Some studies have suggested that these poorly reactive minerals, which are dominantly present in the silt and sand fraction, are not actively involved in the aggregation process (Elliott et al., 1991; Six et al., 2000b). However, fractionation studies have shown that silt and sand particles are the dominant constituents of water-stable macro-aggregates (Barberis et al., 1991; Puget et al., 2000). Furthermore, a substantial part of the Fe-(hydr)oxides in soils are associated with silt and sand particles. For example, Barberis et al. (1991) showed, for a range of soils, that about 50% of the Fe_{ox} content of the soil is associated with the silt and sand fraction. A small mass fraction of Fe-(hydr)oxides can already significantly increase the surface area of particles in the silt/sand range due to the extremely small size of the Fe-(hydr)oxides compared to the silt/sand particles. Therefore, we suggest that this 'coating' of Fe-(hydr)oxides facilitates the interaction between larger mineral particles and organic substances and we argue that this Fe-(hydr)oxide 'coating' is in particular effective

for quartz and other poorly reactive minerals that otherwise lack the necessary surface sites to interact with organic substances and to be taken up within the network of organic substances.

In addition to the amorphous Fe-(hydr)oxides, other metal-(hydr)oxides may also enhance aggregation. Considering the role of crystalline Fe-(hydr)oxides first, the lack of a correlation between the Fe_d content and the porosity and fraction of WSA in the Marchfeld CZO (Table E2) shows that the crystalline Fe-(hydr)oxides (Fe_d minus Fe_{ox}) are of less importance than the amorphous Fe-(hydr)oxides (Fe_{ox}), which is in agreement with previous studies (Duiker et al., 2003). Considering the role of Al-(hydr)oxides, correlations between the sum of the Fe_{ox} and Al_{ox} content and soil structure were similar or poorer than correlations with the Fe_{ox} content alone (Table E3,E4). This suggests that Fe-(hydr)oxides are more important for aggregation than Al-(hydr)oxides, which is in line with the results of Duiker et al. (2003). Nevertheless, in other soil types, amorphous Al-(hydr)oxides or allophane may contribute substantially to aggregate formation, depending on the amounts of the respective minerals present in the soil (Asano and Wagai, 2014; Penn et al., 2001). Furthermore, clay minerals may also act as sorbents for humic substances, however, the surface area of Fe-(hydr)oxides in soils is usually much larger than the surface area of clay minerals (Eusterhues et al., 2005). Therefore, in the wide range of soil types used in this study, amorphous Fe-(hydr)oxides are the most important mineral phase contributing to aggregation.

Organic binding agents. SOC shows a strong correlation with the fraction of WSA (Figure 7.2) whereas the fraction of DSA was not correlated to the SOC content (Figure 7.1). The amount of SOC needed to form a certain number of WSA strongly differs among the different study sites (Figure 7.2). Previous studies have suggested that these differences are related to differences in the clay content (Asano and Wagai, 2014). However, our results show that the pH and, to a lesser extent, the Fe_{ox} content, explain the differences in the number of aggregates formed at a certain SOC content. For acidic soils, the same amount of SOC corresponds to a higher fraction of WSA compared to soils with a neutral to slightly alkaline pH (Figure 7.2,7.3). This pH-effect reflects the role of the coagulation conditions, which will be discussed in detail below. In slightly alkaline soils, the fraction of WSA is controlled by the combination of the SOC content, the Fe_{ox} content and the pH (Table 7.3). The fact that the fraction of WSA is controlled by the combination of these factors rather than by the SOC content only, shows that, in addition to the total SOC content, also the interactions between SOC and the Fe-(hydr)oxide 'coatings' as well as the interactions between SOC

itself (coagulation) are of importance for aggregation.

The importance of the Fe-(hydr)oxide 'coating' in facilitating the adsorption of OM on mineral surfaces has been shown in spectroscopic studies, in which OM on silt and sand particles was shown to be present as patches associated with Fe-rich particles rather than as a homogenous layer (Chenu and Plante, 2006; Mikutta et al., 2006; Vogel et al., 2014). OM, in particular HA, has a high affinity for adsorption to Fe-(hydr)oxides and will likely form a monolayer on the Fe-(hydr)oxide surfaces with a thickness of about 1–2 nm (Weng et al., 2008). Although this monolayer of HA may enhance coagulation of clay and Fe-(hydr)oxide particles (Baalousha, 2009; Majzik and Tombacz, 2007), a 1-2 nm thick layer of HA is too thin to overcome the pore spaces in between silt- and sand-sized particles. Thus, a thicker OM layer is needed in order to incorporate silt- and sand-sized particles within the aggregates. The OM layer can be extended by the adsorption of other larger organic compounds, in particular carbohydrates and glomalin. Carbohydrates and glomalin have a much lower affinity for adsorption to Fe-(hydr)oxides than humic acids (Kaiser, 2003), and their association with soil minerals can be explained by the zonal model of Kleber et al. (2007) which describes that organic molecules adsorb in a layered structure on the mineral surfaces. In the contact zone at the Fe-(hydr)oxide surface, HA is strongly bound via ligand exchange and electrostatic attraction. The hydrophobic parts of the adsorbed HA extend into the solution and act as a sorbent for other organic substances, such as carbohydrates and glomalin, that bind to the first layer through hydrophobic interactions and form the second layer. In the outer layer, organic substances are loosely bound via cation bridging and hydrophobic interactions. Following this conceptual model (Kleber et al., 2007), the importance of carbohydrates and glomalin in aggregate formation (Rillig, 2004; Spohn and Giani, 2010) can be explained by their amphiphilic properties, which facilitates the formation of multiple OM layers. Such associations between different types of organic molecules in soils are also consistent with recent views on the supra-molecular structure of humic substances (Sutton & Sposito, 2007). We suggest that this process leads to a sufficiently thick OM layer on the Fe-(hydr)oxide surfaces, which enables the formation of OM bridges between particles and allows these particles to be taken-up within aggregates.

Coagulation conditions – Impact of pH. The strong increase in the fraction of WSA with decreasing pH (Figure 7.3, Table 7.3) can be explained by two pH-dependent processes. First, adsorption of HA to Fe-(hydr)oxides and clay minerals increases with decreasing pH (Feng et al., 2005; Weng et al., 2008) meaning that a lower pH corresponds to a higher loading of HA on the mineral surfaces. Secondly, the tendency of organic and mineral particles

to coagulate increases with decreasing pH, which can be explained by a decrease in the electrostatic repulsive forces among negatively charged substances (Nguetnkam and Dultz, 2011; Oste et al., 2002; Tombacz and Szekeres, 2004). The surface potential of organically-coated particles is controlled by the surface potential of the adsorbed OM (Weng et al., 2011) and was therefore predicted by the NICA-Donnan model (Figure 7.3). For soils with a SOC content below 15 g kg^{-1} , the fraction of WSA followed the predicted surface potential of HA indicating that the stability of the aggregates is controlled by the tendency of these particles to coagulate. In contrast, the fraction of WSA is less dependent on the pH for soils with a SOC content higher than 15 g kg^{-1} , suggesting that a high SOC content compensate a low aggregate stability induced by a low surface potential for coagulation. The independence of pH for soils with a SOC content above 15 g kg^{-1} might indicate that hydrophobic interactions become more important in soils with a higher SOC content. Thus, the increase in aggregate stability with a decrease in pH can be explained by the (i) increase in the thickness of the OM layer on the mineral surfaces and by (ii) the increase in the binding strength between the organically coated particles.

The effect of pH on aggregation cannot be solely attributed to the proton concentration itself since the pH also affects the solubility of multi-valent cations, such as Ca^{2+} , Al^{3+} and Fe^{3+} . For example, the concentrations of Al^{3+} and Fe^{3+} strongly increase with decreasing pH due to dissolution of Fe- and Al-(hydr)oxide minerals, which also enhances coagulation of particles in acidic soils. In calcareous soils, the Ca^{2+} concentration is controlled by the solubility of CaCO_3 and the Ca^{2+} concentration decreases with increasing pH (Weng et al., 2011) enhancing the dispersion of particles with increasing pH. Thus, the pH-dependent solubility of multi-valent cations in soils amplifies the above-described pH effect.

7.5 Conclusions: Key-factors controlling aggregate formation

The processes controlling aggregate formation in soils at the different size-scales and the linkages between soil aggregates and soil porosity are schematically depicted in Figure 7.7. First, Fe-(hydr)oxides are present as a Fe-(hydr)oxide 'coating' on the surfaces of clay, silt and sand-sized particles, and provide adsorption sites for OM on these larger and low to moderately reactive minerals. Secondly, humic and associated organic substances adsorb to the Fe-(hydr)oxides forming a sufficiently thick layer to act as a bridging agent between the various organic-mineral particles. The adsorption of OM and the coagulation of the particles is enhanced towards a lower pH. As such, the combination of the Feox content, SOC content and pH controls the fraction of WSA in soils. If one of the aggregation factors

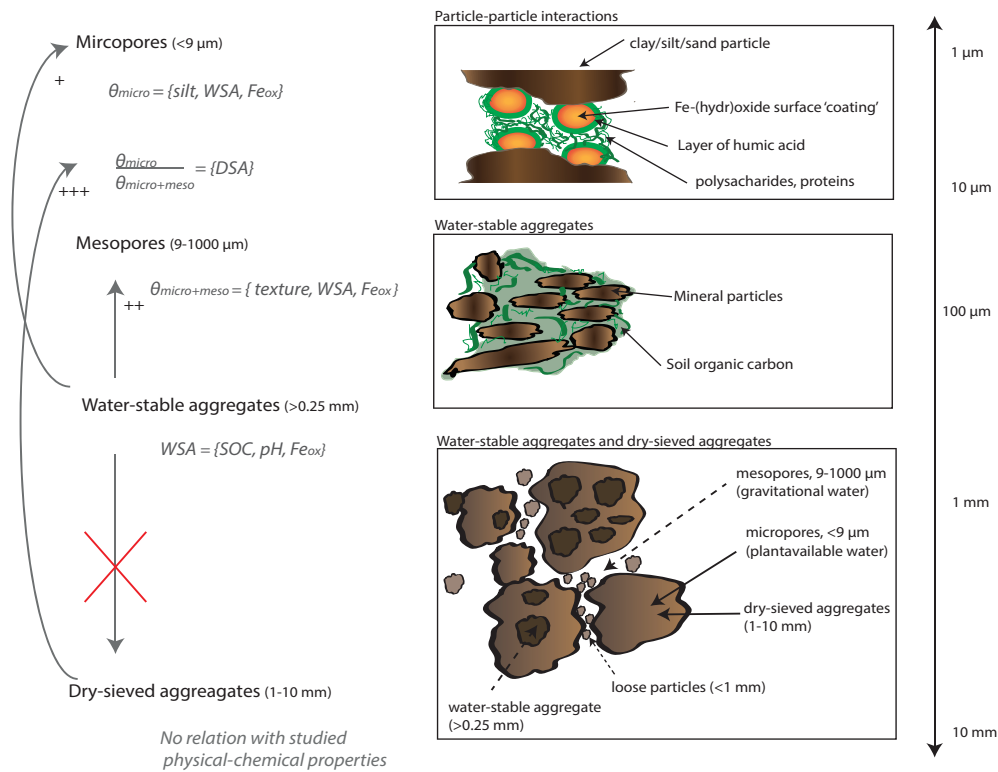


Figure 7.7. Conceptual diagram showing the different size-scales at which aggregate formation occurs and the factors controlling aggregate formation at each size scale. The arrows and corresponding crosses indicate the linkages and between the various physical properties. WSA=water-stable aggregates, DSA= dry-sieved aggregates, Fe_{ox} =oxalate-extractable Fe, SOC=soil organic carbon.

is unfavourable for aggregation, this can be compensated, to a certain extent, by other aggregation factors. For example, a high SOC content can compensate for negative effects of a high pH (Figure 7.2,7.3), and a low pH in combination with a high SOC content can compensate for a low Fe_{ox} content (Figure 7.2 and 7.3).

Considering the different size-scales of aggregates and pores, micropores (< 9 μm) are controlled by the silt content, which determines the inherent porosity of soils, and the Fe-(hydr)oxide content, which determines the additional porosity related to the presence of aggregates (Figure 7.4). The role of Fe-(hydr)oxides is not restricted to the micrometre-sized structures and Fe-(hydr)oxides increase porosity over the whole size-range from micro- to mesopores (Figure 7.5). At the size-scale of the WSA (>250 μm), the contribution of SOC

and pH are more important than the contribution of Fe-(hydr)oxides and there was no effect of texture observed. In contrast, the number of DSA is not controlled by any of the studied physical-chemical parameters or by the number of WSA, suggesting that other aggregation factors such as cementing agents, fungal hyphae or roots control the formation of DSA. Additionally, short-term physical processes like shrinking and swelling may play a major role for the formation of DSA (Horn, 1990). The fraction of DSA is a good indicator for the ratio between micropores and micro+mesopores ($\theta_{30}/\theta_{0.25}$), showing that micropores are dominantly located within DSA whereas mesopores are located in between loose particles and small aggregates (<1 mm).

Our results show that different aggregation factors can be limiting in the different CZO's. Considering the Marchfeld CZO first, the near-alkaline pH of the soils reduces the coagulation potential, which means that a higher SOC and Fe_{ox} content are needed to form the same amount of WSA as compared to soils with a lower pH. The arable sites in the Marchfeld CZO were characterized by a low porosity, low fraction of WSA and low SOC content compared to the forest sites. However, these differences cannot be solely attributed to differences in land use since the Fe_{ox} content was also somewhat lower in the arable sites than in the forest sites. Nevertheless, transitions from forestry to arable farming often coincide with a loss of SOC due to ploughing, lower carbon inputs and high phosphate fertilization levels changing chemical and physical properties of soil (Six et al., 2002; Regelink et al. 2014b; Zehetner et al., 2009) and should therefore be regarded as a threat for the physical quality of soils. In the Koiliaris CZO, the Fluvisols (site K1, K2) are strongly weathered and characterized by a low Fe_{ox} content (amorphous Fe-(hydr)oxides) despite their high Fe_d content (10-25 g kg⁻¹, Table E1). As such, these sites are characterized by a rather low porosity and aggregate stability and can be expected to be susceptible to erosion. In the Slavkov Forest CZO, conditions are favourable for aggregate formation due to the combination of a high SOC content, low pH and high Fe_{ox} content.

Overall, our results have identified amorphous Fe-(hydr)oxides, SOC and pH as the major soil properties that control aggregate formation and porosity in a wide range of soil types, with quantitative relationships that may contribute to strategies towards conserving or improving soil physical properties upon changes in soil management or land use.

References

- Amézketa, E., 1999. Soil Aggregate Stability: A Review. *J. Sustain. Agr.* 14(2-3), 83-151.
- Angers, D.A., 1998. Water-stable aggregation of Québec silty clay soils: Some factors controlling its dynamics. *Soil Till. Res.* 47, 91-96.
- Arias, M., Barral, M.T., Diaz-Fierros, F., 1996. Effects of associations between humic acids and iron or aluminium on the flocculation and aggregation of kaolin and quartz. *Eur. J. Soil. Sci.* 47, 335-343.
- Asano, M., Wagai, R., 2014. Evidence of aggregate hierarchy at micro- to submicron scales in an allophanic Andisol. *Geoderma* 216, 62-74.
- Baalousha, M., 2009. Aggregation and disaggregation of iron oxide nanoparticles; Influence of particle concentration, pH and natural organic matter. *Sci. Total. Environ.* 407, 2093-2101.
- Banwart, S., 2011. Save our soils. *Nature* 474, 151-152.
- Banwart, S., Menon, M., Bernasconi, S.M., Bloem, J., Blum, W.E., Souza, D.M.d., Davidsdotir, B., Duffy, C., Lair, G.J., Kram, P., 2012. Soil processes and functions across an international network of Critical Zone Observatories: Introduction to experimental methods and initial results. *C. R. Geosci.* 344, 758-772
- Barberis, E., Ajmore-Marsan, F., Boero, V., Arduino, E., 1991. Aggregation of soil particles by iron oxides in various size fractions of soil B horizons. *J. Soil Sci.* 42, 525-542.
- Barthès, B.G., Kouakoua, E., Larré-Larrouy, M.C., Razafimbelo, T.M., de Luca, E.F., Azontonde, A., Neves, C.S.V.J., de Freitas, P.L., Feller, C.L., 2008. Texture and sesquioxide effects on water-stable aggregates and organic matter in some tropical soils. *Geoderma* 143(1-2), 14-25.
- Boix Fayos, C., 1997. The roles of texture and structure in the water retention capacity of burnt Mediterranean soils with varying rainfall. *Catena* 31, 219-236.
- Bronick, C.J., Lal, R., 2005. Soil structure and management: A review. *Geoderma* 124(1-2), 3-22.
- Brubaker, S.C., Holzhey, C.S., Brasher, B.R., 1993. Estimating the water-dispersible clay content of soils. *Soil Sci. Soc. Am. J.* 56, 1227-1232.
- Calabi-Floody, M., Bendall, J.S., Jara, A.A., Welland, M.E., Theng, B.K.G., Rumpel, C., de la Luz Mora, M., 2011. Nanoclays from an Andisol: Extraction, properties and carbon stabilization. *Geoderma* 161(3-4), 159-167.
- Chenu, C., Plante, A.F., 2006. Clay-sized organo-mineral complexes in a cultivation chronosequence: revisiting the concept of the 'primary organo-mineral complex'. *Europ. J. Soil Sci.* 57(4), 596-607.
- Currie, J.A., 1966. The volume and porosity of soil crumbs. *J. Soil Sci.* 17(1), 24.
- Curtin, D., Steppuhn, H., Selles, F., 1994. Effect of magnesium on cation selectivity and structural stability of sodic soils. *Soil Sci. Soc. Am. J.* 57(5), 1277-1283.
- Dane, J.H., Topp, G.C., 2002. *Methods of soil analysis. Part 4-Physical methods.* SSA Book Series. Soil Science Society of America, Madison.
- Dexter, A.R., 1988. Advances in characterization of soil structure. *Soil Tillage Res.* 11, 199-238.
- Dilkova, R., Kerchev, G., Kercheva M., 1998. Evaluating and grouping of soils according to their susceptibility to anthropogenic degradation. *Advances in GeoEcology* 31, Catena Verlag, Reiskirchen, 125-131.
- Duiker, S.W., Rhoton, F.E., Torrent, J., Smeck, N.E., Lal, R., 2003. Iron (hydr)oxide crystallinity effects on soil aggregation. *Soil Sci. Soc. Am. J.* 67(2), 606-611.
- Elliott, E.T., Palm, C.A., Reuss, D.E., Monz, C.A., 1991. Organic matter contained in soil aggregates from a tropical chronosequence: Correction for sand and light fraction. *Agr. Eco. Environ.* 34, 443-451.
- Eusterhues, K., Rumpel, C., Kogel-Knabner, I., 2005. Organo-mineral associations in sandy acid forest soils: importance of specific surface area, iron oxides and micropores. *Europ. J. Soil Sci.* 56, 753-763.

- Feng, X., Simpson, A.J., Simpson, M.J., 2005. Chemical and mineralogical controls on humic acid sorption to clay mineral surfaces. *Org. Geochem.* 36, 1553-1566
- Fernández-Ugalde, O., Barré, P., Hubert, F., Virto, I., Girardin, C., Ferrage, E., Caner, L., Chenu, C., 2013. Clay mineralogy differs qualitatively in aggregate-size classes: clay-mineral-based evidence for aggregate hierarchy in temperate soils. *Europ. J. Soil Sci.* 64(4), 410-422.
- Haynes, R., Swift, R., 1990. Stability of soil aggregates in relation to organic constituents and soil water content. *J. Soil Sci.* 41(1), 73-83.
- Hiemstra, T., Antelo, J., Rahnemaie, R., Riemsdijk, W.H.v., 2010. Nanoparticles in natural systems I: The effective reactive surface area of the natural oxide fraction in field samples. *Geochim. Cosmochim. Ac.* 74(1), 41-58.
- Holmgren, G.G.S., 1967. A rapid citrate-ditionite extractable iron procedure. *Soil Sci. Soc. Am. J.* 31(2), 210-211.
- Horn, R., Aggregate characterization as compared to soil bulk properties. *Soil Tillage Res.* 17, 265-289
- Igwe, C.A., Zarei, M., Stahr, K., 2009. Colloidal stability in some tropical soils of southeastern Nigeria as affected by iron and aluminium oxides. *Catena* 77(3), 232-237.
- Kaiser, K., 2003. Sorption of natural organic matter fractions to goethite (α -FeOOH): effect of chemical composition as revealed by liquid-state ^{13}C NMR and wet-chemical analysis. *Org. Geochem.* 34, 1569-1579
- Kercheva, M., Rousseva, S., Dimitrov, E., Nenov, M., Shishkov, T., 2011. Soil aggregation estimates in CZO- Fuchsenbigl. *App. Geochem.* 26 Supplement, S57-59
- Kleber, M., Sollins, P., Sutton, R., 2007. A conceptual model of organo-mineral interactions in soils: self-assembly of organic molecular fragments into zonal structures on mineral surfaces. *Biogeochem.* 85, 9-24
- Kögel-Knabner, I., Guggenberger, G., Kleber, M., Kandeler, E., Kalbitz, K., Scheu, S., Eusterhues, K., Leinweber, P., 2008. Organo-mineral associations in temperate soils: Integrating biology, mineralogy, and organic matter chemistry. *J. Plant Nutr. Soil Sci.* 171(1), 61-82.
- Kram, P., Hruska, J., Shanley, J.B., 2012. Streamwater chemistry in three contrasting monolithologic Czech catchments. *Appl. Geochem.* 27, 1854-1863.
- Lair, G.J., Zehetner, F., Hrachowitz, M., Franz, N., Maringer, F.J., Gerzabek, M.H., 2009a. Dating of soil layers in a young floodplain using iron oxide crystallinity. *Quat. Geochronol.* 4(3), 260-266.
- Lair, G.J., Zehetner, F., Khan, Z.H., Gerzabek, M.H., 2009b. Phosphorus sorption-desorption in alluvial soils of a young weathering sequence at the Danube River. *Geoderma* 149(2), 39-44.
- Lindsay, W.L., 1979. *Chemical Equilibria in Soils*. Wiley-Interscience.
- Lipiec, J., Walczak, R., Witkowska-Walczak, B., Nosalewicz, A., Slowińska-Jurkiewicz, A., Sławiński, C., 2007. The effect of aggregate size on water retention and pore structure of silt loam soils of different genesis. *Soil Tillage Res.* 97, 239-246.
- Luxmoore, R.J. 1980. Micro-, meso-, and macroporosity of the soil. *Soil Sci. Soc. Am. J.* 45, 671-672
- Majzik, A., Tombacz, E., 2007. Interaction between humic acid and montmorillonite in the presence of calcium ions II. Colloidal interactions: Charge state, dispersing and/or aggregation of particles in suspension *Org. Geochem.* 38(8), 1330-1340.
- Mehra, O.P., Jackson, M.L., 1960. Iron oxide removal from soils and clays by a dithionite-citrate system buffered with sodium bicarbonate. *Proc. 7th nat. conf. clays* 5, 317-327.
- Mikutta, R., Kleber, M., Torn, M., Jahn, R., 2006. Stabilization of Soil Organic Matter: Association with Minerals or Chemical Recalcitrance? *Biogeochem.* 77(1), 25-56.
- Milne, C.J., Kinniburgh, D.G., Van Riemsdijk, W.H., Tipping, E., 2003. Generic NICA-Donnan model

- parameters for metal-ion binding by humic substances. *Environ. Sci. Tech.* 37, 958-971.
- Montgomery, D.R., 2007. Soil erosion and agricultural sustainability. *Proc. Nat. Acad. Sci. USA* 104, 13268-13272.
- Moraetis, M., Paranychianakis, N.V., Nikolaidis, N.P., Banwart, S., Rousseva, S., Kercheva, M., Nenov, M., Shishkov, T., de Ruiter, P., Bloem, J., Blum, W.E.H., Lair, G.J., van Gaans, P., Verheul, M., 2014. Sediment provenance, soil development, and carbon content in fluvial and manmade terraces at Koiliaris River Critical Zone Observatory. *J. Soil. Sed.* in press.
- Nguetnkam, J.P., Dultz, S., 2011. Soil degradation in Central North Cameroon: Water-dispersible clay in relation to surface charge in Oxisol A and B horizons. *Soil Tillage Res.* 113(1), 38-47.
- Nyamangara, J., Gotosa, J., Mpofu, S., 2001. Cattle manure effects on structural stability and water retention capacity of a granitic sandy soil in Zimbabwe. *Soil Tillage Res.* 62(3), 157-162.
- Oades, J.M., Waters, A.G., 1991. Aggregate hierarchy in soils. *Soil Res.* 29, 815-828
- Oades, J.M., 1993. The role of biology in the formation, stabilization and degradation of soil structure. *Geoderma* 56, 377-400.
- Oste, L.A., Temminghoff, E.J.M., Van Riemsdijk, W.H., 2002. Solid-solution partitioning of organic matter in soils as influenced by an increase in pH or Ca concentration. *Environ. Sci. Technol.* 36, 208-214.
- Pansu, M., Gautheyrou, J., 2006. *Handbook of Soil Analysis: Mineralogical, Organic and Inorganic Methods*. Springer Berlin Heidelberg New York.
- Penn, R.L., Zhu, C., Xu, H., Velben, D.R., 2001. Iron-oxide coatings on sand grains from the Atlantic coastal plain: High-resolution transmission electron microscopy characterization. *Geology* 29(9), 843-846.
- Pronk, G.J., Heister, K., Kögel-Knabner, I., 2011. Iron oxides as major available interface component in loamy arable topsoils. *Soil Sci. Soc. Am. J.* 75(6), 2158-2168.
- Puget, P., Chenu, C., Balesdent, J., 2000. Dynamics of soil organic matter associated with particle-size fractions of water-stable aggregates. *Europ. J. Soil Sci.* 51(4), 595-605.
- Pulleman, M., Jongmans, A., Marinissen, J., Bouma, L., 2003. Effects of organic versus conventional arable farming on soil structure and organic matter dynamics in a marine loam in the Netherlands. *Soil Use Manag.* 19, 147-165.
- Pulleman, M., Marinissen, J., 2004. Physical protection of mineralizable C in aggregates from long-term pasture and arable soil. *Geoderma* 120(3), 273-282.
- Regelink, I.C., Weng, L., Koopmans, G.F., Van Riemsdijk, W.H., 2013. Asymmetric flow field-flow fractionation as a new approach to analyse iron-(hydr) oxide nanoparticles in soil extracts. *Geoderma* 202, 134-141
- Regelink, I.C., Voegelin, A., Weng, L., Koopmans, G.F., Comans, R.N.J., 2014a. Characterization of Colloidal Fe from Soils using Field-Flow Fractionation and Fe K-edge X-ray Absorption Spectroscopy. *Environ. Sci. Technol.* 48, 4307-4316.
- Regelink, I.C., Weng, L., Lair, G.J., Comans, R.N.J., 2014b. Phosphate solubility and competition with organic matter in arable and forest soils explained by adsorption modelling. *Env. Sci. Tech.* submitted.
- Rillig, M.C., 2004. Arbuscular mycorrhizae, glomalin, and soil aggregation. *Can. J. Soil Sci.* 84(4), 355-363.
- Schwertmann, U., 1991. Solubility and dissolution of iron oxides. *Plant Soil* 130, 1-25.
- Sei, J., Jumas, J.C., Olivier-Fourcade, J., Quiquampoix, H., Staunton, S., 2002. Role of iron oxides in the phosphate adsorption properties of kaolinites from the ivory coast. *Clay. Clay Min.* 50(2), 217-222.

- Six, J., Bossuyt, H., Degryze, S., Deneff, K., 2004. A history of research on the link between (micro) aggregates, soil biota, and soil organic matter dynamics. *Soil Tillage Res.* 79(7-31).
- Six, J., Callewaert, P., Lenders, S., De Gryze, S., Morris, S.J., Gregorich, E.G., Paul, E.A., Paustian, K., 2002. Measuring and Understanding Carbon Storage in Afforested Soils by Physical Fractionation. *Soil Sci. Soc. Am. J.* 66(6), 1981-1987.
- Six, J., Elliott, E.T., Paustian, K., 2000a. Soil structure and soil organic matter: II. A normalized stability index and the effect of mineralogy. *Soil Sci. Soc. Am. J.* 64, 1042-1049.
- Six, J., Paustian, K., Elliott, E.T., Combrink, C., 2000b. Soil structure and organic matter: I. Distribution of aggregate-size classes and aggregate-associated carbon. *Soil Sci. Soc. Am. J.* 64, 681-689.
- Spohn, M., Giani, L., 2010. Water-stable aggregates, glomalin-related soil protein, and carbohydrates in a chronosequence of sandy hydromorphic soils. *Soil Biol. Biochem.* 42(9), 1505-1511.
- Stamati, F.E., Nikolaidis, N.P., Schnoor, J.L., 2013. Modeling topsoil carbon sequestration in two contrasting crop production to set-aside conversions with RothC – Calibration issues and uncertainty analysis. *Agr. Ecosyst. Environ.* 165, 190-200.
- Sutton, R., Spósito, G., 2007. Molecular structure in soil humic substances: The new view. *Environ. Sci. Technol.* 31, 9009-9015.
- Tisdall, J.M., Oades, J.M., 1982. Organic matter and water-stable aggregates in soils. *Journal of Soil Science* 33(2), 141-163.
- Tombacz, E., Szekeres, M., 2004. Colloidal behavior of aqueous montmorillonite suspensions: the specific role of pH in the presence of indifferent electrolytes. *Appl. Clay Sci.* 27, 75-94.
- Vogel, C., Mueller, C.W., Höschel, C., Buegger, F., Heister, K., Schulz, S., Schloter, M., Kögel-Knaber, I., 2014. Submicron structures provide preferential spots for carbon and nitrogen sequestration in soils. *Nature Commun.* 5.
- Wattel-Koekkoek, E.J.W., Van Genuchten, P.P.L., Buurman, P., Van Lagen, B., 2001. Amount and composition of clay-associated soil organic matter in a range of kaolinitic and smectitic soils. *Geoderma* 99, 27-49.
- Weng, L., van Riemsdijk, W.H., Hiemstra, T., 2008. Humic nanoparticles at the oxide-water interface: Interactions with phosphate ion adsorption. *Environ. Sci. Tech.* 42, 8747-8752.
- Weng, L., Vega, F.A., Van Riemsdijk, W.H., 2011. Competitive and Synergistic Effects in pH Dependent Phosphate Adsorption in Soils: LCD Modeling. *Environ. Sci. Tech.* 45(19), 8420-8428.
- Wösten, J., Pachepsky, Y.A., Rawls, W., 2001. Pedotransfer functions: bridging the gap between available basic soil data and missing soil hydraulic characteristics. *J. Hydrol.* 251(3), 123-150.
- Zehetner, F., Lair, G.J., Gerzabek, M.H., 2009. Rapid carbon accretion and organic matter pool stabilization in riverine floodplain soils. *Global Biogeochem. Cy.* 23(4).
- Zehetner, F., Lair, G.J., Maringer, F.-J., Gerzabek, M.H., Hein, T., 2008. From sediment to soil: floodplain phosphorus transformations at the Danube River. *Biogeochem.* 88(2), 117-126.

Chapter 8

General Discussion

Inge C. Regelink

8.1 Introduction

Nanoparticles are nanometre-sized solid particles which have a high sorption capacity due to their small size and consequently large specific surface area (SSA)(Hochella et al., 2008). Mineral nanoparticles can be released from soils and transported to the aquatic environment (Kretzschmar et al., 1999) where they act as carriers for phosphorus (P) and trace metals (Neubauer et al., 2013; Plathe et al., 2013). Furthermore, nanoparticles dominate the surface area that is available for adsorption of soil organic carbon (SOC) and phosphate (PO_4) in the soil and consequently play an important role in the sequestration of SOC and PO_4 as well as in controlling their concentrations in the soil solution (Hiemstra et al., 2010a, Mikutta et al., 2011). Additionally, Fe-(hydr)oxide nanoparticles play an important role in the formation of organo-mineral assemblages (Asano and Wagai, 2014; Pronk et al., 2011) and aggregates in soils (Chapter 7). Therefore, the overall objective of this thesis was to characterize nanoparticles in soils and to understand their role in the above mentioned soil processes.

To enable the characterisation of nanoparticles in soil extracts and water samples, novel analytical techniques were needed. In this PhD thesis, I used Asymmetric Flow Field-Flow Fractionation in combination with an UV analyser and High-Resolution Inductively Coupled Plasma Mass-Spectroscopy (HR-ICP-MS) for the fractionation and characterization of nanoparticles in soil extracts and in runoff waters (Chapter 2–5). Additionally, I made use of Extended X-ray Absorption Fine Structure (EXAFS) spectroscopy to unravel the speciation the Fe-containing nanoparticles (Chapter 3). These results provide new insights into the characteristics of Fe-(hydr)oxide nanoparticles and the role of inorganic nanoparticles in colloid-facilitated transport of P (Chapter 4) and trace metals (Chapter 5). In Chapter 6, I used a mechanistic surface complexation (SC) model in order to predict the competitive interactions between organic matter (OM) and PO_4 for adsorption to Fe-(hydr)oxide surfaces. My results provide new insights into the effect of high PO_4 levels on OM sequestration by metal-(hydr)oxides, and into the effect of OM adsorption to metal-(hydr)oxides on PO_4 solubility in soils. Thereafter, I show that Fe-(hydr)oxides play an important role in formation of aggregates and porosity and as such, improve the water retention capacity and physical properties of the soil (Chapter 7).

In this last chapter, I will discuss the major findings of my PhD thesis and their implications and I will give suggestions for further research. First, I will discuss various analytical approaches that can be used to measure the size-distribution of Fe-(hydr)oxide nanoparticles in soils. Second, I will discuss the role of mineral nano-colloids in

the transport of P from agricultural fields on clay soils to adjacent surface waters and their potential contribution to eutrophication of surface waters. Third, I will discuss the potential contribution of Fe-(hydr)oxides to the sequestration of organic carbon (OC) in soils, considering also the effect of high PO_4 levels and the uncertainties in the chosen SC modelling approach. Fourth, I will discuss the role of Fe-(hydr)oxides in the formation of organo-mineral aggregates and their impact on soil physical properties.

8.2 Iron-(hydr)oxide nanoparticles in soils: How small are they?

The sorption capacity of Fe-(hydr)oxide nanoparticles is strongly related to their specific surface area (SSA) and thus to the size-distribution of the Fe-(hydr)oxides in the soil. Previous studies have estimated that average sizes of metal-(hydr)oxides in soils vary between 1-10 nm (Eusterhues et al., 2005; Hiemstra et al., 2010a). However, the presence of such extremely small (1-10 nm) Fe-(hydr)oxide particles in soil is remarkable because small particles are thermodynamically unstable and tend to increase in size and crystallinity over time (Burlinson and Penn, 2005). The existence of nanosized particles in soils might be explained by the co-precipitation of Fe with dissolved organic carbon (DOC) since DOC effectively inhibits polymerization and further growth of freshly precipitated Fe-(hydr)oxide particles (Eusterhues et al., 2008; Schwertmann et al., 2005). Nevertheless, further experimental evidence is needed to verify the presence of such small particles in soils. However, determination of the size-distribution or SSA of Fe-(hydr)oxides in soils is still a major analytical challenge.

My objective of Chapter 2 and 3 was to develop a method for the extraction and subsequent size-fractionation of Fe-(hydr)oxide nanoparticles using AF4 coupled to online HR-ICP-MS. The first challenge in using this approach is to extract the Fe-(hydr)oxide nanoparticles from the soil as intact and colloidally stable particles. Since there is hardly any knowledge on how to disperse nanoparticles from soils, I tested several new extraction methods for this purpose (Chapter 2, 3). My results show that Na-pyrophosphate extracted most Fe-(hydr)oxide nanoparticles from soils, which can be explained through the replacement of humic substances by pyrophosphate on the Fe-(hydr)oxide surfaces and the subsequent release of Fe-(hydr)oxides due to the dispersion of organo-mineral aggregates (Chapter 2). Quantification of the amount of free (i.e. not associated with clay minerals) Fe-(hydr)oxide nanoparticles in the soil extracts revealed that only a part (5-37%) of the oxalate-extractable Fe was extracted as free Fe-(hydr)oxides by a combination of Na-pyrophosphate

and ultrasonic treatment (Chapter 2 and 3). The remaining part of the Fe-(hydr)oxide particles is likely bound to other mineral particles. The fact that the binding between Fe-(hydr)oxides and other mineral particles cannot be broken by the combination of ultrasonic treatment and Na-pyrophosphate strongly limits our ability to disperse Fe-(hydr)oxides as free particles and to determine the size-distribution of these Fe-(hydr)oxides. This problem cannot be overcome by using stronger extractants such as Na-hydroxide or ammonium-oxalate since these extractants will dissolve rather than disperse Fe-(hydr)oxides. As such, only a fraction of the soil Fe-(hydr)oxides can be dispersed as free particles meaning that the size-distribution can only be determined for a part of the Fe-(hydr)oxides in the soil. Another constraint in analysing the size-distribution of Fe-(hydr)oxide nanoparticles by AF4 is that the aggregation state of the freely dispersed Fe-(hydr)oxide particles cannot be elucidated from the Fe-signal only. The free Fe-(hydr)oxide particles cover a rather wide size-range (1–150 nm) (Chapter 2 and 3) and it is unknown whether this size-range represents the size-range of single particles or of aggregated particles. In the latter case, the diameter of the Fe-(hydr)oxide particles would be seriously overestimated by AF4, leading to a serious underestimation of the SSA. It might be possible to elucidate the aggregation state of the Fe-(hydr)oxide particles from the P/Fe ratio of the particles. However, in this PhD thesis, the measurement of colloidal P concentrations in the Na-pyrophosphate extracts was inhibited by the large salt peak of P eluting from the Na-pyrophosphate extracts and as such, the P/Fe ratio could not be used as an indicator for the aggregation state in these extracts. Further research is needed to enable the measurement of low concentrations of colloidal P in solutions with high concentrations of dissolved P, which might be achievable by using a longer focussing time during the AF4 run. Overall, AF4 provides experimental evidence for the existence of nano-sized Fe-(hydr)oxides in soils however, this approach cannot be used to derive the full SSA of the Fe-(hydr)oxides in the soil due to the low fraction of Fe-(hydr)oxides dispersed from the soil as free particles and due to uncertainties regarding the presence of aggregated Fe-(hydr)oxides in the soil extracts.

An alternative approach to provide evidence for the size of Fe-(hydr)oxide nanoparticles in soils is the visualisation of particles using Scanning Electron Microscopy (SEM) in combination with detection of the elemental composition using Energy Dispersive X-ray (EDX) spectrometry. Figure 8.1 shows the SEM photographs and corresponding EDX spectra of a bulk soil that was also used in Chapter 3 (soil nr.17) for the characterization of Fe in the colloidal fraction. The photographs and EDX spectra show the presence of smaller Fe-rich particles, which are about 100–500 nm in size, on the surfaces of larger Si-rich or Si/Al-

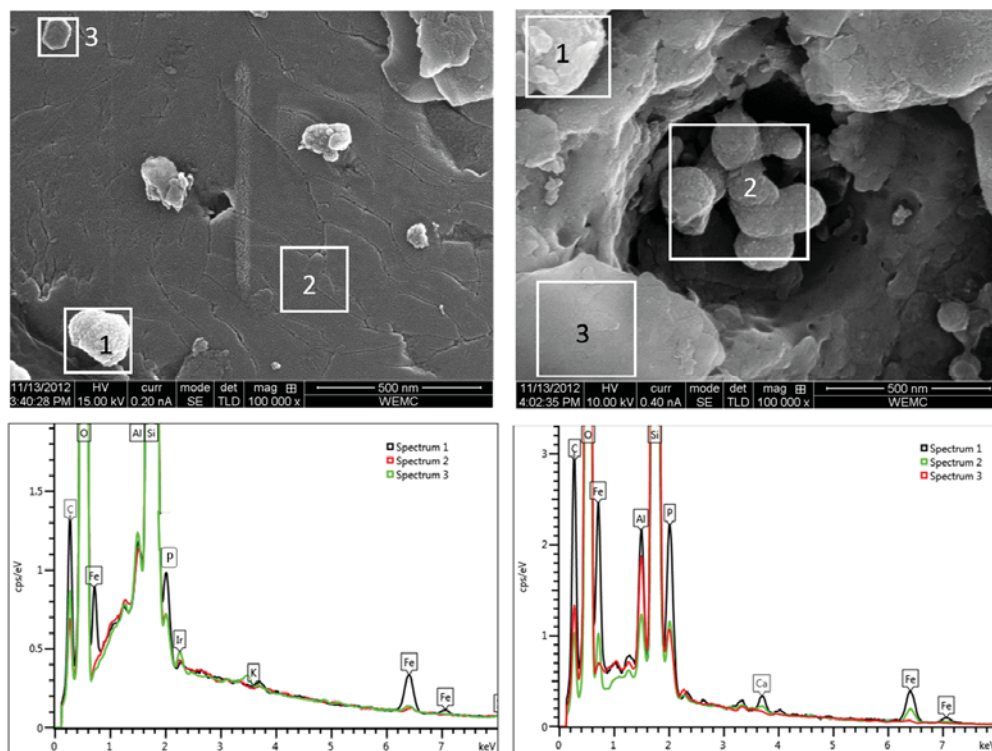


Figure 8.1. Scanning electron microscopy (SEM) photographs and energy dispersive X-ray (EDX) spectra collected for a top soil taken from a Dutch agricultural field (soil nr. 17 in Chapter 3).

rich minerals. Additionally, the right photo shows an example of aggregated nanoparticles. The diameters of these Fe-rich particles are large compared to the smallest size of the Fe-(hydr)oxide nanoparticles detected by AF4 in the Na-pyrophosphate extracts of these soils (2–5 nm, Chapter 3). Visualisation of the very small Fe-(hydr)oxide nanoparticles may be hampered because these particles are likely completely embedded within organo-mineral aggregates and because of their small contribution to the overall soil mass. Generally, Fe-(hydr)oxide nanoparticles represent less than 5% of the soil mass. Therefore, identifying Fe-(hydr)oxide nanoparticle in the soil by SEM is extremely difficult and can be considered as searching for a needle in a haystack.

Previous studies have estimated the average size of Fe-(hydr)oxide nanoparticles in soils based on SSA of the soil, scaled to the metal-(hydr)oxide content of the soil. For example, Eusterhues et al. (2005) estimated the particle size of Fe-(hydr)oxides in some forest soils from surface area measurements using the N_2 -BET adsorption method after oxidation of the

SOC by oxidation, and found an average particle size of about 10 nm. Such in-situ methods have the advantage that possible artefacts due to particle extraction are prevented. However, drawbacks of this method are that the OM layer needs to be removed from the mineral surfaces by oxidation in order to obtain a reliable measurement of the mineral SSA. It is unknown whether the use of strong oxidizing agents affects the SSA of the soil minerals. Furthermore, this method is not selective for metal-(hydr)oxides but quantifies the SSA of all mineral particles in the soil (Eusterhues et al., 2005; Kaiser and Guggenberger, 2003). A milder and more selective approach was recently developed by Hiemstra et al. (2010a) who estimated the SSA of metal-(hydr)oxides in a series of agricultural soils based on their phosphate-buffering behaviour derived from desorption experiments. Interpretation of the desorption data by a SC model allows to derive the SSA and corresponding average particle size (1–10 nm) of the metal-(hydr)oxides in the soil. This method selectively determines the surface area of the Fe+Al(hydr)oxides, since these minerals generally dominate the PO_4 adsorption capacity of the soil (Chapter 6). However, since the SSA is derived by SC modelling, possible discrepancies between the adsorption behaviour or site density of the natural metal-(hydr)oxides versus the synthetic Fe-(hydr)oxides that were used to derive the adsorption parameters can lead to uncertainties in the predicted SSA of the metal-(hydr)oxides. Furthermore, it is assumed that OM associated with the metal-(hydr)oxides is desorbed due to the addition of activated carbon, whereas it is uncertain if black carbon indeed leads to a complete removal of the mineral-associated OM. As such, Hiemstra et al. (2010) proposed that the derived SSA should be interpreted as an ‘effective’ SSA rather than as the actual SSA. If OM is present on the metal-(hydr)oxide surfaces, the phosphate buffering behaviour will be affected which will lead to an underestimation of the SSA of the metal-(hydr)oxides. This problem might be overcome by using more aggressive techniques to remove organic matter, or by improving SC models so that the effect of organic matter on the phosphate desorption curves can be described. Further improvements in this method are important since the SSA of the metal-(hydr)oxide fractions is an important input parameter in SC modelling. The results from the different analytical approaches described above, except the SEM, have in common that they all provide evidence for the presence of 1–10 nm sized Fe-(hydr)oxide particles in soils. However, no relation was found between the effective SSA of the metal-(hydr)oxides and the size or concentration of Fe-(hydr)oxide nanoparticles found in the soil extracts (Chapter 3). The different approaches are based on different principles and all have their own advantages and disadvantages and the choice for the ‘best’ method depends on the research question to be answered.

8.3 Colloid-facilitated transport: Is the release of mineral colloids from clay soils an important source for eutrophication of surface waters?

The excessive use of P fertilizers and animal manure makes agriculture one of the major sources contributing to phosphorus enrichment of surface waters, with often serious water quality problems such as algal blooms as a consequence (Correl, 1998). The impact of P losses on eutrophication is not necessarily related to the total phosphorus concentration, but depends on the speciation of the P entering the surface waters since different P species vary strongly in their bioavailability to algae (Ekholm, 1994). Previous studies have tried to address this problem by linking the bioavailability of P to operationally defined P fractions (Salm et al., 2012; Turner et al., 2002). One of these fractions is the dissolved PO_4 , which is readily bioavailable and thus of major concern with respect to eutrophication. In sandy soils with a high P saturation status, transport of P to the ground- and surface waters is dominated by dissolved PO_4 (Siemens et al., 2008). In contrast, transport of P from clay soils to adjacent surface waters is dominated by colloidal (<0.45 μm) and the particulate P (>0.45 μm) (Salm et al., 2012, Toor et al., 2005). Over a period of 5 years, these two fractions were together responsible for 70% of the P entering the surface waters adjacent to an experimental field site on a heavy clay soil in the Netherlands (Salm et al., 2012). It is commonly believed that the colloidal P fraction is dominantly associated with clay minerals and is poorly available for biota (Uusitalo et al., 1999). However, experimental evidence for the speciation of colloidal P is still poor. This lack of knowledge hampers a quantitative understanding of the contribution of colloidal P from agricultural sources to eutrophication of surface waters in agricultural regions dominated by clay soils. Therefore, in Chapter 4, I unravelled the speciation of the colloidal P fraction in drain and trench waters taken from a fertilized clay field using AF4 coupled to online HR-ICP-MS. In this paragraph, I will elaborate further on the implications of my findings with respect to the role of mineral colloids in the transport of P from fertilized clay soils to the aquatic environment and the consequence for eutrophication.

In Chapter 4, I unravelled the nature of the colloidal P fraction in pipe drain and trench waters collected from a fertilized clay soil in The Netherlands. The water samples were collected at three sampling times at different timespans after manure application and analysed using AF4 coupled to HR-ICP-MS. For the samples taken one week and six months after manure application, the AF4 results showed that P in the colloidal fraction co-elutes with mineral colloids consisting of Si, Al, and Fe. The particulate fraction could

not be analysed by AF4 due to their larger size but, using regression analysis, I show that the speciation of P in the particulate fraction is similar to that in the colloidal fraction. Thus, my results show that the transport of colloidal and particulate P in drain and trench waters from this clay soil should be explained by the association between P and mineral particles present in the waters. However, based on the AF4 fractograms (Chapter 4), the mineralogy of the mineral colloids that facilitate P transport remains elusive. For example, it is uncertain whether the Fe co-eluting with the Si/Al peak represents Fe that is incorporated within the clay mineral structure, or represents Fe-(hydr)oxide nanoparticles associated with the clay minerals. The difference between these two Fe species is relevant because of the much higher adsorption capacity of Fe-(hydr)oxides for PO_4 compared to clay minerals (Sei et al., 2002, Chapter 6). The high affinity of P for adsorption to Fe-(hydr)oxides suggests that the association of P with the inorganic minerals should be explained by the presence of Fe-(hydr)oxide particles. However, in Chapter 2, I argue that the release of Fe-(hydr)oxide nanoparticles to the soil pore water is unlikely to occur because my results showed that dispersion of Fe-(hydr)oxides as free particles was inhibited in mild extractants such as NaCl due to the strong interactions between Fe-(hydr)oxides and OM. In Chapter 3, I solved this apparent contradiction about whether Fe-(hydr)oxides can or cannot be released from soils under conditions similar as in the soil pore water by using a combination of AF4-HR-ICP-MS and EXAFS. For the clay soil, my results showed that the release of free Fe-(hydr)oxides in a mild extractant was indeed inhibited but, Fe-(hydr)oxides associated with clay minerals were dispersed in considerable concentrations. Thus, Fe-(hydr)oxides associated with clay minerals seem responsible for the presence of colloidal P in the drain and trench waters collected from the clay soil. Also in a recent AF4 study about P-speciation in stream waters, Fe-(hydr)oxides were found to be of higher importance for transport of P than clay minerals (Gottselig et al., 2014).

With respect to eutrophication, both the amount of P and the bioavailability of the species entering the surface waters are of importance. Colloidal and particulate P are not directly available for algae and are therefore often considered as less harmful for the environment compared to the dissolved PO_4 , which is directly bioavailable (Ekholm, 1994). However, over time, the bioavailability of the colloidal and particulate P, which are dominated by PO_4 adsorbed to clay-oxide particles, strongly depends on the geochemical reactions that can occur in the water and sediment. Desorption experiments have shown that a part of the mineral-associated PO_4 can be released over time, especially when solution concentrations of PO_4 are low (Uusitalo et al., 1999). Furthermore, colloids will settle down and redox

processes within the sediment layers will affect the long-term availability of the mineral-associated PO_4 . For example, it has been shown that iron-rich sediments can sequester substantial amounts of PO_4 under oxic conditions, whereas release of PO_4 occurs under reducing conditions due to reduction and subsequent dissolution of the Fe-(hydr)oxide minerals (Loeb et al., 2008; Roden and Edmonds, 1997; Rozan et al., 2002). Subsequently, the released PO_4 can be transported from the sediment to the oxic water phase, where it either remains present as dissolved PO_4 or where it can precipitate with Fe and Ca to form Fe-Ca-P minerals (Voegelin et al., 2010). These Fe-Ca-P minerals are characterized by a small size (<400 nm), poorly ordered structure and large P/Fe ratio (0.5–0.7) (Kaegi et al., 2010; Voegelin et al., 2010). As such, these particles can be expected to have high colloidal stability and solubility, and their presence in river water samples shows that they have a high mobility in the environment (Vega and Weng, 2013). Overall, the contribution of mineral-associated P to eutrophication strongly depends on the local geochemical conditions but, over time, it seems likely that the majority of the mineral-associated PO_4 can become available for uptake by algae and thus contributes to eutrophication. As such, in agricultural regions dominated by clay soils, colloidal and particulate P species should be considered as a potential threat for surface water quality, meaning that soil management actions should not solely focus on the reduction of dissolved PO_4 losses, but should also pay attention to the reduction of colloidal and particulate P losses.

8.4 Iron-(hydr)oxide nanoparticles as sorbents: How can we predict the organic matter loading on Fe-(hydr)oxides?

Soils can provide long-term storage of OC and can as such act as a sink for CO_2 , thereby mitigating the greenhouse effect caused by elevated levels of CO_2 . Therefore, the OC-sequestration potential of soils has received increasing attention during the last decades (Eusterhues et al., 2005; Kögel-Knabner et al., 2008; Six et al., 2002; Zehetner et al., 2009). SOC can be physically stabilized due to adsorption to minerals and incorporation within micro-aggregates, and SOC can be (bio)chemically stabilized due to the inherent recalcitrance of specific OM fractions or due to unfavourable conditions for biodegradation (Kalbitz et al., 2005; Six et al., 2002). The physical stabilization by minerals, in particular Fe-(hydr)oxides, plays an important role in the long-term stabilization of OM in soils (Kaiser et al., 2002; Mikutta et al., 2006). The interactions between OM and metal-(hydr)oxides plays an important role throughout this thesis. For example, my results show that Fe-

(hydr)oxide nanoparticles are strongly associated with the OM fraction in the soil and that these organic-mineral assemblages are of high mechanical strength (Chapter 2, 3). Further experimental evidence for the specific role of Fe-(hydr)oxides in carbon sequestration is given by the SEM photographs and corresponding EDX spectra collected for an agricultural soil (Figure 8.1). The EDX spectra, which were collected for subfractions of the SEM photographs, show that the Fe-rich particles are also enriched in C and P. The coincidence between C and P on the Fe-rich particles shows that both OM and P, likely in the form of PO₄, adsorb to these particles and as such compete for adsorption, which is in line with my modelling study described in Chapter 6. In contrast to the Fe-rich particles, there was no C or P detected at the surfaces of the larger Si-rich minerals, which are likely quartz minerals. Thus, OM does not form a homogenous monolayer on the surfaces of the quartz minerals but adsorbs preferentially to Fe-rich particles that are present on the surfaces of the larger quartz minerals, which is in line with previous observations (Kaiser et al., 2002; Mikutta et al., 2006). This finding supports my conceptual model that I describe in Chapter 7, in which I propose that Fe-(hydr)oxide nanoparticles act as sorption sites for OM on larger and poorly reactive minerals.

However, despite the above described evidence for the importance of Fe-(hydr)oxides in the sequestration of SOC, our quantitative understanding of the amount of SOC that can be sequestered by Fe-(hydr)oxides under different conditions is still poor. The potential amount of SOC that can be stabilized by Fe-(hydr)oxides can be estimated from the size of the Fe-(hydr)oxide particles in combination with the thickness of the OM layer on the Fe-(hydr)oxide surface. I estimated the amount of SOC that can adsorb to Fe-(hydr)oxides particles with a diameter of 2, 4, 6 and 10 nm, respectively (Figure 7.3). This size-range corresponds to the average sizes of metal-(hydr)oxides that can be expected in natural soils (Chapter 2,3) (Eusterhues et al., 2005; Hiemstra et al., 2010a). I assumed that OM forms a monolayer with a thickness of 1.5 nm, which is similar to the size of the humic acids extracted in Na-pyrophosphate as determined by AF4 (Chapter 2,3) and I assumed that the density of the mineral and organic substances amounts to 3.5 and 1.25 kg dm⁻³, respectively (Hiemstra et al., 2010). With increasing particle size (2–10 nm), the OM loading decreases from 3.0 to 1.2 mg C m⁻², which can be explained by the decrease in the curvature of spherical particles with increasing particle size. This range in predicted OM loadings is similar to the range of values derived from experimental studies (1.1–4.8 mg C per m⁻²) (Dümig et al., 2012; Eusterhues et al., 2005; Hiemstra et al., 2010b; Kaiser and Guggenberger, 2003; Weng et

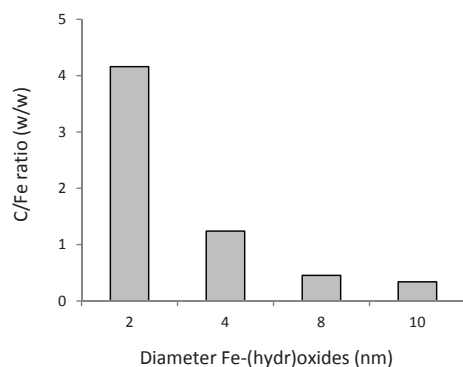


Figure 8.2. The predicted C/Fe ratio as a function of the diameter of the Fe-(hydr)oxide particles. The Fe-(hydr)oxide particles (3.5 kg dm^{-3}) are assumed to be spherical and to be covered with a monolayer of organic matter with a thickness of 1.5 nm and a bulk density of 1.25 kg dm^{-3} .

al., 2007). The calculated C/Fe ratio of the organic-Fe-(hydr)oxide assemblages (Figure 7.3) decreases from 4.1 to 0.3 with an increase in particle size from 2 to 10 nm. Thus, small (<4 nm) Fe-(hydr)oxide nanoparticles have a large capacity to adsorb OM whereas the larger particles hardly contribute to the overall adsorption capacity of the soil. Assuming that the oxalate-extractable Fe fraction represents the small Fe-(hydr)oxide particles, a soil with a Fe_{ox} content of 4 g Fe kg^{-1} , which is within the common range for Dutch soils (Hiemstra et al., 2010), can stabilize up to 16 g C kg^{-1} soil, which corresponds to a SOC content of 1.6%. Overall, this simple calculation shows that a small amount of 1–4 nm sized Fe-(hydr)oxide particles can stabilize a large amount of OC, which shows the importance of developing experimental techniques to quantify the size-distribution of Fe-(hydr)oxide particles in soils.

Another constraint in predicting the OC sequestration capacity of the Fe-(hydr)oxide fraction is the uncertainty in the prediction of the OM loading on the mineral surfaces. The above calculated OM loading represents the maximum amount of OM that can be physically placed near the Fe-(hydr)oxide surface assuming a mono-layer coverage. However, the actual OM loading might be much lower since the amount of OM adsorbed also depends on (i) the characteristics of the OM, such as its molecular weight, number of carboxylic groups and hydrophobicity and on (ii) the solution chemistry, such as the pH, ionic strength, and concentrations of divalent cations and anions, particularly PO₄ (Antelo et al., 2007; Filius et al., 2000; Weng et al., 2007). These adsorption interactions can be described by SC models (Hiemstra et al., 2013; Weng et al., 2008) and therefore, I made

use of an advanced SC model to predict the OM loading on metal-(hydr)oxide surfaces in arable and forest soils collected from the floodplains of the Danube river. My results show that the OM loading on the metal-(hydr)oxides is 2–28 times lower in the topsoils of the PO_4 -rich arable fields compared to the PO_4 -poor forests. Therefore, my results suggest there is a casual relationship between the high PO_4 levels in the arable soils and the low OM loading on the metal-(hydr)oxide surfaces, which implies that excessive P fertilization leads to a decrease in the C-stabilization potential of the soil. The predicted OM loading is substantially lower in arable soils for which the $\text{P}_{\text{ox}}/(\text{Fe}_{\text{ox}}+\text{Al}_{\text{ox}})$ ratio is larger than 0.3. Such high $\text{P}_{\text{ox}}/(\text{Fe}_{\text{ox}}+\text{Al}_{\text{ox}})$ ratios are very common in well-fertilized agricultural soils (De Bolle et al., 2013; Koopmans et al., 2006; Maguire and Sims, 2002; Reijneveld et al., 2010). As such, my findings suggest that carbon sequestration is inhibited in soils with such high phosphate levels, which is the case in many agricultural soils in the Western world.

The above described results about the effect of high PO_4 levels on the SOC-sequestration potential were derived by SC modelling and the OM loadings were predicted based on the observed distribution of PO_4 between the adsorbed and dissolved phase. However, there are several factors that may lead to uncertainties in these model predictions. First, model outcomes can be affected by uncertainties in the input variables. The SSA of the metal-(hydr)oxides is an important but uncertain input variable in SC modelling. The SSA is commonly estimated from the oxalate- and dithionite-extractable amounts of metal-(hydr)oxides (Chapter 6), although estimated and measured values for the SSA might differ substantially (Hiemstra et al., 2010a). As a consequence, the calculated PO_4 loading and the derived OM loading also depend on the chosen SSA of the metal-(hydr)oxide fraction. Second, uncertainties in modelling OM adsorption in soils may arise from the complex nature of the OM fraction in soils. In the chosen modelling approach (Chapter 6), only adsorption of fulvic acid was considered whereas OM is in reality a complex mixture of various OM species (Eusterhues et al., 2007; van Zomeren and Comans, 2007; von Lützow et al., 2007). These different compounds can be expected to vary in their affinity for adsorption to metal-(hydr)oxides and, as a consequence, adsorption of OM in soils is still difficult to predict with SC models. As such, the level of competition between PO_4 and OM may substantially differ in soils compared to batch experiments with fulvic and humic acids. Third, SC models assume instantaneous equilibrium whereas adsorption and desorption of OM and PO_4 in soils are commonly far from equilibrium (Antelo et al., 2007). Non-equilibrium might lead to erroneous predictions of the amount of adsorbed OM in PO_4 -rich

soils. For example, model predictions suggest immediate desorption of most OM adsorbed to mineral surfaces upon addition of high levels of PO_4 , whereas experimental results show only a minor increase in concentrations of dissolved organic carbon upon PO_4 addition (Zhang & Zhang, 2010). As such, the magnitude of the interactions between PO_4 and OM in natural soils is still uncertain.

SC model predictions might be improved by verification with experimentally determined OM loadings. However, verification of the modelling results with experimental data is hampered by our ability to measure the amount of OM associated with the metal-(hydr)oxide fraction because currently available physical-chemical fractionation methods for SOC do not correspond to specific stabilization mechanisms and hence do not describe specific SOC pools (von Lützow et al., 2007). For example, I showed that the amount of organic matter extracted in Na-pyrophosphate cannot be used as a measurement for the oxide-associated organic matter (Chapter 5). Also, density fractionation seems unsuitable to quantify the amount of mineral-associated OC, since the distribution of OC between the dense and light fraction strongly depends on the chosen cut-off between the two fractions and there is no consensus about the 'best practice' for distinguishing between particulate and mineral-associated OC (Chenu and Plante, 2006; Kögel-Knabner et al., 2008). As such, further research should focus on the development of more selective approaches to determine the amount of oxide-associated carbon in order to verify model predictions. Sequential desorption experiments, in which the amount of DOC released from the mineral surfaces is quantified, might provide a better indicator for the OM loading on the metal-(hydr)oxide surfaces. A sequential desorption approach is needed since the DOC concentration in the first extract is mainly of biological origin and strongly affected by the pre-treatments (i.e. drying, storage, Kaiser et al., 2001) whereas the DOC in the subsequent extracts can be expected to be released from the soil solid phase. Development of an experimental approach to quantify the OM loading on Fe-(hydr)oxides is not only important for further development of SC models. My results in Chapter 6 show that PO_4 solubility, at a similar PO_4 loading, strongly depends on the OM loading on the metal-(hydr)oxide surfaces. Development of a simple indicator for the OM loading, as proposed above, will lead to better predictions of PO_4 solubility in soils. Additionally, this knowledge will give insight into how PO_4 availability can be optimized by adjusting the content and composition of the OM through the addition of organic amendments.

8.5 Soil aggregate formation: Do nanoparticles affect soil physical properties?

The physical structure of the soil plays a crucial role in the agricultural productivity and water retention capacity of the soils. Yet, intensive land use and poor agricultural management practices have led to a decline in the quality of the soil structure, leading to a decrease in the agricultural productivity and water retention capacity of soils worldwide (Banwart, 2011; Montgomery, 2007). The decrease in the buffering and water-holding capacity of soils is in particular of concern because climate change is expected to lead to more precipitation extremes and more prolonged periods of drought in the near future (Frei et al., 2006). However, despite the extensive knowledge on aggregation mechanisms (Bronick and Lal, 2005; Six et al., 2004), a quantitative understanding of the relationships between physical-chemical properties and the soil structure is still lacking which was therefore one of the key objectives in this PhD thesis.

In Chapter 2 and 3, I provide evidence for the strong association between Fe-(hydr)oxides and organic matter and for the high mechanical strength of the organic-mineral assemblages in soils. Such organic-mineral assemblages fall within the size-range of nano- to micrometers (Asano and Wagai, 2014; Pronk et al., 2011) and thus, my results show that Fe-(hydr)oxides control the amount and stability of nano- and micro-aggregates in soils. However, other soil physical parameters, in particular the number of water-stable aggregates (WSA) and the water-retention capacity of the soil, are more relevant to assess the physical quality of the soil. Therefore, I studied the linkages between major physical-chemical soil properties (texture, Fe-(hydr)oxides, organic matter and pH), aggregate fractions, and porosity (Chapter 7). The porosity and the number of WSA correlated significantly with the Fe-(hydr)oxide content of the soil. Overall, I showed that formation of WSA is controlled by the Fe-(hydr)oxide content, the SOC content and the tendency of particles to coagulate (i.e. pH and concentration of cations) (Chapter 7). Considering the role of Fe-(hydr)oxides in aggregate formation, I suggest that Fe-(hydr)oxides are associated with larger clay/silt and sand-sized particles and as such, provide adsorption sites for organic substances on these otherwise poorly reactive particles. Therefore, Fe-(hydr)oxides enable poorly reactive particles to be taken up in the network of organic substances. So far, the role of Fe-(hydr)oxides in the formation of soil aggregates and pores is poorly recognized. For example, models describing aggregate formation in soils predict the amount of mineral-associated carbon from the clay content of the soil (Malamoud et al., 2009; Stamati et al., 2013) rather than from the Fe-(hydr)oxide content. Therefore, model predictions can be improved by including the role of Fe-(hydr)oxides, pH and the composition of the cations in the soil, since all these parameters affect aggregation (Chapter 7).

8.6 Conclusions

In this thesis, I characterized nanoparticles in soil extracts and water samples and I studied the contribution of nanoparticles to colloid-facilitated transport, OC-sequestration and formation of soil aggregates. First, I have provided experimental evidence for the existence of nano-sized (1- 10 nm) Fe-(hydr)oxides in soils using AF4 coupled to HR-ICP-MS. Because of their small size and consequently large SSA, Fe-(hydr)oxides play an important role in various soil processes. Second, I discussed the role of Fe-(hydr)oxides and clay minerals in colloid-facilitated transport of trace metals and P. I unravelled the speciation of colloidal P in drain and trench waters by AF4, which had remained unresolved in previous studies using classical physico-chemical fractionation only. So far, studies characterizing colloids in environmental water samples are still scarce and the nature of the colloidal fraction is, therefore, still poorly understood. As such, further research is needed in order to improve our understanding of the mobility and bioavailability of trace metals and P associated with colloids. Third, I studied the role of Fe-(hydr)oxide nanoparticles in the sequestration of OC and PO_4 in soils. I showed that the amount of OM adsorbed to Fe-(hydr)oxides depends on the PO_4 loading on the Fe-(hydr)oxides, suggesting that high P levels lead to a decrease in OM adsorption. I discussed the limitations of the chosen modelling approach and the lack of analytical techniques that allow for an experimental verification of the predicted OM loadings on Fe-(hydr)oxide surfaces. As such, further research using both mechanistic modelling and improved experimental techniques is needed to verify the magnitude of the interaction between PO_4 adsorption and the OM desorption in soils. A better quantitative understanding of the adsorption interactions between PO_4 and OM will also improve model predictions of PO_4 solubility in soils. Furthermore, this knowledge will give insight into how PO_4 availability can be optimized by adjusting the content and composition of the OM through the addition of organic amendments. Fourth, I discussed the role of Fe-(hydr)oxides in the formation aggregates and pores. My results show that the Fe-(hydr)oxides improve aggregate stability and porosity in soils. The role of Fe-(hydr)oxides in the formation of aggregates and pores has been underestimated so far. This mechanism should therefore receive more attention in further studies on soil physical properties. A better mechanistic understanding of the processes controlling aggregation and porosity, and thus the water-holding and buffering capacity of soils, is of concern because climate change is expected to lead to more precipitation extremes and more prolonged periods of drought in the near future.

References

- Antelo, J., Arce, F., Avena, M., Fiol, S., López, R., Macías, F., 2007. Adsorption of a soil humic acid at the surface of goethite and its competitive interaction with phosphate. *Geoderma* 138(1–2), 12–19.
- Asano, M., Wagai, R., 2014. Evidence of aggregate hierarchy at micro- to submicron scales in an allophanic Andisol. *Geoderma* 216, 62–74.
- Burleson, D.J., Penn, R.L., 2005. Two-step growth of goethite from ferrihydrite. *Langmuir* 22(1), 402–409.
- Chenu, C., Plante, A.F., 2006. Clay-sized organo-mineral complexes in a cultivation chronosequence: revisiting the concept of the ‘primary organo-mineral complex’. *Eur.J. Soil Sci.* 57, 596–607.
- Correl, D.L., 1998. The role of phosphorus in eutrophication of receiving waters: A review. *J. Environ. Qual.* 27, 261–266.
- De Bolle, S., De Neve, S., Hofman, G., 2013. Rapid redistribution of P to deeper soil layers in P saturated acid sandy soils. *Soil Use Manag.* 29(s1), 76–82.
- Dümig, A., Häusler, W., Steffens, M., Kögel-Knabner, I., 2012. Clay fractions from a soil chronosequence after glacier retreat reveal the initial evolution of organo–mineral associations. *Geochim. Cosmochim. Ac.* 85, 1–18.
- Ekholm, P., 1994. Bioavailability of phosphorus in agriculturally loaded rivers in southern Finland. *Hydrobiologia* 287(2), 179–194.
- Eusterhues, K., Rumpel, C., Kögel-Knabner, I., 2005. Organo-mineral associations in sandy acid forest soils: importance of specific surface area, iron oxides and micropores. *Eur.J. Soil Sci.* 56, 753–763.
- Eusterhues, K., Rumpel, C., Kögel-Knabner, I., 2007. Composition and radiocarbon age of HF-resistant soil organic matter in a Podzol and a Cambisol. *Org. Geochem.* 38(8), 1356–1372.
- Eusterhues, K., Wagner, F.E., Häusler, W., Hanzlik, M., Knicker, H., Totsche, K.U., Kögel-Knabner, I., Schwertmann, U., 2008. Characterization of ferrihydrite-soil organic matter coprecipitates by X-ray diffraction and Mössbauer spectroscopy. *Environ. Sci. Technol.* 42(21), 7891–7897.
- Filius, J.D., Hiemstra, T., Van Riemsdijk, W.H., 2000. Adsorption of fulvic acid on goethite. *Geochim. Cosmochim. Ac.* 64(1), 51–60.
- Gottselig, N., Bol, R., Nischwitz, V., Vereecken, H., Amelung, W., Klumpp, E., 2014. Distribution of Phosphorus-Containing Fine Colloids and Nanoparticles in Stream Water of a Forest Catchment. *Vad. Zone J.* 13
- Hiemstra, T., Antelo, J., Rahnemaie, R., van Riemsdijk, W.H., 2010a. Nanoparticles in natural systems I: The effective reactive surface area of the natural oxide fraction in field samples. *Geochim. Cosmochim. Ac.* 74(1), 41–58.
- Hiemstra, T., Antelo, J., van Rotterdam, A.M.D., van Riemsdijk, W.H., 2010b. Nanoparticles in natural systems II: The natural oxide fraction at interaction with natural organic matter and phosphate. *Geochim. Cosmochim. Ac.* 74(1), 59–69.
- Hiemstra, T., Mia, S., Duhaut, P.B., Molleman, B., 2013. Natural and Pyrogenic Humic Acids at Goethite and Natural Oxide Surfaces Interacting with Phosphate. *Environ. Sci. Technol.* 47(16), 9182–9189.
- Hochella, M.F., Lower, S.K., Maurice, P.A., Penn, R.L., Sahai, N., Sparks, D.L., Twining, B.S., 2008. Nanominerals, mineral nanoparticles, and Earth systems. *Science* 319(5870), 1631–1635.
- Kaegi, R., Voegelin, A., Folini, D., Hug, S.J., 2010. Effect of phosphate, silicate, and Ca on the morphology, structure and elemental composition of Fe(III)-precipitates formed in aerated Fe(II) and As(III) containing water. *Geochim. Cosmochim. Ac.* 74(20), 5798–5816.
- Kaiser, K., Klaupenjohann, M., Wolfgang, Z. 2001. Sorption of dissolved organic carbon in soils: effects of soil sample storage, soil-to-solution ratio, and temperature. *Geoderma* 99, 317

- Kaiser, K., Eusterhues, K., Rumpel, C., Guggenberger, G., Kögel-Knabner, I., 2002. Stabilization of organic matter by soil minerals — investigations of density and particle-size fractions from two acid forest soils. *J. Plant Nutr. Soil Sci.* 165(4), 451-459.
- Kaiser, K., Guggenberger, G., 2003. Mineral surfaces and soil organic matter. *Eur. J. Soil Sci.* 54(2), 219-236.
- Kalbitz, K., Schwesig, D., Rethemeyer, J., Matzner, E., 2005. Stabilization of dissolved organic matter by sorption to the mineral soil. *Soil Biol. Biochem.* 37, 1319-1331.
- Kögel-Knabner, I., Guggenberger, G., Kleber, M., Kandeler, E., Kalbitz, K., Scheu, S., Eusterhues, K., Leinweber, P., 2008. Organo-mineral associations in temperate soils: Integrating biology, mineralogy, and organic matter chemistry. *J. Plant Nutr. Soil Sci.* 171(1), 61-82.
- Koopmans, G.F., Chardon, W.J., Dekker, P.H.M., Romkens, P.F.A.M., Schoumans, O.F., 2006. Comparing different extraction methods for estimating phosphorus solubility in various soil types. *Soil Sci.* 171, 103-116.
- Kretzschmar, R., Borkovec, M., Grolimund, D., Elimelech, M., 1999. Mobile subsurface colloids and their role in contaminant transport. *Adv. Agron.* 66, 121-193.
- Loeb, R., Lamers, L.P., Roelofs, J.G., 2008. Prediction of phosphorus mobilisation in inundated floodplain soils. *Environ. Poll.* 156(2), 325-331.
- Maguire, R.O., Sims, J.T., 2002. Soil Testing to Predict Phosphorus Leaching Published as Paper no. 1710 in the journal series of the Delaware Agricultural Experiment Station. *J. Environ. Qual.* 31(5), 1601-1609.
- Malamoud, K., McBratney, A.B., Minasny, B., Field, D.J. 2009. Modelling how carbon affects soil structure. *Geoderma* 149, 9-26
- Mikutta, R., Kleber, M., Torn, M., Jahn, R., 2006. Stabilization of Soil Organic Matter: Association with Minerals or Chemical Recalcitrance? *Biogeochem.* 77(1), 25-56.
- Neubauer, E., von der Kammer, F., Knorr, K.H., Peiffer, S., Reichert, M., Hofmann, T., 2013. Colloid-associated export of arsenic in stream water during stormflow events. *Chemical Geology* 352(0), 81-91.
- Plathe, K.L., von der Kammer, F., Hassellöv, M., Moore, J.N., Murayama, M., Hofmann, T., Hochella Jr, M.F., 2013. The role of nanominerals and mineral nanoparticles in the transport of toxic trace metals: Field-flow fractionation and analytical TEM analyses after nanoparticle isolation and density separation. *Geochim. Cosmochim. Ac.* 102(0), 213-225.
- Pronk, G.J., Heister, K., Kögel-Knabner, I., 2011. Iron Oxides as Major Available Interface Component in Loamy Arable Topsoils. *Soil Sci. Soc. Am. J.* 75(6), 2158-2168.
- Reijneveld, J.A., Ehlert, P., Termorshuizen, A., Oenema, O., 2010. Changes in the soil phosphorus status of agricultural land in the Netherlands during the 20th century. *Soil Use Managem.* 26(4), 399-411.
- Roden, E., Edmonds, J., 1997. Phosphate mobilization in iron-rich anaerobic sediments: microbial Fe (III) oxide reduction versus iron-sulfide formation. *Archiv für Hydrobiologie* 139(3), 347-378.
- Rozan, T.F., Taillefert, M., Trouwborst, R.E., Glazer, B.T., Ma, S., Herszage, J., Valdes, L.M., Price, K.S., Luther III, G.W., 2002. Iron-sulfur-phosphorus cycling in the sediments of a shallow coastal bay: Implications for sediment nutrient release and benthic macroalgal blooms. *Limnol. Oceanogr.* 47(5), 1346-1354.
- Salm, C.v.d., Toorn, A.v.d., Chardon, W.J., Koopmans, G.F., 2012. Water and nutrient transport on a heavy clay soil in a fluvial plain in The Netherlands. *J. Environ. Qual.* 41(1), 229-241.
- Schwertmann, U., Wagner, F., Knicker, H., 2005. Ferrihydrite-Humic Associations. *Soil Sci. Soc. Am. J.* 69(4), 1009-1015.

- Sei, J., Jumas, J.C., Olivier-Fourcade, J., Quiquampoix, H., Staunton, S., 2002. Role of iron oxides in the phosphate adsorption properties of kaolinites from the ivory coast. *Clay. Clay Min.* 50(2), 217-222.
- Siemens, J., Ilg, K., Pagel, H., Kaupenjohann, M., 2008. Is colloid-facilitated phosphorus leaching triggered by phosphorus accumulation in sandy soils? *J. Env. Qual.* 37, 2100-2107
- Six, J., Conant, R.T., Paul, E.A., Paustian, K., 2002. Stabilization mechanisms of soil organic matter: Implications for C-saturation of soils. *Plant. Soil* 241, 155-176.
- Stamati, F.E., Nikolaidis, N.P., Banwart, S., Blum, W.E.H. A coupled carbon, aggregation and structure turnover (CAST) model for topsoils. *Geoderma*, 211, 51-64
- Toor, G.S., Condon, L.M., Cade-Menun, B.J., Di, H.J., Cameron, K.C. 2005. Preferential phosphorus leaching from an irrigated grassland soil. *Eur. J. Soil Sci.* 56, 155-168
- Turner, B.L., McKelvie, I.D., Haygarth, P.M., 2002. Characterisation of water-extractable soil organic phosphorus by phosphatase hydrolysis. *Soil Biol. Biochem.* 34(1), 27-35.
- Uusitalo, R., Yli-Halla, M., Turtola, E., 1999. Suspended soil as a source of potentially bioavailable phosphorus in surface runoff waters from clay soils. *Wat. Res.* 34(9), 2477-2482.
- van Rotterdam, A.M.D., Bussink, D.W., Temminghoff, E.J.M., van Riemsdijk, W.H., 2012. Predicting the potential of soils to supply phosphorus by integrating soil chemical processes and standard soil tests. *Geoderma* 189–190(0), 617-626.
- van Zomeren, A., Comans, R.N.J., 2007. Measurement of Humic and Fulvic Acid Concentrations and Dissolution Properties by a Rapid Batch Procedure. *Environ. Sci. Technol.* 41(19), 6755-6761.
- Vega, F.A., Weng, L., 2013. Speciation of heavy metals in River Rhine. *Water Research* 47(1), 363-372.
- Voegelin, A., Kaegi, R., Frommer, J., Vantelon, D., Hug, S.J., 2010. Effect of phosphate, silicate, and Ca on Fe(III)-precipitates formed in aerated Fe(II)- and As(III)-containing water studied by X-ray absorption spectroscopy. *Geochim. Cosmochim. Ac.* 74(1), 164-186.
- von Lützow, M., Kögel-Knabner, I., Ekschmitt, K., Flessa, H., Guggenberger, G., Matzner, E., Marschner, B., 2007. SOM fractionation methods: Relevance to functional pools and to stabilization mechanisms. *Soil Biol. Biochem.* 39(9), 2183-2207.
- Weng, L., Riemsdijk, W.H.v., Hiemstra, T., 2008. Humic Nanoparticles at the Oxide-Water Interface: Interactions with Phosphate Ion Adsorption. *Environ. Sci. Tech.* 42, 8747-8752.
- Weng, L., Van Riemsdijk, W.H., Hiemstra, T., 2007. Adsorption of humic acids onto goethite: Effects of molar mass, pH and ionic strength. *J. Colloid Interf. Sci.* 314, 107-118.
- Zehetner, F., Lair, G.J., Gerzabek, M.H., 2009. Rapid carbon accretion and organic matter pool stabilization in riverine floodplain soils. *Global Biogeochem. Cycl.* 23(4).
- Zhang, M. & Zhang, H. 2010. Co-transport of dissolved organic matter and heavy metals in soils induced by excessive phosphorus applications. *J. Environ. Sci.* 22, 598-606.

Appendices

Appendix A: Supporting Information Chapter 2

Appendix B: Supporting Information Chapter 3

Appendix C: Supporting Information Chapter 4

Appendix D: Supporting Information Chapter 6

Appendix E: Supporting Information Chapter 7

Appendix A

Supporting information to Chapter 2:

Asymmetric flow field-flow fractionation as a new approach to analyse iron-(hydr)oxide nanoparticles in soil extracts

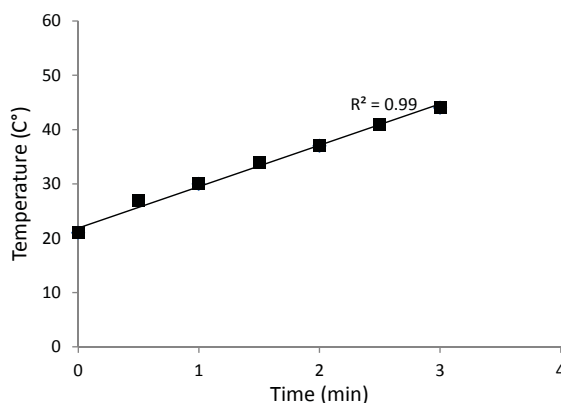


Figure A1. Calorimetric determination of the power output of the Hielscher UP400s ultrasonicator, 24 kHz, operated with a 22 mm probe-tip at 80% amplitude. The temperature increase of the isolated beaker filled with 200 g water was measured at time intervals of 0.5 min and the power output was calculated using the equation:

$$P = m_w c_w \Delta T / t + H$$

where P is the power (W), m_w is the mass of the water (g), c_w is the specific heat capacity of the water ($4.18 \text{ J g}^{-1} \text{ K}^{-1}$), ΔT is the difference in temperature, t is the sonication time and H is the energy loss by conduction (J s^{-1}), which is negligibly small in an isolated system. The power output at 80% amplitude amounted to 106 W.

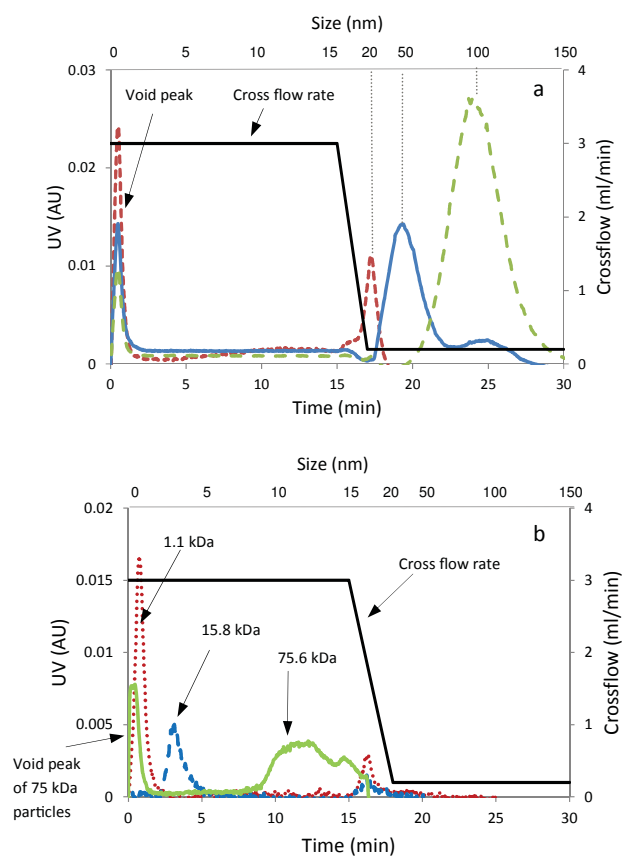


Figure A2. Calibration of AF4 using polystyrene particle with a known diameter of 20, 50 and 100 nm (a) and polystyrene-sulfonate and standards with a known molecular weight of 1.1, 15.8 and 75.6 kDa. Running conditions are given in the main text. The carrier was 3 mM NaHCO_3 for the polystyrene-sulfonate particles and 3 mM NaHCO_3 + 0.01% SDS (w/v) for the polystyrene particles.

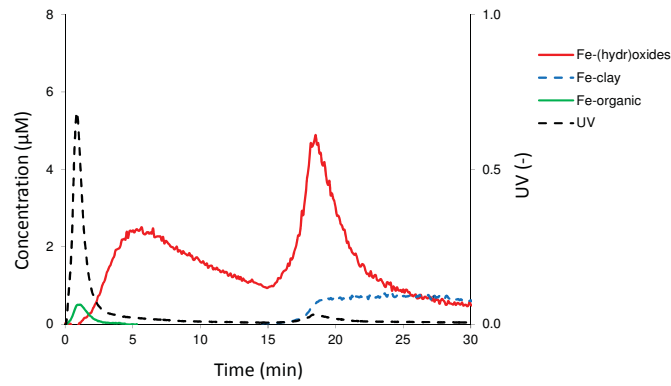


Figure A3. Distribution of Fe between DOM, (hydr)oxides and clays in the fractogram of the NaOH extract of the Bh2 horizon. The assumptions used to calculate the distribution are described in the main text.

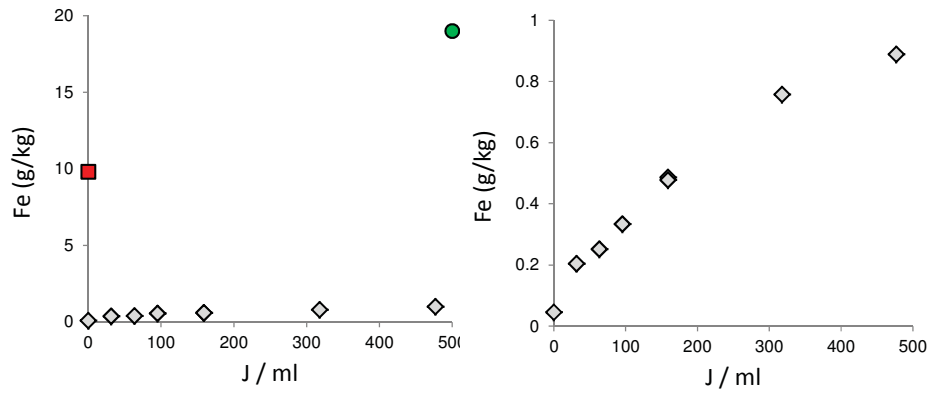


Figure A4. Iron concentration (diamonds) as a function of the amount of ultrasonic energy applied to a NaHCO_3 - soil suspension of the Bh2-horizon at a large (left) and small (right) scale. Iron concentrations were measured in the supernatants after centrifugation (3000 rpm, 30 min). Iron-concentrations in the pyrophosphate (square) and pyrophosphate + ultrasonication (sphere) extracts are given for comparison.

Appendix A

Table A1. Effect of injection time and Al(OH)₃ concentration on the amount of P and Al recovered in the void peak during AF4-fractionation.¹

Solution	Injection time (min)	P-Recovery (%)	Al-Recovery (%)
2 mM Na ₄ P ₂ O ₇	5	7	n.d.
2 mM Na ₄ P ₂ O ₇	11	<1	n.d.
2 mM Na ₄ P ₂ O ₇ + 0.2 mM AlOH ₃	5	29	56
2 mM Na ₄ P ₂ O ₇ + 0.2 mM AlOH ₃	7	31	65
2 mM Na ₄ P ₂ O ₇ + 0.2 mM AlOH ₃	11	15	43

¹The amount of P recovered in the void peak (t: 0.5 min) from a Na-pyrophosphate solution with and without Al(OH)₃ was determined using a crossflow rate of 3 ml min⁻¹ and injection time as indicated in the table.

2 mM Na₄P₂O₇. Recovery of P from the Na₄P₂O₇ solution is low and decreases with increasing injection time. This shows that the chosen injection time of 11 min is sufficiently long to remove more than 99% of the truly dissolved P.

2 mM Na₄P₂O₇ + 0.2 mM AlOH₃. Pyrophosphate is in surplus compared to Al, therefore one can expect that the majority of the Al³⁺ is complexed with pyrophosphate. The recovery of both P and Al are significant and recoveries do not decrease with increasing in injection time. In the presence of Al, the recovery of P is 4 to 15 times higher compared to the recovery of P in the absence of Al.

These results show that Al-pyrophosphate complexes are formed in the mixture of Al and pyrophosphate. These complexes cannot pass the AF4-membrane and therefore elute in the void peak. In soil extracts, pyrophosphate can be expected to form similar complexes with monomeric Fe and Al, which were initially bound to the soil organic matter.

Appendix B

Supporting information to Chapter 3:

Characterization of Colloidal Fe from Soils using Field-Flow Fractionation and Fe K-edge X-ray Absorption Spectroscopy

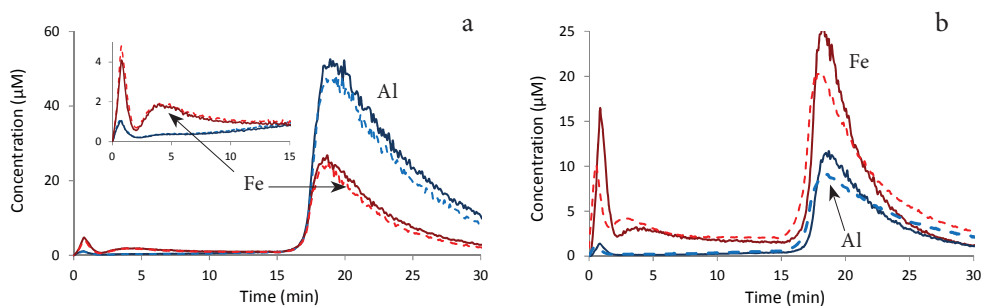


Figure B1. Reproducibility of the AF4-HR-ICP-MS analyses for the Fe (red lines) and Al (blue lines) signal. (a) Colloids extracted with Na-pyrophosphate from soil 7. Both AF4 runs were performed with the same extract and on the same day. (b) Colloids extracted with Na-pyrophosphate from soil 3. Runs were performed on replicate extracts and analysed on different measuring days.

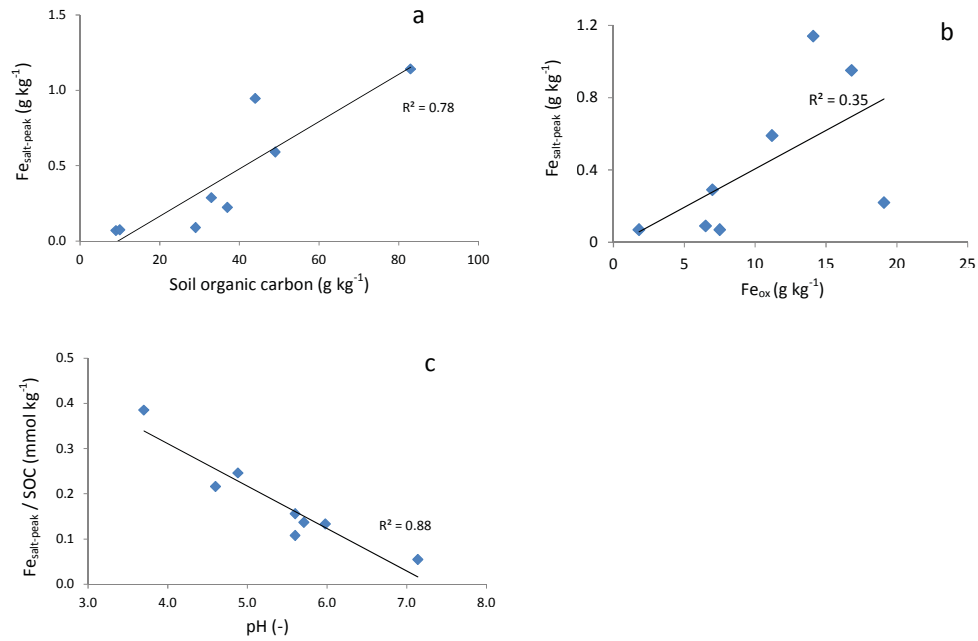


Figure B2. (a) Correlation between the amount of Fe eluting in the salt-peak and the SOC content, (b) correlation between the amount of Fe eluting in the salt-peak and the Fe_{ox} content and (c) correlation between the amount of Fe eluting in the salt-peak scaled to the SOC-content and the pH. The results show that the amount of Fe eluting in the salt-peak of a Na-pyrophosphate extracts increases with increasing SOC content, and decreases with increasing pH whereas the correlation with the Fe_{ox} content is poor. These findings support our reasoning that the Fe eluting in the salt peak was originally present as monomeric Fe adsorbed to SOC (see main text).

Appendix C

Supporting information to Chapter 4:

Characterization of Colloidal Phosphorus Species in Drainage Waters from a Clay Soil Using Asymmetric Flow Field-Flow Fractionation.

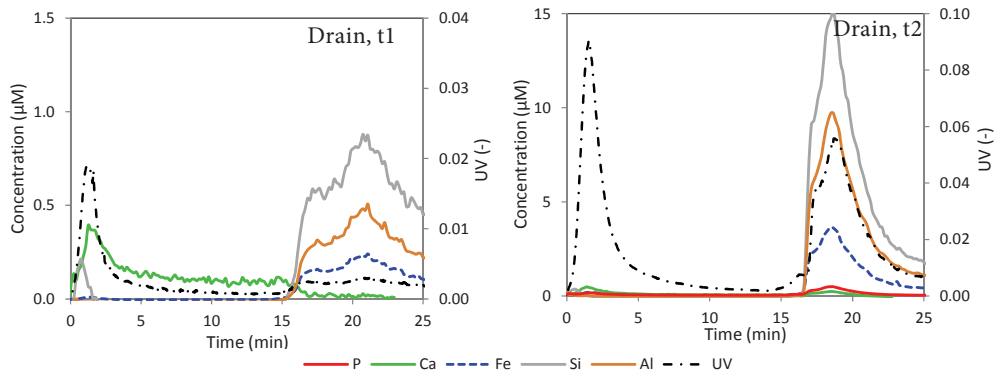


Figure C1. AF4 fractograms of the pipe drain waters collected at t1 (left) and t2 (right). For t1, P concentrations were below the detection limit.

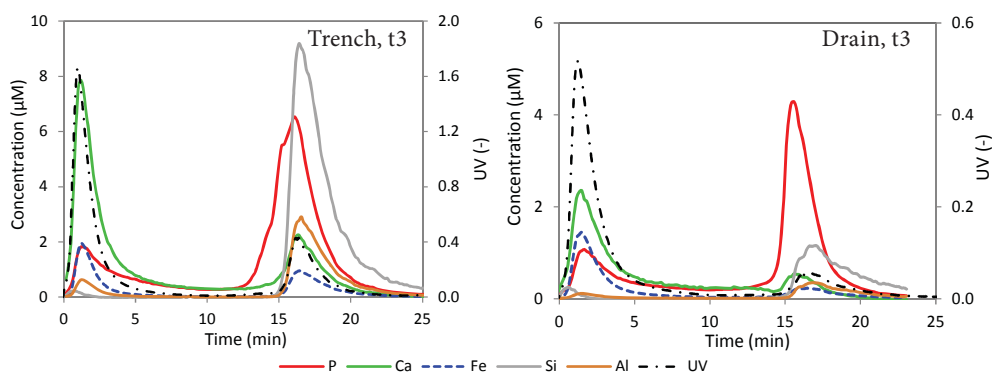


Figure C2. AF4 fractograms of the second set of pipe drain and trench waters collected at t3. The two sets of trenches and pipe drains were treated as replicates.

Appendix D

Supporting information to Chapter 6:

Adsorption competition between phosphate and organic matter on metal-(hydr)oxides in arable and forest soils explained by mechanistic adsorption modelling

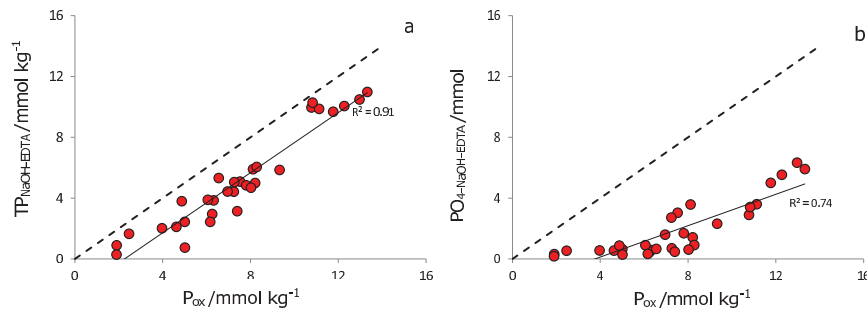


Figure D1. (a) NaOH-EDTA extractable total P ($TP_{NaOH-EDTA}$) content as a function of oxalate-extractable P (P_{ox}). (b) NaOH-EDTA extractable PO_4 content as a function of P_{ox} . The dotted line shows the 1:1 line.

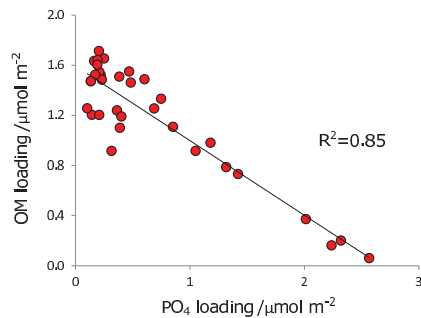


Figure D2. Correlation between the PO_4 loading and the predicted effective OM loading on the oxide surfaces. The PO_4 loading was calculated from the NaOH-EDTA extractable PO_4 content, scaled to the surface of the Fe+Al-(hydr)oxides and the OM loading was predicted by SC-modelling. Details are described in the main text.

Table D1. Ionic composition, free ion activities^a and ion activity products^b of the water-extracts

Nr.	Site	Total ion concentrations							Free ion activities ^a				Ion activity products (IAP) of the water-extracts ^b			
		pH	Ca	PO ₄	Mg	Na	CO ₃	Ca ²⁺	PO ₄ ³⁻	Mg ²⁺	Na ⁺	CO ₃ ²⁻	CaHPO ₄ logK: -19.25	Ca ₃ (PO ₄) ₂ logK: -28.92	HCa ₄ (PO ₄) ₃ logK: -46.89	Ca ₅ (PO ₄) ₃ OH logK: -58.00
		(-)	(-log(M))							(log(M))						
1	F1/1	7.8	2.86	5.44	3.58	4.52	2.42	3.02	10.38	3.73	4.55	5.02	-21.2	-29.8	-35.4	-52.4
5	F1/2	8.2	2.89	5.69	3.62	4.76	2.46	3.04	10.25	3.78	4.79	4.69	-21.4	-29.6	-34.8	-51.8
7	F1/3	8.1	2.82	5.70	3.60	4.76	2.38	2.99	10.34	3.77	4.80	4.69	-21.4	-29.7	-34.9	-51.9
9	F2/1	7.9	2.76	5.17	3.42	4.52	2.32	2.94	10.01	3.60	4.56	4.79	-20.9	-28.8	-33.9	-50.8
10	F2/1	7.9	2.81	5.34	3.51	4.36	2.40	2.98	10.23	3.68	4.40	4.93	-21.1	-29.4	-34.7	-51.7
11	F2/1	8.1	3.03	6.23	3.71	4.28	2.66	3.16	10.81	3.85	4.31	4.96	-22.0	-31.1	-37.0	-54.1
12	F2/1	8.2	3.10	6.09	3.78	4.36	2.73	3.22	10.53	3.90	4.39	4.91	-21.9	-30.7	-36.3	-53.5
13	F2/1	8.2	3.19	6.18	3.86	4.41	2.84	3.30	10.57	3.98	4.43	4.99	-22.1	-31.0	-36.7	-54.0
15	F2/2	8.3	2.87	5.39	3.53	4.52	2.46	3.03	9.86	3.69	4.55	4.59	-21.1	-28.8	-33.5	-50.5
18	F2/3	8.1	2.76	5.63	3.39	4.13	2.35	2.95	10.27	3.58	4.17	4.62	-21.3	-29.4	-34.5	-51.4
21	F3/1	8.0	2.77	5.54	3.32	4.88	2.30	2.96	10.30	3.51	4.93	4.68	-21.3	-29.5	-34.7	-51.7
22	F3/1	7.8	2.83	5.65	3.47	5.06	2.42	3.00	10.61	3.63	5.10	5.03	-21.4	-30.2	-36.1	-53.1
23	F3/1	8.0	2.85	6.05	3.51	5.06	2.46	3.01	10.74	3.68	5.10	4.80	-21.8	-30.5	-36.2	-53.2
24	F3/1	8.2	3.06	6.44	3.71	4.88	2.70	3.19	10.89	3.84	4.91	4.88	-22.3	-31.3	-37.2	-54.4
26	F3/1	8.2	2.99	6.40	3.67	4.88	2.62	3.13	10.92	3.81	4.92	4.85	-22.2	-31.2	-37.1	-54.2
27	F3/1	8.4	3.09	6.63	3.78	4.88	2.75	3.22	10.92	3.91	4.91	4.77	-22.5	-31.5	-37.3	-54.5
29	F3/2	8.2	2.80	5.77	3.52	5.06	2.40	2.97	10.36	3.69	5.10	4.64	-21.5	-29.6	-34.8	-51.8
32	F3/3	8.1	2.86	5.98	3.56	4.88	2.78	3.01	10.56	3.72	4.92	5.02	-21.7	-30.1	-35.6	-52.6

Table D1. continued.

Nr.	Site	pH	Total ion concentrations							Free ion activities ^a					Ion activity products (IAP) of the water-extracts ^b				
			Ca	PO ₄	Mg	Na	CO ₃	Ca ²⁺	PO ₄ ³⁻	Mg ²⁺	Na ⁺	CO ₃ ²⁻	CaHPO ₄	Ca ₃ (PO ₄) ₂	HCa ₄ (PO ₄) ₃	Ca ₅ (PO ₄) ₃ OH			
		(-)	(log (M))																
35	F4/1	8.3	3.12	5.01	3.71	4.58	2.73	3.24	9.37	3.84	4.61	4.83	-20.9	-28.5	-32.8	-50.0			
36	F4/1	8.2	3.12	4.88	3.73	4.46	2.83	3.24	9.29	3.84	4.48	4.98	-20.8	-28.3	-32.6	-49.8			
37	F4/1	8.3	3.15	6.52	3.84	4.36	2.86	3.26	10.82	3.95	4.39	4.91	-22.4	-31.4	-37.2	-54.4			
38	F4/1	8.5	3.25	6.44	3.92	4.32	3.02	3.35	10.58	4.02	4.34	4.94	-22.4	-31.2	-36.7	-54.0			
39	F4/1	8.6	3.39	6.63	4.01	4.41	3.14	3.47	10.61	4.09	4.43	4.93	-22.7	-31.6	-37.2	-54.6			
40	F4/2	8.4	3.14	4.87	3.73	4.36	2.78	3.26	9.15	3.85	4.39	4.80	-20.8	-28.1	-32.2	-49.4			
42	F4/3	8.3	3.14	5.10	3.77	4.66	2.80	3.25	9.42	3.89	4.69	4.86	-21.0	-28.6	-33.0	-50.2			
44	F5/1	8.3	3.25	5.47	3.65	4.88	2.59	3.37	9.96	3.77	4.91	5.09	-21.4	-30.0	-35.2	-52.6			
45	F5/1	8.3	2.93	5.80	3.67	5.06	2.39	3.07	10.22	3.81	5.09	4.70	-21.6	-29.7	-34.7	-51.8			
46	F5/1	8.4	2.78	5.42	3.50	4.58	2.75	2.95	9.91	3.68	4.62	4.51	-21.1	-28.7	-33.3	-50.2			
47	F5/1	8.4	3.09	7.49	3.86	4.76	2.90	3.21	11.73	3.98	4.79	4.73	-23.3	-33.1	-39.7	-56.9			
48	F5/1	8.5	3.25	7.49	3.92	4.76	2.98	3.36	11.67	4.03	4.78	4.85	-23.4	-33.4	-40.0	-57.4			
50	F5/1	7.7	3.33	7.49	3.98	4.76	3.14	3.43	11.56	4.08	4.78	4.84	-23.5	-33.4	-39.9	-57.3			
51	F5/2	8.3	3.52	7.49	4.13	4.88	2.60	3.59	12.37	4.20	4.90	5.81	-23.7	-35.5	-43.8	-61.4			
55	F5/3	8.3	2.96	5.37	3.64	4.88	2.60	3.11	9.73	3.79	4.92	4.65	-21.2	-28.8	-33.3	-50.4			

^aFree ion activities of the water-extracts were calculated with the speciation model Ecosat, using the pH and measured solution concentrations of Na, Ca, Mg, CO₄ and PO₄ and dissolved organic carbon (DOC) as input parameters. The aqueous speciation reactions and their equilibrium constants were taken from Hiemstra et al. (2010a). ^bIon activity products calculated for CaHPO₄ (log K = log Ca²⁺ + log PO₄³⁻ - pH), Ca₃(PO₄)₂ (log K = 3 log Ca²⁺ + 2 log PO₄³⁻), HCa₄(PO₄)₃ (log K = -pH + 4 log Ca²⁺ + 3 log PO₄³⁻), and Ca₅(PO₄)₃OH (log K = 5 log Ca²⁺ + 3 log PO₄³⁻ + log OH). Solubility products and corresponding log K values were taken from Lindsay et al. (1979) and numbers in bold indicate that the solutions are saturated with respect to the corresponding mineral phase.

Table D2. Table of surface species in the CD-MUSIC model^a

Surface species	=FeOH ^{0.5}	=Fe ₃ O ^{0.5}	Δz_0	Δz_1	Δz_2	H ⁺	Na ⁺	Ca ²⁺	Cl ⁻	NO ₃ ⁻	PO ₄ ³⁻	CO ₃ ²⁻	H ₃ SOM	logK
=FeOH ^{0.5}	1	0	0	0	0	0	0	0	0	0	0	0	0	0
=FeOH ₂ ^{0.5}	1	0	1	0	0	1	0	0	0	0	0	0	0	9.0
=FeOH ^{0.5} ...Na ⁺	1	0	0	1	0	0	1	0	0	0	0	0	0	-0.60
=FeOH ₂ ^{0.5} ...Cl ⁻	1	0	1	-1	0	1	0	0	1	0	0	0	0	8.55
=FeOH ₂ ^{0.5} ...NO ₃ ⁻	1	0	1	-1	0	1	0	0	0	1	0	0	0	8.32
=Fe ₃ O ^{0.5}	0	1	0	0	0	0	0	0	0	0	0	0	0	0
=Fe ₃ OH ^{0.5}	0	1	1	0	0	1	0	0	0	0	0	0	0	9.0
=Fe ₃ O ^{0.5} ...Na ⁺	0	1	0	1	0	0	1	0	0	0	0	0	0	-0.60
=Fe ₃ OH ^{0.5} ...Cl ⁻	0	1	1	-1	0	1	0	0	1	0	0	0	0	8.55
=Fe ₃ OH ^{0.5} ...NO ₃ ⁻	0	1	1	-1	0	1	0	0	0	1	0	0	0	8.32
=(FeO) ₂ ^{-0.54} PO ₂ ^{1.46}	2	0	0.46	-1.46	0	2	0	0	0	0	1	0	0	29.72
=FeO ^{0.22} PO ₂ OH ^{1.28}	1	0	0.28	-1.28	0	2	0	0	0	0	1	0	0	27.63
=FeOH ₂ Ca ²⁺	1	0	0.31	1.69	0	0	0	1	0	0	0	0	0	3.23
=FeOH ^{0.5} CaOH ⁺	1	0	0.31	0.69	0	-1	0	1	0	0	0	0	0	-6.42
FeOH ^{0.5} ...Ca ²⁺	1	0	0	2	0	0	0	1	0	0	0	0	0	1.8
=Fe ₃ O ^{0.5} ...Ca ²⁺	0	1	0	2	0	0	0	1	0	0	0	0	0	1.8
=FeOH ₂ ^{0.5} ...CO ₃ ²⁻	1	0	1	-2	0	0	0	0	0	0	0	1	0	10.22
=Fe ₃ OH ^{0.5} ...CO ₃ ²⁻	0	1	1	-2	0	0	0	0	0	0	0	1	0	10.22
=(FeO)(FeOH ₂) ⁻ OM	3	0	2.1	-2.6	-0.5	0	0	0	0	0	0	0	1	25 ^b

^aTable gives the formation reactions of surface species with charge distribution (Δz) and affinities (logK) using the extended Stern layer option with C1 = 0.93 and C2 = 0.75 F/m², all taken from Hiemstra et al.(2010a)

^bThe amount of adsorbed OM was fitted by the model using a high K-value which has no physical meaning. The derivation of the charge distribution of the (FeO)(FeOH₂)⁻OM species is described in the main text.

Appendix E

Supporting information to Chapter 7:

Mechanistic linkages between soil aggregates, soil porosity and physical-chemical soil properties

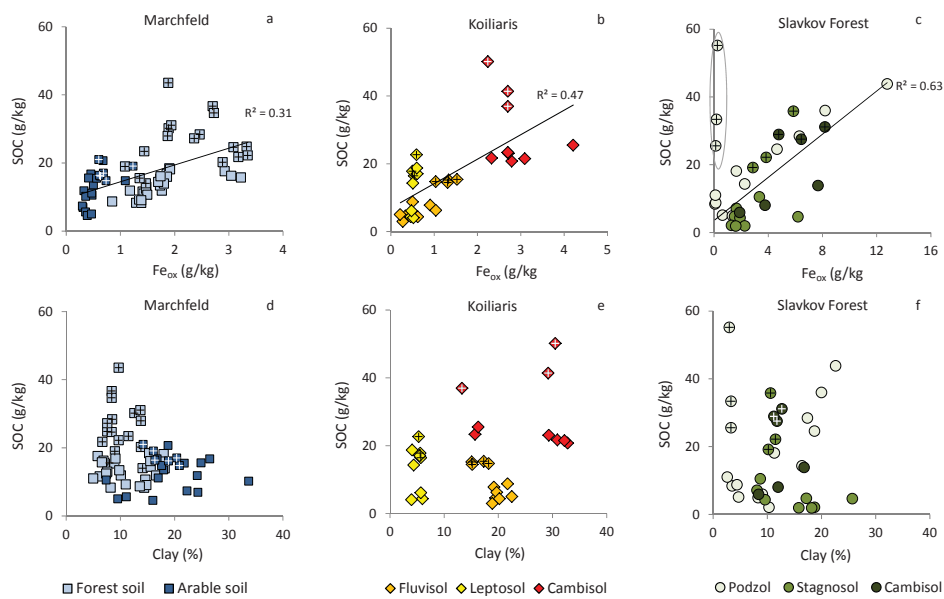


Figure E1. The soil organic carbon (SOC) content as a function of the oxalate-extractable Fe (Fe_{ox}) content (a-b) and the clay content (d-f) for the Marchfeld, Koiliaris and Slavkov Forest CZO.

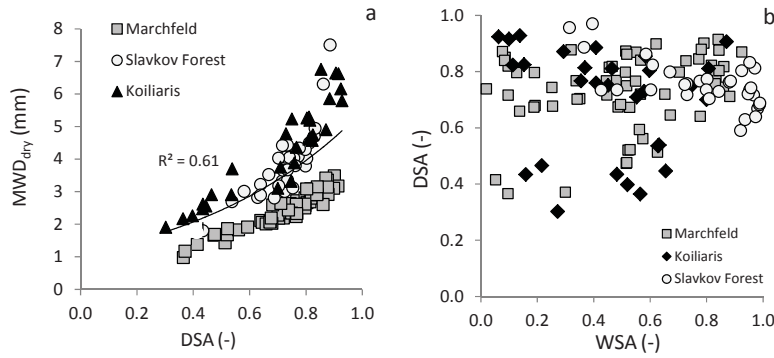


Figure E2. (a). Dry-sieved aggregates expressed as the mean-weight diameter (MWD_{dry}) as a function of the dry-sieved aggregates expressed as the fraction larger than 1 mm (DSA) (w/w). (b). The fraction of DSA as a function of the fraction of water-stable aggregates larger than 0.25 mm (WSA) (w/w).

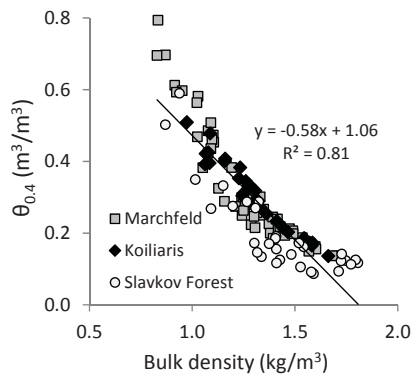


Figure E4. The micro-mesoporosity, defined as the water content at 0.25 kPa, as a function of the bulk density for all soil samples from the three CZO's.

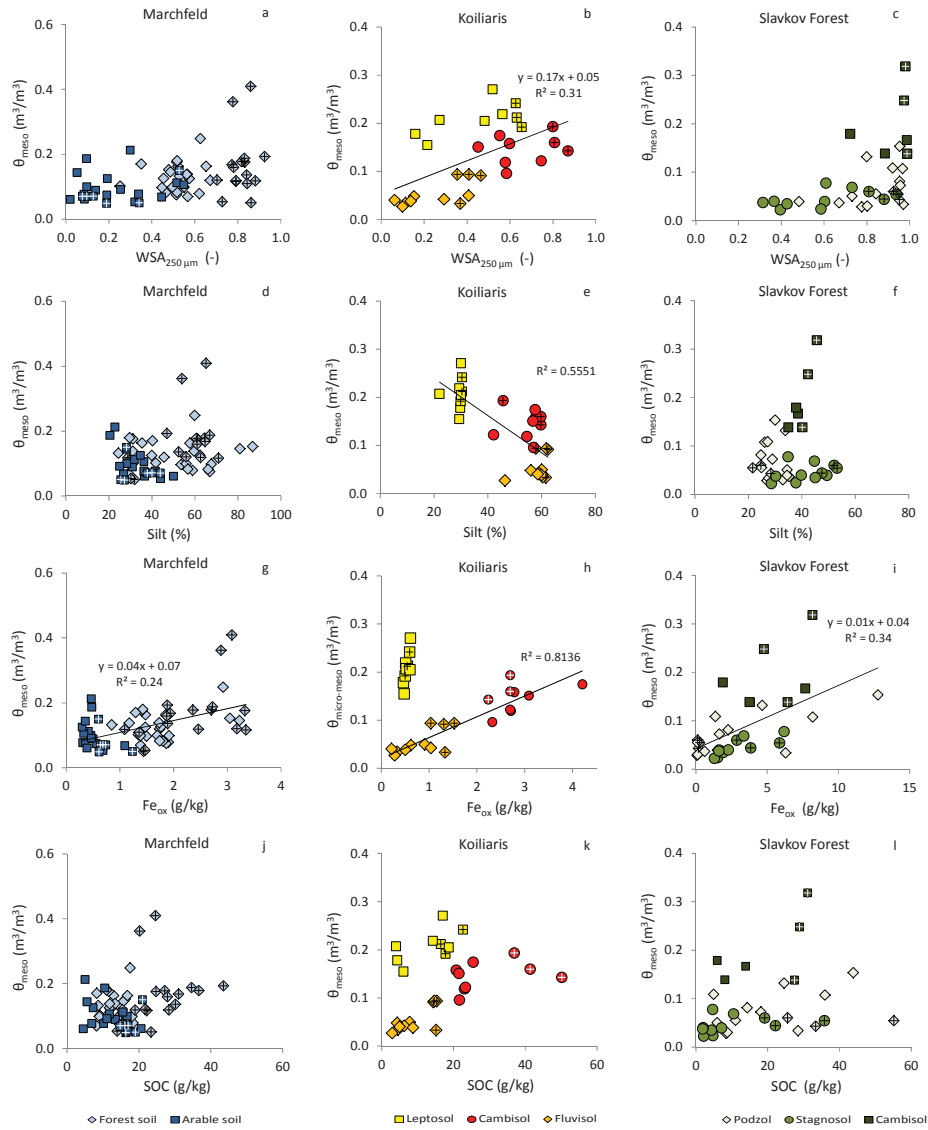


Figure E3. The mesoporosity as a function of the fraction water-stable aggregates (WSA) (w/w), the silt content, the Fe-(hydr)oxide content (Fe_{ox}) and the soil organic carbon (SOC) content. For Figure A3-h, the correlation line was drawn for the Fluvisol (K1) and Cambisol only. Mesoporosity was defined as the volume of water stored between 0.25 and 30 kPa.

Table E1. Average, minimum, maximum values of soil physical and chemical properties for collected from three Critical Zone Observatories. *n.m.*: not measured, *n.d.*: not detected.

	Marchfeld CZO (n: 64)			Kolliaris CZO (n:29)			Slavkov Forest CZO (n:33)		
	Average	Min	Max	Average	Min	Max	Average	Min	Max
Dry-sieved aggregates > 1mm (w/w) ^b	0.73	0.36	0.91	0.70	0.30	0.81	0.76	0.58	0.97
Water-stable aggregates >0.25 mm (w/w) ^c	0.50	0.02	0.92	0.4	0.1	0.9	0.8	0.3	1.0
Bulk density (g cm ⁻³)	1.3	0.8	1.7	1.3	1.0	1.7	1.4	0.9	1.8
$\theta_{0.25}$ kPa (m ³ m ⁻³) ^d (micro+mesoporosity)	0.32	0.14	0.79	0.30	0.14	0.51	0.21	0.09	0.59
θ_{30} kPa (m ³ m ⁻³) ^d (microporosity)	0.19	0.05	0.58	0.17	0.07	0.35	0.13	0.05	0.35
$\theta_{0.25}$ kPa - θ_{30} kPa (m ³ m ⁻³) ^d (mesoporosity)	0.13	0.05	0.41	0.13	0.03	0.27	0.06	0.01	0.24
Gravel ^e (%)	0	0	0	7	0	16	26	0	58
Coarse sand ^f (%)	2	0	12	6	2	24	30	10	52
Fine sand ^g (%)	30	1	71	29	7	69	23	11	34
Silt ^h (%)	45	21	87	48	22	62	35	22	53
Clay ⁱ (%)	14	5	34	17	4	33	12	3	26
Soil organic carbon (g kg ⁻¹)	17	5	44	21	3	89	17	2	55
C:N ratio (-)	15	11	28	11	16	7	20	13	32
Fe ^j (g kg ⁻¹)	1.5	0.3	3.3	1.4	0.2	4.2	3.3	0.1	12.8
Al ^k (g kg ⁻¹)	<i>n.m.</i>	<i>n.m.</i>	<i>n.m.</i>	1.4	0.2	4.3	2.4	0.2	9.1
pH (-)	7.5	5.9	8.4	7.0	5.5	8.1	4.3	3.3	6.6
CaCO ₃ (g kg ⁻¹)	215	2	386	38	0	160	<i>n.d.</i>	<i>n.d.</i>	<i>n.d.</i>
Fe _d (g kg ⁻¹) ^k	5.2	2.5	8.1	17 ^l	10 ^l	25 ^l	7 ^l	0.4 ^l	17 ^l

^a Mean-weight diameter of the dry-sieved aggregates. ^b Fraction of dry-sieved aggregates larger than 1 mm. ^c Water-stable aggregates, measured by wet-sieving of 1-3 mm sized dry-sieved aggregates, larger than 0.25 mm. ^d Volumetric water-content at various suctions. ^e Gravel content (> 2mm), expressed as a percentage of the whole soil. ^f Coarse sand (0.25–2mm), expressed as a percentage of <2 mm soil mass. ^g Fine sand (0.05–0.25 mm), expressed as a percentage of <2 mm soil mass. ^h Silt (0.002–0.05 mm), expressed as a percentage of <2 mm soil mass. ⁱ Clay (<0.002 mm), expressed as a percentage of <2 mm soil mass. ^j Fe and Al extracted in ammonium-oxalate (amorphous oxides). ^k Fe extracted in Na-bicarbonate-dithionite (crystalline plus amorphous oxides) ^l Analysis performed on a selection of soils and the data is therefore solely used for site-description, not for regression analysis.

Table E2. Correlation table showing the coefficient of determination (R^2) for the soil physical and chemical properties for the Marchfeld CZO (n.s.: not significant at $p < 0.0001$).

Marchfeld (n=64)	DSA _{1mm}	WSA _{0.25mm}	Bulk dens.	$\theta_{0.25}$	θ_{30}	$\theta_{0.25} - \theta_{30}$	$(\theta_{30}/\theta_{0.25})$	Sand	Silt	Clay	SOC	Fe _d	Fe _{ox}	pH	C:N	CaCO ₃
DSA _{1mm} ^a	1															
WSA _{0.25mm} ^b	n.s.	1														
Bulk density	n.s.	0.54	1													
$\theta_{0.25 \text{ kPa}}$ (meso+micro-porosity)	n.s.	0.45	0.86	1												
$\theta_{30 \text{ kPa}}$ (microporosity)	n.s.	0.43	0.74	0.85	1											
$\theta_{0.25 \text{ kPa}} - \theta_{30 \text{ kPa}}$ (mesoporosity)	n.s.	n.s.	0.43	0.52	n.s.	1										
$\theta_{30 \text{ kPa}}/\theta_{0.25 \text{ kPa}}$	0.68	n.s.	n.s.	n.s.	0.33	n.s.	1									
Sand	0.37	n.s.	0.23	0.25	0.38	n.s.	0.39	1								
Silt	n.s.	n.s.	0.45	0.47	0.57	n.s.	0.31	0.87	1							
Clay	n.s.	0.26	0.32	0.29	n.s.	0.27	n.s.	n.s.	n.s.	1						
SOC ^c	n.s.	0.43	0.42	0.47	0.57	n.s.	0.29	n.s.	n.s.	n.s.	1					
Fe _d ^d	n.s.	0.40	0.25	n.s.	0.21	n.s.	n.s.	n.s.	0.28	n.s.	0.21	1				
Fe _{ox} ^e	n.s.	0.50	0.65	0.71	0.71	0.24	n.s.	0.33	0.62	0.38	0.31	0.37	1			
pH	n.s.	0.40	n.s.	n.s.	n.s.	n.s.	n.s.	n.s.	n.s.	n.s.	n.s.	0.48	n.s.	1		
C:N ratio	0.26	n.s.	n.s.	n.s.	n.s.	n.s.	n.s.	n.s.	n.s.	n.s.	n.s.	0.30	n.s.	n.s.	1	
CaCO ₃	n.s.	n.s.	n.s.	n.s.	n.s.	n.s.	n.s.	n.s.	n.s.	n.s.	n.s.	n.s.	n.s.	0.42	n.s.	1

^aDSA: Dry-sieved aggregates > 1mm

^bWSA: Water-stable aggregates > 0.25 mm

^cSOC: Soil organic carbon

^dFe_d: Dithionite-extractable Fe (total Fe-(hydr)oxides)

^eFe_{ox} and Al_{ox}: oxalate-extractable Fe and Al content (amorphous oxides)

Table E3. Correlation table showing the coefficient of determination (R^2) for the soil physical and chemical properties for the Koiliaris CZO (n.s.: not significant at $p < 0.0001$).

Koiliaris CZO (n=29)	DSA _{1mm}	WSA _{0.25mm}	Bulk dens.	$\theta_{0.25}$	θ_{30}	$\theta_{0.25} - \theta_{30}$	$(\theta_{30}/\theta_{0.25})$	Sand	Silt	Clay	SOC	Fe _{ox}	pH	C:N	CaCO ₃
DSA ^a _{1mm}	1.00														
WSA ^b _{0.25mm}	n.s.	1.00													
Bulk density	n.s.	0.75	1.00												
$\theta_{0.25 \text{ kPa}}$ (meso+microporosity)	n.s.	0.75	0.95	1.00											
$\theta_{30 \text{ kPa}}$ (microporosity)	n.s.	0.46	0.44	0.50	1.00										
$\theta_{0.25 \text{ kPa}} - \theta_{30 \text{ kPa}}$ (mesoporosity)	0.68	n.s.	0.51	0.51	n.s.	1.00									
$\theta_{30 \text{ kPa}}/\theta_{0.25 \text{ kPa}}$	0.92	n.s.	n.s.	n.s.	n.s.	0.78	1.00								
Sand	0.83	n.s.	n.s.	n.s.	0.44	0.46	0.79	1.00							
Silt	0.85	n.s.	n.s.	n.s.	0.32	0.56	0.84	0.94	1.00						
Clay	0.65	n.s.	n.s.	n.s.	0.54	n.s.	0.56	0.87	0.67	1.00					
SOC ^c	n.s.	0.79	0.66	0.75	0.72	n.s.	n.s.	n.s.	n.s.	n.s.	1.00				
Fe _{ox} ^e	n.s.	0.36	0.38	0.33	0.61	n.s.	n.s.	n.s.	n.s.	0.33	0.47	1.00			
pH	n.s.	0.41	0.50	0.47	n.s.	n.s.	n.s.	n.s.	n.s.	n.s.	0.44	0.40	1.00		
C:N ratio	n.s.	0.66	0.55	0.64	n.s.	0.46	n.s.	n.s.	n.s.	n.s.	0.57	n.s.	n.s.	1.00	
CaCO ₃	n.s.	0.33	0.38	0.38	0.68	0.42	n.s.	n.s.	n.s.	0.49	0.48	0.93	0.44	n.s.	1.00

^aDSA: Dry-sieved aggregates > 1mm

^bWSA: Water-stable aggregates > 0.25 mm

^cSOC: Soil organic carbon

^eFe_{ox} and Al_{ox}: oxalate-extractable Fe and Al content (amorphous oxides)

Table E4. Correlation table showing the coefficient of determination (R^2) for the soil physical and chemical properties for the Slavkov Forest CZO (n.s.: not significant at $p < 0.0001$).

Slavkov Forest (n=33)	DSA _{1mm}	WSA _{0.25mm}	Bulk dens.	$\theta_{0.25}$	θ_{30}	$\theta_{0.25} - \theta_{30}$	$(\theta_{30} / \theta_{0.25})$	Sand	Silt	Clay	SOC	Fe _{ox}	pH	C:N	CaCO ₃
DSA _{1mm} ^a	1.00														
WSA _{0.25mm} ^b	n.s.	1.00													
Bulk density	n.s.	0.58	1.00												
$\theta_{0.25 \text{ kPa}}$ (meso+microporosity)	n.s.	n.s.	0.71	1.00											
$\theta_{30 \text{ kPa}}$ (microporosity)	n.s.	n.s.	0.65	0.85	1.00										
$\theta_{0.25 \text{ kPa}} - \theta_{30 \text{ kPa}}$ (mesoporosity)	n.s.	n.s.	0.51	0.79	0.42	1.00									
$\theta_{30 \text{ kPa}} / \theta_{0.25 \text{ kPa}}$	0.33	n.s.	n.s.	n.s.	n.s.	0.46	1.00								
Sand	n.s.	n.s.	n.s.	n.s.	n.s.	0.06	n.s.	1.00							
Silt	n.s.	n.s.	n.s.	n.s.	n.s.	n.s.	n.s.	0.68	1.00						
Clay	n.s.	n.s.	n.s.	n.s.	n.s.	n.s.	n.s.	0.36	n.s.	1.00					
SOC ^c	n.s.	0.50	0.50	n.s.	n.s.	n.s.	n.s.	n.s.	n.s.	n.s.	1.00				
Fe _{ox} ^e	n.s.	n.s.	0.48	0.61	0.72	0.34	n.s.	n.s.	n.s.	0.45	n.s.	n.s.			
pH	n.s.	0.67	n.s.	n.s.	n.s.	n.s.	n.s.	n.s.	n.s.	n.s.	n.s.	n.s.	1.00		
C:N ratio	n.s.	n.s.	n.s.	n.s.	n.s.	n.s.	n.s.	n.s.	n.s.	n.s.	0.34	n.s.	n.s.	1.00	
CaCO ₃	n.s.	n.s.	0.51	0.59	0.52	0.49	n.s.	n.s.	n.s.	0.35	n.s.	n.s.	0.5	n.s.	1.00

^aDSA: Dry-sieved aggregates > 1mm

^bWSA: Water-stable aggregates > 0.25 mm

^cSOC: Soil organic carbon

^eFe_{ox} and Al_{ox}: oxalate-extractable Fe and Al content (amorphous oxides)

Summary

Natural nanoparticles, in particular iron (Fe)-(hydr)oxide nanoparticles, are abundant in soils and play an important role in several soil processes such as colloid-facilitated transport of phosphorus (P) and trace elements and the sequestration of soil organic carbon (SOC) and P within the solid phase. However, our mechanistic and quantitative understanding of the role of Fe-(hydr)oxide nanoparticles in these processes in soils is still poor due to (i) a lack of analytical techniques that enable the characterization of nanoparticles in soils and waters, and (ii) the complexity of the multiple adsorption reactions occurring simultaneously at the surfaces of the nanoparticles. Therefore, the objective of my PhD thesis was to study the role of Fe-(hydr)oxide nanoparticles in the above mentioned soil processes using novel analytical techniques and advanced modelling approaches.

In **Chapter 2**, I developed a new method for the extraction of Fe-(hydr)oxide nanoparticles from soils and subsequent characterization of the particles using Asymmetric Flow Field-Flow Fractionation (AF4) in combination with High-Resolution Inductively-Coupled-Plasma Mass-Spectroscopy (HR-ICP-MS). Colloids were extracted from the soil as intact particles using a dilute Na-pyrophosphate solution and ultrasonic treatment. The AF4 results show that colloidal Fe was present as Fe-(hydr)oxide nanoparticles of 2–10 nm in size and as Fe associated with Si-Al clay particles of 20–150 nm. However, the nature of the latter Fe species could not be elucidated from the AF4 fractograms only. Maximum concentrations of Fe-(hydr)oxide nanoparticles were found at a particle diameter of 5 nm, and the concentrations corresponded to 16–47% of the amorphous Fe-(hydr)oxide content of the soil. The high abundance of small Fe-(hydr)oxide nanoparticles found in this Podzol is typical for this soil type. These nanoparticles were not released from the soil using ultrasonic treatment in the absence of Na-pyrophosphate, showing that interactions between Fe-(hydr)oxides and organic matter are of high mechanical strength. Overall, in this chapter, I have provided the first experimental evidence obtained by AF4-HR-ICP-MS for the extremely small size of Fe-(hydr)oxide nanoparticles in soils.

I continued the characterization of colloidal Fe in **Chapter 3** using a combination of two novel and complementary analytical techniques; AF4-HR-ICP-MS and X-ray absorption spectroscopy (XAS). The combination of these two novel analytical techniques enabled me to quantify the contribution of Fe-(hydr)oxides and substituted Fe within the clay minerals to the amount of Fe co-eluting with the clay minerals for four soils, which remained

unresolved based on AF4 fractograms only as revealed in Chapter 2. Quantification of these two Fe species in the soil extracts is important because Fe-(hydr)oxides are of higher importance for colloid-facilitated transport than clay minerals due to the higher adsorption capacity of Fe-(hydr)oxides compared to clay minerals. Combined results of AF4 and XAS for colloids extracted from different soils show that a significant part of the colloidal Fe was present as Fe-(hydr)oxides. Depending on the soil, the Fe-(hydr)oxides were dominantly dispersed as free nanoparticles or as nanoparticles attached to clay minerals. Remarkably, the XAS results show that the speciation of Fe in the colloidal fractions closely resembles the speciation of Fe in the bulk soil, indicating that dispersion of colloidal Fe from the studied soils was rather unselective. As such, the size and speciation of the colloidal Fe strongly differ between different soil types. Overall, I show that Fe-(hydr)oxides can be released from the soil as colloids and may as such facilitate the transport of trace elements and P in soils and surface waters.

In **Chapter 4**, I studied the contribution of organic and mineral colloids to the transport of P from fertilized grassland fields to adjacent surface waters. Leaching of P from agricultural land to surface waters contributes to the eutrophication of surface waters. In addition to dissolved P species, also colloidal P (<0.45 μm) and particulate P (>0.45 μm) fractions contribute substantially to the transport of P. However, the speciation of these P fractions is still poorly understood, meaning that the source, mobility, and bioavailability of the colloidal and particulate P in runoff waters are still poorly known. Therefore, I studied the speciation of P in colloidal fractions using AF4 in combination with HR-ICP-MS. The water-samples were collected from an existing field-experiment on a heavy clay soil in the Netherlands. Water samples were collected after an rainfall event at different sampling times corresponding to different P management practices. The total P concentration increased with a factor 60 and 4, respectively, when samples were taken after application of dairy slurry and the solid fraction of dairy slurry compared to the situation where no P was applied for at least 7 months. The speciation of the colloidal fractions differs between the sampling times. AF4 results of the colloidal P fraction show that P co-eluted with colloidal clay and Fe-(hydr)oxide particles when no manure was applied for at least 7 months. A similar speciation of the colloids was found for the water samples taken after application of the solid manure fraction. In contrast, after application of dairy slurry, the colloidal P was dominated by phospholipids, which is a water-soluble organic P species abundantly

present in manure. The particulate P fraction could not be analysed by AF4 due to its large size ($>0.45\ \mu\text{m}$) but, using regression analysis, I show that the speciation of the particulate P fraction resembled the speciation of the colloidal P fraction. These pronounced differences in P speciation among different sampling times had remained unresolved in previous studies using classical physico-chemical fractionation only, showing the added value of AF4-HR-ICP-MS for the characterization of natural colloids in environmental research. Furthermore, these results show that the speciation and concentration of the colloidal and particulate P fractions strongly depend on the pretreatment of manure and on the weather conditions during manure application.

In **Chapter 5**, I studied the distribution of trace metals between organic and mineral colloids in a water-extract of a soil. The mineral colloidal fraction contains clay minerals and likely also Fe-(hydr)oxide that are associated with these clay minerals. The contribution of inorganic colloids to the total colloidal concentration decreased in the order: lead (Pb), P, zinc (Zn), nickel (Ni) and copper (Cu). As such, AF4-HR-ICP-MS provides evidence for the relative adsorption affinity of these metals for adsorption to organic versus inorganic colloids. The results suggest that also inorganic colloids, in addition to organic colloids, can contribute substantially to the transport of trace metals in soils.

In **Chapter 6**, I changed my focus from the characterization of nanoparticles to the adsorption processes occurring at surfaces of the metal-(hydr)oxide nanoparticles and their implications for organic carbon (OC) sequestration and phosphate (PO_4) solubility. In soils, metal-(hydr)oxide nanoparticles dominate the surface area that is available for adsorption of PO_4 and organic matter (OM). The competition for adsorption between phosphate and OM affects the soluble PO_4 concentrations as well as the amounts of OM adsorbed to metal-(hydr)oxides. Using a mechanistic surface complexation model, I explained the adsorption interactions in 33 calcareous soils taken from arable and forest fields. I found that the water-soluble PO_4 concentrations were poorly related to the PO_4 loading on the metal-(hydr)oxides. Instead, at a similar PO_4 loading, PO_4 solubility increased with increasing SOC content, which was mechanistically explained by the model by a higher OM loading on the metal-(hydr)oxides and thus a stronger competition for adsorption. As such, PO_4 solubility, relative to the PO_4 loading, was higher in the organic-rich forest soils than in the organic-poor arable soils. Therefore, I suggest that organic amendments increase phosphate

solubility and may thus increase plant uptake of P. Additionally, the model predictions allowed for a prediction of the OM loading on the metal-(hydr)oxide surfaces within the soils. The predicted OM loading was 2 to 28 times lower in the arable fields than in the forest fields, which I explain by replacement of OM by PO_4 in the arable fields. Therefore, I suggest that high levels of P fertilization may, over time, lead to a decline of the OC-sequestration potential of arable soils due to a loss of OM adsorbed to metal-(hydr)oxides.

In **Chapter 7**, I developed a new conceptual model describing the formation of soil aggregates from single particles. My results show that Fe-(hydr)oxides play an important role in the formation of aggregates and pores and, as such, increase aggregate stability and water retention capacity in soils. I explain the role of Fe-(hydr)oxides by their tendency to attach to larger clay and quartz minerals, thereby providing sorption sites for humic substances on these otherwise low to moderately reactive minerals. I suggest that such a 'coating' of Fe-(hydr)oxides is particularly important for silt and sand particles to be taken up in the network of organic substances. In addition to Fe-(hydr)oxides, also the SOC content and the pH, which is an indicator for the tendency of particles to coagulate, play an important role in determining the amount and stability of soil aggregates.

In **Chapter 8**, I discuss my main findings and I define the remaining knowledge gaps. Since there is an increasing interest in knowledge about phosphate availability and stabilization of organic carbon, I conclude that the development of methods to determine the size and surface area of Fe-(hydr)oxides in soils should receive further attention. I also conclude that more experimental work is needed to validate the model predictions about phosphate and organic matter adsorption in soils and to make the outcomes of this work applicable in agriculture.

Overall, in this PhD thesis, I have provided the first experimental evidence for the small size of Fe-(hydr)oxide nanoparticles in soils using AF4 coupled to HR-ICP-MS and I showed that Fe-(hydr)oxide nanoparticles play an important role in colloid-facilitated transport, OC-sequestration and formation of soil aggregates. This knowledge is important in order to maintain and improve the ability of soils to provide essential soil functions such as food production, sequestration of OC, and retention of water.

Samenvatting

Nanodeeltjes van ijzer(Fe)-(hydr)oxide komen van nature voor in bodems en spelen daar een belangrijke rol in diverse processen. Zo zijn Fe-(hydr)oxide nanodeeltjes belangrijk voor de vastlegging van organisch stof en fosfaat in de bodem omdat zij, door hun extreem kleine afmeting, een uitzonderlijk grote oppervlakte:volume verhouding hebben. Daarnaast kan, vanwege de sterke interacties tussen Fe-(hydr)oxiden en organische stof, verwacht worden dat deze nanodeeltjes de vorming van bodemaggregaten beïnvloeden. Verder kunnen nanodeeltjes in de vorm van colloïden het transport van fosfaat en sporenmatalen, welke een hoge affiniteit hebben voor adsorptie aan Fe-(hydr)oxiden, in bodem en water faciliteren. Ons begrip van de rol van Fe-(hydr)oxide nanodeeltjes in deze bodemprocessen is echter beperkt vanwege (i) een gebrek aan analytische technieken waarmee de deeltjesgrootte en chemische samenstelling van nanodeeltjes in bodem- en watermonsters gekarakteriseerd kunnen worden en (ii) de complexiteit van de adsorptieprocessen welke plaatsvinden aan het oppervlak van de nanodeeltjes. Mijn PhD thesis heeft daarom als doel om de rol van Fe-(hydr)oxide nanodeeltjes in de bovengenoemde processen beter te begrijpen, daarbij gebruikmakend van moderne analytische technieken en geavanceerde adsorptie modellen.

Fe-(hydr)oxide nanodeeltjes zijn belangrijk voor de vastlegging van organische stof en fosfaat in de bodem. De hoeveelheid organische stof en fosfaat die aan nanodeeltjes gebonden kan worden hangt af van de oppervlakte:volume verhouding van de deeltjes welke sterk toeneemt met een afnemende grootte van de nanodeeltjes. Echter, goede analytische technieken om de deeltjesgrootte van nanodeeltjes in de bodem te bepalen ontbreken. Daarom heb ik in **hoofdstuk 2** een methode ontwikkeld om nanodeeltjes uit de bodem te extraheren en om de grootte en chemische samenstelling van de nanodeeltjes te analyseren met behulp van Asymmetric Flow Field-Flow Fractionation (AF4) in combinatie met High-Resolution Inductively-Coupled-Plasma Mass-Spectroscopy (HR-ICP-MS). Voor de gekozen podzol grond kunnen Fe-(hydr)oxide nanodeeltjes als intacte colloïden uit de bodem geëxtraheerd worden met behulp van ultrasone trillingen en een oplossing van natrium-pyrofosfaat. De resultaten laten zien dat 16 tot 47% van de amorfe Fe-(hydr)oxiden in de bodem aanwezig is als Fe-(hydr)oxide nanodeeltjes welke slechts 2 tot 10 nm groot zijn. In de bodem zijn de Fe-(hydr)oxide deeltjes sterk gebonden aan de organische stof. De belangrijkste bevinding van dit hoofdstuk is het directe bewijs (d.m.v. AF4-HR-ICP-MS) voor de aanwezigheid van extreem kleine Fe-(hydr)oxide deeltjes in goed ontwikkelde bodems. Dit toont aan dat Fe-(hydr)oxiden een extreem hoog oppervlak:volume verhouding hebben en daardoor een belangrijke rol kunnen spelen in het vasthouden van fosfaat en organische stof in de bodem.

Naast Fe-(hydr)oxide nanodeeltjes is een groot deel van het Fe in de colloïden geassocieerd met klei mineralen, welke tussen de 20 en 150 nm groot zijn (Hoofdstuk 2 en 3). Dit Fe kan aanwezig zijn in de vorm van Fe-(hydr)oxide of in de vorm van klei mineralen. Deze twee Fe-vormen kunnen echter niet onderscheiden worden op basis van de AF4 fractogrammen. Het is van belang om de bijdrage van deze beide Fe-vormen te kunnen kwantificeren vanwege hun sterk verschillende adsorptie eigenschappen. Dit gaf aanleiding voor het onderzoek in **hoofdstuk 3**, waarin ik naast AF4-HR-ICP-MS ook gebruik van X-ray absorption spectroscopy (XAS). De laatste techniek maakt het mogelijk om de speciatie van het Fe in de colloïdale fractie te bepalen. De resultaten laten zien dat de verhouding tussen amorfe en kristallijne Fe-(hydr)oxide mineralen in de bodemextracten sterk verschilt voor de diverse bodems en sterk afhangt van de verhouding in de bulk grond. Verder laten de resultaten zien dat een significant deel van dit Fe aanwezig is als Fe-(hydr)oxiden welke gebonden zijn aan klei-mineralen. Deze Fe-(hydr)oxide-klei deeltjes kunnen ook geëxtraheerd worden in milde bodemextracten, en spelen daarom mogelijk een belangrijke rol in het transport van o.a. fosfaat vanwege de hoge adsorptiecapaciteit van Fe-(hydr)oxiden.

In **hoofdstuk 4** heb ik de rol van organische en minerale colloïden in de uitspoeling van fosfor (P) van grasland naar het aangrenzende oppervlaktewater bestudeerd. Afspoeling van P van landbouwgronden naar oppervlaktewateren draagt bij aan eutrofiëring. Naast opgelost fosfaat dragen ook colloïdaal (<0.45 µm) en particulier P (>0.45 µm) substantieel bij aan het transport van P. De speciatie van deze colloïdale en particuliere fracties is echter nog onbekend waardoor ook de herkomst, mobiliteit en biobeschikbaarheid van deze fracties slecht begrepen is. Daarom heb ik de speciatie van P in de colloïdale fractie gekarakteriseerd met AF4 in combinatie met HR-ICP-MS. Hiervoor heb ik gebruik gemaakt van watermonsters van een bestaande veldproef op een zware kleigrond in Nederland, welke op verschillende tijdstippen na toepassing van dierlijke mest zijn genomen. De totale P concentratie in de watermonsters nam respectievelijk een factor 60 en 4 toe wanneer neerslag direct volgde na toepassing van drijfmest en de vaste fractie van drijfmest in vergelijking met de situatie waarin geen mest was opgebracht gedurende 7 maanden. De resultaten laten zien dat de speciatie van het colloïdale P afhangt van het tijdstip na bemesting. Wanneer er gedurende 7 maanden geen mest was toegepast, was het colloïdale P voornamelijk geassocieerd met klei en Fe-(hydr)oxide deeltjes. Een vergelijkbare speciatie van de colloïden werd gevonden voor de watermonsters welke kort na de toepassing van de vaste fractie van de dierlijke mest waren genomen. Op deze twee tijdstippen hangt de hoeveelheid colloïdaal P dus sterk af

van de mate waarin klei deeltjes vanuit de bodem dispergeren. Echter, na het opbrengen van drijfmest nam de colloïdale P concentratie sterk toe en was colloïdaal P hoofdzakelijk aanwezig in de vorm van fosfolipiden, een goed-oplosbaar bestanddeel van mest met een hoge biobeschikbaarheid. Deze resultaten laten zien dat de speciatie en concentratie van colloïdaal en particulier P sterk samenhangt met de eventuele voorbehandeling van de drijfmest en de weerscondities (*i.e.* optrede van neerslag) gedurende bemesting. Daarnaast laten deze resultaten zien dat karakterisatie van watermonsters d.m.w. AF4 een sterke meerwaarde heeft t.o.v. klassieke fractioneringstechnieken waarin deze verschillen niet tot uiting komen.

In **hoofdstuk 5** heb de verdeling van sporenmatalen tussen organische en minerale colloïden in een bodem-extract bestudeerd. De bijdrage van de minerale versus organische colloïden verschilde voor de verschillende sporenmatalen en nam af in de volgorde: Pb, Zn, Ni and Cu. Deze resultaten laten zien dat minerale colloïden, welke voornamelijk bestaan uit klei mineralen en Fe-(hydr)oxiden, een belangrijke bijdrage kunnen leveren aan het transport van sporenmatalen in bodems.

In **hoofdstuk 6** richt ik mij op de adsorptie processen welke plaatsvinden op het oppervlak van metaal-(hydr)oxiden (Fe+Al-(hydr)oxiden) in de bodem en de implicaties hiervan voor de vastlegging van organische stof en fosfaat. Het gehalte aan metaal-(hydr)oxiden bepaald in grote mate hoeveel oppervlak er in de bodem beschikbaar is voor de adsorptie van fosfaat en organische stof. Fosfaat en organische stof adsorberen op vergelijkbare wijze aan metaal-(hydr)oxiden en vertonen daarom een sterke competitie voor adsorptie. De hoeveelheid fosfaat die vastgelegd kan worden hangt dus mede af van de hoeveelheid organische stof die geadsorbeerd is en vice versa. Echter, adsorptie-competitie is erg complex en daarom nog slecht begrepen. In hoofdstuk 6 gebruik ik een geavanceerd adsorptie model om de gelijktijdige adsorptie van fosfaat en organische stof te voorspellen. Het model heb ik toegepast op een dataset verzameld voor 33 kalkrijke gronden afkomstig van bosgronden en akkers welke een grote variatie in organische stof en fosfaat gehalte vertoonden. In tegenstelling tot de algemene verwachting was er een slechte correlatie tussen de water-oplosbaar fosfaat concentratie en de hoeveelheid fosfaat geadsorbeerd aan de metaal-(hydr)oxiden. Dit kan ik verklaren doordat de mate van competitie met organische stof verschilde in de diverse bodems. De resultaten laten namelijk zien dat de oplosbaarheid van fosfaat, bij een gelijkblijvende fosfaat-lading, toeneemt met een toenemend organisch stof gehalte in de

bodem. Zo was de oplosbaarheid van fosfaat, voor een vergelijkbare fosfaat-lading, hoger in de bosgronden (rijk aan organische stof) dan in akkergronden (matig gehalte organische stof). Deze bevindingen konden ook verklaard worden aan de hand van het adsorptiemodel en suggereren dat de oplosbaarheid van fosfaat, en daarmee de beschikbaarheid voor planten, verhoogd kan worden door het organisch stof gehalte van de bodem te verhogen. Met hetzelfde model heb ik de lading van de organische stof op de metaal-(hydr)oxiden, welke de mate van competitie met fosfaat bepaalt, berekend. De geschatte organische stof lading was 2 tot 28 keer lager in de akkergronden dan in de bosgronden. Ik suggereer dat de lage organische stof lading in de akkergronden verklaard kan worden door de hoge fosfaat gehalten in deze bodems. Zodoende suggereer ik dat overbemesting met fosfaat op de lange termijn kan leiden tot een afname in het organisch stof gehalte van de bodem.

In **hoofdstuk 7** heb ik een nieuw conceptueel model ontwikkeld welke de vorming van bodemaggregaten vanuit losse bodemdeeltjes beschrijft. Mijn werk laat zien dat Fe-(hydr)oxide een belangrijke rol speelt in de vorming van micro-aggregaten en daarmee de porositeit van de bodem verbeterd. De rol Fe-(hydr)oxide in aggregaat vorming kan verklaard worden door de sterke binding van Fe-(hydr)oxide nanodeeltjes aan klei-, silt- en zanddeeltjes. Hierdoor worden bindingsplekken voor organische stof gecreëerd op deze anders matig reactieve bodemdeeltjes. Ik suggereer dat deze 'coating' van Fe-(hydr)oxiden vooral van belang is om silt- en zanddeeltjes bindingen te laten vormen met organische stof en op te laten nemen in aggregaten. Naast Fe-(hydr)oxide bepalen ook het organisch stof gehalte en de pH, welke een goede indicator voor de mate van coagulatie blijkt te zijn, de hoeveelheid en stabiliteit van de bodemaggregaten en het volume van de poriën.

In **hoofdstuk 8**, de algemene discussie, werp ik een kritische blik op mijn resultaten en de gekozen aanpak, en de bespreek ik de kennisgaten. Gezien de toenemende vraag naar kennis over fosfaat beschikbaarheid en organische stof stabilisatie concludeer ik dat verdere ontwikkeling van methoden om de deeltjesgrootte en het oppervlak van metal-(hydr)oxiden in de bodem te bepalen belangrijk is. Ook concludeer ik dat er meer experimenteel werk nodig is om de modelvoorspellingen over de competitie tussen fosfaat en organische stof beter te valideren en om deze nieuwe kennis toepasbaar te maken.

Al met al laten de resultaten van deze thesis zien dat Fe-(hydr)oxide nanodeeltjes een belangrijke rol spelen in de vastlegging van fosfaat en organische stof in de bodem, colloïdaal transport in bodem en water, en in het bepalen van de bodemfysische eigenschappen.

Dankwoord

Dankwoord

Dit proefschrift is het resultaat van vier en half jaar onderzoek. Het was voor mij een periode met ups en downs, zoals een promotieonderzoek voor menigeeen verloopt. Eenmaal voltooid kijk ik tevreden terug op een waardevolle en leerzame tijd. Natuurlijk was dit proefschrift nooit tot stand gekomen zonder de support, in welke vorm dan ook, van de vele geweldige mensen om mij heen. Ik wil jullie daar dan ook enorm voor bedanken!

Allereerst wil ik mijn directe begeleiders bedanken: Willem van Riemsdijk, Liping Weng en Rob Comans. Willem, ik wil je bedanken voor je vertrouwen in mij en het project. Jouw enthousiasme over mijn werk en discussies over de resultaten zorgde altijd weer voor nieuwe inspiratie. Liping, ik wil je bedanken voor je inhoudelijke input en de vrijheid die je me gegeven hebt om mijn eigen ideeën uit te werken. Rob, onze samenwerking begon twee-en-half jaar geleden. Je ben altijd oprecht geïnteresseerd en enthousiast, en je goede en scherpe feedback op mijn manuscripten gaf mij altijd weer de energie en het vertrouwen om verder te gaan. Minstens zo belangrijk, je betrokkenheid beperkt zich niet tot de werkvloer maar ook op persoonlijk vlak bood je altijd een luisterend oor. Bedankt daarvoor!

Naast mijn begeleiders heb ik ook ontzettend veel steun en plezier gehaald uit de samenwerking met mijn andere co-auteurs. Gerwin, onze samenwerking begon toevallig vanwege jouw interesse in AF4 maar ook daarna zijn we veel contact blijven houden. Ik kon altijd bij je binnen lopen voor grote en kleine vragen. Je persoonlijke betrokkenheid en je inhoudelijke en mentale support heb ik altijd erg gewaardeerd! Al met al kan ik wel stellen dat je een grote bijdrage hebt geleverd aan de voltooiing van dit boekje! Erwin, vier jaar geleden hebben wij op basis van mijn MSc thesis mijn allereerste publicatie geschreven en je motiveerde mij om een promotieonderzoek te gaan doen. Ik ben blij dat ik je advies heb opgevolgd! Ook daarna bleef je een betrokken collega en ik heb onze gesprekken erg gewaardeerd. Ik wens je het allerbeste! Andreas Voegelin, I want to thank you for sharing your data and knowledge on EXAFS spectroscopy which resulted in Chapter 3 of this thesis. I have really appreciated your enthusiasm about the work and your critical feedback on many versions of the manuscript. Cathelijne, wat begon met een toevallige ontmoeting bij de koffieautomaat is uiteindelijk uitgemond in een leuke samenwerking. Je bent altijd vol energie en ik heb in korte tijd veel van je geleerd bij het schrijven van het zevende hoofdstuk van dit proefschrift!

Natuurlijk wil ik ook mijn directe (oud)collega's van de vakgroep 'bodemkwaliteit' bedanken. Dorien, het is al weer bijna vier jaar geleden dat wij een kamer deelden. Ik had me voor de start van mijn PhD geen beter kamergenootje kunnen wensen! Jij zat op dat moment al in de eindfase van je PhD en als beginnend PhD'er kon ik met al mijn vragen en onzekerheden bij jou terecht. Angie, het was super om jou drie-en-een-half jaar als kamergenoot te hebben gehad en lief en leed met elkaar te kunnen delen. Je bent altijd enthousiast en in voor een borrel, etentje of feestje. Helemaal top dat je nu mijn paranimf wilt zijn! Karst en Andreas, ons PhD traject is grotendeels gelijktijdig verlopen. Het was altijd fijn om zo even bij jullie naar binnen te lopen en de frustraties en successen in alle fasen met elkaar te delen! Of course I also want to thank my other office mate, Yunyu, and all other colleagues in the Soil Quality department for the nice chats during the coffee breaks, including the home-made cakes on 'cake-Wednesday'.

De afgelopen jaren heb ik ook vele uurtjes doorgebracht in het lab. Gerlinde, jij was altijd beschikbaar voor de kleine en grote vragen rondom mijn experimenten en een gezellig babbeltje. Peter, wij hebben heel wat tijd samen bij de ICP-MS doorgebracht. Mede door jou flexibiliteit en enthousiasme hebben we goede resultaten geboekt! Verder wil ik ook alle andere medewerkers van het laboratorium bedanken voor hun hulp!

This PhD project was part of the EU-project SoilTrEC and I want to thank all project partners for their support, inspiring discussions and feedback on my papers and presentations. I have really enjoyed the annual meetings, field trips and workshops that were organised by the project. Jaap, vanuit Wageningen zijn wij per auto naar Oostenrijk, Zwitserland en Tsjechië geweest om bodemmonsters te nemen van de SoilTrEC sites. Ik kan me deze tripjes, die voor ons beide toch ook een soort van vakantie waren, nog goed herinneren. Jeroen, ik heb erg genoten van onze reis naar Colorado voor een conferentie en de aansluitende vakantie waarin we naar de meest indrukwekkende parken in Colorado en Utah zijn geweest.

Verder wil ik mijn oud-studiegenootjes Anneke, Danielle, Justine, Marina en Velda bedanken. Omdat we allemaal nog aan Wageningen verbonden zijn, was een spontane lunchafspraak of vrijdagmiddagborrel altijd zo te regelen. Dat moeten we zeker blijven voorzetten! Verder wil ik mijn oud-huisgenootjes van Haarweg 193 bedanken, Paulien, Thomas, Bart, Evert-Jan, Diederik en Lars. Ook al zijn de meeste van ons Wageningen

Dankwoord

ontvlogen, het is altijd weer leuk om bij elkaar te zijn. Ik hoop dat we ook in de toekomst regelmatig contact houden! Paulien, ik vind het superleuk dat je mij op het podium wilt bijstaan!

De afgelopen jaren stonden zeker niet alleen in het teken van promoveren. Ook buiten mijn werk om zijn er natuurlijk vele mensen belangrijk geweest voor het plezier in mijn vrije tijd en tijdens de andere leuke en belangrijke veranderingen van de afgelopen jaren. Allereerst wil ik daarvoor mijn ouders, schoonouders, broers, zussen, zwagers en schoonzussen bedanken. Ook al begrepen jullie misschien niet altijd waar ik zo druk mee was, jullie staan altijd voor ons klaar! Daarnaast natuurlijk alle vrienden, bedankt voor de vele gezellige avondjes, feestjes en andere leuke momenten! De laatste en belangrijkste plek in dit dankwoordje heb ik uiteraard gereserveerd voor mijn man en beste maatje, Niels. De afgelopen vier jaar is er veel veranderd in ons leven, we zijn verhuisd, hebben we ons huis van top en teen verbouwd en we zijn getrouwd. Ik vind het helemaal geweldig dat we nu samen een kleintje verwachten! Bedankt dat je er altijd voor mij bent!

Curriculum Vitae
and
List of Publications

Curriculum Vitae

Inge C. Regelink was born on April 7th, 1986 in Toldijk, the Netherlands. She completed secondary school (VWO, Ulenhof College, Doetinchem) in 2004 and, in the same year, she started her BSc study 'Soil, Water and Atmosphere' at Wageningen University. For her BSc, she specialized in soil science, and followed a minor in environmental biotechnology. For her BSc thesis, she studied the role of redox processes in the restoration of peat lands. She gained her BSc degree in 2007 (*cum laude*), and she continued her MSc education at Wageningen University. During her MSc, she specialized in soil chemistry and followed a minor in environmental technology. She did her internship at the soil department of the consultancy and engineering firm Witteveen+Bos (Deventer, the Netherlands) where she conducted a literature study on the environmental impact of rocket fuel spillages in Kazakhstan and obtained hands-on experience in various soil remediation projects. She did her MSc thesis at the department of Soil Quality of Wageningen University where she studied the geochemical processes that control the mobility of nickel in heavily contaminated sandy aquifers. This thesis work resulted in her first scientific publication. In July 2009, she received her MSc degree (*cum laude*) in Soil Science. In the same year, she had a temporary job at the company BLGG AgroXpertus in Oosterbeek/Wageningen where she worked on improving predictions of nutrient availability in agricultural soils. In October 2009, she continued her career in scientific research and started her PhD research within the EU-project 'SoilTrEC' (Soil Transformations in European Catchments) at the department of Soil Quality of Wageningen University, which resulted in this PhD thesis.

List of publications

Published

Regelink, I.C., Voegelin, A., Weng, L., Koopmans, G.F., Comans, R.N.J. (2014) *Characterization of colloidal Fe from soils using Field-Flow-Fractionation and Fe K-edge X-ray absorption spectroscopy*. Environmental Science and Technology 48, 4307

Regelink, I.C., Koopmans, G.F., van der Salm, C., Weng, L., van Riemsdijk, W.H. (2013) *Characterization of colloidal phosphorus species in drainage waters from a clay soil using Asymmetric Flow Field-Flow Fractionation*. Journal of Environmental Quality 42, 464

Regelink I.C., Weng, L., Koopmans, G.F., van Riemsdijk, W.H. (2013) *Asymmetric Flow Field-Flow Fractionation as a new approach to analyse iron-(hydr)oxide nanoparticles in soil extracts*. Geoderma 202-203, 134

Regelink I.C., Weng, L., van Riemsdijk, W.H. (2011) *The contribution of organic and mineral colloidal nanoparticles to element transport in a podzol soil*. Applied Geochemistry 26, S241.

Regelink I.C., Temminghoff, E.J.M. (2011) *Ni adsorption and Ni-Al LDH precipitation in a sandy aquifer: An experimental and mechanistic modeling study*. Environmental Pollution 159, 716

Submitted

Regelink, I.C., Weng, L., Lair, G.J., Comans, R.N.J. *Adsorption competition between phosphate and organic matter on metal-(hydr)oxides in arable and forest soils explained by mechanistic adsorption modelling*.

Regelink, I.C., Stoof, C.R., Weng, L., Rouseva, S., Lair, G.J., Kram, P., Nikolaidis, N., Kercheva, M., Banwart, S., Comans, R.N.J. *Mechanistic linkages between soil aggregates, soil porosity and soil physical-chemical properties*.

Koopmans, G.F., Hiemstra, T., Regelink, I.C., Molleman, B., Comans, R.N.J. *Asymmetric flow field-flow fractionation of manufactured silver nanoparticles in soil solutions*.



*Netherlands Research School for the
Socio-Economic and Natural Sciences of the Environment*

D I P L O M A

For specialised PhD training

The Netherlands Research School for the
Socio-Economic and Natural Sciences of the Environment
(SENSE) declares that

Inge C. Regelink

born on 7 April 1986 in Steenderen, The Netherlands

has successfully fulfilled all requirements of the
Educational Programme of SENSE.

Wageningen, 7 November 2014

the Chairman of the SENSE board

Prof. dr. Huub Rijnaarts

the SENSE Director of Education

Dr. Ad van Dommelen

The SENSE Research School has been accredited by the Royal Netherlands Academy of Arts and Sciences (KNAW)



K O N I N K L I J K E N E D E R L A N D S E
A K A D E M I E V A N W E T E N S C H A P P E N



The SENSE Research School declares that **Ms Inge Regelink** has successfully fulfilled all requirements of the Educational PhD Programme of SENSE with a work load of 37.4 ECTS, including the following activities:

SENSE PhD Courses

- o Environmental Research in Context (2010)
- o Speciation and Bioavailability (2010)
- o Oral presentation on the Goldschmidt conference entitled: 'Results of an interdisciplinary research project on aggregate formation in European CZO's' (2013)

Other PhD and Advanced MSc Courses

- o PhD Competence Assessment (2010)
- o Physical Modelling (2010)
- o Improve your Writing (2012)
- o Scientific Writing (2013)
- o Soil Aggregation and Carbon Workshop, Vienna, Austria (2013)
- o Interpersonal Communication for PhD Students (2013)
- o Adobe InDesign (2013)
- o Career Assessment (2013)

External Training at a foreign research institute

- o Training on Field-Flow Fractionation, Postnova Analytics, Germany (2010)

Oral Presentations

- o *Iron-(hydr)oxide nanoparticles in soils; Extractability, size-distribution and interactions with organic matter.* GES2011 (Geochemistry of the Earth's Surface), Student Symposium, 30 May- 2 June 2011, Boulder, United States
- o *Analysis of nanoparticles using AF4.* Sense Nano-meeting, 8 November 2012, Wageningen, The Netherlands
- o *Characterization of Fe-(hydr)oxide nanoparticles using state-of-the-art techniques.* EGU2013 (European Geosciences Union), 7-11 April 2013, Vienna, Austria
- o *Results of an interdisciplinary research project on aggregate formation in European CZO's.* Goldschmidt 2013, 26-29 August 2013, Florence, Italy

SENSE Coordinator PhD Education

Dr. ing. Monique Gulickx

This research was financially supported by the European Commission within the FP 7 Project “Soil Transformations in European Catchments” (SoilTrEC).

Financial support from Wageningen University for printing this thesis is gratefully acknowledged.

Thesis layout and cover design: Inge Regelink